Characterisation of the reversible formate dehydrogenases of *Shewanella.*

Jonathan Alexander Davies

PhD

University of East Anglia

September 2017

Abstract

The reversible action of tungsten or molybdenum-containing formate dehydrogenase (FDH) enzymes in reducing CO_2 to formate has been proposed for storing renewably produced electricity with concomitant CO_2 sequestration. Previous attempts have highlighted the unfeasibility of using purified enzyme systems for biotechnological purposes. In response the possibility of using the exoelectrogenic bacteria *Shewanella oneidensis* in association with a cathode to drive intracellular CO_2 reduction is proposed. Since the native FDH enzymes of *S.oneidensis* have not been previously studied, this work concerns their characterisation and directionality to inform both on native physiology and possible future biotechnological applications. This thesis demonstrates that the native FDH enzymes of *S.oneidensis* are capable of CO_2 reductase activity. Both forward (K_m 39 μM) and reverse (K_m 1.43 mM) directions of FDH catalysis in whole cell cultures are maximal when cultured in the presence of W. When grown under such conditions, two FDH isoforms (Fdh1αβγ and Fdh2αβγ) contribute to these activities, with protein purification confirming Fdh2αβγ as a tungstoenzyme. CO_2 reductase activity in *S.oneidensis* cultures could be driven by a cathode in simple three electrode electrochemical experiments without exogenous mediators with high coloumbic efficiency, representing an interesting paradigm for future inexpensive microbial electrosynthetic study.

Acknowledgments

Everyone both at UEA and Schlumberger for supporting me during the last four years, financially, academically and otherwise, with special thanks to Marcus, Tom, Julea, David and Seth for guidance and supervision throughout.

My family for shaping and making me who I am today, (Mother, Father, Brother and Sister), the onus is on you.

Laura for humouring my interests and hobbies, in multiple languages.

Mike for the memories and drinks we shared around the world.

In many ways, to many more people, I just want to say Tak, Obrigado, Gracias, Gràcies, Спасибо and Thank you.

Table of Contents

Table of Figures

Abbreviations

ATP – Adenosine triphosphate

ADP – Adenosine diphosphate

BCA - Bicinchoninic acid

BES - Bioelectrochemical systems

CA – Chronoamperometry

cDNA - Complementary DNA

CE – Counter electrode

CoA - Coenzyme A

C_t – Threshold cycle

CV – Cyclic voltammetry

DEAE - Diethyl-aminoethyl

DDM - n-Dodecyl ß-D-maltoside

DNA – Deoxyribonucleic acid

dNTP(s) – Deoxynucleotide(s)

DMSO - Dimethyl sulfoxide

DTT – Dithiothreitol

E – Potential (V)

EDTA - Ethylenediaminetetraacetic acid

EET – Extracellular electron transfer

EPS - Extracellular polymeric substances

F - Faraday's constant

FDH – Formate dehydrogenase

Fdnαβγ - Gene products of SO_0101-0103

Fdh1αβγ - Gene products of SO_4509-4511

Fdh2αβγ - Gene products of SO_4513-4515

FHL – Formate hydrogen lyase complex

g - Gravitational acceleration

gDNA – Genomic DNA

HDCR – Hydrogen dependent CO_2 reductase

HEPES -4-(2-hydroxyethyl)-1-piperazineethanesulfonic acid

ICP-MS - Inductively coupled plasma mass spectrometry

k_{cat} – Enzymatic turnover number

K_m - Michaelis constant

K_s - Monod constant

LB – Lysogeny broth

LDH – Lactate dehydrogenase

MALDI-TOF - Matrix-Assisted Laser Desorption/Ionization Time of Flight (Mass Spectrometry)

MEC – Microbial electrolysis cell

MES - 2-(N-Morpholino) ethanesulfonic acid

MDC – Microbial desalination cell

MFC – Microbial fuel cell

mRNA – Messenger RNA

Mtr – Metal reducing

MQ – Menaquinone

MQH_2 - Menaquinol

MV – Methyl Viologen

NAD(P) - Nicotinamide adenine dinucleotide (phosphate)

NAG -N-Acetylglucosamine

NMR - Nuclear magnetic resonance spectroscopy

OD – Optical density

PCR – Polymerase chain reaction

PFV – Protein film voltammetry

PGD - Pyranopterin guanine dinucleotide

pKa - $-\log_{10}(K_a$, acid dissociation constant)

PMF – Proton motive force

RE – Reference electrode

RNA - Ribonucleic acid

RT-qPCR – Quantitative reverse transcription PCR

Sarkosyl - Sodium lauroyl sarcosinate

SD – Standard deviation

SDS-PAGE - Sodium dodecyl sulphate polyacrylamide gel electrophoresis

SEM – Standard error of the mean

TAE - Tris-acetate-EDTA

Tris – Tris (hydroxymethyl) aminomethane

TMAO - Trimethylamine N-oxide

V_{max} - Maximal velocity (enzymatic)

WE – Working electrode

WT – Wildtype

+W - Growth with 3 μM tungstate

+Mo - Growth with 3 μM molybdate

+W/+Mo - Growth with 3 μM tungstate and molybdate

-W/-Mo - Growth with neither tungstate nor molybdate

1 Introduction

The continued depletion of fossil fuels (Goli et al. 2016) and increases in human population (Gerland et al. 2014) necessitate the development of renewable and efficient energy solutions to meet soaring demand (Pant et al. 2012). A wide range of novel technologies is currently being developed alongside more established methods such as photovoltaic technologies (Panwar et al. 2011). A pertinent, albeit niche, example includes the use of certain exoelectrogenic microorganisms, capable of coupling intracellular metabolism to extracellular electrodes for electricity production in microbial fuel cell (MFC) devices (Franks & Nevin 2010). A principal concern for many of these technologies however is that their fluctuating electrical outputs are not storable, leading to a host of secondary technologies relating to energy storage including the popular hydrogen economy approach which stores this reductive potential in the form of hydrogen (Nikolaidis & Poullikkas 2017). However a range of other technologies are beginning to emerge including those that use carbon based molecules as energy storage. These have a number of benefits including the fact that many are non-volatile liquids capable of being stored using existing infrastructure (Nevin et al. 2011) and when derived from atmospheric carbon dioxide have the added benefit of being carbon neutral, thereby mitigating associated climate change effects (Goli et al. 2016). Despite being an attractive proposition the thermodynamic and kinetic stability of CO_2 (Crable et al. 2011) means that the majority of CO_2 fixation is still performed by natural processes (Ducat & Silver 2013).

Biological autotrophic carbon dioxide (CO_2) fixation, responsible for the prehistoric reservoirs of reduced carbon currently used to meet over 80% of the world's energy requirements (Ducat & Silver 2013), (and concomitantly producing 87% of anthropomorphic CO_2 emissions (Goli et al. 2016)) is also the principal contributor to the (re-)sequestration of atmospheric CO_2, primarily through photosynthetic organisms (Armstrong & Hirst 2011). The majority of such carbon fixation occurs in plants, algae and cyanobacteria via the reductive pentose phosphate pathway (Calvin cycle) (Ladapo & Whitman 1990) which relies on the notoriously slow RuBisCO **(**Ribulose-1,5-bisphosphate carboxylase/oxygenase) enzyme (< $10s^{-1}$) (Maia et al. 2015).

Four other pathways, including the reductive tricarboxylic acid (reductive-TCA) cycle exist for autotrophic growth. These fix CO_2 by incorporating inorganic carbon directly into existing acetyl-coenzyme A (acetyl-CoA) or succinyl-CoA molecules (Ducat & Silver 2013).

A final fifth alternative pathway for autotrophic growth is via the reductive acetyl-CoA (Wood Ljungdahl) pathway, in which (for acetogenic bacteria) CO_2 is initially reduced to formate (Ragsdale & Pierce 2008). The single proton, two electron reduction of CO_2 to formate in this pathway represents a simple and attractive process to be replicated for CO_2 fixation to a renewable energy storage molecule. The accompanying technologies for formate use as a fuel are already developing with formic acid fuel cells being designed with a view to replace traditional lithium ion batteries in small portable devices (Lum et al. 2012). In addition to use as an energy storage solution, formate has also been proposed to be an effective synthon for the fine chemical industry (Reda et al. 2008). However in order to be economically viable the reduction of CO_2 to formate requires a catalyst that operates selectively, efficiently, and under mild conditions (Bachmeier & Armstrong 2015).

Considering the simple underlying chemistry, a variety of chemical catalysis methods have been suggested for the reduction of CO_2 not just to formate but also methanol or CO (Armstrong & Hirst 2011). Of these, examples of ruthenium, iron, manganese, and copper based catalysts have been shown to reduce CO_2 electrochemically, but with poor selectivity and requiring large energy inputs (high overpotentials) (Bassegoda et al. 2014). In a similar manner chemical electrodes, made of lead, mercury, indium, and thallium are capable of direct CO_2 reduction with high specificity but also require high overpotentials (Reda et al. 2008).

Considering the limited success of such chemical approaches, recent focus has returned to biology for inspiration, with extensive study of the family of formate dehydrogenase (FDH) enzymes that catalyse the reaction for the Wood Ljungdahl pathway. After several unsuccessful biomimetic chemical approaches (Groysman & Holm 2007), research has focused on the electrochemical study of purified enzymes, demonstrating reversible, efficient, selective catalysis under mild conditions without significant overpotentials (Bassegoda et al. 2014).

Despite this success it has been stressed that the described enzymatic systems are not economically viable or scalable due to the time and costs associated with enzyme purification and adhesion to an electrode (Armstrong & Hirst 2011). To resolve these limitations it is proposed here that bacterial species capable of interacting with electrodes, for example the model exoelectrogen *Shewanella oneidensis* MR-1 (Logan 2009), could be used as a self-renewing biocatalyst, coupling a cathode to the intracellular reduction of CO_2 by FDH enzymes within the protective environment of the bacterial cell, enabling the benefits of the previously characterised enzymatic catalysis without the need for costly enzyme purification and with the scope for further chemical transformation using the genetically tractable metabolic machinery of *S.oneidensis* (Kane et al. 2013).

Since the biochemistry of the FDH of *S.oneidensis* has not been previously studied, questions about their reversibility and native properties are raised, concerning not just their viability as CO_2 reductase enzymes for biotechnology but also concerning their native function and how they contribute to native microbial physiology. To sufficiently introduce these aspects, four topics will be discussed at length below, (A) the metabolism of formate, (B) the relevant FDH enzymes, (C) An introduction to the relevant physiology of *S.oneidensis*, and (D) the potentially relevant biotechnological and electrochemical applications.

1.1 Formate metabolism

Formate ($HCOO^-$) plays an important role in a variety of different biological contexts and a range of organisms, including humans. Despite this the enzymes responsible for interconversion between formate and CO_2, (FDH), are not seen in higher eukaryotes, restricted to plants and simple eukaryotic organisms such as yeast and prokaryotic life (Maia et al. 2015). Although FDH are not found in higher eukaryotes, formate still plays an important biosynthetic role for serine and nucleic acid metabolism, a role it also plays in plants and many prokaryotes (Bar-even 2016).

In plants and indeed some species of pathogenic bacteria and fungi, formate has been implicated in initiating stress responses (Alekseeva et al. 2011). Extensive research in potato cultivars has revealed the role of FDH as a stress protein in response to chemical stress, low temperature, drought and ultraviolet light (Tishkov & Popov 2004), under these conditions FDH expression is thought to be required to reduce formate and proline accumulation, although the specifics remain unclear. Concerning stress responses in plants and promising the generation of more hardy crop strains (Hanson et al. 2000) this area has received a large amount of academic interest.

The low reduction potential ($E^{0'}$) of the $CO_2/HCOO^-$ couple at -0.42 V (vs SHE at pH 7, 1M formate, CO_2 (g) 1atm) (Armstrong & Hirst 2011) makes it well suited for providing reducing equivalents for reduction of terminal electron acceptors as part of energy generating respiratory chains or fermentation pathways in prokaryotic organisms as well as for energy conservation, including the regeneration of biological reducing agents such as NAD(P)H (Tishkov & Popov 2004). In these contexts FDH catalyses the oxidation of formate to CO_2 according to eq. (1.1) below.

$$HCOO^- \rightarrow CO_2 + 2e^- + H^+ \qquad (1.1)$$

When contributing to the respiratory needs of gram negative bacteria, formate oxidation typically occurs in the periplasm and can be coupled to a wide range of electron acceptors that typically generate proton motive force (Wang & Gunsalus 2003) either directly or indirectly.

In many such respiratory chains the electrons abstracted from the oxidation of formate (releasing a proton) in the periplasm are relayed via internal redox centers of FDH enzymes to the cytoplasm for the reduction of quinones in quinone/quinol redox pools (removing cytoplasmic protons). As such catalysis contributes to the establishment of an electrochemical proton gradient across the inner membrane (Jormakka et al. 2002). Such reduced quinones then transfer the reducing equivalents to terminal electron acceptors, which may in turn contribute further to PMF generation as seen in Figure 1-1 (**A**).

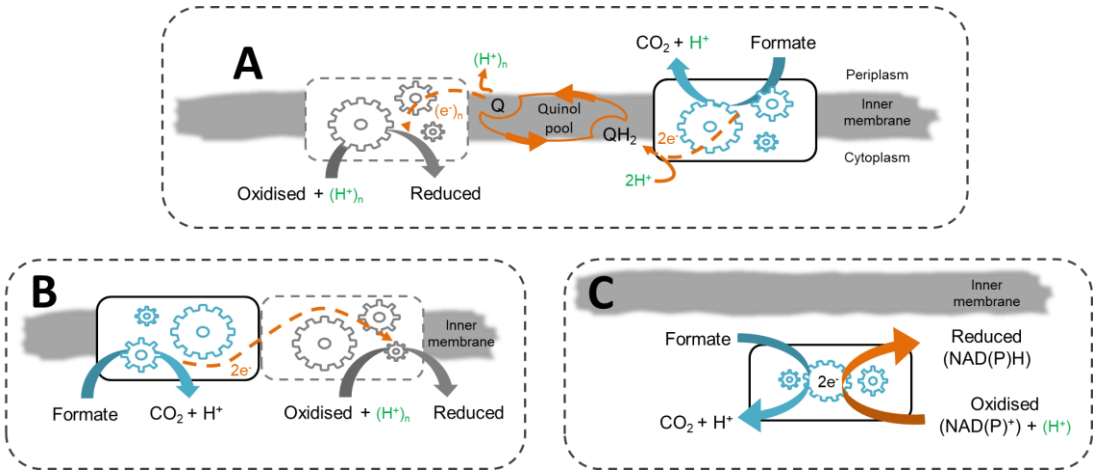

Figure 1-1 Formate linked energy generation/conservation in gram negative bacteria.
(A) *Overview of a simple redox loop demonstrating the periplasmic oxidation of formate by FDH coupled to reduction of a quinone pool and subsequent reduction of a terminal electron acceptor, where the pictured example is cytoplasmically facing as proposed when coupled to nitrate reductase (Jormakka, S Törnroth, et al. 2002).* ***(B)*** *Overview of FDH in complex with coupled reductase, as seen for FHL complex for which the associated protein is a hydrogenase enzyme. Both FDH and coupled protein partner are presented here as cytoplasmically facing as proposed for FHL of E.coli.* ***(C)*** *Overview of simple FDH enzymes responsible for energy conservation by regeneration of reduced species such as NADH, presented here in the cytoplasm as has been demonstrated for a range of organisms including several methylotrophic bacteria and Cupriavidus necator (previously Ralstonia eutropha) (Maia et al. 2015). In all panels protons contributing to PMF generation are coloured green.*

The canonical example of such a redox loop has been extensively described for *E.coli*, linking a FDH, (FDH-N) with a nitrate reductase enzyme, NarGHI. FDH-N and NarGHI couple to generate proton motive force in a simple redox loop (Jormakka et al. 2003b), achieved through opposite orientations of the two enzymes in the inner membrane, seen in Figure 1-1 (**A**), and linkage through the menaquinone pool. In this loop formate is first oxidised by FDH-N, producing CO_2 and a single proton in the periplasm, the electrons produced are shuttled through the redox centres of FDH-N to a cytoplasmic b type heme where two cytoplasmic protons are utilised in the reduction of menaquinone. This menaquinol is then free to traverse the membrane until it is oxidised in the

menaquinol oxidation site of Nar, releasing the two protons into the periplasm, finally the electrons from this oxidation shuttle though redox centers in Nar to be delivered to the cytoplasmic active site where nitrate is reduced to nitrite, incorporating another two cytoplasmic protons. In summary one such cycle of this loop removes four cytoplasmic protons and provides three periplasmic protons, a net contribution of seven per complete cycle (Jormakka et al. 2003b; Bagramyan & Trchounian 2003).

Other than nitrate, FDH enzymes have been shown to be able to couple to a wide range of other terminal electron acceptors including nitrite, trimethylamine N-oxide, dimethyl sulfoxide, sulphate, polysulphide, fumarate, carbon dioxide, arsenate, Fe^{3+}, oxygen, protons and $NAD(P)^{+}$ (Maia et al. 2015) (Wang & Gunsalus 2003).

Not all of these acceptors require intermediary redox pools and indeed not all are periplasmic and contribute to PMF in the manner described above. For example certain simple FDH enzymes are cytoplasmic and contribute to energy conservation simply by coupling formate oxidation to the regeneration of NAD(P)H, Figure 1-1 (**C**) (Tishkov & Popov 2004). Others are membrane associated but simply bypass the need for redox shuttles, instead forming protein complexes allowing direct electron transfer. The most commonly recognised complex concerning FDH are formate-hydrogen lyase (FHL) complexes, where FDH is found in association with a hydrogenase, allowing formate oxidation to be coupled to proton reduction (Bagramyan & Trchounian 2003), either as a terminal electron acceptor allowing removal of unwanted reducing equivalents in the form of diffusible hydrogen, as a way of storing reducing equivalents for later re-oxidation by hydrogenases capable of re-oxidising dihydrogen or even for detoxifying formate accumulation as described below. The thermodynamic driving force for this reaction is small, but thought to be favoured due to the volatility of the products (hydrogen and CO_2) (McDowall et al. 2014).

The most well characterised FHL complex is that of *E.coli*. A FDH (FDH-H, hydrogenase associated) is associated with a nickel-iron hydrogenase enzyme (Rossmann et al. 1991) conceptualised in Figure 1-1 (**B**). Such a FHL complex is thought to contribute to energy conservation in a distinct manner to the previously described periplasmic FDH enzymes, indeed FDH-H is

cytoplasmically facing and expressed during mixed fermentation when formate accumulates in the cytoplasm, the accumulation of such organic acids can dissipate proton motive force by acidifying the cytoplasm so by removing formate and protons, FHL is thought to prevent these toxic effects (Bagramyan & Trchounian 2003).

In actuality two FHL complexes exist in *E.coli*, both use the same FDH-H component but differ in the associated hydrogenase. FHL-1 uses Hyd-3 whereas FHL-2 uses Hyd-4 (Andrews et al. 1997). In both cases the hydrogenase is of the NiFe variety (Bagramyan & Trchounian 2003). Recently a functional FHL-1 complex has been purified from *E.coli* which retains FHL activity *in vitro* (McDowall et al. 2014) and an arrangement for the component subunits in the membrane has been suggested with numerous comparisons having been made to complex one (McDowall et al. 2014). Even more recently this FHL complex has been shown to be reversible, both *in vitro* and *in vivo*, capable of catalysing the oxidation of hydrogen and reduction of CO_2 although only under artificial conditions and such formate assimilation is not thought to play a role in native metabolism (Pinske & Sargent 2016). However it has been proposed that such a system may have allowed pyruvate synthesis before the evolution of the required glycolytic pathways (McDowall et al. 2014).

Although formate is usually considered an electron donor as described above, certain metabolic pathways use formate assimilation as a biomass precursor. They are not numerous however, with a pKa of 3.75, (Maia et al. 2015) formate tends to be deprotonated, making it a poor electrophile. It is also a poor nucleophile due to the difficulty in establishing a negative charge on the single carbon atom. To enable formate assimilation those pathways that do exist either first activate formate via phosphorylation (at the cost of ATP) or use radical reaction chemistry.

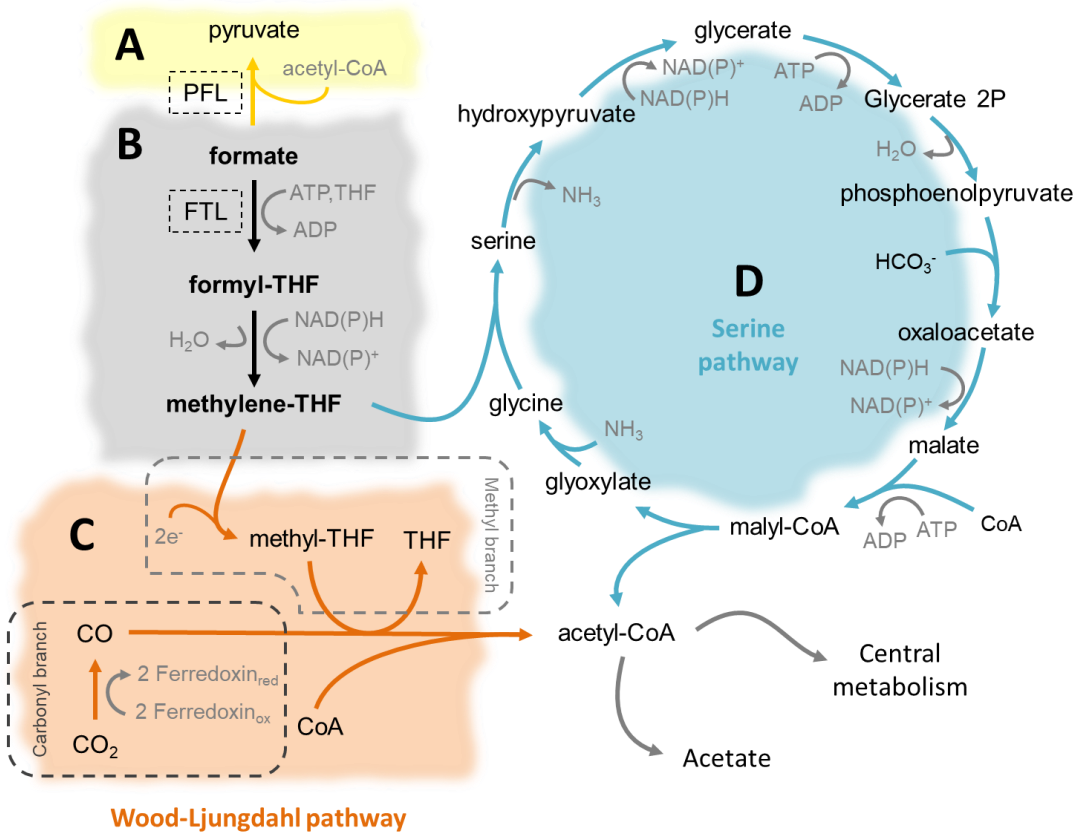

Figure 1-2 Formate assimilation pathways.
(A) Condensation of formate and acetyl-CoA by pyruvate formate lyase (PFL). (B) Activation of formate by formate-tetrahydrofolate ligase (FTL) and subsequent condensation to methylene-THF. (C) Overview of Wood-Ljungdahl pathway for acetogenic bacteria with branches contributing methyl and carbonyl groups for acetyl-CoA formation indicated. (D) Metabolically expensive (requiring multiple reducing equivalents) serine pathway.

There are two known mechanisms for formate assimilation used for microbial growth and both use an initial step catalysed by formate-tetrahydrofolate ligase (FTL) seen in Figure 1-2 (**B**). FTL catalyses two reactions, the initial phosphorylation of formate to formyl-phosphate, followed by reaction with tetrahydrofolate (THF) to form formyl-THF (Bar-even 2016). This electrophilic molecule is then further converted to methylene-THF. Methylene-THF can then enter two distinct pathways for formate assimilation, the bacterial Wood-Ljungdahl pathway, or serine pathway, described below.

The Wood Ljungdahl pathway, or reductive acetyl-CoA (Coenzyme A) pathway Figure 1-2 (**C**), is used by both acetogenic (Ragsdale & Pierce 2008) and methanogenic (Borrel et al. 2016) microorganisms for carbon fixation. In acetogenic bacteria is it used to make acetate for ATP synthesis, or the fixed carbon is used for biomass generation. In archaeal methanogens the pathway

can also be coupled to methanogensis, thermodynamically more favourable than acetogenesis (Ragsdale & Pierce 2008).

The pathway can be largely split into two branches, the carboxyl branch, which provides the carboxyl group for acetyl CoA formation (via reduction of CO_2 to CO) (Figure 1-2) and the methyl branch, which provides a methyl group. The methyl group in methanogenic archaea is derived from the direct reduction of CO_2 to formyl-methanofuran and so does not involve a formate intermediate (Borrel et al. 2016), for this reason the methanogenic Wood-Ljungdahl pathway is not discussed further here. The methyl branch of the acetogenic Wood-Ljungdahl pathway does involve formate, typically derived from the reduction of CO_2, (by FDH enzymes, discussed subsequently) (Ragsdale & Pierce 2008) followed by further reductions to formyl-THF, methylene-THF, and then methyl-THF seen in Figure 1-2 (**B** + **C**). The methyl and carboxyl groups are then combined with CoA to form acetyl-CoA by an acetyl CoA synthase complex outlined in Figure 1-2. The resultant acetyl-CoA can then be used to generate ATP via acetogenesis or directed into central metabolism, in acetogenic bacteria this is predominantly via pyruvate synthase (Bar-even 2016).

The second pathway for formate assimilation is via the serine pathway, exploiting the same initial reactions as the Wood-Ljungdahl pathway, with the sequential reduction of formate to methylene-THF, which then joins glycine to make serine. Serine then cycles through phosphoenolpyruvate, oxaloacetate and malate, as seen in Figure 1-2 (**D**), which is combined with CoA to make malyl-CoA before cleavage to glyoxylate (returns to glycine) and acetyl CoA. The produced acetyl CoA can then be used for biomass production by entering central metabolism. Both the glyoxylate shunt (via acetyl-CoA to succinate) or ethylmalonyl-coA pathways have been shown to support such growth (Bar-even 2016).

The serine and Wood-Ljungdahl pathways are the only known methods of formate assimilation capable of supporting microbial growth. Other pathways, including the reductive glycine pathway are capable of assimilating formate, but this cannot be coupled to growth (Bar-even 2016). Another method of formate assimilation which has been shown to be theoretically possible, but until recently not demonstrated experimentally, is the direct reduction of formate and acetyl-coA to pyruvate by a pyruvate-formate lyase (PFL) enzyme (Figure 1-2

A). This enzyme is normally considered to generate ATP from the conversion of pyruvate to formate and acetyl CoA during anaerobic fermentation but has been shown to be reversible *in vivo* in *E.coli* using a strain unable to assimilate acetate via the glyoxylate shunt therefore relying on PFL formate fixation (Zelcbuch et al. 2016).

Although not an example of formate assimilation, it is also worth noting that formate is capable of serving as the sole carbon source for some organisms by being oxidised to CO_2, generating reducing equivalents that can be used to fix CO_2 by other pathways, for example the well-known Benson-Bassham-Calvin cycle (Biel & Fomina 2015), 3-hydroxypropionate cycle or the reductive tricarboxylic acid cycle (reverse Krebs cycle) (Huugler et al. 2005).

Finally formate is also an important metabolite in bacterial syntrophic interactions, secreted in conjunction with dihydrogen as a way of facilitating internal redox balancing during a number of fermantaion pathways. These metabolites are then scavenged by syntrophic partners (Maia et al. 2015) (Kane et al. 2016).

1.2 Formate dehydrogenases (FDH)

1.2.1 Metal independent FDH.

The simplest category of formate dehydrogenase (FDH) enzymes are characterised by their oxidation of formate coupled to NAD^+ reduction, (Figure 1-1 (**C**)) and so are commonly referred to as NAD^+ dependent FDH (EC 1.2.1.2). Such enzymes are simple single subunit or homodimers lacking complicated metal cofactors and are found abundantly in a variety of organisms including aerobic bacteria, yeasts, fungi and plants (Maia et al. 2015). Due to the simplicity of formate oxidation such enzymes are often used as model enzymes for studying hydride ion transfer in dehydrogenases and so have been characterised thoroughly. Considering the lack of redox cofactors, catalysis in these enzymes is thought to proceed by the enzyme positioning formate and NAD^+ in close proximity and allowing the direct hydride transfer between the two (Maia et al. 2015).

In plants such metal independent/NAD^+ dependent FDHs are mitochondrial proteins and have been shown to be found in a variety of different species ranging from English oak (*Quercus robur*) to potato (*Solanum tuberosum*) (Alekseeva et al. 2011). The distinctive feature of plant FDHs is an N-terminal signal peptide responsible for transport from the cytoplasm into the mitochondria (Alekseeva et al. 2011). NAD^+ dependent FDHs are also found in methylotrophic microbial species with extended N-terminal proline rich rigid loop which give rise to a significantly higher thermostability than FDHs from other sources (Tishkov & Popov 2004).

Industrial applications for these types of NAD^+ dependent FDHs are becoming more commonplace, principally in enzymatic syntheses (Ernst et al. 2005). Due to increasingly stringent demands for ultra-pure optically active chiral compounds for pharmaceutical usage, enzymatic systems are being increasingly turned to due to their extremely high stereospecificity, in particular dehydrogenases (Tishkov & Popov 2004). However, many of these enzymes use (costly) NADH as a cofactor making these reactions economically unviable without a way to regenerate the cofactor, a role in which FDH excels (Figure 1-3) and is already fulfilling in the industrial production of L-leucine for Degussa (Leuchtenberger et al. 2005).

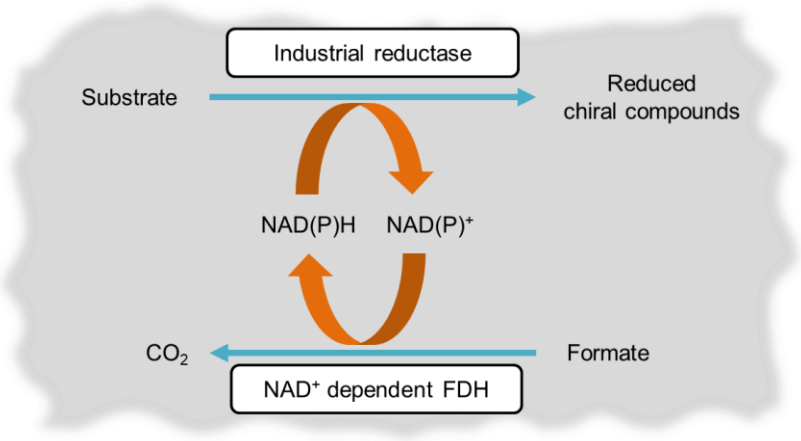

Figure 1-3 FDH regenerating NAD(P)+ in the industrial synthesis of chiral compounds.

From a protein engineering perspective, the plant FDH from Soybean (*Glycine max*) (SoyFDH), has garnered particular interest due to its remarkably low Michaelis constant for both formate (K_m = 0.6 mM) and NAD^+ (K_m = 5.7 µM) (Alekseeva et al. 2011). All previously studied NAD^+ dependent FDHs demonstrated similar Michaelis constants for formate, (ranging from 3-10 mM) and NAD^+ (ranging from 35-90 µM) in part due to their high degree of homology, with all sharing at least 55% sequence identity (Tishkov & Popov 2004). SoyFDH has been a focus of research due to its potential as a enzymatic catalyst for NADH regeneration in the synthesis of optically active compounds (Alekseeva et al. 2011) described above.

In a similar manner the higher thermostability of bacterial FDHs make them attractive for an industrial NADH regenerative role. In particular a FDH of *Pseudomonas sp*. 101 is the most thermostable NAD^+ dependent FDH investigated (Tishkov et al. 1993) and is often quoted as a standard by which other such FDH enzymes are compared. Extensive mechanistic studies and multiple crystal structures have been solved for this enzyme (Tishkov & Popov 2004). Attempts have been made to change the specificity of such enzymes from NAD^+ to $NADP^+$ to widen their industrial applications, allowing the regeneration of NADPH in chemical syntheses, important considering the significantly higher cost of NADPH over NADH (Katzberg et al. 2010).

CO_2 reductase activity exhibited by NAD^+ dependent FDHs is not normally considered, principally due to its irrelevance to the normal physiological role of

the enzyme and its unfavourable thermodynamics, (the reduction potential of NAD^+ is more positive than that of CO_2, (-0.32 V and -0.42 V respectively) (Reda et al. 2008; Olson et al. 2000), despite this several examples of CO_2 reductase activity by NAD^+ dependent FDH enzymes have been reported. The FDH from *Candida boidinii* CbFDH is a very well characterised example of a reversible NAD^+ dependent FDH (Slusarczyk et al. 2000) with published values for CO_2 reduction substrate-binding affinity and turnover number of 31.28 mM and 0.015/s respectively (Choe et al. 2014). However these rates are still very low and have prompted research into more efficient enzymes. A recent study found FDH from *Thiobacillus sp. KNK65MA* (TsFDH) had a 21 fold higher CO_2 reduction turnover number and favoured the reduction over oxidation more than 85 times more than the previous CbFDH (Choe et al. 2014). This higher CO_2 reductase activity of TsFDH over CbFDH was attributed to the extended C-terminal end of the protein which interacts with the substrate binding channel (Choe et al. 2014). CO_2 reductase activity has also been seen in NADPH specific FDHs, where NADPH produced by photosystem one is coupled to the reduction of CO_2 *in vivo* creating a light driven CO_2 fixation mechanism (Ihara et al. 2013).

Although such NAD^+ dependent FDH reduction catalysis is interesting, and free of the complications of oxygen sensitive cofactors, maximal specific activities of 12.2, 9.5, 8.7, and 4.0 mU/mg enzyme at pH 5.5, 6.0, 6.5, and 7.0, were seen for TsFDH, the fastest of these enzymes, (Choe et al. 2014), importantly still far lower than those reported for metal dependent FDHs.

1.2.2 Metal dependent FDH.

In contrast to the previously discussed FDHs, another group of FDHs exist, expressed exclusively by prokaryotes (Maia et al. 2015) referred to as metal dependent FDHs. These FDHs are characterised by formate oxidation at a metal containing active site. This active site couples, not to NAD^+, but to ferredoxins and/or cytochromes (EC 1.2.2.1) in the catalytic subunit, (Jormakka, S Törnroth, et al. 2002). Significantly however such enzymes may then subsequently pass these electrons to other associated proteins/subunits which reduce protons, quinones or $NAD(P)^+$ (Reda et al. 2008). As such examples of metal dependent/NAD^+ dependent FDH activity can be observed, but these use NAD^+ only as a subsequent electron acceptor.

The metal containing active sites of such FDH enzymes can either coordinate a mononuclear Mo atom, collectively referred to as Mo-FDH, or a mononuclear W atom, referred to as W-FDH (Jormakka et al. 2003a). In either case in such FDH enzymes the metal is coordinated by four sulphur atoms from the cis-dithiolene groups of two pyranopterin guanine dinucleotide (PGD) cofactors in addition to two other groups, either a selenium or sulphur atom (from a selenocysteine or cysteine residue) and an additional terminal sulpho group (Maia et al. 2015). Such coordination places the Mo-FDH in the dimethyl sulfoxide (DMSO) reductase family (family III) of molybdoenzymes, characterised by containing a Mo-bisPGD cofactor (Magalon et al. 2011). Although demonstrating the same coordination W-FDH are often categorised separately as tungstoenzymes but collectively with the DMSO reductase family have been referred to as molybdenum/tungsten-bis pyranopterin guanosine dinucleotide enzymes (Mo/W-bis PGD) (Maia et al. 2015).

In contrast to the metal independent/NAD^+ dependent FDH enzymes the active site of metal dependent FDH enzymes is thought to directly mediate transfer of electrons for catalysis, with the redox active site metal cycling between a 6+ and 4+ oxidation state during catalysis (Silva et al. 2011). Other generally conserved features of the active site include a catalytically essential arginine and histidine residue in addition to the selenocysteine/cysteine residue contributing to the metal coordination sphere, although each of these features is discussed further in the context of individual proteins to avoid ambiguity.

Other than the identity of the active site, Mo/W-bis PGD enzymes are a heterogeneous group of proteins consisting of a variable number of subunits with a diverse range of redox centers (typically variable numbers of ferredoxins, but also including flavins and both b and c type hemes). These less conserved subunits often coordinate electron transfer elements that allow them to fulfil a range of functions, from membrane associated interaction with quinones to the regeneration of NADH in the cytoplasm (Jormakka, S Törnroth, et al. 2002) (Figure 1-1). To use the sub-classification method used to describe DMSO reductase family molydoenzymes, these can be generalised as those belonging to the three subunit membrane bound complex iron-sulphur molybdoenzyme (CISM) group (here the complex iron-sulphur Mo/W-bis PGD (CISMW) group), or the simpler soluble single subunit variety (Magalon et al. 2011) although not all studied Mo/W-bis PGD enzymes fall into these categories.

Over the past twenty years multiple reaction mechanisms have been proposed for Mo/W-bis PGD FDH enzymes. Many of these were based on the resolved crystal structure of the FDH-H enzyme from *E.coli* in which a terminal hydroxyl group, coordinated to the catalytic Mo atom, was proposed to play an important part in catalysis (Jormakka et al. 2002). Subsequent re-evaluation of the crystallographic data suggests this ligand to be a terminal sulpho group, as described above, not just in this enzyme, but in all known W-FDH and Mo-FDH enzymes (Maia et al. 2017). Other mechanistic suggestions involved the active role of the widely, but not absolutely, conserved SeCys residue in the two electron, one proton abstraction from formate to generate CO_2 (Maia et al. 2015). However in light of combined experimental data from a variety of sources an elegant alternative catalytic mechanism is currently thought to apply to all known Mo/W-bis PGD FDH enzymes, regardless of the presence of a selenocysteine residue (Yu et al. 2017). This mechanism suggests a reversible direct hydride transfer reaction involving the terminal sulpho group as seen in Figure 1-4 and described below (Niks et al. 2016). In the following description only the Mo center will be discussed for clarity, but the described mechanism also applies for W-FDH.

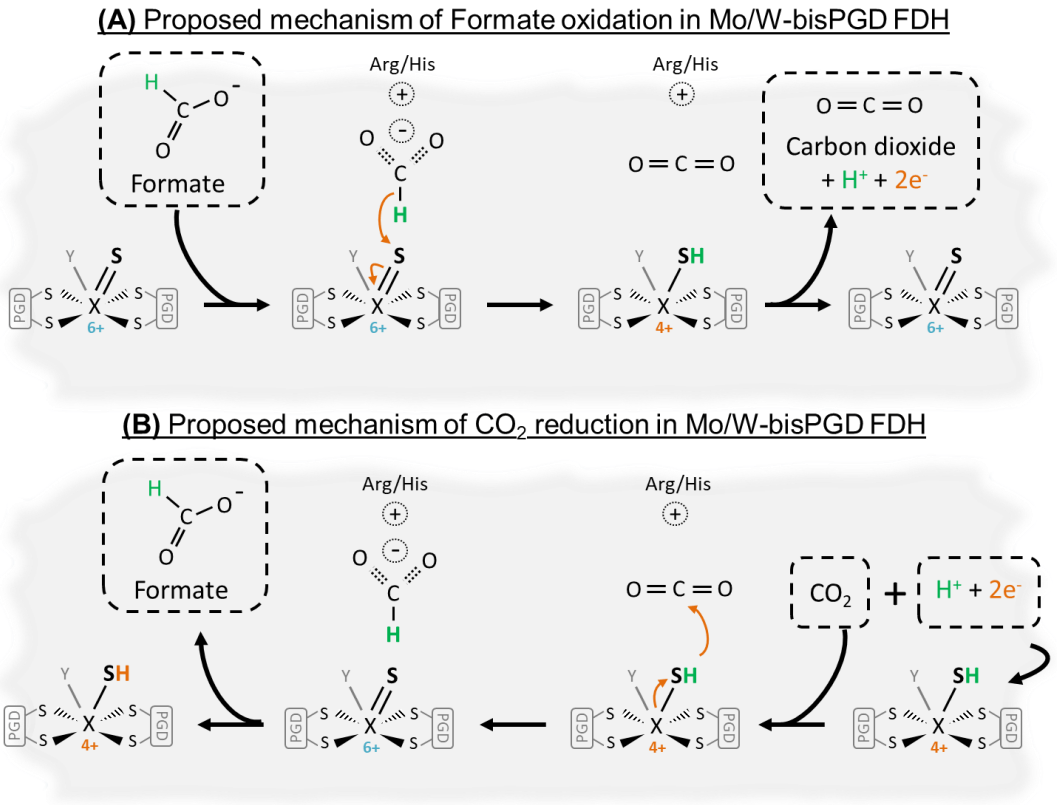

Figure 1-4 Proposed mechanism for reversible catalysis by Mo/W-bisPGD FDH enzymes.
*Where X represents either the redox active W or Mo atom and Y either a selenium or sulphur atom (from selenocysteine or cysteine respectively) which complete the hexacoordinate binding sphere of the catalytic metal with four sulphur ligands from two PGD cofactors and a terminal sulpho group. This sulpho group can either be deprotonated to act as a hydride acceptor for formate oxidation (**A**) or protonated to act as a hydride donor for CO_2 reduction (**B**) (Maia et al. 2016)(Yu et al. 2017). Hydrogen relating to hydride transfer coloured green in both reactions.*

In the proposed mechanism the oxidation state of the metal plays an essential part in catalysis by determining the protonation state of the sulpho group, the pKa values for the oxidised and reduced metals being dramatically different. When the metal is reduced, the protonated group is expected (Mo^{4+}-SH) which is capable of acting as a hydride donor for CO_2 reduction. In contrast when the metal is oxidised the deprotonated group is expected (Mo^{6+}=S) which is an effective hyride acceptor for formate oxidation (Maia et al. 2016). The oxidation state of the active site metal (and therefore direction of catalysis) is influenced by the remaining redox centers of the protein which can either supply electrons to reduce the active site (Mo^{4+}-SH) for CO_2 reduction or accept them to maintain the oxidised (Mo^{6+}=S) for formate oxidation (Maia et al. 2016).

To expand, formate oxidation is initiated by formate binding to the oxidised active site, the conserved arginine and histidine residues thought to correctly orient the C-H group of formate for effective hydride transfer to the Mo^{6+}=S

group, resulting in the reduced Mo^{4+}-SH moiety, catalysis is then completed by the diffusion of CO_2 out of the active site and transfer of two electrons from the metal centre via other redox centers to re-generate the oxidised Mo^{6+}, which as a result of the pKa, becomes deprotonated for the next catalytic cycle (Maia et al. 2016).

In contrast CO_2 reduction is initiated by CO_2 binding to the reduced active site, the conserved arginine and histidine residues thought to correctly orient the carbon atom of CO_2 for effective hydride transfer from the Mo^{4+}-SH group, resulting in the oxidised Mo^{6+}=S, catalysis is then completed by the diffusion of formate out of the active site and reduction of the metal centre by other redox centers to re-generate Mo^{4+}, which as a result of the pKa, becomes protonated for the next catalytic cycle (Maia et al. 2016).

This proposed mechanism does not consider the Se atom (from selenocysteine) or the S atom (of the alternative cysteine residue) to directly contribute to catalysis, instead having them simply complete a hexa-coordination sphere for the active site metal (Yu et al. 2017). It is possible this coordination is important in regulating the reduction potential of the metal or it has also been proposed this steric hindrance would prevent these enzymes from promiscuously catalysing oxygen transfer reactions seen by other members of the DMSO reductase family (Maia et al. 2017). Despite this, it has not been demonstrated that such a sixth ligand is necessary for catalysis, and may not even be present in the presence of substrate as suggested by one FDH-H crystal structure (Raaijmakers & Romao 2006), although considering the energetic burden required for selenocysteine incorporation it seems likely to have some function.

1.2.2.1 Previously characterised FDH

The most well characterised example of such metal dependent FDHs is FDH-N from *E.coli*. With several high resolution crystal structures and numerous expression studies it is by far the most well characterised FDH of this type and discussion of common/unique structural elements in other such enzymes is best done by first describing in turn FDH-N and the other FDHs of *E.coli* to provide meaningful comparisons.

FDH-N consists of three subunits, the periplasmic catalytic α subunit containing a Mo containing active site and a single 4Fe4S cluster, the transmembrane ß

subunit which contains four more 4Fe4S clusters and the membrane bound γ cytochrome b subunit (Jormakka et al. 2002) (Figure 1-5). The redox centres of these three subunits allow electrons from the oxidation of formate in the periplasm to be passed through the membrane to reduce menaquinone in the cytoplasm as seen in Figure 1-5 (B) (Sawers 1994). All distances between redox centers in this schematic are within 14 Å allowing effective electron transfer (Jormakka et al. 2003b). Although not shown in Figure 1-5, FDH-N crystallises in a trimer, thought to be physiologically relevant, giving it an overall mushroom shaped topology in the membrane (Jormakka et al. 2002).

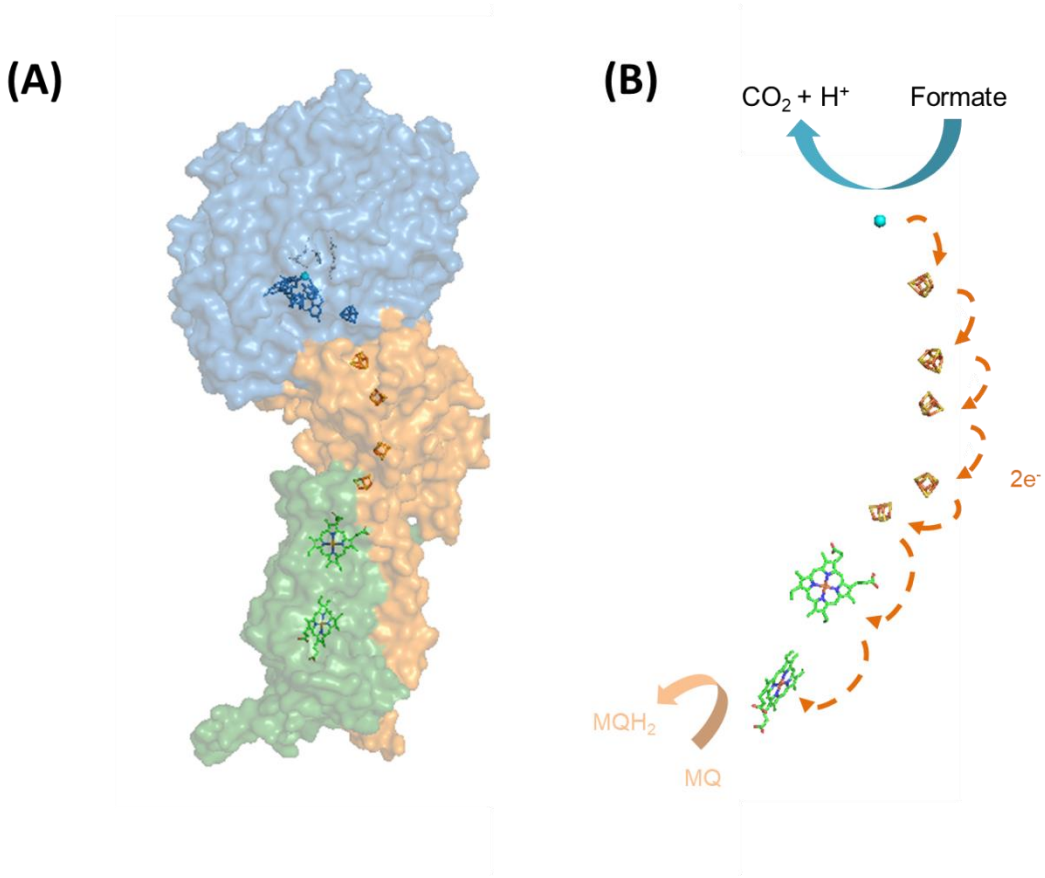

Figure 1-5 Structure of respiratory FDH-N from E.coli.
(A) Surface representation of the heterotrimer with the catalytic α subunit and associated Mo-bisPDG and 4Fe4S cofactors shown in blue, β subunit and four associated 4Fe4S clusters shown in orange and γ subunit with associated b type hemes shown in green (in which the redox active iron is shown in red, coordinated by four nitrogen atoms (dark blue). Also shown are relevant $Secys_{\alpha 196}$, $His_{\alpha 197}$ and $Arg_{\alpha 446}$ residues coloured blue. (B) Transfer of electrons during formate oxidation within FDH-N via redox active Mo atom (light blue) via ferredoxins and cytochromes to menaquinone (MQ) binding site. Figure made using pymol and PBD file 1KQF.

The α subunit of FDH-N is very similar to those solved for other similar FDHs including FDH-H from *E.coli* and DgW-FDH from *Desulfovibrio gigas* (Raaijmakers et al. 2002) as well as catalytic subunits from related enzymes

including DMSO reductase and periplasmic nitrate reductase (Jormakka, S Törnroth, et al. 2002).

The redox active Mo metal is coordinated by four sulphur atoms from the two pterin cofactors in addition to the selenium atom of a selenocysteine residue ($SeCys_{\alpha196}$) and a final sixth sulpho ligand. The active site is completed by the inclusion of $His_{\alpha197,}$ the nitrogen of which had been proposed to abstract the proton from formate during previous mechanistic models of oxidative catalysis, and $Arg_{\alpha446}$ (found at the bottom of the substrate binding pocket) which is thought to correctly orient formate within the active site (Maia et al. 2015). The active site itself is found buried in a substrate channel containing multiple positively charged residues thought to be important for substrate interaction (Jormakka et al. 2003b). As well as containing the active site this subunit also contains a [4Fe-4S] cluster, referred to as FeS-0, to which electrons from the active site are passed (Jormakka et al. 2003a).

The ß subunit of FDH-N is principally responsible for electron transfer through the inner bacterial membrane, a process it achieves using a further 4 [4Fe-4S] clusters designated FeS1-4, using such notation, electrons pass from the α subunit to FeS-1 then FeS-4, FeS-2 and finally FeS-3, in likeness to an electrical wire. Such clusters can be identified genetically from the repeated [4Fe-4S] cluster binding motif, (CxxCxxCxnCP, or slight variations, where n represents 36-38 residues) (Jormakka et al. 2003b). These type of electron transfer domains are common among membrane bound oxidoreductases and can also be found in [NiFe] hydrogenase, succinate dehydrogenase, nitrate reductase and countless others (Yoch & Carithers 1979). The C terminal end of this subunit includes a transmembrane helix which anchors it to the membrane allowing it to associate with the membrane bound γ subunit.

The γ subunit, a membrane bound cytochrome b, consists of 4 transmembrane helices which coordinate two b type heme groups, the first, heme b (periplasmic) is located on the periplasmic side of the membrane and receives electrons from the final FeS cluster in the ß subunit, which it then passes onto the second heme, heme b (cytoplasmic), which can reduce menaquinone directly, with the menaquinone oriented in close proximity after binding to a histidine residue ($His_{\gamma169}$) (Jormakka et al. 2003b). Like the above ferredoxin moieties such

hemes are common electron transfer elements with comparable subunits found in NiFe-hydrogenase, thiosulfate reductase and fumarate reductase enzymes (Jormakka et al. 2003a).

As well as FDH-N, the genome of *E.coli* also encodes two other FDH isoenzymes. The first, FDH-O (formerly FDH-Z), shares the same three subunit composition as FDH-N, as well as a high degree of sequence homology including the presence of the selenocysteine residue, with FDH-N antibodies also binding strongly to FDH-O (Abaibou et al. 1995). FDH-O is in contrast to FDH-N however as it is expressed aerobically, or more specifically, independently of FNR/ArcA or O_2 or nitrate levels (Abaibou et al. 1995). It is proposed to link the aerobically expressed nitrate reductase, Nar-Z, in a respiratory loop akin to that explained for FDH-N allowing *E.coli* to generate PMF from formate and nitrate whilst the predominant enzymes for these conditions, FDH-N and Nar-A, are synthesised (Wang & Gunsalus 2003). Finally there is some evidence that FDH-O can couple to O_2 as a terminal electron acceptor (Abaibou et al. 1995) due to this it is sometimes called formate oxidase (Sawers 1994). This proposed role has been reinforced by the finding that FDH-O may form part of a supercomplex assembly containing FDH with *bo₃* and *bd* oxygen reductases (Sousa et al. 2011).

The final FDH of *E.coli* (FDH-H) forms a FHL catalysing the cytoplasmic oxidation of formate to CO_2 and molecular hydrogen as described previously (Bagramyan & Trchounian 2003). FDH-H is predominantly thought to be a single subunit enzyme (Boyington & Gladyshev 1997), although it has been suggested that *hycB*, found in the *hyc* operon of *E.coli* may have pleiotropic effects and act as a small additional FDH-H subunit (Bagramyan & Trchounian 2003). Importantly the large main catalytic subunit of FDH-H is very similar to the α subunit of FDH-N, containing an intrinsic selenocystiene ($SeCys_{140}$) coordinating the redox active molybdenum atom in combination with four sulphur atoms from the two PGD cofactors and another sulphur completing the coordination sphere as seen from multiple resolved crystal structures (Boyington & Gladyshev 1997). As seen for FDH-N, the conserved Arg_{333} and His_{141} residues complete the active site and an 4Fe-4S cluster is located in the same subunit thought to facilitate electron transfer from the active site (Boyington & Gladyshev 1997).

This catalytic subunit of FDH-H is encoded by *fdh*F, a monocistronic gene that is supressed by both O_2 and nitrate and upregulated by formate (Bagramyan & Trchounian 2003). This is in line with the reported role of FHL, expressed during fermentation in *E.coli* to detoxify formate and neutralise the pH in the cytoplasm (Bagramyan & Trchounian 2003).

Other than FDH-N and FDH-H of *E.coli*, the W-FDH of *Desulfovibrio gigas* is the only other metal dependent FDH for which a crystal structure has been resolved (Moura et al. 2004). Composed of two subunits, the large α subunit resembles the catalytic subunit of FDH-N and FDH-H containing a single 4Fe4S cluster and a bis-PGD containing active site with catalytically important His_{159}, and Arg_{407} and $SeCys_{158}$ residues, the last being thought to coordinate the W along with the two PGD cofactors with the final ligand being the mechanistically vital terminal sulpho group (Raaijmakers et al. 2002). This FDH differs from FDH-H and FDH-N with the presence of a disulphide bridge close to the active site on the protein surface, which when reduced widens the formate cleft allowing catalysis. It has been proposed that the oxidation of such a disulphide bridge would allow careful regulation under aerobic conditions, preventing substrate entry, possibly explaining why this FDH is found to not be irreversibly inactivated by oxygen (Raaijmakers et al. 2002).

Physiologically this enzyme is thought to couple periplasmic formate oxidation to the reduction of periplasmic c type cytochromes (Raaijmakers et al. 2002) for PMF generation as is thought to be the case for a number of *Desulfovibrio* species. For such sulphate reducing bacteria formate is an important electron donor and the FDH of this genus have been extensively studied and are remarkably diverse (Silva et al. 2011). In contrast to the dimeric W-FDH of *D.gigas, D.desulfuricans* oxidises formate with a trimeric selenocysteine containing Mo-FDH (Maia et al. 2015) and *D.alaskensis* and *D.vulgaris* both contain three FDH isoforms. Of these six, four have been studied, a W-FDH from *D.alaskensis,* a Mo-FDH from *D.vulgaris,* and more intriguingly an isoform from each strain that retains FDH activity when grown with W or Mo (Mota et al. 2011)(Silva et al. 2011). This ability to incorporate either metal for formate oxidation is thought to be a result of the environment of such sulphate reducers, which are likely to experience high sulphide concentrations, conditions that

reduce the bioavailability of Mo (Silva et al. 2011), and so the redundancy may represent a selective advantage.

Despite this, sulphate reducing bacteria are not the only prokaryotes that have been demonstrated to contain FDH isoforms capable of catalysis with either W or Mo, for example the selenocysteine containing FDH of the methanogenic archaea *Methanococcus vannielii* (Maia et al. 2015) which physiologically couples to F420, a flavin derived cofactor commonly used in methanogens (Doddema & Vogels 1978). The Mo-FDH of another methanogen, *Methanobacterium formicium* couples to F420 in a similar way (Schauer & Ferry 1980) and is notable as it lacks a selenocysteine residue, containing cysteine instead (Maia et al. 2015).

Other examples include the methylotroph *Methylobacterium sp.* RXM which is thought to contain only a single metal dependent/NAD^+ dependent enzyme that can incorporate either metal (Maia et al. 2015). The methylotroph *Mycobacterium vaccae* is also thought to be able to substitute both metals, although here a Mo-FDH is favoured (Laukel et al. 2003). Formate oxidation is critical for a wide range of methylotrophic bacteria (Chistoserdova et al. 2004) and as such multiple metal-dependent FDH enzymes other than those mentioned above have been studied including an NAD^+ dependent W-FDH of *Methylobacterium extorquens* AM1 (Laukel et al. 2003).

In addition to the above, a range of other metal dependent FDH enzymes thought to physiologically oxidise formate have been studied, including, but not limited to, the NAD^+ dependent Mo-FDHs of *Cupriavidus necator* (previously *Ralstonia eutropha*) (Niks et al. 2016), *Methylosinus trichosporium*, *Cupriavidas oxalaticus*, and *Rhodobacter capsulatus*, (which all contain cysteine rather than selenocysteine) (Maia et al. 2015), as well as the preferentially W-FDH enzymes of *Campylobacter jejuni* (Smart et al. 2009) and the gram positive *Eubacterium acidaminophilum* (Graentzdoerffer et al. 2003).

Whilst several of the above enzymes that physiologically catalyse the oxidation of formate have been shown to be reversible under non-physiological conditions, including FHD-H of *E.coli* (Pinske & Sargent 2016), the NAD^+ dependent FDHs of *Pseudomonas oxalaticus* (Ruschig et al. 1976) and the FDH of *Cupriavidus necator* (FdsABG) (Yu et al. 2017) to name three, many more enzymes have been

studied for their physiologically relevant CO_2 reductase catalysis and are explored below.

The most obvious examples are those metal dependent FDH enzymes from acetogens involved in the first reduction of CO_2 to formate in the acetogenic Wood-Ljungdahl pathway. The first such described enzyme was the selenocysteine containing, $NADP^+$ dependent, W-FDH from *Moorella thermoacetica*, (previously *Clostridium thermoaceticum)*, a model acetogen (Ragsdale & Pierce 2008). Subsequent examples include the $NAD(P)^+$ dependent W-FDH enzymes of *Clostridium formicoaceticum* and *Clostridium carboxidivorans* (Maia et al. 2015), and the Mo-FDH of *Clostridium pasteurianum* (Liu & Mortenson 1984).

Another Mo-FDH thought to physiologically catalyse CO_2 reduction is that of another acetogen, *Acetobacterium woodii*, in complex with a hydrogenase enzyme that catalyses hydrogen oxidation, in effect creating a reverse formate hydrogen lyase system, referred to as a hydrogen-dependent carbon dioxide reductase (HDCR) (Schuchmann & Müller 2013).

One of the most well characterised examples of physiologically releveant CO_2 reductase activity is by the FDHs of *Syntrophobacter fumaroxidans*, which expresses two W-FDHs (de Bok et al. 2003). Both of these enzymes, FDH-1 and FDH-2, show extremely high levels of CO_2 reductase activity, with specific activities, determined using dithionite-reduced methyl viologen as the electron donor, of 900 U/mg and 89 U/mg for FDH-1 and FDH-2 respectively (de Bok et al. 2003) Importantly the two are thought to be functionally distinct.

The first W-FDH, FDH-1 is similar to those described for other acetogenic bacteria, fixing CO_2 for the Wood- Ljungdahl pathway (de Bok et al. 2003) whilst FDH-2 is implicated in syntrophic interactions. the CO_2 reductase activity of FDH-2 thought to be responsible for removing unwanted reducing equivalents, in the form of formate, which can then be excreted and oxidised by syntrophic partners, hydrogen has been described to play a similar role for syntrophic exchange of reducing equivalents but formate is increasingly recognised as a common alternative (Stams & Plugge 2009).

Both FDH-1, consisting of three subunits, and FDH-2, a heterodimer, have been purified and have been found to be selenocysteine containing W-FDH enzymes. Interestingly both required reducing conditions, using dithionite, at all stages for successful purification (de Bok et al. 2003), a precaution noted for purification of a number of other W-FDHs from *M. thermoacetica* and *E. acidaminophilum* (de Bok et al. 2003) but not in the case of *D. gigas* (Almendra et al. 1999).

In addition, partially reducing conditions were required to assay *in vitro* activity both for CO_2 reduction using methyl viologen and formate oxidation using methyl or benzyl viologen (de Bok et al. 2003). When conducting such assays 'reactivation' times of up to 10 minutes with redox dyes were required before assaying to see maximal rates (de Bok et al. 2003). This may be attributed to 'reductive activation' a relatively well characterised phenomena in equivalent molybdoenzymes where the reduction of the active site Mo-PGD cofactor is required for a catalytically active form of an enzyme (Jacques et al. 2014). A phenomena proposed for other DMSO reductase family members (Fourmond et al. 2008).

The fact that both FDHs of *Syntrophobacter fumaroxidans* contain W and exhibit CO_2 reductase activity is probably not coincidental, all of the above examples catalysing physiologically relevant CO_2 reduction are W-bis PGD enzymes rather than Mo-bis PGD, with the exception of those from *C.pasteurianum and A.woodi*. From a thermodynamic perspective W-FDH enzymes, rather than Mo-FDH enzymes, are better suited for reductive catalysis as although the two metals have very similar chemical and catalytic properties (Silva et al. 2011), the reduction potential of W^{4+} is lower than that of Mo^{4+} (Armstrong & Hirst 2011). Despite this it seems that Mo-FDH enzymes are also capable of reversible catalysis, as seen in the examples above and even more are thought to be reversible under non-physiological conditions (Bassegoda et al. 2014).

1.2.2.2 Electrochemical studies of enzymatic CO_2 reduction

Prokaryotic metal dependent FDH enzymes from multiple sources have been investigated in protein film voltammetry (PFV) studies. The fact that these enzymes physiologically couple to independent redox partners, commonly quinones, distinct hydrogenase enzymes or nicotinamide adenine dinucleotides

makes them well suited to electrochemical study (Reda et al. 2008). When adhered to an electrode such proteins are able to donate electrons generated from the oxidation of formate directly to an electrode or accept them for the reduction of CO_2 (Figure 1-6) (Reda et al. 2008).

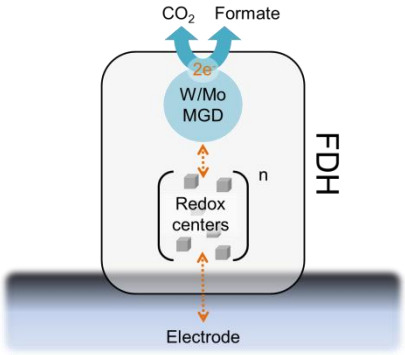

Figure 1-6 Schematic overview of electrochemical study of isolated FDH enzymes.
Reversible electron transfer shown in orange from electrode to adhered enzyme via a variable number of redox centers to the buried pterin active site with either coordinated Mo or W atom. Structure and number of additional redox sites varies dependent on studied enzyme, typically consisting of one of more ferredoxins and/or hemes. Depending on potential electrode can either provide the two electrons required for the reduction of CO_2 to formate or accept those produced by formate oxidation (Reda et al. 2008).

Of those FDH enzymes that have been electrochemically studied FDH1 from *Syntrophobacter fumaroxidans* represents the first to establish an important paradigm. This heterotrimeric enzyme contains a buried selenocysteine coordinated tungstopterin cofactor where catalysis takes place. When coupled to an electrode this active site is thought to be linked by an extensive chain of over nine iron-sulphur clusters (Reda et al. 2008). Importantly CO_2 reduction could be observed on an electrode by FDH1 with high faradaic efficiency and at low over-potentials (just below the reduction potential) with currents of -80 μA cm^{-2} at -0.8 V vs SHE at pH 5.9 (Reda et al. 2008). A reduction potential of -0.389 V was determined at pH 7.0 for this system, with the value changing with pH. Formate oxidation could also be electrochemically measured at potentials above the reduction potential with a maximum current of 500 μA cm^{-2} at +0.2 V vs SHE at pH 8.

Although study of FDH1 established FDH enzymes as viable electrocatalysts for CO_2 reduction other examples have followed. Whereas FDH1 contained multiple iron-sulphur clusters FDH-H from *E.coli* contains only a single [4Fe-4S] cluster making it a simpler system to work with and theoretically less problematic to overexpress. Similarly to FDH1, PFV experiments on FDH-H revealed

reversible FDH catalysis with CO_2 reduction observed at low overpotentials with maximal CO_2 reduction rates of -80 μA cm^{-2} and formate oxidation rates of 180 μA cm^{-2}. Under comparable conditions the the previously studied FDH1, demonstrated rates of 5 μA cm^{-2} for CO_2 reduction and 160 μA cm^{-2} for formate oxidation (Bassegoda et al. 2014). That FDH-H can catalyse these reactions when coupled to an electrode faster than FDH1, especially the reverse reduction of CO_2, under certain conditions is interesting considering the typical assertion that W containing FDH enzymes are better suited to driving CO_2 reduction due to their comparatively lower reduction potentials (Crable et al. 2011). The limitations of FDH1 may lie with the higher number of FeS clusters causing a bottleneck in electron transfer from an electrode.

The emphasis of this thesis is the reduction of CO_2 to formate but it should also be noted that carbon monoxide dehydrogenase (CODH) enzymes have also been electrochemically studied for the reduction of CO_2 to CO. The Ni containing CODH I of *Carboxydothermus hydrogenoformans* has been shown to be an effective reversible electrocatalyst when adhered to an electrode capable of facile CO_2 reduction at low overpotentials (Parkin et al. 2007). Other examples include the Ni containing CODH from *Moorella thermoacetica* which instead of being performed as a classical PFV experiment used methyl viologen as a mediator to allow CO_2 reduction to CO at potentials below -0.57 vs SHE (Shin et al. 2003). The use of methyl viologen as an electrochemical mediator for enzymatic CO_2 reduction is not new and indeed has been used to show that the FDH of *Pseudomonas oxalaticus* could generate formate from CO_2 as early as the 1980s (Parkinson & Weaver 1984). Unfortunately its use as a mediator especially at high concentrations has been described as undesirable due to its relative cost and significant toxicity (Suntres 2002).

1.3 *Shewanella oneidensis*

The *Shewanella* genus encompasses a range of gram negative, facultative anaerobes in the γ-Proteobacteria class found in a wide range of aquatic environments including both marine and freshwater sediments or living as symbionts or epibionts within higher aquatic organisms (Hau & Gralnick 2007). Named in honour of Dr. James Shewan, the *Shewanella* genus contains approximately 40 species capable of using a wide range of terminal electron acceptors during respiration. These include the reduction of trimethylamine-N-oxide (TMAO) to trimethylamine, sulphur/polysulphide/sulphite/thiosulphate to H_2S, Dimethylsulphoxide (DMSO) to dimethylsulphide, arsenate to arsenite, fumarate to succinate, nitrate to nitrite, Fe(III) to Fe(II), Mn(III and IV) to Mn(II), Although the above have all been shown to support respiratory growth *Shewanella* is also able to reduce a wide range of other compounds, including a range of radioactive and toxic compounds such as uranium (VI), technetium (^{99}TcVII), plutonium and arsenic (Beliaev et al. 2005) (Hau & Gralnick 2007) (Fredrickson et al. 2008) (Pinchuk et al. 2011).

In addition to their versatility regarding respiratory substrates *Shewanella* species are commonly characterised by their ability to produce omega-3 fatty acids. The role of these lipids is unclear but they have been suggested to play a role in respiration, symbiotic relationships with higher organisms, or the ability for psychrotolerant growth, (i.e. at temperatures below 5^{o}C), another hallmark of the genus, although the temperature optimum for many species is much higher (Hau & Gralnick 2007).

Shewanella oneidensis MR-1, isolated from lake Oneida, is the best characterised *Shewanella* species, widely used as a model organism for a range of potential biotechnological purposes, broadly concerning its versatile range of terminal electron acceptors, which is hoped to be exploited for the bioremediation of several of the above substrates including U(VI) and (^{99}TcVIII) for which the reduced forms are insoluble and therefore less likely to contaminate water sources. In addition *S.oneidensis* has received considerable attention due to its ability to use electrodes as terminal electron acceptors as described in the microbial fuel cell section, in such a context *S.oneidensis* is referred to as an exoelectrogen (Logan 2009) and is discussed later.

This ability to use a wide range of terminal electron acceptors is in part due to extensive metabolic and regulatory plasticity. *Shewanella oneidensis* contains high numbers of signal transduction proteins, including chemotaxis proteins, thought to allow exquisite regulation of metabolic pathways in response to changing environmental factors and available substrates (Fredrickson et al. 2008). *S.oneidensis* has an extensive and complicated electron transport system, with 42 c type cytochromes encoded in the genome (Beliaev et al. 2005). Many of these have unknown function but others are better understood including the components of the metal reducing (Mtr) pathway (Figure 1-7 (**A**).

For electrons from internal respiration to be coupled to the reduction of insoluble extracellular metals such as Fe(III) or Mn (III or IV) the insulating outer membrane presents a problem. To resolve this, *S.oneidensis* constitutively expresses the Mtr pathway, consisting principally of OmcA, MtrC, MtrA, MtrB, CymA and STC (Coursolle et al. 2010). Two decahaem proteins, MtrA and MtrC, traverse the outer membrane, orientated by the porin MtrB (Edwards et al. 2015), the heme groups of these proteins are arranged in a chain like configuration and allow intracellular electrons to shuttle across the membrane, in likeness to an electrical wire (Davies et al. 2017). This MtrCAB complex receives electrons from the menaquinone pool, via CymA (and STC) which serve as intracellular electron transfer elements (Qian et al. 2011). In addition to these transfer proteins and the MtrCAB complex, another decaheme protein, OmcA, is also encoded on the same mtr operon, sharing a high degree of homology to MtrC and thought to act in a similar way as a terminal reductase for iron reduction (Liang et al. 2009).

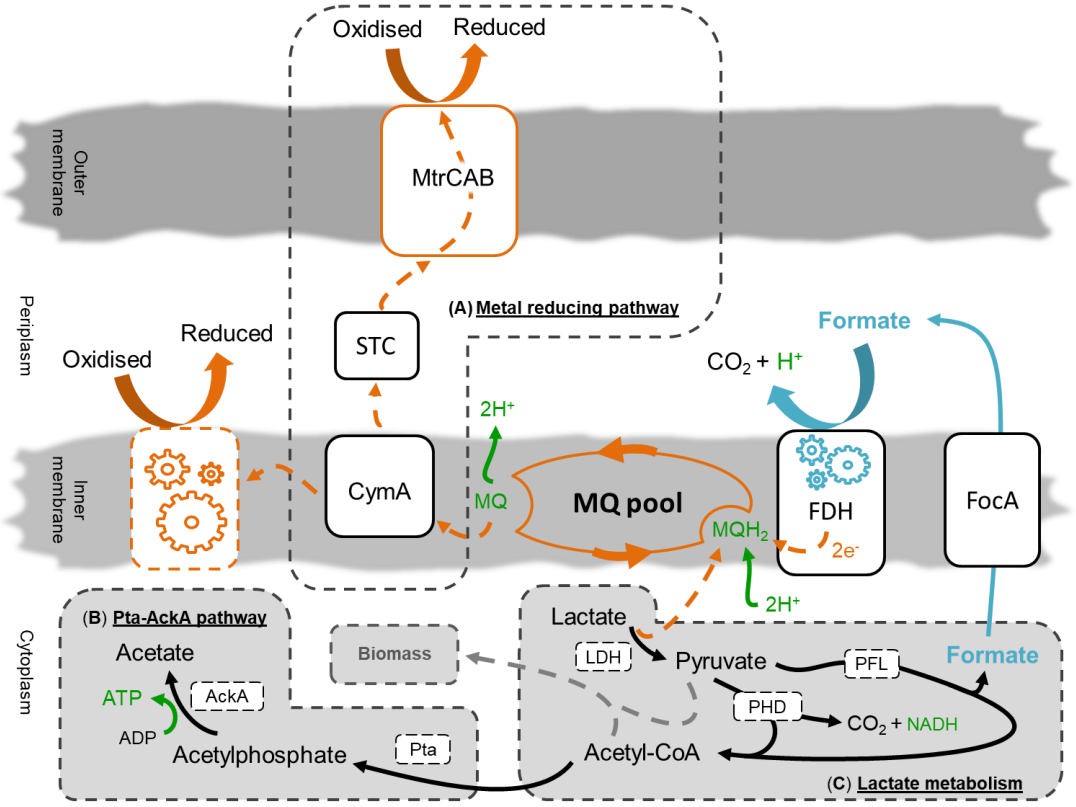

Figure 1-7 Anaerobic respiratory pathways of S.oneidensis MR-1.
*(**C**) Lactate metabolism when provided as sole electron donor and carbon source. Lactate oxidation catalysed by lactate dehydrogenase (LDH) and the resultant pyruvate is either cleaved to acetyl-CoA and formate by pyruvate-formate lyase (PFL) or to acetyl-coA and CO_2 by pyruvate dehydrogenase (PDH). Both pyruvate or acetyl-coA can enter central metabolism for generation of biomass. Alternatively acetyl-CoA can enter the Pta-AckA pathway (**B**) where substrate level phosyphorylation by the combined action of acetate kinase (AcKA) and acetyltransferase (Pta) contributes to anaerobic ATP synthesis. Formate, produced by PFL is exported into the periplasm by the formate transporter (FocA) where it is oxidised by FDH enzymes. Resultant electrons are shuttled to cytoplasmic menaquinone (MQ) reduction sites where they are reduced to menaquinol (MQH_2). This MQ pool couples either directly to terminal reductases (represented in orange) or via CymA, as seen for the metal reducing pathway (**A**) couples to extracellular electron acceptors. Electron transfer occurs via CymA, via STC to the outer membrane cytochromes MtrC and MtrA, coordinated by the porin MtrB. MtrC and OmcA (not shown) are proposed to transfer electrons via a variety of mechanisms (see text). Electron transfer shown in orange, formate metabolism in blue and processes contributing to energy conservation or generation in green.*

Considering the ability of *S.oneidensis* to couple not only to extracellular minerals but also electrodes, the specifics of extracellular electron transfer (EET) continue to be the focus of multiple research groups. The described Mtr pathway has been shown to be important for such interactions, but the direct interaction of the terminal reductases of the pathway with extracellular minerals are not the only proposed mechanisms of EET. Other mechanisms include the role of electron shuttles such as flavins or low molecular weight Fe complexes which may act to transfer electrons from the cofactors of MtrC and OmcA to the surface of insoluble mineral/electrode surfaces (Edwards et al. 2015). In addition, outer membrane extensions coated with the terminal

reductases MtrC and OmcA have been suggested, called nanowires, in line with extended conductive structures seen in other iron reducing bacteria such as *Geobacter* species (Bond et al. 2012).

In addition to being able to use a wide range of terminal electron acceptors, the carbon metabolism pathways of *S.oneidensis* are also remarkably diverse. The genome of *S.oneidensis* encodes pathways for the catabolism of multiple organic acids, fatty acids, amino acids, peptides and nucleotides, with many proposed to be able to act as sole electron donor and carbon source (Fredrickson et al. 2008). However not all of these have been experimentally corroborated, with most experimental studies using the well-established lactate, pyruvate, formate or hydrogen, or more recently N-acetylglucosamine, (NAG) (the primary component of chitin) (Kane et al. 2016), when selecting an electron donor for defined growth studies.

The metabolism of lactate, pyruvate, formate and hydrogen are all intimately connected in *S.oneidensis* (Figure 1-7 (**C**)). Lactate is able to be used as sole carbon and energy source for both aerobic and anaerobic growth (Pinchuk et al. 2009). Lactate is initially oxidised to pyruvate using membrane-bound lactate dehydrogenase complexes specific for the L or D isomer (Lld encoded by SO_1520-1518 and Dld encoded by SO_1521 respectively) with concomitant reduction of a quinone molecule (Brutinel & Gralnick 2012).

The produced pyruvate is either oxidised by the action of a pyruvate dehydrogenase (PDH) complex (aceEFG (SO_0424 to SO_0426)) to acetyl CoA and CO_2 with the reduction of a NAD^+ molecule, or converted to acetyl CoA and formate by a pyruvate formate-lyase enzyme (pflB encoded by SO_2912) (Kouzuma et al. 2015).

At this stage during aerobic respiration acetyl CoA can enter the tricarboxylic acid (TCA) cycle where it is completely oxidised to CO_2 (Kouzuma et al. 2015). In contrast, during anaerobic respiration the produced acetyl-CoA enters the phosphotransacetylase-acetate kinase (Pta-AckA) pathway (Figure 1-7 (**B**)). This pathway consists of the conversion of acetyl-CoA to acetylphosphate (by acetyltransferase (pta encoded by SO_2916) and subsequent conversion to acetate by acetate kinase (ackA encoded by SO_2915). This last substrate-level

phosphorylation step is considered the major source of ATP synthesis during anaerobic respiration (Hunt et al. 2010).

Formate, from the cleavage of pyruvate to formate and acetyl-coA by PFL during anaerobic respiration in the cytoplasm is transported by a bidirectional formate transporter (FocA, encoded by SO_2911) into the periplasm where its oxidation by FDH enzymes (discussed in detail below) is thought to contribute to proton motive force by driving the reduction of the menaquinone pool (Kane et al. 2016) (abstracting cytoplasmic protons) in a redox loop with CymA (Marritt et al. 2012), which is thought to act as a hub diverting electrons to available terminal electron acceptor pathways including the described Mtr pathway or via simpler systems such as a periplasmic fumarate reductase (Maier et al. 2003).

Several older publications claim that formate could be used as the sole carbon and electron source for growth of *S.oneidensis* (Scott & Nealson 1994). In such cases it was suggested that formate assimilation would occur by entering the energetically expensive serine cycle, but more recent bioinformatics approaches concluded this would not be energetically viable, suggesting the only viable method of formate assimilation would be via the action of a pyruvate-formate lyase complex in reverse (Fredrickson et al. 2008), a reaction that has never been observed to be physiologically relevant *in vivo*, not just in *S.oneidensis*, but any known organism (Bar-even 2016). Indeed it is widely considered that *S.oneidensis* is not capable of formate assimilation and the initial observations were in fact the result of amino acids present in the growth media acting as the carbon source, whilst formate acted only as electron donor (Fredrickson et al. 2008).

Hydrogen has been shown to be able to act as an electron donor in *S.oneidensis* coupled to reduction of both soluble and insoluble terminal electron acceptors (Liu et al. 2002). In addition, the reverse reaction has also been suggested to occur in *S.oneidensis* under anaerobic conditions with the depletion of terminal electron acceptors (Meshulam-Simon et al. 2007). In such a scenario formate oxidation has been suggested to couple to proton reduction catalysed by the two periplasmic hydrogenases of *S.oneidensis* (Pinchuk et al. 2011). *S.oneidensis* encodes both a Fe-Fe, hydrogen producing type hydrogenase (HydAB, encoded by SO_3920-SO_3926) and a reversible Ni-Fe type (HyaB, encoded by SO_2089 to SO_2099) (Meshulam-Simon et al. 2007).

Due to apparent coupling of formate oxidation to proton reduction the presence of a FHL complex has been proposed in *S.oneidensis* (Meshulam-Simon et al. 2007). Several papers claim that the presence of an assigned *fdh* gene in the middle of the *hydAB* operon, (SO_3922) is evidence for the existence of a cotranscribed FHL complex consisting of a FDH and HydAB (Meshulam-Simon et al. 2007). However the gene product in question bears similarity only to the γ subunit of known FDH enzymes and is unlikely to catalyse formate oxidation, more likely acting as an electron transfer element for the hydrogenase complex. Despite this a periplasmically facing FHL complex in *S.oneidensis* is still possible, the described hydrogenases complexing with the FDH enzymes described in detail below. Alternatively formate oxidation could couple to proton reduction via the menaquinone pool as suggested by some authors (Serres & Riley 2006).

The genome of *S.oneidensis* MR-1 encodes three periplasmic FDH complexes. All three are heterotrimers similar in topology to the respiratory FDH enzymes of *E.coli*, FDH-N and FDH-O, consisting of a catalytic α subunit and ß and γ subunits for subsequent electron transfer from the α subunit. As detailed above these proteins are thought to act as primary dehydrogenases, contributing to PMF maintenance across the cytoplasmic membrane and the reduction of the menaquinone pool (Mordkovich et al. 2013). The three FDH complexes are encoded by SO_0101-SO_0103, henceforth referred to as **Fdnαβγ**, SO_4509-SO_4511 (**Fdh1αβγ**) and SO_4513-SO_4515 (**Fdh2αβγ**) as seen in Figure 1-8.

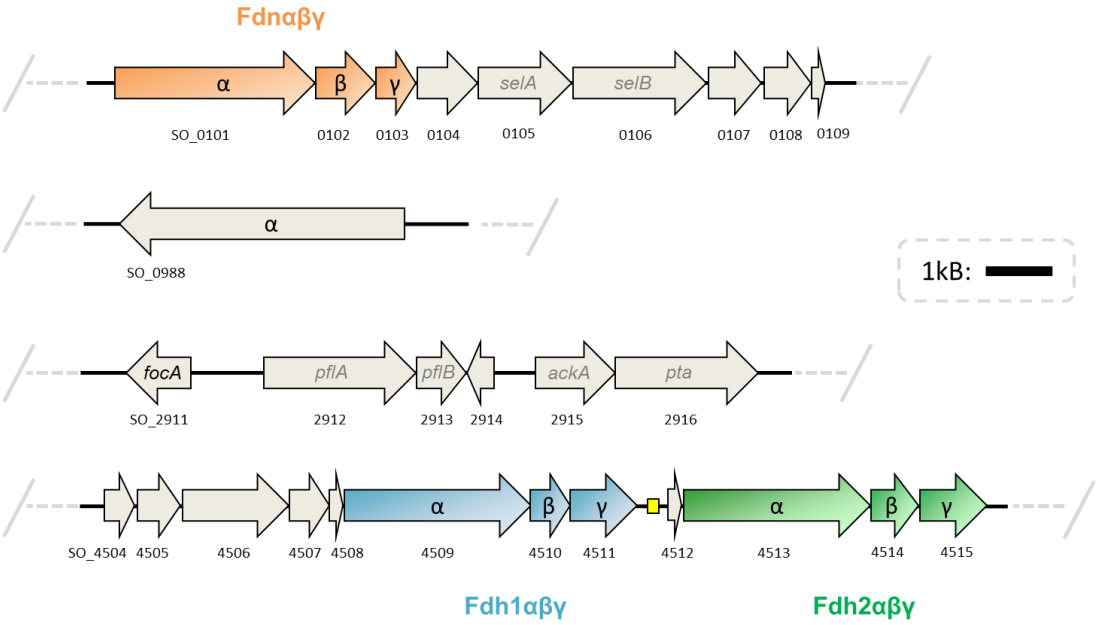

Figure 1-8 Genetic loci concerning formate metabolism in S.oneidensis MR-1.
Respiratory heterotrimeric FDH complexes coloured in orange blue and green respectively, consisting of Mo/W-bis PGD and 4Fe4S binding α catalytic subunit, β subunit coordinating a further four ferredoxins and a cytochrome b, quinone binding, γ subunit. SO_0988 encodes a further isolated α catalytic subunit. Bidirectional formate transporter encoded by SO_2911 upstream of pyruvate formate lyase (PFL) machinery and components of the Pta-AckA pathway (see text). Remaining genes in grey (excluding SO_2914) thought to be accessory proteins for FDH assembly or activity. Predicted binding site of transcriptional regulator EtrA shown in yellow.

The first of these FDHs, Fdnαβγ, is encoded by the region SO0101-0103. This is thought to be orthologous to FDH-N in *E.coli* (ecFDH-N for clarity), coupling formate oxidation to nitrate reduction in a respiratory loop, contributing to PMF, a role supported by microarray data which found the cluster to be significantly upregulated in response to nitrate (Beliaev et al. 2005). Fdnαβγ shares a high degree of sequence homology with the equivalent subunits in ecFDH-N, specifically 63%, 56% and 42% for the α, β and γ subunits respectively. Importantly the residues responsible for binding of the catalytic Mo/W-bis PGD and 4Fe4S cofactors in the α subunit are also found, in addition to those for binding of four further ferredoxins in the β subunit and two b type heme groups in the γ subunit. The fdnαβγ genes lie directly upstream of the accessory proteins encoded by 0101-0108, of which SO_0104 and SO_0107 are thought to encode homologs of FdhE (Lüke et al. 2008) and FdhD (Schlindwein et al. 1990) in *E.coli*, responsible for correct Fdnαβγ maturation and assembly. SO_0105 and SO_0106 encode the proteins SelA and SelB required for the incorporation of the selenocysteine residue predicted by a UGA codon in the catalytic Fdnα subunit (Axley et al. 1991).

The other two respiratory FDH complexes, Fdh1αβγ and Fdh2αβγ, are thought to have resulted from an ancestral gene duplication event (Kane et al. 2016) and are found together in the genome. Indeed at the amino acid level the α subunits (74% identical, 85% similar), β subunits (88% identical, 94% similar) and γ subunits (54% identical, 70% similar) are highly conserved. Like the Fdnαβγ isoform the α subunits are predicted to contain both a catalytically important Mo/W-bis PGD and 4Fe4S cofactor. Likewise the β subunits are predicted to bind a further four ferredoxins and the γ subunit to contain two b type hemes and a quinone binding site. Indeed the only distinguishing feature of these isoforms is the lack of the selenocysteine residue predicted in the Fdn isoform, replaced in these enzymes by a cysteine residue (Cys_{193} in both proteins). In a genetic context Fdh1αβγ is preceded by the genes SO_4504 to 4508, these are accessory proteins of unknown function. Notably a homolog of one of these, the small tat sequence containing protein (FdhX) encoded by SO_4508, also proceeds Fdh2αβγ in the form of SO_4512.

Despite the predicted similarities between the two isoforms Fdh1αβγ and Fdh2αβγ it has been suggested they are under distinct regulatory control, primarily due to the presence of a binding site (ACTGTTCTAGATCAAA) for the transcriptional regulator EtrA upstream of SO_4512 (Figure 1-8). This is supported by study of an EtrA deletion strain, in which SO_4512-4515 (Fdh2) expression was repressed and SO_4508-4511 (Fdh1) expression, in contrast, was not (Cruz-García et al. 2011). The transcriptional regulator EtrA (electron transport regulator protein) is thought to play a comparable role to Fnr (fumarate and nitrate reduction regulator) in *E.coli*, sharing 73% amino acid sequence identity and restoring wild type physiology to an *E.coli fnr* deletion mutant (Cruz-García et al. 2011). Both are thought to act as transcription regulators in response to the presence of oxygen, but whilst Fnr is considered absolutely essential for anaerobic respiration in *E.coli* (Gao et al. 2010) the analogous EtrA in *S.oneidensis* is instead thought to fine tune metabolic responses, the alternative global regulator CRP (cyclic-AMP receptor protein) adopting many of the functions of Fnr in *E.coli* and being essential for anaerobic growth (Gao et al. 2010).

Other than the three heterotrimeric FDH complexes described above the genome of *S.oneidensis* also encodes a single orphaned FDH α subunit encoded

by SO_0988 predicted to contain both Mo/W-bis PGD and 4Fe4S cofactors. In contrast to the other described α subunits SO_0988 does not contain a tat binding sequence suggesting it remains within the cytoplasm. However the inability of a deletion strain lacking the three respiratory isoforms (FdnαβγFdh1αβγ and Fdh2αβγ) to grow suggests SO_0988 alone is not capable of substituting for their activity (Kane et al. 2016).

1.4 Electrochemical applications

Electrochemistry is used to study exoelectrogenic bacteria (such as *Shewanella*) in a variety of different contexts, from fundamental academic research that characterises and explores the native microbial physiology to industrially focussed biotechnologies that exploit the interactions of these bacteria with electrodes. Of course the two areas are fundamentally connected, with better understanding of the physiological processes allowing improvements to biotechnological designs and biotechnological applications resulting in increased academic research spending.

One principal area of academic research is elucidating how electrogenic bacteria are able to interact with electrodes, allowing for future improvements of biotechnologies that exploit them. Three principal mechanisms have been suggested, direct electron transfer from the bacteria to electrodes via dedicated cytochrome proteins on the cell surface (Richardson et al. 2012), transfer through conductive nanowires (Kumar et al. 2015) and via mediators, either exogenous or those produced by the cell (Marsili et al. 2008), illustrated in Figure 1-9 and previously discussed in the context of *S.oneidensis*.

When discussing biotechnologies relating to electrogenic bacteria the term bioelectrochemical systems (BESs) is frequently used (Pant et al. 2012). BESs encompass a wide range of emergent technologies that share a common paradigm. In all such systems bacteria exploit exogenous electrodes as either electron acceptors or electron donors, coupling them to their internal metabolism (Figure 1-9).

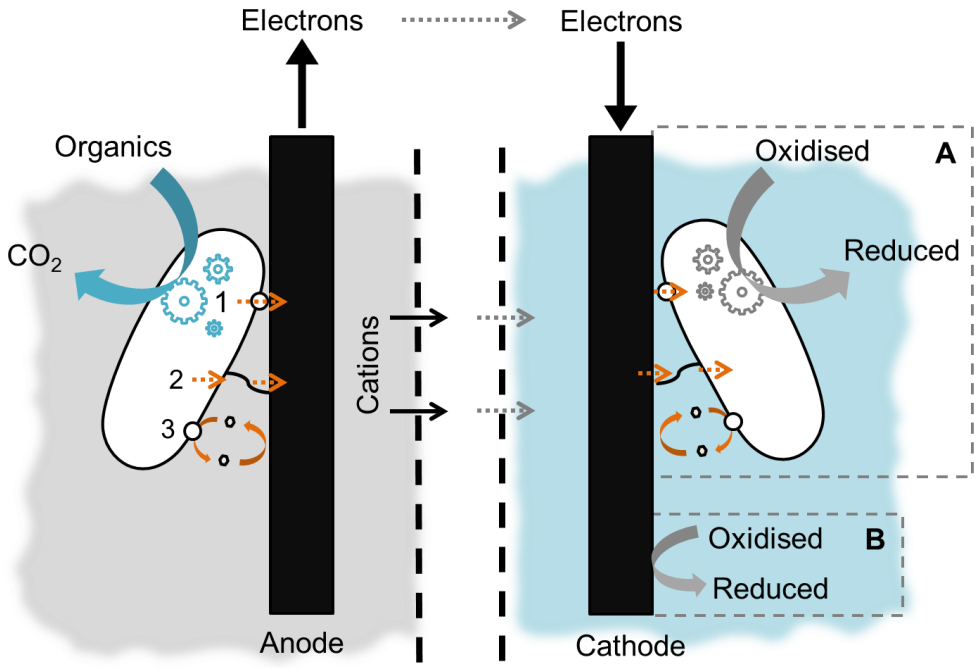

Figure 1-9 Schematic overview of bioelectrochemical systems (BESs).
*BESs can include either an anodic compartment (left) a cathodic compartment (right) or both, separated by an ion permeable exchange membrane (dashed black lines). In the anodic compartment of a BES, exoelectrogenic bacteria use extracellular electrodes as electron acceptors coupled to internal catabolism to generate electrical current. The cathodic compartment can either be abiotic (**B**), as in MFC devices, or biotic (**A**) where exoelectrogenic bacteria accept reducing equivalents from a cathode for intracellular reduction reactions. Also shown in orange are the three commonly accepted modes of electron transfer from electrogenic bacteria to electrodes (1) Direct electron transfer, (2) Transfer through conductive nanowires (3) Mediated electron transfer, although these mechanisms are thought to overlap, see text.*

Although this underlying principle is relatively simple, the permutations and applications are varied. The most common BESs are microbial fuel cells (MFCs) in which electrogenic bacteria transfer electrons generated from their intracellular catabolism to an extracellular electrode, generating an electrical current (Logan et al. 2006). Microbial electrolysis cells (MECs) expand on this premise, coupling the current produced in the biotic anodic compartment to reduce protons in a connected cathodic compartment (Kadier et al. 2016). Microbial electrosynthesis (MES) focuses solely on the cathodic compartment and concerns the use of a cathode to drive intracellular reductive metabolism to products of commercial value (Rabaey & Rozendal 2010). An overview of these concepts is seen in Figure 1-9 but a detailed exploration of each in addition to other more niche applications using the same principles follow.

1.1.1 Microbial fuel cells (MFCs)

The concept of microbial electricity generation, the fundamental concept behind microbial fuel cells (MFCs) has been studied sporadically for over a century (Potter 1911), with the first commercial patent filed in 1967 by John Davis (Pant et al. 2012). Despite this history it is only in the last few decades that research in this area has intensified in response to a growing need for environmentally sustainable energy sources (Lovley & Nevin 2011).

As outlined above and in Figure 1-9, MFCs operate due to bacterial colonisation of an anode, which acts as a terminal electron acceptor, accepting electrons generated from intracellular oxidation reactions, principally catabolism of a range of organic molecules to CO_2 (Yi-chi et al. 2015). The bioenergetics of this process is sufficient to support the respiratory needs of these microbes and when connected to a distinct cathode, a continuous current can be produced from the self-sustaining bacterial culture, requiring only a continued source of oxidisable substrates (Logan et al. 2006).

The flow of electrons from the anode to cathode requires charge balance and so many MFCs include ion permeable exchange membranes to allow cations in the anolyte to migrate to the cathode as seen in Figure 1-9 (Rahimnejad et al. 2014).

The cathodic compartment coupled to the biotic anode in a MFC was classically aerobic, allowing the abiotic reduction of oxygen to water at the cathode surface (Bullen et al. 2006). However subsequent variations have demonstrated a variety of other molecules that can accept the electrodes at the cathode, including ferricyanide, nitrate or sulphate with others providing the basis for other BESs, including MECs, MES systems, and microbial remediation cells (MRCs), which are discussed subsequently (Wang & Ren 2013).

The first MFC examples used defined substrates, principally acetate, glucose or other simple substrates in the anodic compartment. To make them economically attractive they have since been demonstrated to function with a wide range of different waste waters, from a range of industrial and domestic sources, allowing the partial decomposition of organic waste and simultaneous energy production. More ambitious devices also incorporate polymer degrading bacteria in combination with electrogenic bacteria, the polymer degraders breaking down

polymers into simple molecules that electrogenic bacteria can couple to electricity production (Wang & Ren 2013).

Of all the BESs, MFCs are the most well established, and significant advances have been made in many aspects of their design. Of these the most significant are the development of single chamber MFCs with an air cathode that bypass the need for the costly cation exchange membranes that prevented many previous iterations being economically viable (Pant et al. 2012). The use of multiple stacked MFCs in series or parallel has also allowed significant increases in both voltage and current (another shortcoming of early devices), as well as increased substrate oxidation (Aelterman et al. 2006). Other developments such as tubular MFCs, with improved flow to reduce resistance and various other improvements have culminated in a significant increase in the power output of these devices. A previous study concluded that MFCs would need to produce more than 0.5 kW/m^3 to be commercially and environmentally viable (Pant et al. 2012), Current laboratory scale MFCs have been shown to produce 2.87 kW/m^3 of power (Wang & Ren 2013), making their future use promising.

Despite the significant improvements to MFC devices, several issues and considerations remain, successful scaling of these technologies to an industrial level being the most concerning. It has been repeatedly shown that the maximum power density generated by a MFC is not proportional to the surface area of the anode (Pant et al. 2012)(Logan et al. 2006), suggesting the power outputs seen for small laboratory scale experiments extrapolated to larger scales may be optimistic. In addition to issues with scaling, MFCs must prove themselves to be viable in comparison with other competing technologies, for example anaerobic digesters, and so the need for further improvements to these technologies still exists.

Improvements to MFC design, including those discussed above typically use electrochemistry as a quantative way of studying various design elements (Menicucci et al. 2006) including choice of anode material, (Hindatu et al. 2017) the nature of the coupled cathode (Franks & Nevin 2010), and other material or electrical component improvements (Logan et al. 2006).

Electrochemistry is also used to study those aspects of the MFC relating to the bacteria themselves and ways to exploit existing physiological responses to promote power generation (Logan 2009). Study of microbe-anode interactions is a common area of study with a variety of perspectives including those studying/optimising the relevant biochemical, microbiological and material aspects. For recent reviews of these aspects see (Santoro et al. 2017), (Kumar et al. 2015) and (Hindatu et al. 2017) respectively.

All of these approaches however use electrochemistry to ultimately assess the improvements made by their investigations, typically quoted as maximum power outputs (Yi-chi et al. 2015) or in the case of more fundamental research by more refined cyclic voltammetry or chronoamperometry data.

Although many envisage the future of MFCs as intrinsically linked to waste water treatment a variety of other applications for MFC exist, with some in current, albeit niche, commercial use. For example, sediment MFCs, (also referred to as benthic MFCs) exploit the natural potential difference on the ocean floor, the anode is embedded in the anoxic sediment capable of supporting bacterial growth and the cathode in the oxic seawater above, allowing current generation for marine sensors, with a number of successful long term tests having already been carried out (Franks & Nevin 2010).

Other variations include microbial solar cells, which add a layer of complexity to existing MFC designs by having the substrates used by electrogenic bacteria being provided by photosynthesis by either plants, photoautotrophic bacteria or algae *in situ* (Strik et al. 2011).

Another use for MFCs exploits the potential difference between anode and cathode to drive water desalination in microbial desalination cells (MDCs). At their simplest, these devices resemble MFCs with an extra third compartment between anodic and cathodic compartments, as current flows from anode to cathode, anions (including Cl^-) in the central chamber migrate to the anode and cations (including Na^+) migrate to the cathode through anion and cation exchange membranes respectively to balance the transferred charge, as a result the central compartment becomes desalinated (Saeed et al. 2015).

1.1.2 Microbial remediation cells (MRCs)

The ability of BES's to oxidise or reduce a range of compounds has already been alluded to. In the case of MFCs, the removal of organic waste from wastewater is a convenient benefit to what is primarily a means of producing energy, however in certain cases the bioremediation effects of such devices can be of more significance than their energy production.

A principal example of such bioremediation is for decolourisation of dyes from the textile industry. The dye Congo red has been effectively degraded in BESs devices with concomitant current production and the toxic azo dyes have also been shown to be detoxified both by oxidation and reduction in the anodic and cathodic chambers of BES's respectively (Pant et al. 2012).

The use of microbial remediation devices has also been used to accelerate subsurface bioremediation. By coupling an aerobic cathode on the surface to an anode in contaminated area the oxidation of petroleum contaminants and diesel, ethanol, 1,2-dichloroethane and pyridine have been shown to be dramatically accelerated (Wang & Ren 2013). This concept can also be extended to waste water treatment, which although not able to produce electrical current has been shown to improve wastewater treatment processes in a procedure referred to as microbial electrochemical snorkelling (Erable et al. 2011).

In contrast to the above anodic remediation devices a poised cathode can also be colonised for bioremediation, both in the environment and in dedicated MRC devices, the reduction of chlorinated solvents, perchlorate (Wang & Ren 2013), chromium, uranium (Cheng et al. 2012) as well as denitrification (Rabaey & Rozendal 2010) have all been shown.

1.1.3 Microbial electrolysis cells (MECs)

First conceived in 2005, microbial electrolysis cells are an extension of MFC technologies. The electrons generated from the microbial decomposition of organic substrates in the anodic compartment are not used to generate electrical power, but instead are combined with the additional voltage required to drive proton reduction to dihydrogen at the cathode, with a view to use hydrogen as a renewable energy source (Pant et al. 2012). In earlier devices this extra voltage had to be externally provided, but recent versions exploit complex reverse

electrodialysis techniques to prevent external input of power (Kadier et al. 2016). As with their parent MFC predecessors, the ion exchange membrane components proved limiting and the development of membrane-less MEC devices has allowed higher hydrogen production, although a common drawback is the generation of methane by methanogens. Although this generation of methane is largely seen as a hindrance it has recently also been considered as a fuel in its own right, as described in the microbial electrosynthesis discussion below (Eerten-jansen et al. 2012).

1.1.4 Microbial electrosynthesis (MES)

The term microbial electrosynthesis was first used in 2010 to refer to the reduction of CO_2 to multi carbon compounds by microbes on a cathode but has since been widely expanded and redefined as any microbial synthesis of chemical compounds in electrochemical cells, (Rabaey & Rozendal 2010) thus accounting for the wide range of transformations possible using BESs.

Using the above definition the above MEC devices would fall under this classification as the hydrogen synthesis at the chemical cathode is microbially driven at the anode (Hasany et al. 2016). More varied applications become available however when the cathode is also colonised, allowing access to the full diversity of reductive microbial metabolism.

The use of a bacterial community catalysing a reductive transformation using electrons from a cathode is an attractive prospect for a number of reasons. Primarily biocathodes are favoured over conventional chemical alternatives due to their relatively cheap cost and potential to self-regenerate in addition to their ability to act as biocatalysts for a wide range of substrates, allowing both bioremediation or synthesis of a range of value-added chemicals (Sharma et al. 2014) and as such study in this field has intensified in the last decade.

The supply of electrons from a cathode to influence microbial metabolism can have a diverse range of uses as explored below, it can be used to drive and exploit respiration or influence the flux of metabolites in fermentation pathways to drive production of useful metabolites, a process referred to as electrofermentation (Sharma et al. 2014). Electrofermentation has already been used to demonstrate the effective production of L-glutamic acid and other

research hopes to drive production of butanol and ethanol (Rabaey & Rozendal 2010).

The first microbial electrosynthetic reactions concerned the reduction of CO_2 to small organic molecules, principally acetate, that could potentially be used as renewable energy sources, these transformations being particularly attractive considering the concomitant removal of CO_2 and fuel production. This area has remained a focus of the field, with the biocathodic reduction of CO_2 being used to produce acetate, methane, syngas, hydrogen, ethylene, methanol, dimethyl ether and urea with varying degrees of success (Sadhukhan et al. 2016). Of these the most promising remain acetate and methane and are discussed in turn below.

The reduction of CO_2 to acetate by acetogenic bacteria has remained a focus of many research groups since the first demonstration by cultures of *Sporomusa ovata* capable of generating acetate, and small quantities of 2-oxobutyrate, from a cathode and CO_2 alone (Nevin et al. 2010). Physiologically acetogenic bacteria naturally produce acetate using hydrogen as an electron donor, but a wide range of organisms including various *Clostridia* species and *Sporomusa* species appear able to use a cathode to provide these reducing equivalents (Wang & Ren 2013).

The reduction of CO_2 to methane by methanoogenic bacteria is also of considerable interest, as previously mentioned the generation of methane in MECs was considered problematic, but recently a number of research groups have focused on optimising methane generation at a cathode surface as an alternative fuel source in a process known as electromethanogensis (Sadhukhan et al. 2016). Electromethanogensis has since been shown in pure cultures of the archaeon *Methanobacterium palustre* with high efficiency (Cheng et al. 2009). However the production of methane is not ideal, methane itself is a potent greenhouse gas, indeed per molecule, it absorbs infrared radiation much more strongly than carbon dioxide (Lashof & Ahuja 1990). This problem is compounded by issues with methane being gaseous which raises issues with transportation infrastructure, indeed leakage is already a considerable issue (Alvarez et al. 2012).

Considering some of the issues with acetate or methane as fuels many research groups have retained the focus on renewable fuel sources but instead have

addressed the generation of more complex fuel molecules, often using simple organic molecules such as pyruvate, formate, acetyl-coenzyme A, acetate or methane as building blocks (Khosravanipour et al. 2017). Considerable work has been invested in the transformation of acetate to ethanol using microbial electrosynthesis, (Rabaey & Rozendal 2010) with current examples requiring the use of mediators such as methyl viologen (Wang & Ren 2013). In a similar manner the diversion from acetyl coenzyme A conversion to acetate in acetogenic bacteria to more desirable fuel products such as butanol has also been the focus of work re-engineering the metabolism of *Clostridium ljungdahlii* (Rosenbaum & Henrich 2014). Other studies have investigated acetyl-CoA as a building block for the formation of various other alcohols and long chain fatty acids (Rosenbaum & Henrich 2014).

Alternative microbial electrosynthesis studies have focused on more niche reductive transformation reactions, these are less concerned with renewable energy production and address more the generation of high value compounds, i.e. those of more commercial value than their precursors. A relevant example is the bioanode driven production of hydrogen peroxide from the reduction of oxygen at a chemical cathode (Pant et al. 2012). The produced hydrogen peroxide can then be sold to a variety of industries where it is frequently used for Fenten reaction chemistry (Rabaey & Rozendal 2010). In a similar manner the consumption of protons at the cathode of BES devices and corresponding rise in pH values has been used to make caustic solutions intended for industrial use as cheap disinfectants (Wang & Ren 2013). Reduction of fumarate to succinate is another commonly studied transformation having been shown by *Anaeromyxobacter dehalogenans* (Nevin et al. 2011), cultures of *Actinobacillus succinogenes* when mediated by neutral red (Rabaey & Rozendal 2010) and in non-mediated systems by the model organisms *Geobacter metallireducens* (Rabaey & Rozendal 2010) and *Shewanella oneidensis* (Ross et al. 2011). Other examples of value-added products being investigated for microbial electrosynthesis include various precursors for polymers and carbonate species for construction industries (Sadhukhan et al. 2016).

Microbial electrosynthesis has also been used for bioremediation with the reduction of unwanted waste products, as already partially described for MRC devices. Of these denitrification has been particularly well studied (Blackall et

al. 2007), with the reduction of nitrate to nitrite being demonstrated without mediators or hydrogen acting as an intermediate for a pure culture of *Geobacter metallireducens* (Gregory et al. 2004). Other demonstrated examples of microbial electrosynthetic bioremediation include the degradation of phenol (Sharma et al. 2014) and recovery of phosphate as struvite (Wang & Ren 2013). More unusual applications involve the recovery of various nanomaterials including nanomagnets, nanocatalysts and quantum dots (Sadhukhan et al. 2016).

Information on the range of bacterial species capable of accepting electrons from cathodes is remarkably sparse considering the interest in the area. As already previously mentioned a range of acetogenic bacteria have been shown to be able to accept reducing equivalents from cathodes including many of the gram positive *Clostridium* species including *C. beijerinckii,, C. acetobutylicum, C. saccharobutylicum, C. pasteurianum and C. ljungdahlii* (Khosravanipour et al. 2017). Other acetogenic bacteria including several *Sporomusa* species, thought to be phylogenetically related to *Clostridia* (Yutin & Galperin 2013) and *Moorella thermoacetica,* a model acetogen, have also been studied (Nevin et al. 2011).

Model organisms have been the focus of a number of other reported microbial electrosynthetic investigations, including the model dechlorinator *Anaeromyxobacter dehalogenans* for the reduction of dehalogenate-2-chlorophenol (Nevin et al. 2011), the model methanogen, *Methanobacterium palustre* for methane production and the model exoelectrogens *Geobacter sulfurreducens* (Rabaey & Rozendal 2010) and *Shewanella oneidensis* (Ross et al. 2011) for the reduction of fumarate. Importantly in the case of *S.oneidensis* the well characterised Mtr pathway was proposed to function in reverse to enable such catalysis (Ross et al. 2011).

A variety of other studies have studied bacterial communities and co-cultures in which those species responsible for cathode interactions are not always apparent (Hasany et al. 2016). Indeed through the use of exogenously added mediators a wide range of bacterial species not typically considered as electrotrophs have been studied (Khosravanipour et al. 2017).

A surprisingly unexplored area is the use of chemolithotrophs such as *Acidithiobacillus ferrooxidans* (Yarzábal et al. 2002) in microbial electrosynthesis systems. These species oxidise extracellular iron in order to obtain reducing equivalents for CO_2 fixation or ATP generation although the underlying mechanisms are currently largely unclear. A few examples do exist however including study of *Rhodopseudomonas palustris* with a consideration for microbial electrosynthesis (Doud & Angenent 2014) and the cultivation of certain iron-oxidising bacteria on cathodes including *Mariprofundus ferrooxydans* PV-1 (Summers et al. 2013). One limitation however may be the extensive time required to culture such organisms making them unfeasible for economic exploitation (Yarzábal et al. 2002).

Knowledge of the mechanisms of electron transfer from a cathode to biocatalysts has already been highlighted as being of fundamental importance for future development of microbial electrosynthesis technologies. Despite this little is known, even relating to those systems closest to commercialisation (Lovley 2011).

The simplest mechanism of electron transfer between cathodes and microbes is through the use of exogenously added mediators, these cycle between redox states, transferring electrons from the cathode surface to the biocatalysts. Common examples of mediators include neutral red, thionin and methyl viologen (Park & Zeikus 2000), although higher potential alternatives such as Anthraquinone-2,6-disulfonate (AQDS) can also be used (Thrash et al. 2007). Disadvantages of such systems is that many mediators can be unstable or toxic necessitating their removal from electrosynthetic products which can be costly (Rabaey & Rozendal 2010).

Certain bacterial species appear to secrete their own mediators to act in a similar capacity to those described above, many of these are secondary metabolites including various flavin molecules (Marsili et al. 2008) and phenazines (Wang et al. 2013), but sulphur species produced by *Pelobacter carbinolicus* have also been observed (Rabaey & Rozendal 2010).

Hydrogen generated at the surface of a cathode has been shown to drive reductive metabolism for electrosynthesis in a manner similar to that described for the mediators described above. Hydrogen has been used to promote

denitrification (Sakakibara & Kuroda 2004), acetate production in acetogens and poly-ß-hydroxybutyrate production by *Cupriavidus necator* (Rabaey & Rozendal 2010). Despite these successes hydrogen also has a number of drawbacks including its low solubility compared to the above mediators and energetically inefficient generation at an uncatalysed electrode which requires overpotentials below -0.41V vs SHE (Rabaey & Rozendal 2010). It is relevant to mention that for electrosynthetic conversions requiring particularly low potentials the accompanying electrolysis and hydrogen production can complicate analysis. This becomes a particular obstacle when trying to demonstrate that electron transfer proceeds without the presence of hydrogen.

Another mechanism suggested for electron transfer to electrodes is the involvement of iron species, which like the mediators and dihydrogen above, cycle between redox states shuttling between the cathode and biocatalyst (Rabaey & Rozendal 2010). Such a mechanism is already recognised as a metabolic strategy used by iron oxidising bacteria and has been shown to be applicable for cathodic interactions by *Rhodopseudomonas palustris* (Doud & Angenent 2014).

Concerning co-culture and bacterial community studies it is relevant to highlight that not all species involved in microbial electrosynthetic processes need interact with the cathode. In such scenarios, electrotrophs may accept electrons from a cathode, producing intermediate building block organic molecules like acetate or formate which are syntrophically provided to other species which further reduce them to the final, more complex, electrosynthetic products (Rabaey & Rozendal 2010).

Of most interest are the mechanisms by which certain bacteria accept electrons directly from cathodes, i.e. direct electron transfer. Examples of such interactions are restricted to those model organisms principally studied as iron-reducers including *Geobacter sulfurreducens* (Rabaey & Rozendal 2010) and *Shewanella oneidensis* (Liang et al. 2009). The anodic interactions of both species are well documented, but in contrast relatively little is known about their ability to couple to cathodes. It is tempting to assume that many of the metabolic elements responsible for anodic and cathodic interactions would overlap but that does not seem entirely the case (Rabaey & Rozendal 2010).

In *Geobacter* species the intensively studied outer-surface Omc cytochromes (Liang et al. 2009) required for utilising electrodes as electron acceptors, have been demonstrated to play no major part in electron transfer into cells (Strycharz et al. 2011). This is in direct contrast to *Shewanella oneidensis* where the equally intensively studied Mtr pathway is thought to be reversible and responsible for both electron shuttling in and out of cells (Ross et al. 2011).

Despite recent advances in the field, such technologies are still in their infancy and require considerable more study to make them commercially viable. These technologies share many of the concerns presented for the future of MFCs including the viability of scaling many of these processes (Sharma et al. 2014). Many of the issues concern economic viability and relate to several points regarding efficiency including high overpotentials and internal resistances observed for certain transformations (Pant et al. 2012). Other considerations include limitations imposed by substrate/ion diffusion (Rabaey & Rozendal 2010), pH changes (Pant et al. 2012) as well as bacterial electron uptake limiting production and the unavailability of desired metabolic functions (Rosenbaum & Henrich 2014). Many of these issues may be resolved by engineering and electronic refinements, with a variety of unexplored configurations and improvements having already been proposed (Recio-garrido et al. 2016). The last two constraints however concerning improved microbe-cathode interactions and metabolic diversity will require a developed understanding of the fundamental biochemistry underlying these processes and advances in the field will likely come from synthetic biology approaches to optimise both electrode interactions and optimise the relevant metabolic pathways (Rabaey & Rozendal 2010).

1.5 Perspective

As introduced at the beginning of this literature review, the following work aims to determine whether *S.oneidensis* MR-1 is capable of acting as a biocatalyst for CO_2 reduction and subsequently determining whether such activity can be driven by a cathode as a potential biotechnological energy storage system for the simultaneous production of formate and fixation of CO_2. To do this the native FDH enzymes of *S.oneidensis* must first be characterised and their normal physiological role explored. As such this project will simultaneously inform on the role of the key anaerobic metabolite formate during the respiration of the model organism *S.oneidensis* MR-1.

1.6 References

Abaibou, H., Pommier, J. & Benoit, S., 1995. Expression and characterization of the *Escherichia coli* fdo locus and a possible physiological role for aerobic formate dehydrogenase. *Journal of Bacteriology*, 177(24), pp.7141–7149.

Aelterman, P., Rabaey, K. & Verstraete, W., 2006. Continuous Electricity Generation at High Voltages and Currents Using Stacked Microbial Fuel Cells. *Environmental Science and Technology*, 40(10), pp.3388–3394.

Alekseeva, A.A., Savin, S.S. & Tishkov, V.I., 2011. NAD + -dependent Formate Dehydrogenase from Plants. *Acta Naturae*, 3(11), pp.39–54.

Almendra, M.J. et al., 1999. Purification and characterization of a tungsten-containing formate dehydrogenase from *Desulfovibrio gigas*. *Biochemistry*, 38(49), pp.16366–72.

Alvarez, R. a et al., 2012. Greater focus needed on methane leakage from natural gas infrastructure. *Proceedings of the National Academy of Sciences of the United States of America*, 109(17), pp.6435–40.

Andrews, S. et al., 1997. A 12-cistron *Escherichia coli* operon (hyf) encoding a putative proton-translocating formate hydrogenlyase system. *Microbiology*, (1 997), pp.3633–3647.

Armstrong, F. a & Hirst, J., 2011. Reversibility and efficiency in electrocatalytic energy conversion and lessons from enzymes. *Proceedings of the National Academy of Sciences of the United States of America*, 108(34), pp.14049–54.

Axley, M.J., Böck, A. & Stadtman, T.C., 1991. Catalytic properties of an *Escherichia coli* formate dehydrogenase mutant in which sulfur replaces selenium. *Proceedings of the National Academy of Sciences of the United States of America*, 88(19), pp.8450–4.

Bachmeier, A. & Armstrong, F., 2015. Solar-driven proton and carbon dioxide reduction to fuels - lessons from metalloenzymes. *Current opinion in chemical biology*, 25C, pp.141–151.

Bagramyan, K. & Trchounian, A., 2003. Structural and functional features of formate hydrogen lyase, an enzyme of mixed-acid fermentation from *Escherichia coli*. *Biochemistry. Biokhimiiâ*, 68(11), pp.1159–70.

Bar-even, A., 2016. Formate Assimilation: The Metabolic Architecture of Natural and Synthetic Pathways. *Biochemistry*, 55, pp.3851–3863.

Bassegoda, A. et al., 2014. Reversible Interconversion of CO_2 and Formate by a Molybdenum-Containing Formate Dehydrogenase. *Journal of the American Chemical Society*, 136(44), pp.15473–6.

Beliaev, A. et al., 2005. Global transcriptome analysis of *Shewanella oneidensis* MR-1 exposed to different terminal electron acceptors. *Journal of bacteriology*, 187(20), pp.7138–45.

Biel, K. & Fomina, I., 2015. Benson-Bassham-Calvin cycle contribution to the organic life on our planet. *Photosynthetica*, 53(June), pp.161–167.

Blackall, L.L. et al., 2007. Microbial ecology meets electrochemistry: electricity-driven and driving communities. *The ISME Journal*, 1, pp.9–18.

de Bok, F. a. M. et al., 2003. Two W-containing formate dehydrogenases (CO_2-reductases) involved in syntrophic propionate oxidation by *Syntrophobacter fumaroxidans*. *European Journal of Biochemistry*, 270(11), pp.2476–2485.

Bond, D.R. et al., 2012. On electron transport through *Geobacter* biofilms. *ChemSusChem*, 5(6), pp.1099–105.

Borrel, G., Adam, P.S. & Gribaldo, S., 2016. Methanogenesis and the Wood – Ljungdahl Pathway: An Ancient, Versatile, and Fragile Association. *Genome Biol. Evol.*, 8(6), pp.1706–1711.

Boyington, J. & Gladyshev, V., 1997. Crystal structure of formate dehydrogenase H: catalysis involving Mo, molybdopterin, selenocysteine, and an Fe4S4 cluster. *Science*, 275(4), p.1305.

Brutinel, E.D. & Gralnick, J.A., 2012. Preferential Utilization of D -Lactate by *Shewanella oneidensis*. *Applied and environmental microbiology*, 78(23), pp.8474–8476.

Bullen, R. a. et al., 2006. Biofuel cells and their development. *Biosensors and Bioelectronics*, 21(11), pp.2015–2045.

Cheng, S. et al., 2009. Direct biological conversion of electrical current into methane by electromethanogenesis. *Environmental science & technology*, 43(10), pp.3953–8.

Cheng, Y., Holman, H. & Lin, Z., 2012. Remediation of Chromium and Uranium Contamination. *Elements*, (April), pp.107–112.

Chistoserdova, L. et al., 2004. Multiple Formate Dehydrogenase Enzymes in the Facultative

Methylotroph *Methylobacterium extorquens* AM1 Are Dispensable for Growth on Methanol. *Journal of bacteriology*, 186(1), pp.22–28.

Choe, H. et al., 2014. Efficient CO2-Reducing Activity of NAD-Dependent Formate Dehydrogenase from *Thiobacillus* sp. KNK65MA for Formate Production from CO_2 Gas. *PloS one*, 9(7), p.e103111.

Coursolle, D. et al., 2010. The Mtr respiratory pathway is essential for reducing flavins and electrodes in *Shewanella oneidensis*. *Journal of bacteriology*, 192(2), pp.467–74.

Crable, B.R. et al., 2011. Formate formation and formate conversion in biological fuels production. *Enzyme research*, 2011, p.532536.

Cruz-García, C. et al., 2011. Fnr (EtrA) acts as a fine-tuning regulator of anaerobic metabolism in *Shewanella oneidensis* MR-1. *BMC microbiology*, 11(1), p.64.

Davies, J.A., Clarke, T.A. & Butt, J.N., 2017. Making Connections: An Amphiphilic Ferrocene Stimulates Bacterial Electricity Production. *Chem*, 2(2), pp.164–167.

Doddema, H. & Vogels, G., 1978. Improved Identification of Methanogenic Bacteria by fluorescenece microscopy. *Applied and environmental microbiology*, 36(5), pp.752–754.

Doud, D.F.R. & Angenent, L.T., 2014. Toward Electrosynthesis with Uncoupled Extracellular Electron Uptake and Metabolic Growth : Enhancing Current Uptake with Rhodopseudomonas palustris. *Environmental Science and Technology Letters*, 56, pp.351–355.

Ducat, D. & Silver, P., 2013. Improving Carbon Fixation Pathways. *Current Opinion In Chemical Biology*, 16, pp.337–344.

Edwards, M.J. et al., 2015. Redox Linked Flavin Sites in Extracellular Decaheme Proteins Involved in Microbe-Mineral Electron Transfer . *Nature Publishing Group*, 5(11677).

Eerten-jansen, M.C.A.A. Van et al., 2012. Microbial electrolysis cells for production of methane from CO2 : long-term performance and perspectives. *International Journal of Energy Research*, 36, pp.809–819.

Erable, B., Etcheverry, L. & Bergel, A., 2011. From microbial fuel cell (MFC) to microbial electrochemical snorkel (MES): maximizing chemical oxygen demand (COD) removal from wastewater. *Biofouling*, 7014(July).

Ernst, M. et al., 2005. Enantioselective reduction of carbonyl compounds by whole-cell biotransformation, combining a formate dehydrogenase and a (R)-specific alcohol dehydrogenase. *Applied microbiology and biotechnology*, 66(6), pp.629–34.

Fourmond, V. et al., 2008. Major Mo(V) EPR signature of *Rhodobacter sphaeroides* periplasmic nitrate reductase arising from a dead-end species that activates upon reduction. Relation to other molybdoenzymes from the DMSO reductase family. *The journal of physical chemistry.*

B, 112(48), pp.15478–86.

Franks, A. & Nevin, K., 2010. Microbial Fuel Cells, A Current Review. *Energies*, pp.899–919.

Fredrickson, J.K. et al., 2008. Towards environmental systems biology of *Shewanella*. *Nature reviews. Microbiology*, 6(8), pp.592–603.

Gao, H. et al., 2010. Physiological Roles of ArcA , Crp , and EtrA and Their Interactive Control on Aerobic and Anaerobic Respiration in *Shewanella oneidensis*. *PloS one*, 5(12).

Gerland, P. et al., 2014. World population stabilization unlikely this century. *Scientific Reports*, 346(6206).

Goli, A. et al., 2016. An overview of biological processes and their potential for CO_2 capture. *Journal of Environmental Management*, 183, pp.41–58.

Graentzdoerffer, A. et al., 2003. Molecular and biochemical characterization of two tungsten- and selenium-containing formate dehydrogenases from *Eubacterium acidaminophilum* that are associated with components of an iron-only hydrogenase. *Archives of Microbiology*, pp.116–130.

Gregory, K.B., Bond, D.R. & Lovley, D.R., 2004. Graphite electrodes as electron donors for anaerobic respiration. *Environmental microbiology*, 6(6), pp.596–604.

Groysman, S. & Holm, R.H., 2007. Synthesis and Structures of Bis (dithiolene) tungsten (IV , VI) Thiolate and Selenolate Complexes : Approaches to the Active Sites of Molybdenum and Tungsten Formate Dehydrogenases. *Inorganic chemistry*, 46(10), pp.1826–1832.

Hanson, A., Gage, D. & Shachar-Hill, Y., 2000. Plant one-carbon metabolism and its engineering. *Trends in plant science*, 1385(1997), pp.81–87.

Hasany, M., Mardanpour, M.M. & Yaghmaei, S., 2016. Biocatalysts in microbial electrolysis cells : A review. *International journal of hydrogen energy*, 41, pp.1477–1493.

Hau, H.H. & Gralnick, J. a, 2007. Ecology and biotechnology of the genus *Shewanella*. *Annual review of microbiology*, 61(August), pp.237–58.

Hindatu, Y., Annuar, M.S.M. & Gumel, A.M., 2017. Mini-review : Anode modification for improved performance of microbial fuel cell. *Renewable and Sustainable Energy Reviews*, 73(June 2015), pp.236–248.

Hunt, K.A. et al., 2010. Substrate-Level Phosphorylation Is the Primary Source of Energy Conservation during Anaerobic Respiration of *Shewanella oneidensis* Strain MR-1. *J. Bacteriol.*, 192(13), pp.3345–3351.

Huugler, M. et al., 2005. Evidence for Autotrophic CO_2 Fixation via the Reductive Tricarboxylic Acid Cycle by Members of the ε Subdivision of Proteobacteria. *Journal of Bacteriology*, 187(9), pp.3020–3027.

Ihara, M. et al., 2013. Light driven CO_2 fixation by using cyanobacterial photosystem I and NADPH-dependent formate dehydrogenase. *PloS one*, 8(8), p.e71581.

Jacques, J.G.J. et al., 2014. Reductive activation in periplasmic nitrate reductase involves chemical modifications of the Mo-cofactor beyond the first coordination sphere of the metal ion. *Biochimica et biophysica acta*, 1837(2), pp.277–86.

Jormakka, M., Törnroth, S., et al., 2002. Molecular basis of proton motive force generation: structure of formate dehydrogenase-N. *Science*, 295(March), pp.1863–1868.

Jormakka, M., Törnroth, S., et al., 2002. Purification and crystallization of the respiratory complex formate dehydrogenase-N from *Escherichia coli*. *Acta Crystallographica Section D: Biological Crystallography*, 58(1), pp.160–162.

Jormakka, M., Byrne, B. & Iwata, S., 2003a. Formate dehydrogenase – a versatile enzyme in changing environments. *Current Opinion in Structural Biology*, 13(4), pp.418–423.

Jormakka, M., Byrne, B. & Iwata, S., 2003b. Protonmotive force generation by a redox loop mechanism. *FEBS Letters*, 545(1), pp.25–30.

Kadier, A. et al., 2016. A comprehensive review of microbial electrolysis cells (MEC) reactor designs and configurations for sustainable hydrogen gas production. *Alexandria Engineering Journal*, 55(1), pp.427–443.

Kane, A.L. et al., 2016. Formate metabolism in *Shewanella oneidensis* generates proton motive force and prevents growth without an electron acceptor. *Journal of Bacteriology*, 198(8), pp.1337–1346.

Kane, A.L., Bond, D.R. & Gralnick, J. a, 2013. Electrochemical analysis of *Shewanella oneidensis* engineered to bind gold electrodes. *ACS synthetic biology*, 2(2), pp.93–101.

Katzberg, M. et al., 2010. Engineering cofactor preference of ketone reducing biocatalysts: A mutagenesis study on a γ-diketone reductase from the yeast *Saccharomyces cerevisiae* serving as an example. *International journal of molecular sciences*, 11(4), pp.1735–58.

Khosravanipour, A. et al., 2017. Microbial electrosynthesis of solvents and alcoholic biofuels from nutrient waste: A review. *Journal of Environmental Chemical Engineering*, 5(1), pp.940–954.

Kouzuma, A. et al., 2015. Catabolic and regulatory systems in *Shewanella oneidensis* MR-1 involved in electricity generation in microbial fuel cells. *Frontiers in Microbiology*, 6(JUN), pp.1–11.

Kumar, R. et al., 2015. Exoelectrogens in microbial fuel cells toward bioelectricity generation : a review. *International journal of energy research*, (February), pp.1048–1067.

Ladapo, J. & Whitman, W.B., 1990. Method for isolation of auxotrophs in the methanogenic archaebacteria : Role of the acetyl-CoA pathway of autotrophic CO_2 fixation in

Methanococcus maripaludis. *Proceedings of the National Academy of Sciences of the United States of America*, 87(August), pp.5598–5602.

Lashof, D.A. & Ahuja, D.R., 1990. Relative contributions of greenhouse gas emissions to global warming. *Nature*, 344(6266), pp.529–531.

Laukel, M. et al., 2003. The tungsten-containing formate dehydrogenase from *Methylobacterium extorquens* AM1: Purification and properties. *European Journal of Biochemistry*, 270(2), pp.325–333.

Leuchtenberger, W., Huthmacher, K. & Drauz, K., 2005. Biotechnological production of amino acids and derivatives: current status and prospects. *Applied microbiology and biotechnology*, 69(1), pp.1–8.

Liang, S. et al., 2009. The roles of outer membrane cytochromes of *Shewanella* and *Geobacter* in extracellular electron transfer. *Environmental microbiology reports*, 1(4), pp.220–7.

Liu, C. et al., 2002. Reduction kinetics of Fe(III), Co(III), U(VI), Cr(VI), and Tc(VII) in cultures of dissimilatory metal-reducing bacteria. *Biotechnology and bioengineering*, 80(6), pp.637–49.

Liu, C. & Mortenson, L., 1984. Formate Dehydrogenase of *Clostridium pasteurianum*. *Journal of bacteriology*, 159(1), pp.375–380.

Logan, B.E., 2009. Exoelectrogenic bacteria that power microbial fuel cells. *Nature Reviews Microbiology*, 7, pp.375–381.

Logan, B.E. et al., 2006. Microbial fuel cells: Methodology and technology. *Environmental Science and Technology*, 40(17), pp.5181–5192.

Lovley, D.R., 2011. Powering microbes with electricity: direct electron transfer from electrodes to microbes. *Environmental microbiology reports*, 3(1), pp.27–35.

Lovley, D.R. & Nevin, K.P., 2011. A shift in the current: new applications and concepts for microbe-electrode electron exchange. *Current opinion in biotechnology*, 22(3), pp.441–8.

Lüke, I. et al., 2008. Biosynthesis of the respiratory formate dehydrogenases from *Escherichia coli* : characterization of the FdhE protein. *Archives of Microbiology*, 190, pp.685–696.

Lum, K., Kamarudi, K. & Daud, W.R.W., 2012. Overview on Dirrect Formic Acid Fuel Cells (DF AFCs) as an Energy Source. *APCBEE Procedia*, 3, pp.33–39.

Magalon, A. et al., 2011. Molybdenum enzymes in bacteria and their maturation. *Coordination Chemistry Reviews*, 255(9–10), pp.1159–1178.

Maia, L.B. et al., 2016. Reduction of Carbon Dioxide by a Molybdenum-Containing Formate Dehydrogenase: A Kinetic and Mechanistic Study. *Journal of the American Chemical Society*, 138(28), pp.8834–8846.

Maia, L.B., Moura, I. & Moura, J.J.G., 2017. Molybdenum and tungsten-containing formate

dehydrogenases: aiming to inspire a catalyst for carbon dioxide utilization. *Inorganica Chimica Acta*, 455(2), pp.350–363.

Maia, L.B., Moura, J.J.G. & Moura, I., 2015. Molybdenum and tungsten - dependent formate dehydrogenases. *J Biol Inorg Chem*, 20, pp.287–309.

Maier, T.M. et al., 2003. Identification of the gene encoding the sole physiological fumarate reductase in *Shewanella oneidensis* MR-1. *J. Basic Microbiol*, 43(4), pp.312–327.

Marritt, S.J., Lowe, T.G. & Bye, J., 2012. A functional description of CymA , an electron- transfer hub supporting anaerobic respiratory flexibility in *Shewanella*. *J. Biochem.*, 444, pp.465–474.

Marsili, E. et al., 2008. *Shewanella* secretes flavins that mediate extracellular electron transfer. *Proceedings of the National Academy of Sciences of the United States of America*, 105(10), pp.3968–73.

McDowall, J.S. et al., 2014. Bacterial formate hydrogenlyase complex. *Proceedings of the National Academy of Sciences of the United States of America*, 111(38), pp.E3948-56.

Menicucci, J. et al., 2006. Procedure for determining maximum sustainable power generated by microbial fuel cells. *Environmental science & technology*, 40(3), pp.1062–8.

Meshulam-Simon, G. et al., 2007. Hydrogen metabolism in *Shewanella oneidensis* MR-1. *Applied and environmental microbiology*, 73(4), pp.1153–65.

Mordkovich, N.N. et al., 2013. Effect of NAD+-dependent formate dehydrogenase on anaerobic respiration of *Shewanella oneidensis* MR-1. *Microbiology*, 82(4), pp.404–409.

Mota, C.S. et al., 2011. Effects of Molybdate and Tungstate on Expression Levels and Biochemical Characteristics of Formate Dehydrogenases Produced by *Desulfovibrio alaskensis* NCIMB 13491. *Journal of Bacteriology*, 193(12), pp.2917–2923.

Moura, J.J.G. et al., 2004. Mo and W bis-MGD enzymes: nitrate reductases and formate dehydrogenases. *Journal of biological inorganic chemistry*, 9(7), pp.791–9.

Nevin, K.P. et al., 2011. Electrosynthesis of Organic Compounds from Carbon Dioxide Is Catalyzed by a Diversity of Acetogenic Microorganisms □. *Applied and environmental microbiology*, 77(9), pp.2882–2886.

Nevin, K.P. et al., 2010. Microbial Electrosynthesis : Feeding Microbes Electricity to Convert carbon Dioxide and Water to Multi Carbon Extracellular Organic Compounds. *mBio*, 1(January), pp.e00103-10.

Nikolaidis, P. & Poullikkas, A., 2017. A comparative overview of hydrogen production processes. *Renewable and Sustainable Energy Reviews*, 67, pp.597–611.

Niks, D. et al., 2016. Spectroscopic and Kinetic Properties of the Molybdenum- containing , NAD+

-dependent Formate Dehydrogenase from *Ralstonia eutropha*. *The Journal of biological chemistry*, 291(3), pp.1162–1174.

Olson, B.J.S.C. et al., 2000. Formate dehydrogenase in *Arabidopsis thaliana*: characterization and possible targeting to the chloroplast. *Plant Science*, 159(2), pp.205–212.

Pant, D. et al., 2012. Bioelectrochemical systems (BES) for sustainable energy production and product recovery from organic wastes and industrial wastewaters. *RSC Advances*, 2, pp.1248–1263.

Panwar, N.L., Kaushik, S.C. & Kothari, S., 2011. Role of renewable energy sources in environmental protection: A review. *Renewable and Sustainable Energy Reviews*, 15(3), pp.1513–1524.

Park, D.H. & Zeikus, J.G., 2000. Electricity Generation in Microbial Fuel Cells Using Neutral Red as an Electronophore. *Applied and Environmental Microbiology*, 66(4), pp.1292–1297.

Parkin, A. et al., 2007. Rapid and Efficient Electrocatalytic CO_2 / CO Interconversions by *Carboxydothermus hydrogenoformans* CO Dehydrogenase I on an Electrode. *Journal of the American Chemical Society*, 129, pp.10328–10329.

Parkinson, B. & Weaver, P., 1984. Photoelectrochemical pumping of enzymatic CO_2 reduction. *Letters to Nature*, 309(10), pp.148–9.

Pinchuk, G.E. et al., 2009. Genomic reconstruction of *Shewanella oneidensis* MR-1 metabolism reveals a previously uncharacterized machinery for lactate utilization. *Proceedings of the National Academy of Sciences of the United States of America*, 106(8), pp.2874–2879.

Pinchuk, G.E. et al., 2011. Pyruvate and lactate metabolism by *Shewanella oneidensis* MR-1 under fermentation, oxygen limitation, and fumarate respiration conditions. *Applied and environmental microbiology*, 77(23), pp.8234–40.

Pinske, C. & Sargent, F., 2016. Exploring the directionality of *Escherichia coli* formate hydrogenlyase : a membrane- - bound enzyme capable of fixing carbon dioxide to organic acid. *MicrobiologyOpen*, 5(5), pp.721–737.

Potter, M.C., 1911. Electrical Effects Accompanying the Decomposition of Organic Compounds. *Proceedings of the Royal Society B: Biological Sciences*, 84(571), pp.260–276.

Qian, Y. et al., 2011. Mapping the iron binding site(s) on the small tetraheme cytochrome of Shewanella oneidensis MR-1. *Biochemistry*, 50(28), pp.6217–24.

Raaijmakers, H., Macieira, S. & Dias, J., 2002. Gene Sequence and the 1.8 Å Crystal Structure of the Tungsten-Containing Formate Dehydrogenase from *Desulfovibrio gigas*. *Structure*, 10(2), pp.1261–1272.

Raaijmakers, H.C.A. & Romao, M., 2006. Formate-reduced *E . coli* formate dehydrogenase H : the reinterpretation of the crystal structure suggests a new reaction mechanism. *J Biol Inorg*

Chem, 11, pp.849–854.

Rabaey, K. & Rozendal, R. a, 2010. Microbial electrosynthesis - revisiting the electrical route for microbial production. *Nature reviews. Microbiology*, 8(10), pp.706–16.

Ragsdale, S.W. & Pierce, E., 2008. Acetogenesis and the Wood-Ljungdahl Pathway of CO_2 Fixation. *Biochimica et Biophysica Acta*, 1784(12), pp.1873–1898.

Rahimnejad, M., Bakeri, G. & Ghasemi, M., 2014. A review on the role of proton exchange membrane on the performance of microbial fuel cell. *Polymers advanced technologies*, 25, pp.1426–1432.

Recio-garrido, D., Perrier, M. & Tartakovsky, B., 2016. Modeling , optimization and control of bioelectrochemical systems. *Chemical Engineering Journal*, 289, pp.180–190.

Reda, T. et al., 2008. Reversible interconversion of carbon dioxide and formate by an electroactive enzyme. *Proceedings of the National Academy of Sciences of the United States of America*, 105(31), pp.10654–8.

Richardson, D.J. et al., 2012. Exploring the biochemistry at the extracellular redox frontier of bacterial mineral Fe(III) respiration. *Biochemical Society transactions*, 40(3), pp.493–500.

Rosenbaum, M.A. & Henrich, A.W., 2014. Engineering microbial electrocatalysis for chemical and fuel production. *Current opinion in biotechnology*, 29, pp.93–98.

Ross, D.E. et al., 2011. Towards electrosynthesis in *Shewanella*: energetics of reversing the mtr pathway for reductive metabolism. *PloS one*, 6(2), p.e16649.

Rossmann, R., Sawers, G. & Böck, A., 1991. Mechanism of regulation of the formate-hydrogenlyase pathway by oxygen, nitrate, and pH: definition of the formate regulon. *Molecular microbiology*, 5(11), pp.2807–14.

Ruschig, U. et al., 1976. CO_2 reduction to formate by NADH catalysed by formate dehydrogenase from *Pseudomonas oxalaticus*. *European journal of biochemistry / FEBS*, 70(2), pp.325–330.

Sadhukhan, J. et al., 2016. A critical review of integration analysis of microbial electrosynthesis (MES) systems with waste biorefineries for the production of biofuel and chemical from reuse of CO2. *Renewable and Sustainable Energy Reviews*, 56, pp.116–132.

Saeed, H.M. et al., 2015. Microbial desalination cell technology : A review and a case study. *Desalination*, 359, pp.1–13.

Sakakibara, Y. & Kuroda, M., 2004. Electric Prompting and Control of Denitrification. *Biotechnology and Bioengineering*, 42(4), pp.535–537.

Santoro, C. et al., 2017. Microbial fuel cells : From fundamentals to applications . A review. *Journal of Power Sources*, 356, pp.225–244.

Sawers, G., 1994. The hydrogenases and formate dehydrogenases of *Escherichia coli*. *Antonie van*

Leeuwenhoek, 66(1–3), pp.57–88.

Schauer, N.L. & Ferry, J.G., 1980. Metabolism of Formate in *Methanobacterium formicicum*. *Journal of Bacteriology*, 142(3), pp.800–807.

Schlindwein, C., Giordano, G. & Santini, C., 1990. Identification and Expression of the *Escherichia coli* fdhD and fdhE Genes , Which Are Involved in the Formation of Respiratory Formate Dehydrogenase. *J. Bacteriol.*, 172(10), pp.6112–6121.

Schuchmann, K. & Müller, V., 2013. Direct and Reversible Hydrogenation of CO_2 to Formate by a Bacterial Carbon Dioxide Reductase. *Science*, 342(December), pp.1382–1386.

Scott, J.H. & Nealson, K.H., 1994. A biochemical study of the intermediary carbon metabolism of *Shewanella putrefaciens*. *Journal of bacteriology*, 176(11), pp.3408–11.

Serres, M.H. & Riley, M., 2006. Genomic analysis of carbon source metabolism of *Shewanella oneidensis* MR-1: Predictions versus experiments. *Journal of bacteriology*, 188(13), pp.4601–9.

Sharma, M. et al., 2014. A critical revisit of the key parameters used to describe microbial electrochemical systems. *Electrochimica Acta*, 140, pp.191–208.

Shin, W. et al., 2003. Highly Selective Electrocatalytic Conversion of CO_2 to CO at - 0 . 57 V (NHE) by Carbon Monoxide Dehydrogenase from *Moorella thermoacetica*. *Journal of the American Chemical Society*, pp.14688–14689.

Silva, S.M. da et al., 2011. Tungsten and molybdenum regulation of formate dehydrogenase expression in *Desulfovibrio vulgaris Hildenborough*. *Journal of bacteriology*, 193(12), pp.2909–16.

Slusarczyk, H. et al., 2000. Stabilization of NAD-dependent formate dehydrogenase from *Candida boidinii* by site-directed mutagenesis of cysteine residues. *European Journal of Biochemistry*, 267(5), pp.1280–1289.

Smart, J.P., Cliff, M.J. & Kelly, D.J., 2009. A role for tungsten in the biology of *Campylobacter jejuni*: tungstate stimulates formate dehydrogenase activity and is transported via an ultra-high affinity ABC system distinct from the molybdate transporter. *Molecular microbiology*, 74(3), pp.742–57.

Sousa, P.M.F. et al., 2011. Supramolecular organizations in the aerobic respiratory chain of *Escherichia coli*. *Biochimie*, 93(3), pp.418–25.

Stams, A.J.M. & Plugge, C.M., 2009. Electron transfer in syntrophic communities of anaerobic bacteria and archaea. *Nature Reviews Microbiology*, 7(august), pp.568–577.

Strik, D.P.B.T.B. et al., 2011. Microbial solar cells : applying photosynthetic and electrochemically active organisms. *Trends in Biotechnology*, 29(1), pp.41–49.

Strycharz, S.M. et al., 2011. Gene expression and deletion analysis of mechanisms for electron transfer from electrodes to *Geobacter sulfurreducens*. *Bioelectrochemistry (Amsterdam, Netherlands)*, 80(2), pp.142–50.

Summers, Z.M., Gralnick, J. a & Bond, D.R., 2013. Cultivation of an obligate Fe(II)-oxidizing lithoautotrophic bacterium using electrodes. *mBio*, 4(1), pp.e00420-12.

Suntres, Z.E., 2002. Role of antioxidants in paraquat toxicity. *Toxicology*, 180, pp.65–77.

Thrash, J.C. et al., 2007. Electrochemical Stimulation of Microbial Perchlorate Reduction. *Environ. Sci. Technol.*, 41(5), pp.1740–1746.

Tishkov, V. et al., 1993. Catalytic Properties and Stability of a Pseudomonas sp. 101 Formate Dehydrogenase Mutants Containing Cys-255-Ser and Cys-255-Met Replacements. *Biochemical and Biophysical Research Communications*, 192(2), pp.976–981.

Tishkov, V. & Popov, V., 2004. Catalytic mechanism and application of formate dehydrogenase. *Biochemistry (Moscow)*, 69(11), pp.1252–1267.

Wang, H. & Gunsalus, R., 2003. Coordinate regulation of the *Escherichia coli* formate dehydrogenase fdnGHI and fdhF genes in response to nitrate, nitrite, and formate: roles for NarL and NarP. *Journal of bacteriology*, 185(17), pp.5076–5085.

Wang, H. & Ren, Z.J., 2013. A comprehensive review of microbial electrochemical systems as a platform technology. *Biotechnology Advances*, 31(8), pp.1796–1807.

Wang, V.B. et al., 2013. Engineering PQS biosynthesis pathway for enhancement of bioelectricity production in *Pseudomonas aeruginosa* microbial fuel cells. *PloS one*, 8(5), p.e63129.

Yarzábal, A. et al., 2002. The High-Molecular-Weight Cytochrome c Cyc2 of Acidithiobacillus ferrooxidans Is an Outer Membrane Protein. *J. Bacteriol.*, 184(1), pp.313–317.

Yi-chi, Z., Zhao-hong, J. & Ying, L.I.U., 2015. Application of Electrochemically Active Bacteria as Anodic Biocatalyst in Microbial Fuel Cells. *Chinese Journal of Analytical Chemistry*, 43(1), pp.155–163.

Yoch, D.C. & Carithers, R.P., 1979. Bacterial Iron-Sulfur Proteins. *Microbiological reviews*, 43(3), pp.384–421.

Yu, X. et al., 2017. Efficient reduction of CO_2 by the molybdenum-containing formate dehydrogenase from *Cupriavidus necator* (*Ralstonia eutropha*). *Journal of Biological Chemistry*, pp.1–20.

Yutin, N. & Galperin, M., 2013. A genomic update on clostridial phylogeny: Gram-negative spore-formers and other misplaced *Clostridia*. *Environmental microbiology*, 15(10), pp.2631–2641.

Zelcbuch, L. et al., 2016. Pyruvate Formate-Lyase Enables Efficient Growth of *Escherichia coli* on Acetate and Formate. *Biochemistry*, 55, pp.2423–2426.

2 Materials and methods

2.1 Buffer preparation

All buffer components were purchased from Sigma™ and buffers made using analytical grade water (Fisher). Adjustments to pH were made using 10 M HCl in small additions until the correct pH was determined by pH electrode (VWR International). All buffers were then vacuum filtered through 0.2 μM filters (Sartorius) to remove insoluble material.

2.2 Minimal media composition

For metal dependent experiments a minimal medium was used. To prevent metal contamination analytical grade water and acid washed glassware/equipment were used for media preparation, 50% Nitric acid was used, followed by three thorough rinses with analytical water. Disposable plastic alternatives to glassware were used to reduce contamination risk where possible.

Basal medium containing 0.46 g/L NH_4Cl, 0.225 g/L K_2HPO_4, 0.225 g/L KH_2PO_4, 0.117 g/L $MgSO_4$, 1 g/L DL-Serine, 1 g/L DL-Arginine, 1 g/L DL-Glutamine, 23.83 g/L HEPES, 3.4 g/L Na Formate and 8 g/L Na Fumarate was adjusted to pH 7.2 using NaOH before autoclaving. Subsequently filter sterilised vitamin and mineral mixes were added at 5 ml/L, these were not autoclaved to avoid precipitation.

Vitamin mix; 0.002 g/L Biotin, 0.002 g/L Folic acid, 0.02 g/L pyridoxine HCl, 0.005 g/L Thiamine, 0.005 g/L Nicotinic acid, 0.005 g/L Pantothenic acid, 0.0001 g/L Vitamin B12, 0.005 g/L p-aminobenzoic acid, 0.005 g/L thioctic acid.

Mineral mix; 1.5 g/L Nitrilotriacetic acid, 0.1 g/L $MnCl_2$, 0.3 g/L $FeSO_4$, 0.17 g/L $CoCl_2$, 0.1 g/L $ZnCl_2$, 0.04 g/L $CuSO_4$, 0.005 g/L $AlK(SO_4)_2$, 0.12 g/L $NiCl_2$, 0.1 g Na_2SeO_4, 0.005 g/L H_3BO_3.

Filter sterile 1.5 mM or 15 mM solutions of Na tungstate and Na molybdate were used to supplement media as required by specific experiments. Such additions did not alter the pH of the media, even at high concentrations.

Unless stated otherwise all references to minimal media experiments in subsequent text refer to those using the above growth medium. A summary table including final concentrations of all components is included for ease of reference.

Table 2-1 Composition of minimal media used in this work.

Component	Final concentration in mM
HEPES	100.00
Na Formate	50.00
Na Fumarate	50.00
DL-Serine	9.52
DL-Arginine	5.75
DL-Glutamine	6.85
NH_4Cl	8.68
K_2HPO_4	1.29
KH_2PO_4	1.65
$MgSO_4$	0.98
Mineral Component	**Final concentration in µM**
Nitrilotriacetic acid	39.27
Na_2SeO_4	2.65
$MnCl_2$	11.90
$FeSO_4$	5.59
$CoCl_2$	3.85
$ZnCl_2$	3.68
$CuSO_4$	1.26
$AlK(SO_4)_2$	0.10
$NiCl_2$	4.62
H_3BO_3	0.40
Na_2WO_4	As specified
Na_2MoO_4	As specified
Vitamin Component	**Final concentration in nM**
Thiamine (B1)	94
Nicotinic acid (B3)	203
Pantothenic acid (B5)	2
Pyridoxine HCl (B6)	147
Biotin (B7)	40
Folic acid (B9)	226
Cobalamin (B12)	18
p-Aminobenzoic acid	182
Thioctic acid	121

2.3 Bacterial strains

A list of the strains used in this thesis including origin and genotype is presented in Table 2-2.

All mutants in this study were created using in frame deletion mutagenesis as routinely described for *Shewanella* (Saltikov & Newman 2003). Briefly, all mutant strains were generated by amplification of approximately 1kb flanking regions upstream and downstream of a deletion target, which when combined in a crossover fusion PCR and cloned into a suicide vector (pSMV3) (Kane et al. 2016) or (pDS3.1) (LS527). Conjugation into *S.oneidensis* allowed for screening of homologous recombinants where the wild type version of a gene was replaced by the truncated version on the suicide plasmid. All mutants used in this work are in frame deletion mutants verified by sequencing. These strains were not generated as part of this work and their origins are detailed in Table 2-2.

Table 2-2 Bacterial strains used during this thesis.
Where Pacific Northwest National Laboratory refers to those strains provided by the group of Dr Liang Shi in Washington, now at Wuhan University.

Strain	Genotype	Origin
Shewanella oneidensis MR-1	Wild Type	(Richardson et al. 2012)
Shewanella oneidensis MR-1 (ΔFdh1)	ΔSO_4509-4511	(Kane et al. 2016)
Shewanella oneidensis MR-1 (ΔFdh2)	ΔSO_4513-4515	(Kane et al. 2016)
Shewanella oneidensis MR-1 (ΔFdn)	ΔSO_0101-0103	(Kane et al. 2016)
Shewanella oneidensis MR-1 (Fdh1+)	ΔSO_0101-0103 ΔSO_4513-4515	(Kane et al. 2016)
Shewanella oneidensis MR-1 (Fdh2+)	ΔSO_0101-0103 ΔSO_4509-4511	(Kane et al. 2016)
Shewanella oneidensis MR-1 (Fdn+)	ΔSO_4509-4511 ΔSO_4513-4515	(Kane et al. 2016)
Shewanella oneidensis MR-1 (ΔFDH)	ΔSO_0101-0103 ΔSO_4509-4511 ΔSO_4513-4515	(Kane et al. 2016)

Strain	Genotype	Origin
Shewanella oneidensis MR-1 (LS527)	ΔSO_1776 (mtrB) ΔSO_1777 (mtrA) ΔSO_1778 (mtrC) ΔSO_1779(omcA) ΔSO_1780(mtrF) ΔSO_1781 (mtrE) ΔSO_1782 (mtrD)	Pacific Northwest National Laboratory
Shewanella amazonensis SB2B	Wild Type	Pacific Northwest National Laboratory
Shewanella baltica OS185	Wild Type	Pacific Northwest National Laboratory
Shewanella baltica OS195	Wild Type	Pacific Northwest National Laboratory
Shewanella baltica OS223	Wild Type	Pacific Northwest National Laboratory
Shewanella loihica PV4	Wild Type	Pacific Northwest National Laboratory
Shewanella putrifaciens 200	Wild Type	Pacific Northwest National Laboratory
Shewanella putrifaciens CN-32	Wild Type	Pacific Northwest National Laboratory
Shewanella putrifaciens W3-18-1	Wild Type	Pacific Northwest National Laboratory
Shewanella sp. ANA-3	Wild Type	Pacific Northwest National Laboratory
Shewanella oneidensis MR-4	Wild Type	Pacific Northwest National Laboratory
Shewanella oneidensis MR-7	Wild Type	Pacific Northwest National Laboratory

2.4 *Shewanella* growth in minimal media

Single bacterial colonies from LB-agar plates were inoculated into 100 ml LB liquid cultures grown aerobically at 30°C with agitation. After 24 h 50 ml aliquots of cultures were centrifuged at 5540 x g for 15 min. Cell pellets were then washed thrice, each wash consisting of centrifugation at 5540 x g for 15 min followed by resuspension in 25 ml of basal medium in an attempt to prevent metal introduction from inoculum.

After the final wash each 50 ml pellet was re-suspended in 5 ml of basal media. These were then diluted to an OD_{600} of 8 using additional basal media. 2 ml/L was then used to inoculate minimal media growth experiments (i.e. a 2 % inoculum). Experiments monitoring growth were conducted in 500 ml Durans with septum sealed lids that could be pierced to take samples to determine OD_{600} readings. The same lids were used for 1 L or 5 L Duran growths for protein purifications.

Once inoculated, each Duran was sparged with N_2 gas passed through a 0.45 μm filter and a needle submerged in the media for 10 min to remove oxygen from the headspace of the Duran and promote anaerobicity. Durans were then incubated at 30°C without agitation for 10/24 h for RNA extraction/colorimetric assay analysis respectively.

2.5 *Shewanella* growth in LB

Lysogeny broth was prepared from premixed powder (Formedium) of which 25 g was dissolved per litre of distilled water. Once prepared, the media contained 10 g/L tryptone, 10 g/L NaCl and 10 g/L yeast extract.

Single bacterial colonies from LB-agar plates were inoculated into 100 ml LB liquid cultures grown aerobically at 30°C with agitation or anaerobically as described below.

Experiments monitoring anaerobic growth were conducted in 500 ml Durans with septum sealed lids that could be pierced to take samples to determine OD_{600} readings. Note sodium fumarate was supplemented at 50 mM to act as a terminal electron acceptor in these experiments. Once inoculated each Duran was sparged with N_2 gas passed through a 0.45 μm filter and a needle

submerged in the media for 10 min to remove oxygen from the headspace of the Duran and promote anaerobicity. Durans were then incubated at 30°C without agitation for 24 h.

2.6 Bacterial growth analysis

Analysis of growth curves in Chapter 5 was performed by determining three parameters for each growth trace, corresponding to lag, exponential and stationary phases of growth (Zwietering et al. 1990). An example trace analysis is shown in Figure 2-1.

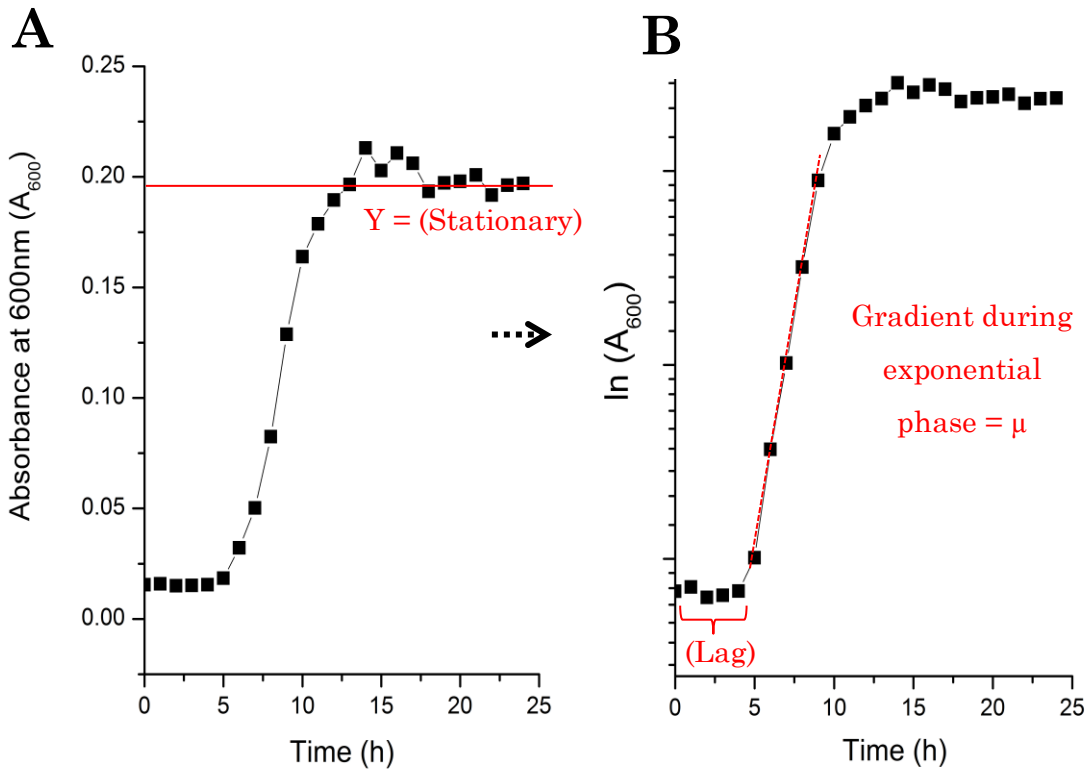

Figure 2-1 Example of growth curve analysis.
(A) *Data plotted on linear axis demonstrating calculation of absorbance during stationary phase ($A_{Stationary}$). A semi-log plot (B) is then used for determination of both lag phase duration and specific growth rate (μ) where μ equals the gradient of a linear trend line fitted through points during exponential growth.*

The average absorbance during stationary phase ($A_{stationary}$) was determined by the mean absorbance at 600 nm for the last five time points during stationary phase. For those traces which did not enter stationary phase during the 24 h duration of the experiment instead the final absorbance value at 24 h is presented. Population size is taken to be equivalent to turbidity in these

experiments, a common and established approach (Monod 1949) but which could be complimented with alternative metrics (cfu/ml) that take into consideration the viability of the cells within the cultures (Owens & Legan 1987).

Parameters for both lag and exponential phases were analysed by use of a semi-log plot, where the natural logarithm of the absorbance at 600nm is plotted against time (Figure 2-1). The duration of the lag phase was defined by the length of time in hours where changes in OD_{600} were not detected prior to entering exponential growth.

To report on the exponential phase of growth, specific growth rates (μ) were calculated by determining the gradient of a linear trendline during exponential growth, typically seen between 5 and 10 h of growth. Such specific growth rates were also used to study growth kinetics (Owens & Legan 1987) as detailed in the next section.

2.7 Monod constant determination

Specific growth rates (μ) were determined in triplicate for each concentration of formate investigated. The resultant data were plotted and fitted by OriginPro 8.5 software to the Nonlinear curve fit:Hyperbl function, to represent the Monod eq. below (2.1):

$$\mu = \mu_{max} \frac{S}{K_s + S} \tag{2.1}$$

Where μ_{max} is the maximum specific growth rate, S is the substrate (formate) concentration, and K_s is the half velocity or Monod constant (Owens & Legan 1987).

2.8 ICP analysis

A quadrupole based ICP mass spectrometer, Thermo Elemental X Series 1 (Thermo Scientific, Bremen, Germany) equipped with Peltier impact bead spray chamber, glass expansion concentric nebuliser, Cetac ASX 520 auto sampler and Plasma lab Software was used for ICP-MS measurements. ICP-MS measurements were carried out using the standard mode with Xi cones. Elements that were measured: 98 Mo, 186 W. All standards and samples were measured in triplicate, with relative standard deviations lower than 2%.

2.9 Polymerase chain reaction

MyTaq™ DNA polymerase (Bioline) was used for low fidelity PCR amplification. Each 20 µl reaction was prepared on ice and contained 10 µl Mytaq polymerase master mix (2x), 8.2 µl of nuclease free water, 0.4 µl of Forward primer (20 µM) and 0.4 µl of Forward primer (20 µM) and 1 µl of DNA template (100 ng/µl). A PCR program was run using a TC-512 Thermal cycler (Techne) consisting of an initial denaturation step at 95°C for 120 s. This was followed by 35 cycles of denaturation at 95°C for 15 s, template annealing at 59°C for 15 s and polymerase extension at 72°C for 10 s. A final extension step at 72°C for 300 s completed the program and the resultant product was visualised using agarose gel electrophoresis.

2.10 Agarose gel electrophoresis

DNA was visualised using agarose gel electrophoresis, the negatively charged phosphate backbone of DNA causes it to migrate to the anode in an applied electric field whilst the physical properties of the gel cause slower migration of larger DNA fragments allowing size separation. Agarose gels, 1% (w/v) were made by melting 1.2 g of agarose in 120 ml TAE buffer (45 mM Tris-acetate, 1 mM EDTA, pH 8.0). When cool enough to avoid evaporation, 10 µl of 10 mg/ml ethidium bromide (Sigma-Aldrich) was added for DNA visualisation. Loading dye, (40% sucrose (w/v), 20% Orange G (w/v) 40% H_2O) was mixed 1:10 with DNA before loading on gel. Hyperladder™ 1 kb (Bioline) was run on all gels for size identification. A voltage of 120 V was applied across the gel submerged in

TAE buffer and once complete a BioRad Gel Doc XR UV transilluminator and BioRad Quantity One imaging software were used for visualisation.

2.11 Genomic DNA extraction

Genomic DNA extraction from WT *Shewanella oneidensis* MR-1 was performed using a QIAGEN Genomic prep kit according to the manufacturer's instructions, DNA was notably eluted in nuclease free water, not the provided elution buffer, to avoid interference with subsequent analysis. DNA was extracted from bacterial culture derived from a single bacterial colony from an LB-agar plate inoculated into 10 ml LB liquid culture grown aerobically at 30°C with agitation for 24 h.

2.12 RNA extraction

Throughout the entire RNA extraction meticulously clean working conditions were maintained to prevent RNAse contamination. All surfaces and equipment were regularly cleaned with both Distel detergent (Tristel solutions) and RNase Zap™ (Ambion) and filtered pipette tips were used exclusively (TipOne® range from Starlab).

Cells were harvested at mid-exponential growth for RNA extraction, as determined from previous growth studies, typically upon reaching an OD_{600} of 0.1. A 50 ml aliquot of culture was centrifuged at 5540 x g for 15 min at 4°C before being added to a pestle and mortar filled with liquid nitrogen and surrounded by solid carbon dioxide. The pellet was then ground to a fine dust in the mortar before allowing the liquid nitrogen to evaporate and being transferred to a 50 ml falcon tube. TRI reagent (Sigma) was added at 2 ml per 50 ml pellet followed by 0.4 ml chloroform (99.99% purity) the mix was then vortexed for 15 s before centrifugation at 18000 x g for 10 min in a 5424 microcentrifuge (*Eppendorf*). The upper aqueous phase was then collected. Direct-zol RNA extraction kit (Zymo Research) was then used according to the manufacturer's instructions, including a DNase treatment step using TURBO-DNase (Ambion). RNA was eluted in nuclease free water to avoid interference with subsequent analysis.

RNA quality and quantity were then confirmed using a combination of nanodrop (Nanodrop One, ThermoScientific), Experion automated electrophoresis (according to manufacturer's instructions) and PCR (described above) using primers for the constitutively expressed MtrA (SO_1777) to confirm absence of gDNA. Primers used:

Table 2-3 PCR primers for SO_1777 fragment used as gDNA marker

Forward primer	5' AAGAACTGCCTAAAAATGAAAAACCTA 3'
Reverse primer	5' GCGCTGTAATAGCTTGCCA 3'

2.13 Reverse Transcription

All reagents supplied as part of SuperScript™ II Reverse Transcripase kit (Invitrogen). RNA (2 µg) in 11 µl nuclease free water was combined with 1 µl 10 mM dNTPs and 1 µl Random primers (300 ng/µl) before incubation 5 min at 65°C, followed by 1 min on ice. To each reaction 4 µl 5x First strand buffer and 2 µl 0.1M Dithiothreitol were added. Reaction was then incubated at 25°C for 2 min before adding 1 µl Superscript™ II reverse transcriptase. Incubation steps at 25°C for 12 min, 42°C for 50 min and 70°C for 15 min followed using a TC-512 Thermal cycler (Techne). After a final 2 min on ice, 180µl nuclease free water was added to each reaction to complete cDNA preparation.

2.14 RT-qPCR

Real time quantitative PCR (Rt-qPCR) was performed using an AriaMx Real-Time PCR system (Aligent technologies). Each 20 µl reaction contained 10 µl SensiFAST mix (Bioline), 8.2 µl nuclease free water, 0.4 µl 20 µM Forward primer, 0.4 µl 20 µM Reverse primer and 1 µl of template. The template was either cDNA, one of a series of dilutions of gDNA (100 ng/µl – 0.1 ng/µl), water in the case of a no template control (NTC) or mRNA in the case of a reverse transcriptase control (RT). 96-well full-skirt plates (Bioline) were used for Real time PCR reactions, sealed with multi-well caps (Bioline) and kept on ice throughout preparation to avoid RNA degradation. The PCR program used consisted of an initial denaturation step at 95°C for 3 min, followed by 40 cycles of 95°C for 5 s, 60°C for 10 s, and 72°C for 5 s. During the run the system was set

to detect the florescence emitted by the SYBER Green dye as it intercalated in the accumulating double stranded DNA.

Note that each gene investigated, including the housekeeping gene RecA, required a distinct set of primers, detailed in Table 2-4.

Table 2-4 RT-qPCR primers for cDNA amplification

Primer name	Primer sequence
SO_0101 Forward primer	5' GCATTCCTTCTGGGTGTGAT 3'
SO_0101 Reverse primer	5' GAGAATAGGCCGTCATGGAA 3'
SO_4509 Forward primer	5' GCGACCCAATTTGAAACCTA 3'
SO_4509 Reverse primer	5' CAATCCCCACCTTTTTAGCA 3'
SO_4513 Forward primer	5' CGTAAAAACGGCGTGTACCT 3'
SO_4513 Reverse primer	5' AGATTCGAATAGCGGCTGAA 3'
SO_3430 (RecA) Forward primer	5' AACCCAGAAACCACAACG 3'
SO_3430 (RecA) Reverse primer	5' ACCAACCACCTCATCACC 3'

To analyse the resultant data, standard curves were constructed for each investigated gene by plotting C_t against gDNA concentration. C_t is defined as the PCR cycle number when florescence exceeds an arbitrary threshold value. From these calibration curves, the gradients were used to determine primer pair efficiencies. All primer pairs used in the following work had primer efficiencies between 96% and 100% allowing qualitative comparisons. C_t values for unknown samples could then be used to interpolate a quantity of cDNA for each gene. These absolute quantification values were then normalised to the housekeeping gene RecA and the relative expression presented for discussion.

2.15 Cell preparation/quantification for colourimetric assays.

To prepare culture samples for assay analysis, 50 ml of culture grown for 24 h in either LB or minimal media were centrifuged at 5540 x g for 15 min. Cell pellets were then washed thrice, each wash consisting of centrifugation at 5540 x g for 15 min followed by resuspension in 2 ml of 100 mM HEPES pH7.2 to clean the cells and remove metabolites. After the final wash cell pellets were either flash frozen at -80°C for later use or for immediate use resuspended in 1ml of 100 mM

HEPES pH7.2. This preparation was used when describing whole cell samples in subsequent colourimetric assays.

Pellets, rather than cell suspensions, were flash frozen in liquid nitrogen, as when frozen in solution noticeable decreases in specific activity were observed. Note that lysed and fractionated samples were not suitable for frozen storage as evident by decreased FDH activities.

2.16 Cell lysis - Sonication

After preparatory washes described above, 25 µl of EDTA free protease inhibitor cocktail (Roche), made from 1 tablet dissolved in 10 ml of distilled water was added to prevent subsequent protein degradation. Cells were then sonicated (SONICS Vc50) on ice for 40 s in 10 s bursts (25 Watts) to prevent heat denaturation. Samples were kept on ice where possible after this step to try and limit degradation.

2.17 Membrane separation for enzymatic localisation studies.

Following cell lysis by sonication described above, membrane components were ultracentrifuged at 205,076 x g (42000 rpm) for 2 h (45Ti rotor, Beckman Optima XL-100k). The supernatant was retained and represents the soluble cellular fractions whilst the pelleted components represent membrane containing fractions.

2.18 BCA assay

To determine protein concentration, BCA reagent (*Sigma*) was used according to the manufacturer's instructions. To do this, 25 ml of BCA reagent A was combined with 500 µl 4% (w/v) copper (II) sulphate pentahydrate solution to make a working reagent. 200 µl of this was combined with 25 µl of either BSA standard or unknown sample and incubated at 37°C for 30 min for the colorimetric change to develop. Unknown samples were run in quadruplet at two different dilutions to ensure consistent estimations. The absorbance at 562 nm was then recorded using a plate reader (FLUOstar Omega, BMG Labtech) in a Nunc™ 96-Well Polypropylene MicroWell™ plate (ThermoFisher Scientific) without lid to avoid condensation issues. A 6 point standard curve was

generated using a serial dilution in the range of 1-0 mg/ml of BSA. This produced a standard curve with an R^2 value over 0.99. Unknown protein concentrations were then interpolated from the standard curve. Note when determining protein concentration in whole cell samples, these were first lysed via sonication as described in 2.16.

2.19 Bradford assay

As a complementary technique to the BCA assay, Bradford reagent (BioRad) was used according to the manufacturer's instructions. A standard curve was first generated using a serial dilution with a top standard of 10 µg ranging down to 1 µg lysozyme, each standard was measured in triplicate. This produced a standard curve with an R^2 value over 0.99. Unknown samples were then analysed in triplicate at two different volumes to ensure consistent estimations. All Bradford assays were either run in 1.1 ml volumes in 1.5 ml cuvettes; 1 ml Bradford reagent, 100 µl sample, or in a 96 well plate using a volume of 210 µl; 200 µl Bradford reagent, 10 µl sample. Regardless of scale, absorbance at 595nm was recorded and protein concentrations interpolated from the standard curve.

2.20 FDH activity assay.

Assays were conducted in 4 ml glass cuvettes containing 1940 µl of 100 mM HEPES pH 7.2, 10 µl 100 mM methyl viologen (Final: 0.5 mM) and 40 µl of sample prepared as described above (either whole cells, lysed cells or cellular fractions). Each cuvette was then sealed with a no.9 suba seal and three layers of parafilm. Each cuvette was then sparged for 25 min under a N_2 atmosphere to remove any atmospheric oxygen. The cuvette was then inverted 5 times and absorbance measured at 578 nm for 600 s with a 0.2 s interval between measurements in a spectrophotometer (Hitachi U-3310). For the first 100 s the background absorbance change was observed, After 100 s, 10 µl of 2 M Na formate solution (Final: 10 mM) was added to the cuvette (which was taken out and inverted 5 times before being returned. Note with substrate final reaction volume was 2 ml. If FDH activity was present the absorbance at 578 nm rose after substrate addition, the gradient of this first linear section of increasing absorbance is referred to as an initial rate (v_0) which can be used in a variety of

ways, either comparatively or to establish kinetic constants. A typical data plot for formate oxidation is seen in Figure 2-2.

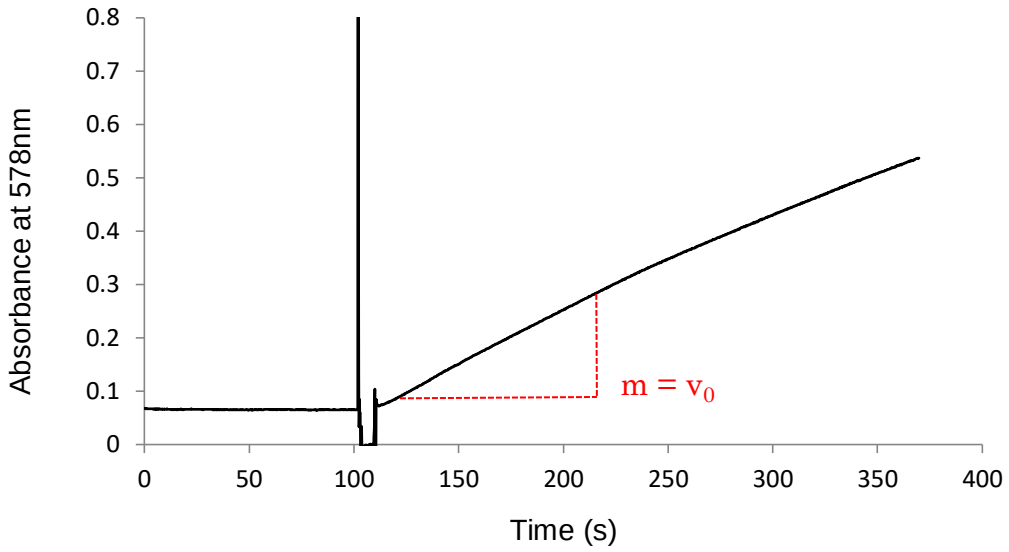

Figure 2-2 *Typical Initial rate (v_0) determination for formate oxidation assay. Determined from first linear section of increasing absorbance after addition of 10mM formate at 100 s.*

For studies involving azide inhibition of enzymatic activity, a 2 M stock of sodium azide (Sigma) was added at appropriate concentrations to reaction cuvettes before sparging with nitrogen. Assays were otherwise conducted as previously described.

2.21 CO_2 reductase activity assay

Assays were conducted in 4 ml glass cuvettes containing 1940 µl of 100 mM HEPES pH 7.2, 10 µl 100 mM methyl viologen (Final: 0.5 mM) and 40 µl of sample prepared as described above (either whole cells, lysed cells or cellular fractions). Each cuvette was then sealed with a no.9 suba seal and three layers of parafilm. Each cuvette was then sparged for 25 min under a N_2 atmosphere to remove any atmospheric oxygen. To each cuvette 2.5 µl of 100 mM dithionite (125 µM in cuvette) was added using a microsyringe (Hamilton). The cuvettes are allowed to stand for 15 min, being inverted 5 times every 5 min to allow cellular background reduction reactions to plateau. The cuvette was then inverted 5 times and absorbance measured at 578 nm for 600 s with a 0.2 s

interval between measurements in a spectrophotometer (Hitachi U-3310). For the first 100 s the background absorbance change was observed. After 100 s, 10 µl of 2 M Na carbonate solution (Final: 10 mM) were added to the cuvette (which was taken out and inverted 5 times before being returned. Note with substrate final reaction volume was 2 ml. If CO_2 reductase activity was present the absorbance at 578 nm fell after substrate addition, the gradient of this first linear section of decreasing absorbance is referred to as an initial rate (v_0) which can be used in a variety of ways, either comparatively or to establish kinetic constants. A typical data plot for CO_2 reduction is seen below in Figure 2-3.

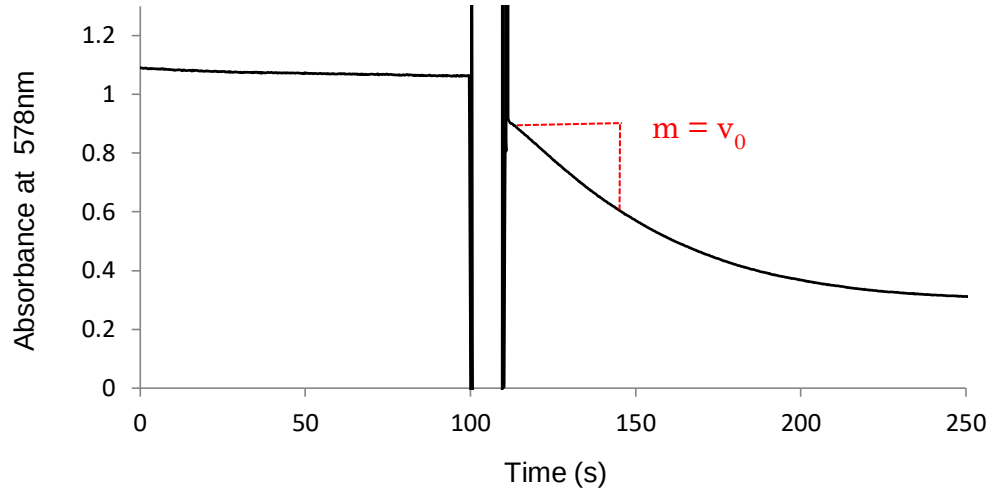

Figure 2-3 Typical Initial rate (v_0) determination for CO_2 reduction assay.
Determined from first linear section of decreasing absorbance after addition of 10mM carbonate at 100 s.

For studies involving azide inhibition of enzymatic activity, a 2 M stock of sodium azide (Sigma) was added at appropriate concentrations to reaction cuvettes before sparging with nitrogen. Assays were otherwise conducted as previously described.

2.22 Fumarate reductase activity assay

Fumarate reductase activity was assayed using methyl viologen, using the same procedure followed for CO_2 reduction assays, only replacing the sodium carbonate substrate with sodium fumarate 99.5% (Sigma).

2.23 Specific activity calculations

Once initial rates had been determined for formate oxidation and CO_2 reduction as absorbance/min further analysis was required to convert into specific activity values. This was done as follows.

By rearranging the Beer-Lambert law, absorbance (A) can be expressed below in eq. (2.2)

$$A = C\ (mM) \times\ \varepsilon\ (mM^{-1}cm^{-1})\ \times l\ (cm) \tag{2.2}$$

Where C represents concentration and ε the extinction coefficient at 578 nm, 9.7 $mM^{-1}\,cm^{-1}$ for methyl viologen (de Bok et al. 2003) and the path length (l) is 1 cm. By rearranging eq. (2.2) and introducing a time component to give eq. (2.3), rates with units of mM/min are calculated.

$$\Delta C\ (mM\ min^{-1}) = \frac{\Delta A\ (min^{-1})}{\varepsilon\ (mM^{-1}cm^{-1}) \times l\ (cm)} \tag{2.3}$$

Since mM = mmol/L = μmol/ml, the units of these measurements can also be written as μmol $ml^{-1}min^{-1}$. As each reaction was conducted in a 2 ml cuvette, multiplication by 2 converts to μmol min^{-1} values, i.e. a quantitative amount of product formed in each reaction. Since each reaction contains 0.04 ml of sample, division by 0.04 converts to μmol min^{-1} ml^{-1}. Since the protein concentration (mg/ml) in each sample had been determined using the described BCA assay, division by these values provided specific activities in μmol min^{-1} mg^{-1} for formation of either the methyl viologen mono-cation (in the case of formate oxidation) or di-cation (for CO_2 reduction). However since formate oxidation or CO_2 reduction are two electron processes, only half the concentration of product will be formed relative to the associated change in measured colourimetric product, this is reflected in the presented specific activities for formate oxidation and CO_2 reduction throughout this work.

2.24 Enzymatic pH dependence studies

For investigating pH dependence for enzymatic assays, 100 mM HEPES was replaced with Mcilvaine buffers of varying pH values, made using varying

concentrations of 0.2 M Na_2HPO_4 and 0.1 M citric acid solutions (McIlvaine 1921). Both solutions were made using analytical grade water and all pH values verified before use.

2.25 NMR

For NMR confirmation of formate production for CO_2 reductase activity, reactions were conducted in 1.5 ml Eppendorfs in an anaerobic environment (UniLabPlus ECO Glovebox workstation, MBraun) with oxygen levels below 0.5 ppm throughout.

Each reaction contained 1 ml of 100 mM HEPES pH7.2, and where appropriate, combinations of 0.5 mM methyl viologen, 5 mM sodium dithionite, 10 mM carbonate, 20 mM sodium azide and 20 µl of 1 mg/ml protein whole cell samples, where the protein concentration was determined by BCA assay and all samples from different growth conditions diluted to 1 mg/ml with 100 mM HEPES pH7.2 prior to the experiment. In each case, the substrate, i.e. sodium carbonate, was added last with 5 inversions of each reaction to mix. Each reaction was allowed to proceed for 30 min at 20°C in the anaerobic glovebox before anaerobic centrifugation in a 5424 microcentrifuge (Eppendorf) at 14000 x g for 10 min. Subsequently 400 µl of the reaction supernatant was mixed with an equal volume of NMR buffer containing 22 mM NaH_2PO_4, 80 mM K_2HPO_4, 14 mM sodium azide and 1 mM trimethylsilylpropanoic acid (TSP) which acted as an internal NMR reference. Once mixed with buffer samples were flash frozen and stored at -20°C.

NMR Samples were run by the Quadram Institute of Bioscience, (previously the Institute for Food Research, Norwich). For analysis, samples were transferred to 5 mm NMR tubes. ^1H NMR spectra were recorded at 600 MHz on a Bruker Avance spectrometer with cryoprobe (Bruker BioSpin) using Topspin 2.0 software. Each ^1H NMR spectrum was acquired with 64 scans, a spectral width of 12300 Hz, an acquisition time of 2.7 s, and a relaxation delay of 3.0 s. The "noesypr1d" presaturation sequence was used to suppress the residual water signal with a low-power selective irradiation at the water frequency during the recycle delay and a mixing time of 10 ms. Spectra were transformed with a 0.3 Hz line broadening, manually phased, baseline corrected, and referenced by setting the TSP methyl signal to 0 ppm. Formate was quantified using the

software Chenomx NMR suite 7.6™ using characteristic resonance peaks and their relative amplitudes to known calibration concentrations.

2.26 Kinetic analysis

For determining kinetic parameters, specific activities were plotted for varying concentrations of substrate, determined in triplicate, and data were fitted by OriginPro 8.5 software to the Nonlinear curve fit:Hyperbl function, to represent the Michaelis-Menten eq. (2.4) below:

$$v_0 = \frac{V_{max}\,[S]}{K_m + [S]} \tag{2.4}$$

Where v_0 is the initial reaction rate, V_{max} is the maximum reaction rate, [S] is the substrate concentration, and K_m is the Michaelis constant (Schnell & Maini 2003). When varying substrate concentrations for these experiments substrates were prepared in a serial dilution to avoid changes in total reaction volume greater than 10 µl.

2.27 Purification of SO_4513

2.27.1 Growth and lysis

In 5 L Durans, 10 L of an MR-1 mutant containing only the SO_4513-4515 FDH isoform, i.e a SO_450101-0103 and SO_4509-4511 deletion strain (Fdh2+), was grown in minimal media anaerobically as described in section 2.4 at 30°C for 22 h.

After growth cells were pelleted aerobically (5540 x g for 20 min, 8°C, JLA8.100 rotor, Beckman Avanti J-20) before resuspending combined pellets in 100 ml of 100 mM HEPES pH7.2. Cells were resuspended/washed three times with 100 ml of 100 mM HEPES pH7.2 buffer, re-pelleting cells between each wash by centrifuging at 5540 x g for 15 min. This was to remove media contaminants which can interfere with subsequent assays

Before lysis, 4 mM Dithiothreitol (DTT) and 500 µl of EDTA free protease inhibitor cocktail (Roche), made from 1 tablet dissolved in 10 ml of distilled water, were added to 50 ml of cell concentrate. DTT was added to help maintain a reducing environment for the protein, an important factor for other FDH

purifications (Jormakka et al. 2002), and the protease inhibitor prevents protein degradation by intracellular proteases released by cell lysis.

Cells were then lysed, keeping lysate on ice throughout. The cell concentrate was passed through a chilled French press cell disruptor (Thermo Fisher) set at 16000 psi twice, producing a transparent red lysate.

Performing the above cell harvesting and lysis purification steps under anaerobic conditions had no effect on measured FDH/CO_2 reductase activities, subsequent purification steps however required anaerobic conditions to avoid loses in activity. Even so, harvesting and lysis were performed quickly followed by sparging of the lysate with N_2 for 15 min in suba sealed (no.53) falcon tubes to remove atmospheric oxygen. All purification steps from this point were conducted in a glovebox (Belle) with oxygen levels below 20 ppm throughout. Aerobic preparations from this point onwards rapidly lost all observable enzymatic activity.

2.27.2 Cell fractionation and inner-membrane solubilisation.

To remove unlysed cells and aggregated cell debris, lysate was sealed anaerobically and centrifuged at 5540 x g for 15 min. The supernatant was then anaerobically diluted to 56 ml using 100 mM HEPES pH7.2 and ultracentrifuged at 205,076 x g (42000 rpm) for 2 h (45Ti rotor, Beckman Optima XL-100k). The supernatant following this ultracentrifugation step is henceforth referred to as the soluble fraction, i.e. anything that did not pellet with the membranes during this procedure.

To limit soluble fraction carryover, the membrane fraction pellet was gently washed with 1 ml of 100 mM HEPES pH 7.2 buffer, being careful not to disturb the pellet. Subsequently the pellet was resuspended in 56 ml of 20 mM MES pH6 with 5 mg/ml sodium lauroyl sarcosinate (sarkosyl) and mixed by agitation in a beaker for 1 hour in the glovebox at ambient temperature (20^{o}C). This step exploits the preferential solubilisation of bacterial inner membranes over outer membranes by sarkosyl (Brown et al. 2010). After this solubilisation step membranes were ultracentrifuged at 45000 x g (19700 rpm) for 1 hour (45Ti rotor, Beckman Optima XL-100k). The pelleted material is henceforth referred

to as the outer membrane fraction, and the supernatant referred to as the inner membrane fraction assuming the selective solubilisation described above.

2.27.3 Anion exchange chromatography

Anion exchange chromatography was used to purify SO_4513 from inner membrane fractions. A 5 ml Q sepharose HP cartridge column was used in combination with an ÄKTA prime plus (GE Healthcare) within a glovebox (Belle). All steps were carried out with a flowrate of 1 ml/min. Initially the column was equilibrated using 25 ml of loading buffer, (20 mM MES buffer pH 6 containing 0.01% DDM and 25 mM NaCl). Once equilibrated, 10 ml of inner membrane fraction was loaded onto the column, followed by a further 25 ml of loading buffer, to remove any non-bound material. Bound SO_4513 was then eluted in 20 ml of elution buffer, (identical to loading buffer but containing 415 mM NaCl), This 20 ml elution was collected following a rise in absorbance at 280 nm using the integrated UV detector.

2.27.4 Size exclusion chromatography

Following the anion exchange separation detailed above, SO_4513 was further purified using a Superdex 200 25 ml size exclusion column. In order to load onto this column the previous 20 ml of purified protein from the Q sepharose column was concentrated down to a combined volume of 0.5 ml using 0.5 ml centrifugal filters (Amicon) which theoretically remove molecules less than 50 kDa in size. This concentration step was performed anaerobically in a 5424 microcentrifuge (Eppendorf) at 14000 x g.

The size exclusion column was run anaerobically in a glovebox (Belle) using an ÄKTA prime plus (GE Healthcare) with all steps carried out with a flow rate of 0.3 ml/min. Initially the column was equilibrated with 75 ml of size exclusion buffer (20 mM HEPES pH7.2 containing 0.01% DDM and 150 mM NaCl). Once equilibrated the protein sample was loaded using a sample loop onto the column. Once loaded, 0.5 ml fractions of eluent were collected using a fraction collector, monitoring absorbance at 280 nm and conductivity. SO_4513 eluted after 15 ml of buffer had been collected, in the first of two UV absorbance peaks. Fractions containing FDH activity, determined using the described methyl viologen assay, were combined and concentrated using 0.5 ml centrifugal filters

(Amicon) removing molecules ≤ 30 kDa in size. This concentration step was performed anaerobically in a 5424 microcentrifuge (Eppendorf) at 14000 x g concentrating to a final volume of 200 µl. This purified SO_4513 was analysed using SDS-PAGE electrophoresis and subsequent mass spectrometry fingerprinting as well as enzymatic activity assays and ICP-MS.

2.27.5 Mass spectrometry – Peptide fingerprinting.

For analysis and identification, protein bands were excised from SDS-PAGE gels, see section 2.27.7, having been stained with InstantBlue Coomassie stain for visualisation. To prepare samples for analysis, bands were first de-stained in LoBind 1.5ml tubes (Eppendorf) containing 30% ethanol at 65°C. This was repeated, with fresh ethanol solution until the band was colourless.

Once clear, the band was washed with a solution of 50 mM ammonium bicarbonate containing 50% (w/v) acetonitrile. This was then replaced with a solution of 10 mM dithiothreitol incubated at 55°C for 30 min.

Once complete this solution was removed and replaced by a 50 mM ammonium bicarbonate. This was kept in darkness, on a Vortex Genie 2 ™ (Scientific industries) at 20°C for 30 min. Subsequently the band was washed with a solution of 50 mM ammonium bicarbonate containing 50% (w/v) acetonitrile followed by a final wash of 50 mM ammonium bicarbonate.

The band was then cut into 1mm by 1mm squares, which were washed with a solution of 50 mM ammonium bicarbonate containing 50% (w/v) acetonitrile followed by a final wash of 50 mM ammonium bicarbonate.

Finally the gel fragments were washed in 100% acetonitrile, which was then removed and the samples sent to the Proteomics facility at the John Innes Centre for tryptic digest and Matrix-Assisted Laser Desorption/Ionization Time Of Flight (MALDI-TOF) Mass Spectrometry. The results were screened against the bacterial UniProt Swiss-Prot/TrEMBL database accounting for common contaminants and digestion by trypsin/P enzyme. Specific parameters included in these searches included a peptide mass tolerance of 50 ppm, variable oxidation, carbamidomethylation and aceylation of N terminal residues and allowance for a single missed cleavage. This search was performed by a dedicated Mascot 2.4 server. Using the above parameters Mascot protein match

scores greater than 85 were judged to be significant ($p<0.05$). In the case of SO_4513 identification a score of 125 was obtained.

2.27.6 Acid digestion for ICP-MS protein analysis.

To determine the metal content of purified SO_4513 protein, 100 µl of 3 µM protein was added to an equal volume of 35% nitric acid and incubated at 95°C for 90 min. Once cooled the sample was centrifuged in a 5424 microcentrifuge (Eppendorf) at 14000 x g for 10 min. The supernatant (200 µl) was added to 1800 µl analytical grade water (Fisher) and the sample run according to the ICP-MS procedure detailed in 2.8. In addition to the protein sample, pure analytical water and standard solutions containing known concentrations of W and Mo were also run as negative and positive controls respectively.

2.27.7 SDS-PAGE

To separate protein samples by size, sodium dodecyl sulphate polyacrylamide gel electrophoresis (SDS-PAGE) was used. Polyacrylamide gels consisted of two parts, the lower resolving gel, which separates depending on proteins differential rates of migration through an acrylamide gel, exploiting the fact that the detergent SDS binds the hydrophobic regions of peptides (Rath et al. 2009) and confers an approximately uniform net negative charge. The upper stacking gel aligns all protein samples by concentrating them between charge fronts that occur under an applied potential at pH 6.8 allowing for higher resolution separation.

Prior to loading on SDS-PAGE gels, samples were denatured by incubation at 70°C for 15 min in TruPAGE™ LDS Sample Buffer (Sigma) supplemented with TruPAGE™ DTT Sample Reducer (Sigma) according to the manufacturer's instructions.

For images prepared for this work, precast TruPAGE™ 4-20% polyacrylamide gradient gels (Sigma) were used, run submerged in TruPAGE™ TEA-Tricine SDS Running Buffer (Sigma) in a Mini-protean II gel electrophoresis tank (BioRad). Gels were run for 70 min at 180 V before staining with InstantBlue Coomassie stain (Expedeon) for 60 min on a rocking platform before being washed and stored in analytical grade water (Fisher).

2.28 Electrochemical cell design

All electrochemical investigations were conducted in a three electrode bioreactor. This bioreactor was specifically designed to facilitate these and future whole cell biochemical experiments and for which a scheme is shown in Figure 2-4.

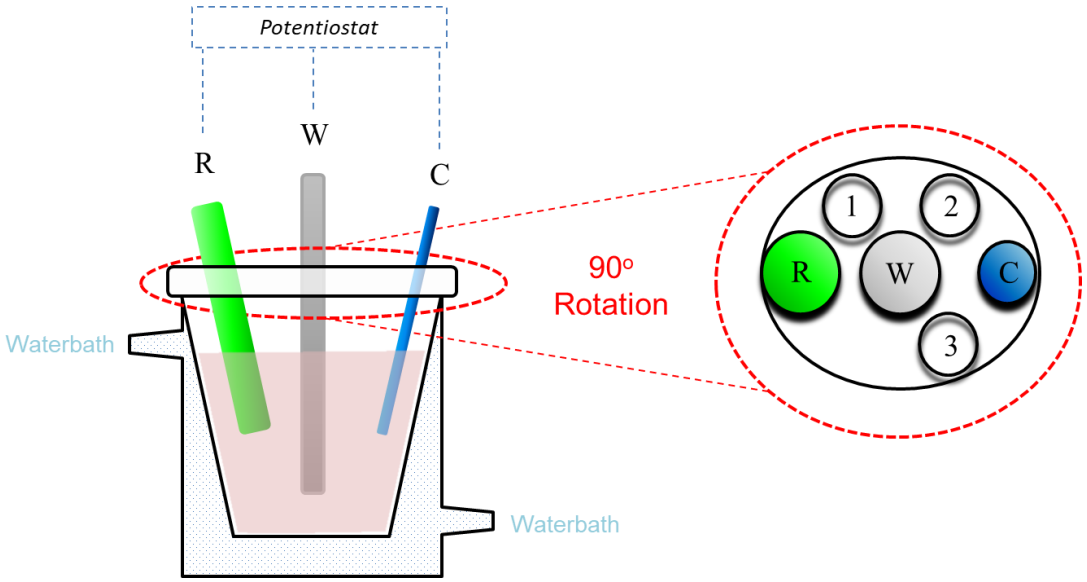

Figure 2-4 Schematic of bioreactor used for electrochemical studies.
Where R, W and C represent reference, working and counter electrodes respectively and 1, 2 and 3 are the remaining apertures for gas/substrate injections during experiments.

To ensure correct potential measurement the reference electrode was designed to be located as close to the working electrode as possible and outside the path of ion migration between WE and CE. This was done to limit the resistance of the electrolyte between WE and RE causing unwanted decreases in the solution potential according to Ohm's law (Harnisch & Freguia 2012).

The cell itself was made in house (University of East Anglia Chemistry Department). The inverted truncated cone shaped reaction chamber holds a maximum volume of 55 ml (working volume 30 ml) and the flattened base allows optional stirring using a magnetic micro stirrer.

An outer water sleeve enables temperature control via an external water bath since more typical incubation methods used for bacterial study are logistically challenging in an anaerobic environment. Cast in one piece the top face contains five apertures, with either a 15mm glass screw thread fitting (for working and

reference electrode) or 13 mm glass screw thread fitting (for counter electrode and remaining apertures). The apertures not containing electrodes are designed for experimental flexibility, two allow for continual gas purging of the cells should the bioreactors be used outside the glovebox and the last allows additions to be made throughout experiments. These apertures are sealed with suba seals (no. 9) during all described experiments and along with all electrodes are further sealed from the external environment with parafilm.

Before each electrochemical experiment each bioreactor was thoroughly cleaned by washing 5 times with ethanol 99.9% (Sigma) followed by a further 5 washes with analytical water, with a resistance below 18.2 MΩ.cm. Remaining water was then evaporated using argon gas. The working, counter and reference electrodes are then assembled as described below and the assembly transferred to the glovebox. Oxygen levels were below 10 ppm throughout all conducted experiments.

Throughout these experiments 102 mm long, 6.15 mm diameter 99.9995% graphite rods (Alfa Aesar) were used as working electrodes. Before use each was polished 10 times with cotton wool coated in aluminium oxide 99.99% (Alfa Aesar) before sonication for 30 s to remove loose imperfections. This polishing step was repeated a further 3 times before rinsing the electrode in analytical water and assembling in the bioreactor with a silicone rubber ring (SciLabware Limited) and cap, further sealed by parafilm.

During each experiment a 7.5 mm Ag/AgCl saturated KCl "Red Rod" reference electrode (Radiometer analytical) was used. After ensuring each electrode contained saturated KCl solution, indicated by KCl crystals, the reference electrode was rinsed with analytical water and assembled in the bioreactor with a silicone rubber ring (SciLabware Limited) and cap, further sealed by parafilm. To convert potentials quoted against this electrode 197 mV was added to all measurements to provide values quoted against SHE (Field et al. 2005).

The counter electrode in all electrochemical studies was made of 10 cm of platinum wire, 0.25mm diameter, 99.9% purity (Sigma Aldrich) threaded through a plastic sleeve filled with the same electrolyte as the remainder of the bioreactor, typically 100mM HEPES, 8.7 mM NH_4Cl, 1.3 mM K_2HPO_4, 1.7 mM KH_2PO_4 and 1mM $MgSO_4$, pH7.2. The counter electrode was isolated from the

analyte by a CoralPor tip (Basi), a porous glass frit commonly used for such purposes (Mousavi & Bühlmann 2013). The counter electrode was then assembled in the bioreactor with a silicone rubber ring (SciLabware Limited) and cap, further sealed by parafilm.

Each electrochemical experiment contained 30 ml of aqueous electrolyte solution containing 100mM HEPES, 8.7 mM NH_4Cl, 1.3 mM K_2HPO_4, 1.7 mM KH_2PO_4 and 1mM $MgSO_4$, pH7.2, i.e. the components of the previously described minimal media without minerals, vitamins, carbon source, electron donor or acceptor. Due to the high buffer concentration pH values, determined by pH probe, did not change by more than 0.1 pH unit from the start to finish of any electrochemical experiment or upon addition of any cell cultures or substrate additions. Experiments were conducted in a faradaic cage to limit electrical interference.

Electrochemical measurements were either made using a DropSens Multipotentiostat µStat 8000P potentiostat (Metrohm) controlled by Dropview 8400 software or an Autolab AUT73338 potentiostat (Metrohm) using NOVA 1.0 software. In both cases the same three electrode cells described above were used. The AUT73338 equipment was predominantly used for its higher sensitivity and was used unless specified otherwise, the multichannel equipment was reserved for those experiments requiring faster throughput and which are highlighted as such in the results.

2.29 Bacterial culture for electrochemistry

Cultures used for electrochemical experiments were grown anaerobically using 50 mM sodium fumarate as electron acceptor according to the above protocols for *S.oneidensis* culture in minimal media. Unless specified otherwise cultures were grown in 1L Durans supplemented with 3 µM sodium tungstate (+W) for 24 h before harvesting for electrochemical study. After growth cells were pelleted aerobically (5540 x g for 20 min, 8°C, JLA8.100 rotor, Beckman Avanti J-20).

Cell pellets for each litre of culture were resuspended/washed three times with 25ml of 100 mM HEPES, 8.7 mM NH_4Cl, 1.3 mM K_2HPO_4, 1.7 mM KH_2PO_4 and 1mM $MgSO_4$, , pH7.2., (the same electrolyte used in bioreactors), re-pelleting

cells between each wash by centrifuging at 5540 x g for 15 min. This was to remove media contaminants and substrates which can interfere with electrochemical analysis. Each litre pellet was finally resuspended in 2 ml of electrolyte. To ensure normalisation cultures were diluted so cell suspensions of the same OD were introduced into the electrochemical cells, subsequent analysis showed comparable protein content (20 mg/ml) as determined by BCA assay. When adding such cultures to bioreactors 2 ml of previous electrolyte was removed and replaced by 2 ml of *S.oneidensis* culture (inoculum), maintaining a reaction volume of 30 ml.

2.30 Cyclic voltammetry

Typical cyclic voltammetry staircase experiments were conducted for the bioreactor set up described above. Each study consisted of two complete scans using the following parameters; Initial potential (Lower vertex potential, E_1) -0.76 vs Ag/AgCl (Sat KCl), Final potential (Upper vertex potential, E_2) 0.22 vs Ag/AgCl (Sat KCl), Step potential: 1mV/s, Scan rate (v): 1mV/s. For those experiments when scan rate was increased, the step potential was scaled accordingly. All experiments were conducted anaerobically with O_2 levels below 10 ppm at 25^{o}C.

2.31 Chronoamperometry

Chronoamperometry experiments were conducted for the bioreactor set up described above. After poising the working electrode at -0.757 vs Ag/AgCl (Sat KCl)(-0.56 V vs SHE) the system was allowed to equilibrate for 5 s before current measurements were taken either every second or 2 min for extended poise experiments. All experiments were conducted anaerobically with O_2 levels below 10 ppm at 25^{o}C.

2.32 First derivative of Cyclic voltammetry traces

Postacquisition analysis of CV data to determine first derivative plots of the catalytic current with respect to applied potential was performed using OriginPro 8.5 software. Derivative data was determined using the mathematics: differentiation tool followed by first order Savitsky-Golay smoothing of data using a 50 point window. Smoothened plots were used only to limit background

noise and were individually confirmed not to mask or distort peak features from unsmoothed datasets.

2.33 Integration of chronoamperometry data.

Postacquisition integration of chronoamperometry data to determine the charge transferred to analyte after addition of sodium carbonate was performed using OriginPro 8.5 software. This was done using the integration gadget, using the absolute area determination and integrating using a constant Y axis value as a baseline, the choice of baseline was determined by the capacitive current observed prior to addition of sodium carbonate and was typically defined as -4 μA.

2.34 References

de Bok, F. a. M. et al., 2003. Two W-containing formate dehydrogenases (CO_2-reductases) involved in syntrophic propionate oxidation by *Syntrophobacter fumaroxidans*. *European Journal of Biochemistry*, 270(11), pp.2476–2485.

Brown, R.N. et al., 2010. Mapping the subcellular proteome of *Shewanella oneidensis* MR-1 using Sarkosyl-based fractionation and LC-MS/MS protein identification. *Journal of Proteome Research*, 9(9), pp.4454–4463.

Field, S.J. et al., 2005. Reductive activation of nitrate reductases. *Dalton Transactions*, 2005(21), pp.3580–3586.

Harnisch, F. & Freguia, S., 2012. A basic tutorial on cyclic voltammetry for the investigation of electroactive microbial biofilms. *Chemistry, an Asian journal*, 7(3), pp.466–75.

Jormakka, M. et al., 2002. Purification and crystallization of the respiratory complex formate dehydrogenase-N from *Escherichia coli*. *Acta Crystallographica Section D: Biological Crystallography*, 58(1), pp.160–162.

Kane, A.L. et al., 2016. Formate metabolism in *Shewanella oneidensis* generates proton motive force and prevents growth without an electron acceptor. *Journal of Bacteriology*, 198(8), pp.1337–1346.

McIlvaine, T., 1921. A buffer solution for colorimetric comparison. *Journal of Biological Chemistry*, pp.183–186.

Monod, J., 1949. The growth of bacterial cultures. *Annual Reviews in M*, 3(Xl), pp.371–394.

Mousavi, M.P.S. & Bühlmann, P., 2013. Reference electrodes with salt bridges contained in nanoporous glass: An underappreciated source of error. *Analytical Chemistry*, 85(19), pp.8895–8901.

Owens, J.D. & Legan, J.D., 1987. Determination of the Monod substrate saturation constant for microbial growth. *FEMS Microbiology Reviews*, 46, pp.419–432.

Rath, A. et al., 2009. Detergent binding explains anomalous SDS-PAGE migration of membrane proteins. *Proceedings of the National Academy of Sciences of the United States of America*, 106(6), pp.1760–5.

Richardson, D.J. et al., 2012. Exploring the biochemistry at the extracellular redox frontier of bacterial mineral Fe(III) respiration. *Biochemical Society transactions*, 40(3), pp.493–500.

Saltikov, C.W. & Newman, D.K., 2003. Genetic identification of a respiratory arsenate reductase. *Proceedings of the National Academy of Sciences of the United States of America*, 100(19), pp.10983–8.

Schnell, S. & Maini, P.K., 2003. A Century of Enzyme Kinetics: Reliability of the K_m and V_{max} Estimates. *Comments on Theoretical Biology*, 8, pp.169–187.

Zwietering, M.H. et al., 1990. Modeling of the bacterial growth curve. *Applied and Environmental Microbiology*, 56(6), pp.1875–1881.

3 FDH characterisation in WT *Shewanella oneidensis* MR-1 in response to metal supplementation

3.1 Media optimisation

In order to study formate metabolism in *S.oneidensis* MR-1 it was necessary to develop an appropriate growth medium. Although many types of minimal media have been used for study of growth of *S.oneidensis* in the past almost all use lactate or pyruvate as the principal energy and carbon source (Pinchuk et al. 2011). Since this investigation was focused on the role of formate, a media using formate as the sole energy source was developed.

Anaerobic growth conditions were used for growth studies due to the proposed role of formate in *S.oneidensis* and its main function contributing to anaerobic respiration and maintenance of proton motive force (Kane et al. 2016). The media was developed using fumarate as a terminal electron acceptor under anaerobic conditions, as opposed to aerobically using oxygen. No growth was observed with aeration, either in the presence or absence of fumarate (Figure 3-1 panel A), suggesting the unsuitability of this media for aerobic growth, and in agreement with the importance of formate in menaquinone coupled anaerobic, and not aerobic, respiration (Kane et al. 2016) when the alternative ubiquinone pool is used (Chen & Wang 2015).

A major consideration for these experiments was the importance of the metals tungsten and molybdenum, essential cofactors for all identified putative FDH enzymes in the genome of *S.oneidensis*. Since this study aimed to examine the impact of each metal it was vital to develop a media without significant traces of either. This proved difficult, despite use of analytical grade water and acid washed equipment, due to the tryptic digests within earlier media iterations, which contained μM concentrations of metal yet were essential carbon sources. These are replaced in the final iteration by the addition of three amino acids, Glutamine, Serine and Arginine which provide the same function yet contain comparatively lower metal traces. Figure 3-1B demonstrates the importance of each of these media components, the electron donor sodium formate, electron

acceptor sodium fumarate and carbon source in the form of the amino acids, without their inclusion no growth was observed. For these media optimisation experiments both sodium tungstate and sodium molybdate were supplemented at 3 μM.

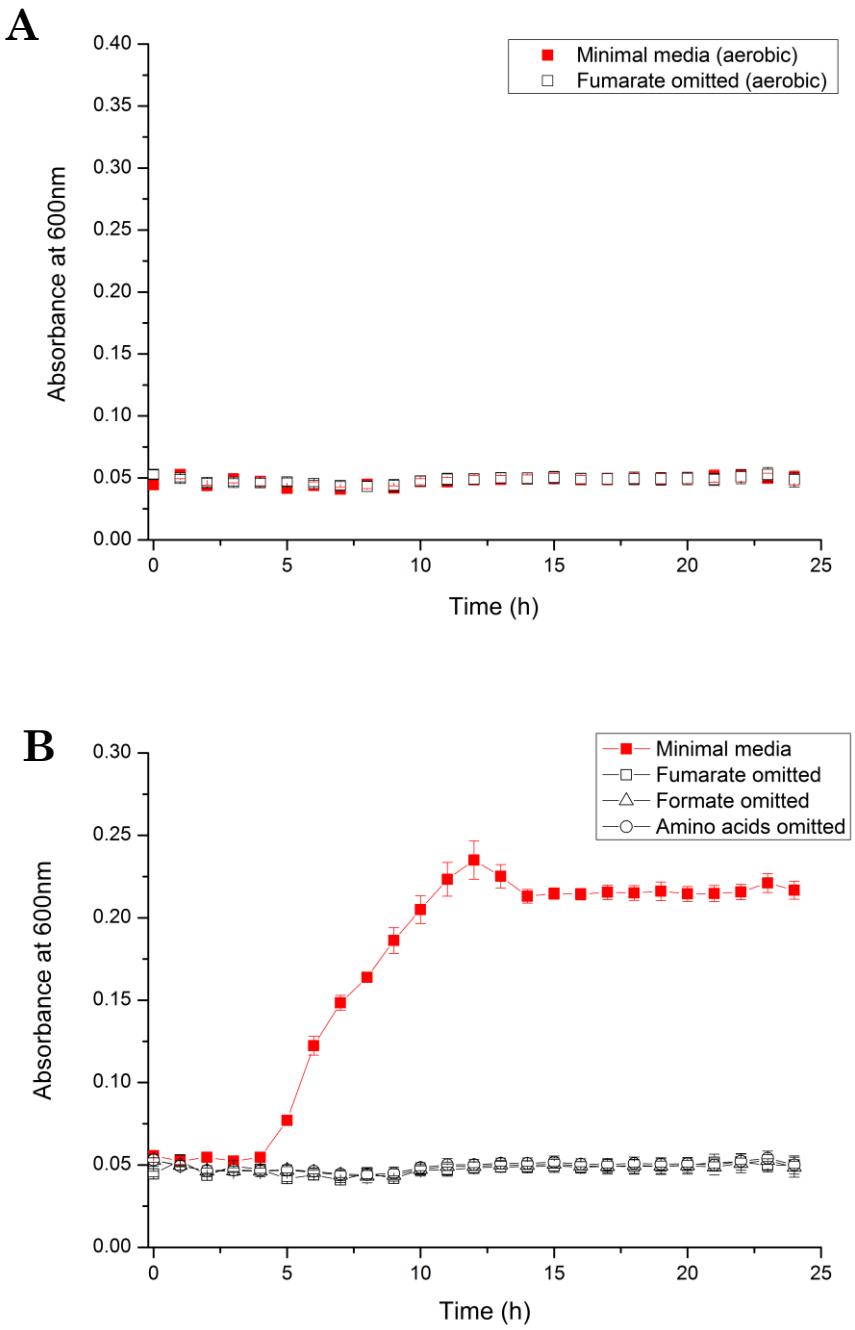

Figure 3-1 Aerobic and anaerobic S.oneidensis growth in formate containing minimal media.
(A) *Aerobic growth not supported in described media with or without addition of sodium fumarate.* ***(B)*** *Anaerobic growth in minimal media highlighting the effect of omitting media components. Complete minimal media as described in Chapter 2 shown in red. Sodium formate and fumarate at 50 mM when included. Amino acids describe glutamine, arginine and serine at 1 g/L. For all conditions sodium tungstate and sodium molybdate were supplemented at 3 μM. Data represents average of three experimental data sets where error bars represent ± SEM.*

3.2 Determination of Monod constant for formate.

Once a suitable growth medium was established, i.e. that described in section 3.1, using 50 mM fumarate as terminal electron acceptor, an optimal amount of formate for growth was determined. As can be seen in Figure 3-2A, maximal OD_{600} values were obtained when media contained 50 mM formate or higher, hence for all subsequent minimal media experiments, 50 mM sodium formate was used as electron donor for growth. By plotting the specific growth rate (μ) against concentration of formate it is possible to graphically represent the Monod equation. This is seen in Figure 3-2B with the derived μ_{max}, 0.272 ± 0.024 h^{-1}, (the maximum specific growth rate of *S.oneidensis* on formate under these growth conditions) and the K_s (Monod constant) of 20.3 ± 6 mM (SEM) (which corresponds to the concentration of formate when the specific growth rate is half that of μ_{max}). Both these cellular kinetic coefficients are direct parallels to the more commonly encountered V_{max} and K_m found in enzyme kinetics.

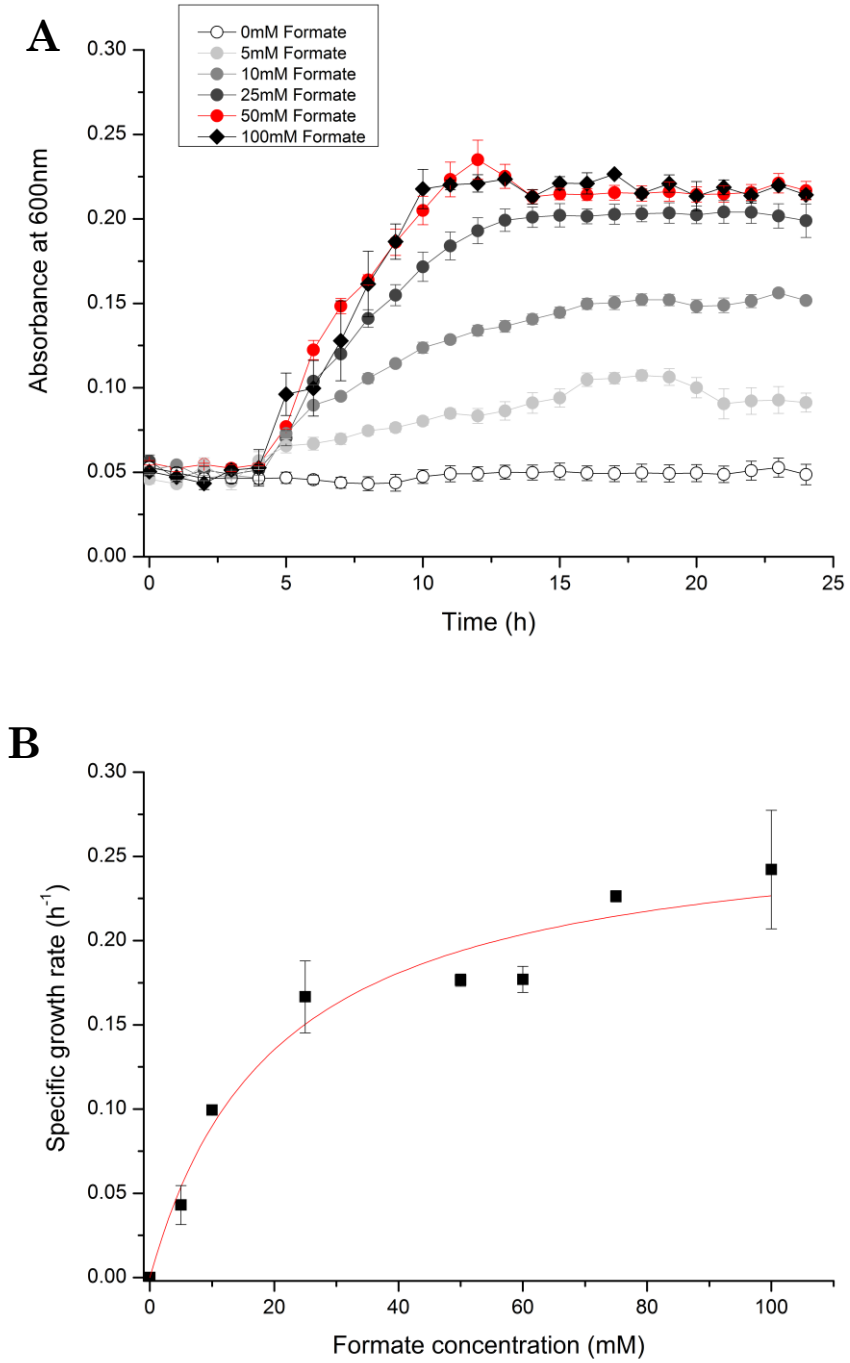

Figure 3-2 Anaerobic S.oneidensis growth in minimal media with sodium formate.
(A) *Growth curves with increasing formate concentration. Maximum* OD_{600} *becomes independent of formate concentration above 50 mM, shown in red. For all conditions sodium tungstate and sodium molybdate were supplemented at 3 µM with sodium fumarate as electron acceptor Data represents average of three experimental data sets where error bars represent ± SEM.* ***(B)*** *Determination of Monod constant. Plot of specific growth rate, µ, determined from* ***(A)*** *as described in Chapter 2 plotted against formate concentration in media. Average of three experimental data sets shown where error bars represent ± SEM. Data was then fitted by OriginPro 8.5 software to Michaelis-Menten hyperbolic function shown in red. From this the* K_s *and* μ_{max} *were determined as described in the text.*

3.3 Growth studies with metal supplementation

Having established a suitable growth medium, the effect of W and Mo supplementation in the optimised media was investigated. Note that for both metals, as in previous experiments, the more bioavailable sodium salts of these metals were used in the form of sodium tungstate and sodium molybdate. The majority of minimal bacterial growth media only include low μM concentrations of these metals, typically in the range of 0.3 μM to 3 μM, only ranging higher in dedicated studies, (Laukel et al. 2003)(Gates et al. 2003)(Kouzuma et al. 2010). Typically only molybdate is included in many experiments, with tungstate only rarely considered (Kisker et al. 1997). Considering this, the following experiments were supplemented with 3 μM tungstate and/or molybdate.

Figure 3-3 shows the effect on growth when 3 μM tungstate (+W), 3 μM molybdate (+Mo), 3 μM of both metal ions (+W/+Mo) or neither metal ions (-W/-Mo) are added to cultures. Notably all four growth conditions supported growth. This deserves attention as the growth condition containing no supplementation (-W/-Mo) was capable of growth on formate, despite apparently lacking the essential metals needed for its enzymatic oxidation. When supplemented with solely tungstate, growth is almost indistinguishable from non-supplemented cultures, this is also true for cultures supplemented with tungstate and molybdate. The only observed increase in growth was when supplemented with molybdate alone.

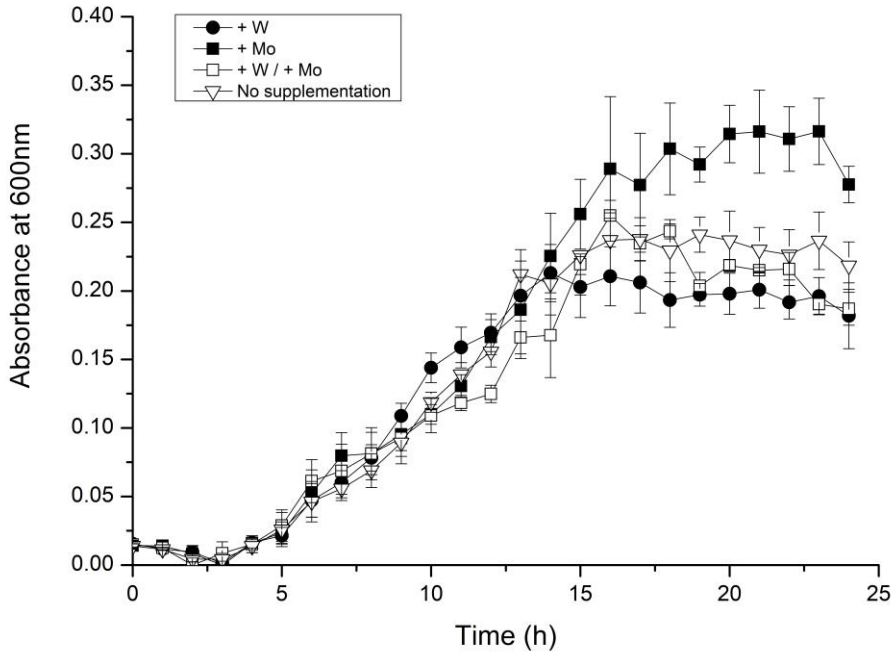

Figure 3-3 Anaerobic growth of S.oneidensis with W/ Mo at 3 µM.
Where metals supplemented as sodium molybdate (+Mo) and/or sodium tungstate (+W). Growth with 50 mM sodium fumarate as electron acceptor in minimal media. Data represents the average of a minimum of three experimental data sets where error bars represent ± SEM.

In order to rationalise the above results, the tungstate and molybdate concentrations in the growth medium were experimentally confirmed. To do this inductively coupled plasma mass spectrometry (ICP-MS) was used to determine metal concentrations in inoculated cultures. ICP-MS data for cultures immediately after inoculation, i.e. at time point 0h in Figure 3-3 are shown in Table 3-1.

Table 3-1 ICP-MS data after 0 h growth during 3 µM metal supplementation growth studies.
Data represents 0.5 ml of media taken immediately after inoculation. Average of at least three experimental replicates shown ± SEM. (3.s.f.) Limits of detection for this dataset were 0.022 µM for W and 0.012 µM for Mo.

	3 µM W Supplementation	3 µM Mo Supplementation	3 µM W + 3 µM Mo Supplementation	Neither supplementation
W concentration (µM)	3.14 ± 0.17	0.073 ± 0.005	3.161 ± 0.1	0.063 ± 0.028
Mo concentration (µM)	0.08 ± 0.015	3.31 ± 0.036	3.52 ± 0.45	0.073 ± 0.012

Expected metal concentrations match those determined using ICP-MS (Table 3-1). However, it is also noticeable that even without supplementation traces of tungstate and molybdate remain at around 70-80 nM. Considering these samples are from inoculated cultures these traces could originate from either the inoculum, despite prior wash steps, or the media itself.

To try and clarify this point ICP-MS was also conducted on media prior to inoculation and on the inoculum independently. The media contained 74 nM ± 15 (SEM) Mo and 112 nM ± 21 (SEM) W suggesting the cause of the trace amounts of metal were due to components of the media itself rather than metal carry over from the inoculum. However the inoculum (after wash steps) did contain both metals, at 744 nM ± 90 (SEM) Mo and 130 nM ± 48 (SEM) W which although considerably higher does not consider that cultures are only inoculated at 2%, meaning metal contributions from the inoculum are small (around 3nM for W and 15nM for Mo) compared to the bulk media. As these traces of metals proved impossible to remove, further analysis was done with this as a caveat, accepting that traces of both metals may complicate analysis.

Table 3-2 ICP-MS data after 24 h growth during 3 μM metal supplementation growth studies. Data represents 0.5 ml of media taken after 24 h growth and subsequent centrifugation. Average of at least three experimental replicates shown ± SEM. (3.s.f.) Limits of detection for this dataset were 0.022 μM for W and 0.012 μM for Mo.

	3 μM W Supplementation	3 μM Mo Supplementation	3 μM W + 3 μM Mo Supplementation	Neither supplementation
W concentration (μM)	3.01 ± 0.153	0.058 ± 0.013	3.121 ± 0.116	0.053 ± 0.010
Mo concentration (μM)	0.053 ± 0.016	3.041 ± 0.218	3.485 ± 0.212	0.059 ± 0.012

Table 3-2 shows ICP-MS data for centrifuged media samples, taken after 24 h of growth, corresponding to the growth seen in Figure 3-3. These experiments were conducted to determine if metal uptake could be observed by *S.oneidensis* cultures, making the assumption that decreases in metal content before and after growth would correspond to uptake by the cells. Although the metal concentration values in Table 3-2 after growth are lower than those at inoculation (i.e, Table 3-1) the relatively large errors associated with these measurements are frequently larger than the decreases in metal concentrations

over the 24 hour period, complicating any analysis. Despite the theoretical possibility of discerning such changes considering the sensitivity of the equipment used, the variability between cultures made this unfeasible without further investment of time. Although it is impossible to quantify exact changes, it can be said that changes of no more than 100 nM were seen for either metal in any of the studied growth conditions, suggesting such concentrations are capable of supporting the growth seen in Figure 3-3.

3.4 Growth studies with increasing metal supplementation.

By careful selection of reagents, using acid washed glassware and analytical water it was possible to limit W and Mo concentrations to 112 nM and 74 nM respectively in the investigated minimal media. These values represent a lower limit to W and Mo in this media but the effect of higher concentrations was unknown. An excess of metal (W or Mo) not capable of facilitating enzymatic formate oxidation may compete with the required metal due to their atomic similarity and therefore inhibit growth. Examples of such phenomena already exist in the literature (Dudev & Lim 2014). As seen in Figure 3-4 increasing sodium tungstate supplementation in the minimal media had no effect on growth even at 150 μM as seen in the green growth trace in panel A. In contrast an equivalent concentration of sodium molybdate supplementation inhibited all growth, (red trace in panel B). Supplementation of both metals at 150 μM had a negligible effect on growth, (blue trace in panel C). Together these results suggest that a high Mo:W ratio (233:1, Table 3-3) is detrimental to growth.

One explanation for the observed results is that sodium molybdate is more cytotoxic to *S.oneidensis* than sodium tungstate in a manner unrelated to FDH inhibition, however supplementation of 150 μM tungstate, molybdate or both metals to equivalently grown anaerobic cultures in LB media (Figure 3-4 panel D), rather than minimal media, show no growth inhibition under any condition, supporting, but not proving, the competitive FDH inhibition explanation since formate is not the principal energy source in these LB growth conditions. A counter proposal that the LB media is able to sequester or chelate and therefore nullify the toxicity of the metals is an avenue that still needs to explored but seems unlikely considering the broad range of microorganisms capable of

growth in LB and the necessity of these metals for many of these organisms (Magalon et al. 2011).

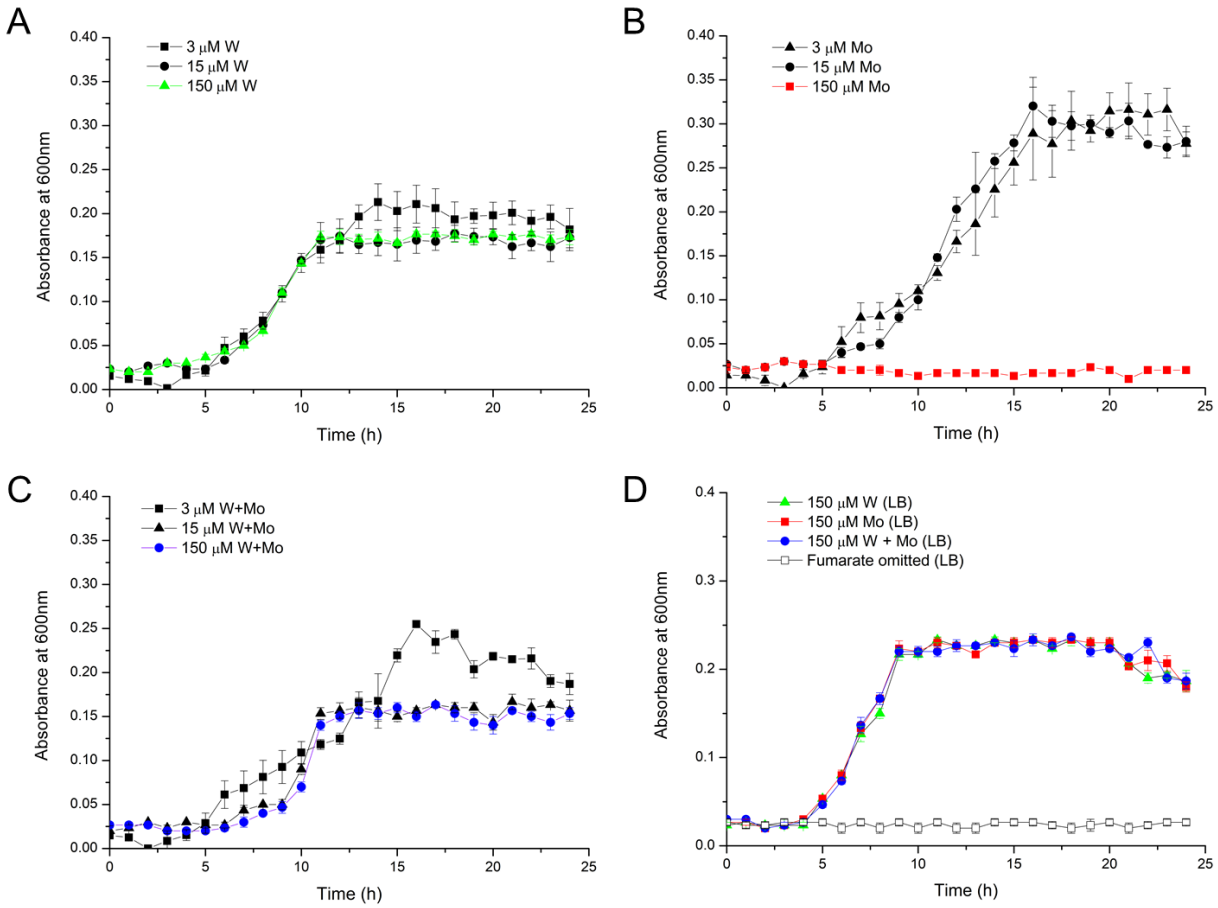

Figure 3-4 S.oneidensis growth with increasing molybdate and tungstate concentrations.
*Growth curves for S.oneidensis MR-1 grown anaerobically with sodium fumarate as electron acceptor in minimal media with 50 mM formate (**A**,**B**,**C**) or LB (**D**) supplemented with sodium molybdate and/or sodium tungstate. Data represents average of a minimum of three experimental data sets where error bars represent ± SEM. (**A**) Increasing tungstate supplementation in minimal media. (**B**) Increasing molybdate supplementation in minimal media. (**C**) Increasing tungstate and molybdate supplementation in minimal media. (**D**) 150 μM metal supplementation in anaerobic LB with 50 mM fumarate as terminal electron acceptor.*

Table 3-3 ICP-MS data after 0 h growth during 150 µM metal supplementation growth studies. Data represents 0.5 ml of media taken immediately after inoculation. Average of at least three experimental replicates shown ± SEM. (3.s.f.)

	150 µM W Supplementation (MM)	150 µM Mo Supplementation (MM)	150 µM W + Mo Supplementation (MM)	150 µM W + Mo Supplementation (LB)
W concentration (µM)	146 ± 5.98	0.612 ± 0.393	165 ± 6.01	165 ± 2.93
Mo concentration (µM)	0.217 ± 0.025	143 ± 6.95	161 ± 9.31	154 ± 3.00

3.5 FDH gene expression in response to metal supplementation.

Having primarily addressed the importance of sodium tungstate and sodium molybdate on bacterial population growth on formate *S.oneidensis*, gene expression in response to these metals was also examined. Considering the focus of this body of work, only the expression of the FDH enzymes were investigated, in particular the putatively catalytic *SO_0101*, *SO_4509* and *SO_4513* (Fdnαβγ, Fdh1αβγ and Fdh2αβγ), thought to be responsible for formate oxidation (Kane et al. 2016). To do this, minimal media cultures grown supplemented with metals at 3 µM as described previously were harvested at mid exponential growth before extracting mRNA and subsequently using RT-qPCR to quantify amplicons for each gene of interest and the constitutively expressed RecA recombinase gene (Yang et al. 2010) used to normalise expression between growth conditions. The relative expression of each gene compared to RecA is presented in Figure 3-5 where sodium tungstate supplementation at 3 µM in the growth media is indicated by +W and sodium molybdate supplementation at 3 µM is indicated by +Mo. The most notable and unexpected change in expression is seen for *SO_0101* which is upregulated solely when neither metal was supplemented (-W/-Mo). Of the other two *fdh* genes of interest *SO_4509* appears upregulated in response to all three metal supplemented conditions, +W, +Mo and +W/+Mo. *SO_4513* is also upregulated when grown +Mo or +W/+Mo but even higher upregulation (1.4 AU) is seen when grown +W.

Any conclusions made have to be carefully considered due to the number of variables involved, but it can be stated with relative confidence that based on these data alone, supplementation with either sodium tungstate and/or

molybdate at 3 μM under these conditions during exponential growth causes an increase in amplicons for *SO_4509* and *SO_4513*, with a particular increase in *SO_4513* amplicons in response to tungstate alone. In addition under these conditions amplicons for *SO_0101* are upregulated when sodium tungstate or molybdate are at low concentrations (specifically around 70-80 nM as determined in Table 3-1).

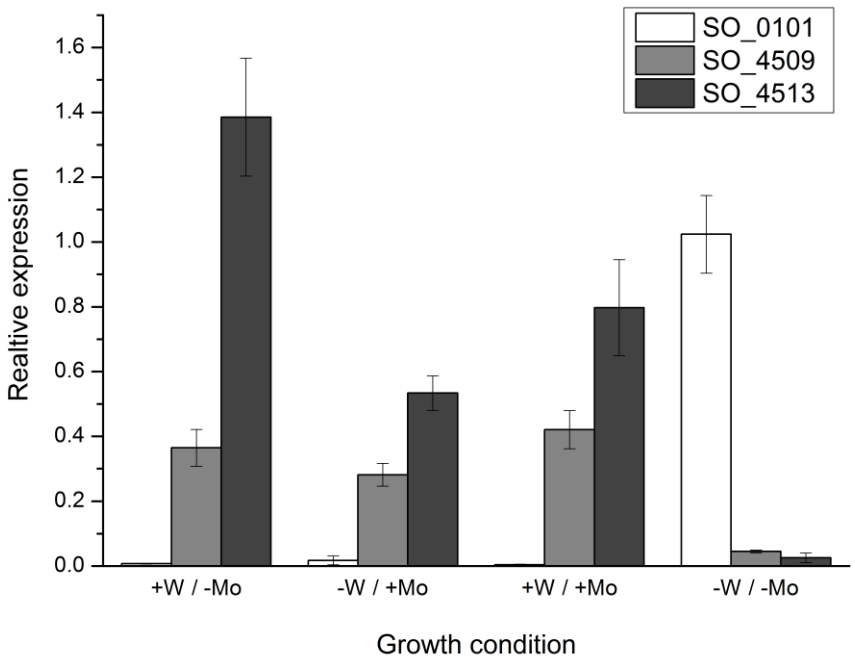

Figure 3-5 Fdh gene expression in response to metal supplementation.
Where +W indicates supplementation of sodium tungstate at 3 μM to anaerobic minimal media and +Mo indicates sodium molybdate supplementation at 3 μM. Data represents absolute determination of amplicon levels normalised to the housekeeping gene RecA in three experiments where error bars represent ± SD.

3.6 FDH activity in response to metal supplementation.

To further characterise the effects sodium tungstate and molybdate have on metabolism of formate in *S.oneidensis* the FDH activity in whole cells was measured. This was carried out to elucidate which of the two metals might be responsible for catalysis of formate oxidation. For these experiments cells were harvested after 24 h of growth in minimal media supplemented with metals at 3 μM as described previously. These cells were then thoroughly washed to remove metabolites that might interfere with the following assay. To monitor formate oxidation the redox dye methyl viologen (MV) was used. By coupling formate

oxidation to reduction of methyl viologen it allows the progress of the reaction to be monitored spectroscopically as the methyl viologen transitions from the colourless $[MV]^{2+}$ state to the blue $[MV^{\cdot}]^{+}$ oxidation state (Illichmanová et al. 2011). The observed absorbance change at 598 nm is then converted to a FDH specific activity normalised using total protein content. The specific activities determined for each growth condition are presented in Figure 3-6 where +W and +Mo indicate sodium tungstate and sodium molybdate growth supplementation at 3 μM respectively in minimal media.

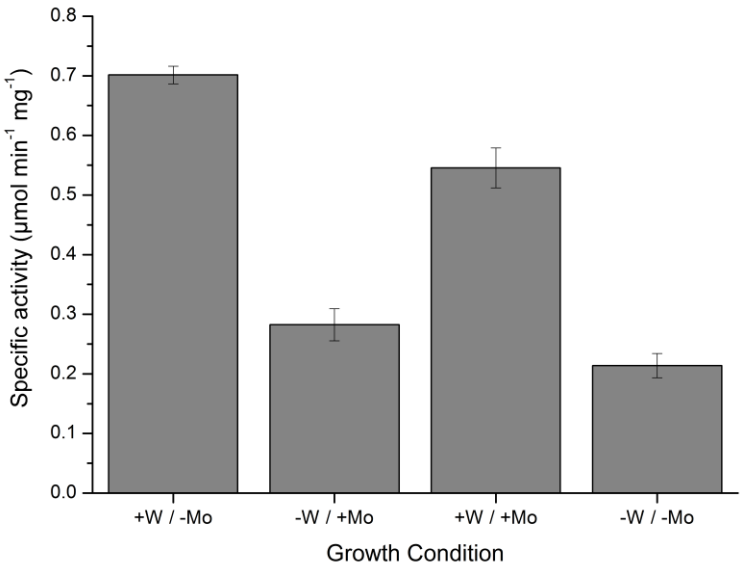

Figure 3-6 FDH activity in response to metal supplementation in minimal growth media.
Where +W indicates sodium tungstate at 3μM and +Mo indicates sodium molybdate at 3μM. Activities obtained using colorimetric methyl viologen assay and normalised to total cellular protein content in samples. Data represents average of a minimum of three experimental data sets where error bars represent ± SEM.

Noticeable changes were observed in FDH activity between growth conditions in Figure 3-6, with the lowest being observed in the control without +W or +Mo supplementation, in keeping with these metals being important for catalysis. +Mo supplementation alone caused a small 0.07 μmol $min^{-1}mg^{-1}$ increase in specific activity. More significant increases were seen with +W or +W and +Mo conditions with increases in specific activity of 0.49 and 0.33 $\mu molmin^{-1}mg^{-1}$ compared to the non-supplemented control. Since the highest increases in FDH activity are seen when tungstate is present it is concluded that tungstate, and not molybdate, is required for maximal FDH activity in these conditions.

3.7 Discussion

Formate is a commonly cited electron donor used to support growth of *S.oneidensis* MR-1 by generating proton motive force (Kane et al. 2016). Although commonly alluded to, the enzymes involved have not been studied thoroughly. This first collection of work aims to clarify and characterise the role formate, and FDH enzymes, play in the metabolism of *S.oneidensis* MR-1.

Although *S.oneidensis* MR-1, and indeed many characterised *Shewanella* strains, have been shown to be able to use formate as an electron donor (Kostka & Nealson 1995) there has been a degree of controversy as to whether it can be used as a sole carbon and energy source, with several older publications claiming this to be true (Scott & Nealson 1994). Bioinformatic modelling studies suggested possible formate assimilation pathways including a pyruvate-formate lyase complex in reverse (acetyl CoA + formate ⇌ pyruvate + CoA) (Fredrickson et al. 2008) or use of enzymes comprising the serine or isocitrate lyase serine pathways combined with elements of the central carbon metabolism for *Shewanella putrefaciens* (Fredrickson et al. 2008)(Serres & Riley 2006). Despite these observations, it was also suggested that carbon could alternatively be sourced from amino acids commonly added as minimal media supplements to previous experiments, namely glutamine, arginine and serine (Fredrickson et al. 2008). Serine in particular has been demonstrated to be a suitable carbon source for growth of *S.oneidensis* (Scott & Nealson 1994). Despite their regular inclusion in minimal media, it should be noted that *S.oneidensis* does not have an auxotrophic dependence on these amino acids and their supplementation is not required for successful growth in other growth conditions.

The data in Figure 3-1 supports this hypothesis, that formate is in fact capable of acting as electron donor, but not sole carbon source, as when the same amino acids were excluded from the minimal media no growth was observed suggesting the importance of both components under these conditions.

Sodium fumarate is used as a terminal electron acceptor in these experiments. Nitrate, nitrite, thiosulfate, trimethylamine N-oxide (TMAO) and dimethyl sulfoxide (DMSO) have also been shown to be effective alternative soluble electron acceptors (Gao et al. 2008). Fumarate was used because the enzymes used to catalyse the reduction of many of these alternative acceptors are

predicted to be molybdopterin containing enzymes and since this study was in part investigating the effect of molybdate on cell growth it was deemed the most appropriate. The reduction of fumarate in *S.oneidensis* is catalysed by FccA, a periplasmic flavocytochrome protein (Maier et al. 2003) with no known requirement for either tungsten or molybdenum in its biosynthesis or expression.

The determination of a substrate affinity constant, or Monod constant (K_s) (Owens & Legan 1987) for formate in *S.oneidensis* MR-1 in the described growth conditions is shown in Figure 3-2. A K_s of 20.4 ± 6 mM was determined. Comparison with other literature values is difficult due to a general lack of standardisation. Not only are there often conflicting experimental results, but multiple methods to determine specific growth and a multitude of mathematical models to fit data (Owens & Legan 1987). The result is that even for glucose in *Escherichia coli*, one of the most well studied examples of cellular kinetics, values for K_s vary by 3 orders of magnitude (Kovarova-Kovar & Egli 1998). Despite this, the values estimated here do not seem unreasonable, similar to K_s values obtained for formate as the sole energy and carbon source in *Pseudomonas oxalaticus* OX1. A specific number is not quoted as depending on the mathematical fitting used values ranged from 0.5-60 mM (Dijkhuizen & Harder 1975) re-emphasising the previous point. Concerning suitability of experimental design and analysis, the approaches used here were chosen for their simplicity. Specific growth rates were determined from batch culture rather than respirometry, i.e. the study of CO_2 or other metabolomic products (Du Plessis et al. 2001) due to experimental limitations and data was computationally fitted by non-linear regression to the hyperbolic Monod equation. This was partially to avoid the biases affecting arrangements such as those often seen in Lineweaver-Burke plots (Schnell & Maini 2003) but also because more complicated models have been the subject of much controversy (Almquist et al. 2014). Although determining specific growth activities from batch cultures is an established procedure, it does make the assumption that cell responses to the substrate in question are immediate, and that cells do not need time to adapt, an assumption that is not always true and further complicates literature comparison (Owens & Legan 1987). The K_s value here will likely only become important in the context of future work when it can be compared to other strains growth under the same conditions.

Both tungsten and molybdenum have been shown to be catalytically important in FDH enzymes in a variety of species (Moura et al. 2004). As yet there is no definitive way of determining the required metal for putative molybdo/tungsto pterin enzymes, and indeed because this is not commonly considered many putative PGD enzymes may require tungsten or at least be able to use it as a substitute in the absence of environmental molybdenum. The oxyanion forms of these metals, tungstate (WO_4^{2-}) and molybdate (MoO_4^{2-}) are the bioavailable forms of these metals found in the environment and both are recognised by the ABC type transporters that transport them across bacterial membranes (Magalon et al. 2011), hence their use over the elemental forms in these studies. Figure 3-3 investigates the effect on growth of supplementing these metals to growth media with the prediction that if one or other metal was essential its absence would prevent growth on formate.

Surprisingly growth was seen without addition of either metal. This is likely to be explained by the ICP-MS analysis of the media which suggests that despite experimental efforts traces of both W (112 nM ± 21 (SEM)) and Mo (74 nM ± 15 (SEM)) remain in the non-supplemented media. It should be noted that ICP-MS quantifies total metal content after acid digestion and a percentage of this metal may not be in a bioavailable form.

Although seemingly low, such levels are in fact comparable to those found in environments where *Shewanella* species are usually found, predominantly aquatic environments. Molybdenum is the most abundant transition metal in surface sea water, present at 100 nM (Butler 1998) whilst an average of around 20 nM has been suggested for lake derived water, with levels rising more than 200 fold in areas affected by quarrying (Hem 1985). To emphasise the differences between different locations, another study found Mo concentrations to vary between three eastern Sierra Nevada rivers from 12 nM to 3200 nM (Johannesson et al. 2000) suggesting natural exposure and abundance can vary greatly. With respect to W, the same study found values ranging from 0.8 nM to 1030 nM in line with the common observation that W is generally found less abundantly than Mo in the current environment (Magalon et al. 2011). Considering these values it is not surprising that the nanomolar range of trace W and Mo found in the media are capable of supporting growth. The ability to effectively scavenge cofactor metals found at such low concentrations is probably

due to the presence of highly specific ABC type transporters. Both putative tungstate, *TupA* (SO_4719) (Kolker et al. 2005) and molybdate *ModA* (SO_3863) and *ModC* (SO_3865) transporters are predicted to exist in *S.oneidensis* MR-1.

The inability to remove nanomolar traces of metals needed for cofactors from media components using standard laboratory techniques has been previously documented (Gates et al. 2003)(Davey et al. 1970) (Bruland et al. 2013). Indeed many studies simply investigate genotypic and phenotypic changes in response to increases in metal availability as opposed to the more absolute absence vs. presence (Sullivan et al. 2013).

Figure 3-3 demonstrates a slight increase of around 0.1 absorbance units in final OD_{600} when cultures were supplemented with molybdate alone prompting the suggestion that Mo is important for FDH activity. However, as discussed in the context of the FDH assay data later, this appears to not be the case. It is therefore important to consider whether this could be a FDH independent phenotype. Although this media was designed to emphasise formate dependent phenotypes, bacterial metabolism is complicated and metabolic bottlenecks are poorly understood in many cases (Goelzer & Fromion 2011). It is entirely possible that another molybdate dependent process limits growth in these conditions, either at a regulatory level or as a cofactor in another molybdopterin protein. Possible candidates for such alternative molybdoenzymes include the DMSO reductases encoded by SO_1429 and SO_4358 (Gralnick et al. 2006), sulphite dehydrogenase (SO_0715), isoquinoline 1-oxidoreductase (SO_3048), thiosulphate reductase / polysulphide reductase (SO_4062) and the periplasmic nitrate reductase *NapA* (SO_0848). It is possible that these enzymes may alleviate some metabolic bottleneck, for example NapA has been shown to dissipate excess reducing energy for redox balance (Gavira et al. 2002) when grown with nitrate, although this is not the case here, a homologous system may exist involving one of the other listed enzymes.

Figure 3-4 demonstrates a seemingly higher toxicity of molybdate than tungstate in the investigated conditions. This can be most easily explained by first hypothesising that W is essential as a cofactor for maximal FDH activity. Making this assumption it is not surprising that increasing tungstate does not seem to affect growth, even at 150 μM. As a continuation of this hypothesis the observed toxicity of molybdate at higher concentrations can also be explained, at

low concentrations of molybdate supplementation (3 μM) the traces of W found in the media may still be effectively scavenged for cofactor incorporation, however if the ratio of Mo:W in the environment increases, the Mo may begin to competitively inhibit W incorporation into enzymes for formate oxidation, which are unable to function and therefore unable to support growth on formate. This is speculative but is supported by the observation that supplementation of both metals at 150 μM restores growth in this media, and using the same rational as before can be explained as the ratio of Mo:W in the environment is no longer biased, preventing competitive inhibition by Mo. Evidence for W and Mo oxyanion antagonism and subsequent enzyme inactivation has several precedents in the literature; a very pertinent example is the tungsten containing FDH of *Campylobacter jejuni* that is negatively affected by excess molybdate during growth (Smart et al. 2009). The opposite relationship is more regularly reported with molybdoenzyme activity inhibited after growth with tungstate (Gates et al. 2003). Both nitrate and sulphite oxidoreductases are typical tungsten-sensitive molybdoenzymes (Smart et al. 2009) in keeping with the previous discussion explaining the higher OD_{600} reached when supplemented with molybdate alone.

An alternative explanation for the results in Figure 3-4 might involve some FDH independent toxicity effect, but this seems unlikely as when equivalent concentrations (150 μM) of tungstate, molybdate and both metals were supplemented to anaerobically grown LB media, which does not use formate as its principal energy source, no differences in growth phenotypes were observed. The exact compounds acting as electron donors in LB are generally accepted as being catabolisable amino acids, with less than 100 μM sugar being present (Sezonov et al. 2007).

Toxicity of transition metals at high concentrations is well documented in the literature (Lemire et al. 2013). However examples of molybdate and tungstate concentrations needed to completely inhibit growth as seen in Figure 3-4 Panel B, tend to be considerable higher, for example complete inhibition of *Paracoccus pantotrophus* growth required concentrations of 100 mM tungstate (Gates et al. 2003) further supporting Mo causing toxicity by competitive antagonism. The ability of *S.oneidensis* to grow despite high concentrations of tungstate has been previously documented, with cultures able to grow up to concentrations of 250

mM (Mumy & Doyle 2010), unfortunately this study did not make comparative measurements with molybdate.

The preceding discussion has not differentiated between different FDH isoforms within *S.oneidensis* MR-1. Three gene clusters have been identified as being important for respiratory formate oxidation, the active heterotrimeric FDH enzymes encoded by SO_0101-0103 (Fdnαβγ), SO_4509-4511 (Fdh1αβγ) and SO_4513-4515 (Fdh2αβγ) (Kane et al. 2016). The previous results have discussed formate oxidation, but it is important to appreciate that the relative contributions of the three isoforms may vary depending on the growth conditions. This was investigated in Figure 3-5 concerning the expression of the catalytically active alpha subunits of these three isoforms, SO_0101, SO_4509 and SO_4513.

Expression of SO_0101 was considerably higher when neither W nor Mo were supplemented in the growth media raising several non-mutually exclusive hypotheses. The first is that SO_0101 does not require either metal for catalysis and is capable of functioning in some Mo/W independent manner and is expressed to compensate when the Mo/W dependent isoforms are unavailable. The second hypothesis is that SO_0101 is repressed by expression of the other isoforms to prevent waste of resources in metabolic redundancy. A further possibility is repression of SO_0101 by either the presence of tungstate and/or molybdate at 3 μM. The final possibility is that this isoform is upregulated in response to low levels of cofactor metal availability and is capable of benefiting from incredibly efficient scavenging mechanisms in a way other isoforms are not, potentially by virtue of SO_0107, a putative assembly/maturation protein, FdhD, or by SO_0108, a protein of unknown function, equivalents of both which are missing in the other two gene clusters. Studies in *E.coli* have demonstrated homologous FdhD proteins to be important for cofactor insertion (Sawers 1994) supporting this line of reasoning. The above scenario could hold true but making the distinction that SO_0101 is downregulated in response to higher concentrations of cofactor metals, as opposed to upregulated without them, without understanding the underlying mechanisms both are possible. Such sensitive but usually complicated changes in metabolic gene expression relating to metal limitation are well recorded, with upregulation of systems better able to make use of available resources (Merchant & Helmann 2012).

Concerning the other two isoforms SO_0509 and SO_4513, the qPCR data suggests that in the four growth conditions studied the SO_4509 isoform was constitutively expressed when tungstate and/or molybdate were supplemented. The SO_4513 isoform was also expressed in these three conditions and was up-regulated most when tungstate alone was added to media. From this data alone it can be suggested that under metal supplemented conditions SO_4509 and SO_4513 are likely to play an important role in formate oxidation, with tungstate being of particular importance for SO_4513. Such enzymatic changes in response to availability of different cofactor metals would not be a unique finding. During Fe^{2+} deprivation there are numerous cases whereby Mn^{2+} is instead incorporated into mononuclear Fe^{2+} enzymes including ribulose-5-phosphate 3-epimerase, cytosine deaminase, peptide deformylase, and threonine dehydrogenase, this particular substitution is not only initiated in response to Fe scarcity, but also in response to oxidative stress as the Mn^{2+} containing enzyme is less susceptible to oxidative inactivation by H_2O_2 (Dudev & Lim 2014).

The gene expression presented here is limited in a number of ways. Initially it only addresses expression of the catalytic alpha subunits, whilst information on expression of other gene cluster proteins including the accessory proteins described above would be of interest as would be expression of the transporters TupA , ModA and ModC . It should also be noted that RNA was extracted for these experiments during mid exponential growth, and further changes may appear in later stages of growth. In addition to the current qPCR data presented here a more thorough future approach would conduct microarray or RNA sequencing experiments to establish all genetic changes in response to W and Mo but this was not the principal focus of this work. A final caveat with this work is that it is not assumed that an increase in mRNA gene transcripts as monitored here necessarily translates into an increase in functional protein, with post translational regulation playing an important role (Greenbaum et al. 2003).

The colorimetric whole cell assays presented in Figure 3-6 add an extra layer of complexity to this discussion. When considering formate oxidation, specific activities are significantly higher when cultures are grown with tungstate, raising a number of further questions and possibilities. 1) There is higher FDH

expression in these conditions, as already suggested above in regards to SO_4513. 2) Only tungstate is capable of being incorporated into active FDH enzymes and the activity in non-tungstate supplemented conditions reflects the enzyme population with tungstate traces in the media. 3) Tungstate may be required for maximal FDH activity not as a cofactor, but as a regulatory element, or both. 4) FDH isoform(s) can contain either tungsten or molybdenum but there is a resultant change in enzyme kinetics, possible evidence for this point comes from the small increase in specific activity when supplemented with Mo compared to the non-supplemented control suggesting at least a proportion of FDH activity is Mo dependent. Since these questions are multi-faceted several experiments in subsequent Chapters will aim to address different elements. The question of whether W is incorporated into a cofactor is addressed by purification of active protein in Chapter 4. The contribution of different isoforms to specific activity is investigated in Chapter 5 with use of mutants to allow examination of each isoform in turn. This Chapter also will attempt to address whether both metals can be incorporated into catalytically active cofactors.

The work presented here begins to explore the role of formate in *S.oneidensis*. The initial aim to simply characterise the microbial physiology and the native systems involving formate oxidation evolved into a more complicated study with a number of interesting findings that suggest far more complicated systems than first expected. It was observed that *S.oneidensis* is capable of effectively scavenging Mo and W at nM concentrations to support growth. Further tungstate supplementation at 3 μM caused increases not only in gene expression for *SO_4513* and *SO_4509* but also in whole cell FDH activity. Combined with the possible inhibitory effects of Mo, but not W on growth, it can be summarised that W seems to play an important role in formate oxidation in *S.oneidensis*. Although unexpected considering the effectiveness of Mo containing enzymes in the majority of bacterial species, with W containing enzymes typically being associated with archaea (Silva et al. 2011) and the natural predominance of Mo in the environment, this is a novel discovery in *Shewanella* and warrants further study, addressed in the following section of work.

3.8 References

Almquist, J. et al., 2014. Kinetic models in industrial biotechnology - Improving cell factory performance. *Metabolic Engineering*, 24, pp.38–60.

Bruland, K.W., Middag, R. & Lohan, M.C., 2013. Controls of Trace Metals in Seawater. *Treatise on Geochemistry: Second Edition*, 8, pp.19–51.

Butler, A., 1998. Acquisition and utilization of transition metal ions by marine organisms. *Science*, 281(5374), pp.207–210.

Chen, Y. & Wang, F., 2015. Insights on nitrate respiration by *Shewanella*. *Frontiers in Marine Science*, 1(January), pp.1–9.

Davey, E.W. et al., 1970. Removal of Trace Metals from Marine Culture Media. *Limnology and Oceanography*, 15(3), pp.486–488.

Dijkhuizen, L. & Harder, W., 1975. Substrate inhibition in *Pseudomonas oxalaticus* OX1: a kinetic study of growth inhibition by oxalate and formate using extended cultures. *Antonie van Leeuwenhoek*, 41(1), pp.135–146.

Dudev, T. & Lim, C., 2014. Competition among metal ions for protein binding sites: Determinants of metal ion selectivity in proteins. *Chemical Reviews*, 114(1), pp.538–556.

Fredrickson, J.K. et al., 2008. Towards environmental systems biology of *Shewanella*. *Nature reviews. Microbiology*, 6(8), pp.592–603.

Gao, H. et al., 2008. Probing regulon of ArcA in *Shewanella oneidensis* MR-1 by integrated genomic analyses. *BMC genomics*, 9(Iii), p.42.

Gates, A.J. et al., 2003. Properties of the periplasmic nitrate reductases from *Paracoccus pantotrophus* and *Escherichia coli* after growth in tungsten-supplemented media. *FEMS Microbiology Letters*, 220(2), pp.261–269.

Gavira, M. et al., 2002. Regulation of nap Gene Expression and Periplasmic Nitrate Reductase Activity in the Phototrophic Bacterium *Rhodobacter sphaeroides* DSM158. *Journal of bacteriology*, 184(6), pp.1693–1702.

Goelzer, A. & Fromion, V., 2011. Bacterial growth rate reflects a bottleneck in resource allocation. *Biochimica et Biophysica Acta - General Subjects*, 1810(10), pp.978–988.

Gralnick, J. a et al., 2006. Extracellular respiration of dimethyl sulfoxide by *Shewanella oneidensis* strain MR-1. *Proceedings of the National Academy of Sciences of the United States of America*, 103(12), pp.4669–74.

Greenbaum, D. et al., 2003. Comparing protein abundance and mRNA expression levels on a genomic scale. *Genome Biol*, 4(February 2017), p.117.

Hem, J.D., 1985. *Study and Interpretation of the Chemical Characteristics of Natural Water*

Illichmanová, a et al., 2011. Nitrate reductase whole-cell assay: side effects associated with the use of benzyl viologen. *Folia microbiologica*, 56(1), pp.72–6.

Johannesson, K.H. et al., 2000. Oxyanion concentrations in Eastern Sierra Nevada Rivers - 3. Boron, Molybdenum, Vanadium, and Tungsten. *Aquatic Geochemistry*, 6(1), pp.19–46.

Kane, A.L. et al., 2016. Formate metabolism in *Shewanella oneidensis* generates proton motive force and prevents growth without an electron acceptor. *Journal of Bacteriology*, 198(8), pp.1337–1346.

Kisker, C., Schindelin, H. & Rees, D.C., 1997. Molybdenum cofator containing enzymes: Structure and Mechanism. *Annu. Rev. Biochem*, 66, pp.233–67.

Kolker, E. et al., 2005. Global profiling of *Shewanella oneidensis* MR-1: expression of hypothetical

genes and improved functional annotations. *Proceedings of the National Academy of Sciences of the United States of America*, 102(6), pp.2099–104.

Kostka, J.E. & Nealson, K.H., 1995. Dissolution and reduction of magnetite by bacteria. *Environmental science & technology*, 29(10), pp.2535–40.

Kouzuma, A. et al., 2010. Disruption of the putative cell surface polysaccharide biosynthesis gene SO3177 in *Shewanella oneidensis* MR-1 enhances adhesion to electrodes and current generation in microbial fuel cells. *Applied and environmental microbiology*, 76(13), pp.4151–7.

Kovarova-Kovar, K. & Egli, T., 1998. Growth Kinetics of Suspended Microbial Cells: From Single-Substrate-Controlled Growth to Mixed-Substrate Kinetics. *Microbiol. Mol. Biol. Rev.*, 62(3), pp.646–666.

Laukel, M. et al., 2003. The tungsten-containing formate dehydrogenase from *Methylobacterium extorquens* AM1: Purification and properties. *European Journal of Biochemistry*, 270(2), pp.325–333.

Lemire, J. a, Harrison, J.J. & Turner, R.J., 2013. Antimicrobial activity of metals: mechanisms, molecular targets and applications. *Nature reviews. Microbiology*, 11(6), pp.371–84.

Magalon, A. et al., 2011. Molybdenum enzymes in bacteria and their maturation. *Coordination Chemistry Reviews*, 255(9–10), pp.1159–1178.

Maier, T.M. et al., 2003. Identification of the gene encoding the sole physiological fumarate reductase in Shewanella oneidensis MR-1. *J. Basic Microbiol*, 43(4), pp.312–327.

Merchant, S.S. & Helmann, J.D., 2012. Elemental Economy. Microbial Strategies for Optimizing Growth in the Face of Nutrient Limitation. *Advances in Microbial Physiology*, 60, pp.91–210.

Moura, J.J.G. et al., 2004. Mo and W bis-MGD enzymes: nitrate reductases and formate dehydrogenases. *Journal of biological inorganic chemistry*, 9(7), pp.791–9.

Mumy, K. & Doyle, T., 2010. Impact of Sodium Tungstate and Tungsten Alloys on the Growth of Selected Microorganisms with Environmental Significance. *Naval Health Research Center Detachment reports*, (July), pp.1–30.

Owens, J.D. & Legan, J.D., 1987. Determination of the Monod substrate saturation constant for microbial growth. *FEMS Microbiology Reviews*, 46, pp.419–432.

Pinchuk, G.E. et al., 2011. Pyruvate and lactate metabolism by *Shewanella oneidensis* MR-1 under fermentation, oxygen limitation, and fumarate respiration conditions. *Applied and environmental microbiology*, 77(23), pp.8234–40.

Du Plessis, C.A. et al., 2001. Development of respirometry methods to assess the microbial activity of thermophilic bioleaching archaea. *Journal of Microbiological Methods*, 47(2), pp.189–198.

Sawers, G., 1994. The hydrogenases and formate dehydrogenases of *Escherichia coli*. *Antonie van Leeuwenhoek*, 66(1–3), pp.57–88.

Schnell, S. & Maini, P.K., 2003. A Century of Enzyme Kinetics: Reliability of the K_m and V_{max} Estimates. *Comments on Theoretical Biology*, 8, pp.169–187.

Scott, J.H. & Nealson, K.H., 1994. A biochemical study of the intermediary carbon metabolism of *Shewanella putrefaciens*. *Journal of bacteriology*, 176(11), pp.3408–11.

Serres, M.H. & Riley, M., 2006. Genomic analysis of carbon source metabolism of *Shewanella oneidensis* MR-1: Predictions versus experiments. *Journal of bacteriology*, 188(13), pp.4601–9.

Sezonov, G., Joseleau-Petit, D. & D'Ari, R., 2007. *Escherichia coli* physiology in Luria-Bertani broth. *Journal of Bacteriology*, 189(23), pp.8746–8749.

Silva, S.M. da et al., 2011. Tungsten and molybdenum regulation of formate dehydrogenase expression in *Desulfovibrio vulgaris Hildenborough*. *Journal of bacteriology*, 193(12), pp.2909–16.

Smart, J.P., Cliff, M.J. & Kelly, D.J., 2009. A role for tungsten in the biology of *Campylobacter jejuni*: tungstate stimulates formate dehydrogenase activity and is transported via an ultra-high affinity ABC system distinct from the molybdate transporter. *Molecular microbiology*, 74(3), pp.742–57.

Sullivan, M.J. et al., 2013. Copper control of bacterial nitrous oxide emission and its impact on vitamin B 12 -dependent metabolism. *Proceedings of the National Academy of Sciences of the United States of America*, 110(49), pp.19926–31.

Yang, Y. et al., 2010. The tricarboxylic acid cycle in *Shewanella oneidensis* is independent of Fur and RyhB control. *BMC microbiology*, 10(1), p.264.

4 Kinetic and protein studies of *Shewanella oneidensis* MR-1 FDH and CO_2 reductase activities

4.1 Suitability of redox dyes for CO_2 reductase assay

Previous work addressed formate oxidation in *S.oneidensis* and began to inform on the importance of the cofactor metals W and Mo from a microbial physiology perspective. Without a more detailed biochemical approach only limited conclusions could be drawn. The formate oxidation assay described in the last chapter was therefore used to further characterise FDH activity and address the possibility of native CO_2 reductase activity in *S.oneidensis*.

Before settling on the methyl viologen assay described in Chapter 3, a number of alternative colourimetric redox dyes were investigated to monitor formate oxidation. Formate-NAD^+ reductase activity was not observed in agreement with previous studies (Mordkovich et al. 2013). However both formate-methyl viologen reductase and formate-benzyl viologen reductase activities were observed at comparable levels (Figure 4-1).

To determine if this FDH activity was reversible a CO_2 reductase assay was also developed. CO_2-methyl viologen oxidase activity was detectable but CO_2-benzyl viologen oxidase activity was not (Figure 4-1). For both cases Na dithionite was used to artificially reduce the viologen to allow its re-oxidation, coupled to CO_2 reduction, to be monitored.

Notably the use of the term CO_2 reductase activity throughout this work is used when describing the activity seen when sodium carbonate is used as a substrate. The use of sodium carbonate to provide CO_2 for CO_2 reductase assays is reported elsewhere (Bassegoda et al. 2014) and was used for experimental ease. It should therefore be clarified that CO_2 in such experiments is derived from the dissociation of Na carbonate in water into CO_2 and other carbonate species. Although the possible implications of this are discussed, experiments using gaseous CO_2 (99.9%) sparged through a reaction cuvette in place of adding Na carbonate solution showed equivalent enzymatic activity, 0.63 ± 0.1 μmolmin-

$^{1}mg^{-1}$ compared to 0.57 ± 0.03 μmol $min^{-1}mg^{-1}$. Importantly, regardless of whether Na carbonate or gaseous CO_2 was used as substrate in these assays, the assay conditions were sufficiently buffered and the pH did not change more than 0.1 pH unit from start to finish.

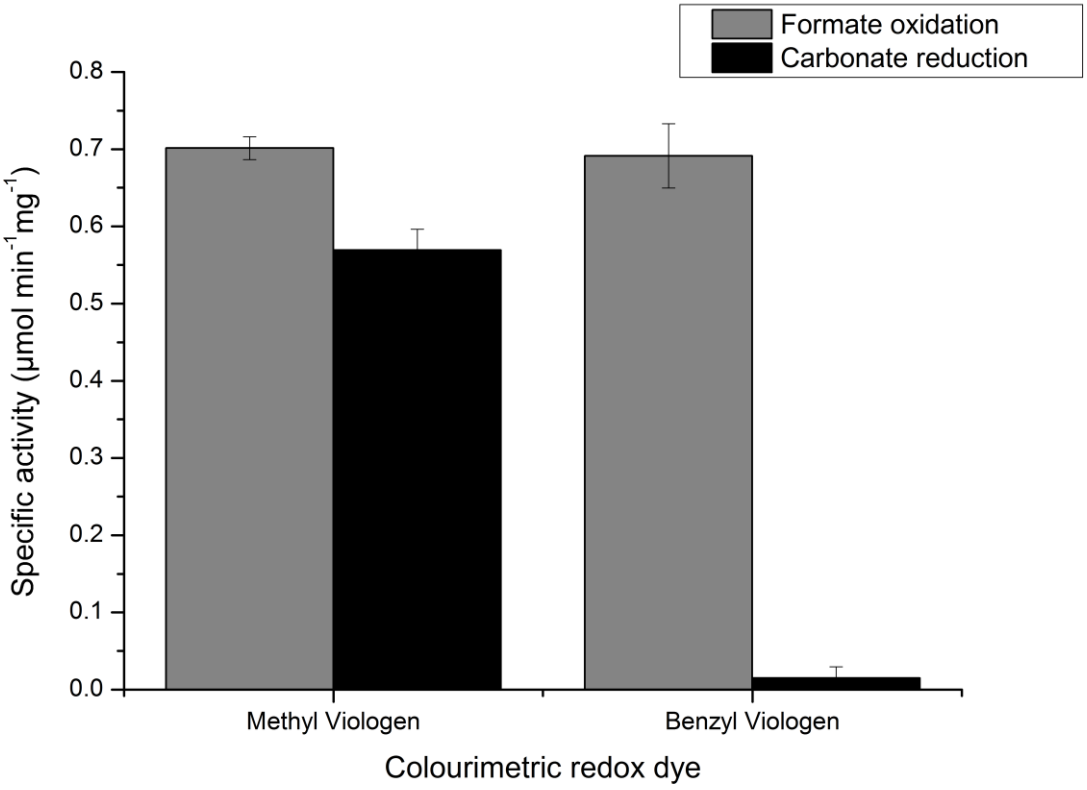

Figure 4-1 Methyl and benzyl viologen coupled FDH and CO_2 reductase activity in S.oneidensis
Viologens used as coupled colourimetric redox dyes with activities normalised to protein content. Cells grown in minimal growth media supplemented with sodium tungstate at 3 μM. Data represents average of a minimum of three experimental data sets where error bars represent ± SEM.

4.2 CO_2 reductase activity in response to metal supplementation.

For all of the above investigations, cells were grown in minimal media supplemented with 3 μM W found to produce the highest FDH activities in Chapter 3. Since FDH activity was metal dependent and the observed CO_2 reductase activity was suspected to be due to FDH enzymes working in reverse, CO_2 reductase activity in these same four conditions was investigated (Figure 4-2). The data for formate oxidation determined in Chapter 3 is also presented here for comparative purposes. CO_2 reductase activity followed the same pattern as formate oxidation, with highest activities when cultures were supplemented

with 3 μM tungstate (+W). When growth was not supplemented (-W/-Mo), or was only supplemented with 3 μM molybdate (+Mo), activities were comparably low, 0.07 ± 0.02 and 0.06 ± 0.01 $\mu molmin^{-1}mg^{-1}$ respectively suggesting W is important for CO_2 reductase activity.

It is also observed that the ratio of CO_2 reduction compared to formate oxidation is also dependent on tungstate supplementation. When grown +W or +W/+Mo, reduction:oxidation ratios of 0.81:1 and 0.92:1 are observed, i.e. in these conditions methyl viologen catalysed CO_2 reduction is approximately equal to formate oxidation. However when grown without tungstate, in +Mo or -W/-Mo growth conditions, ratios of 0.21:1 and 0.34:1 are observed, suggesting formate oxidation is favoured.

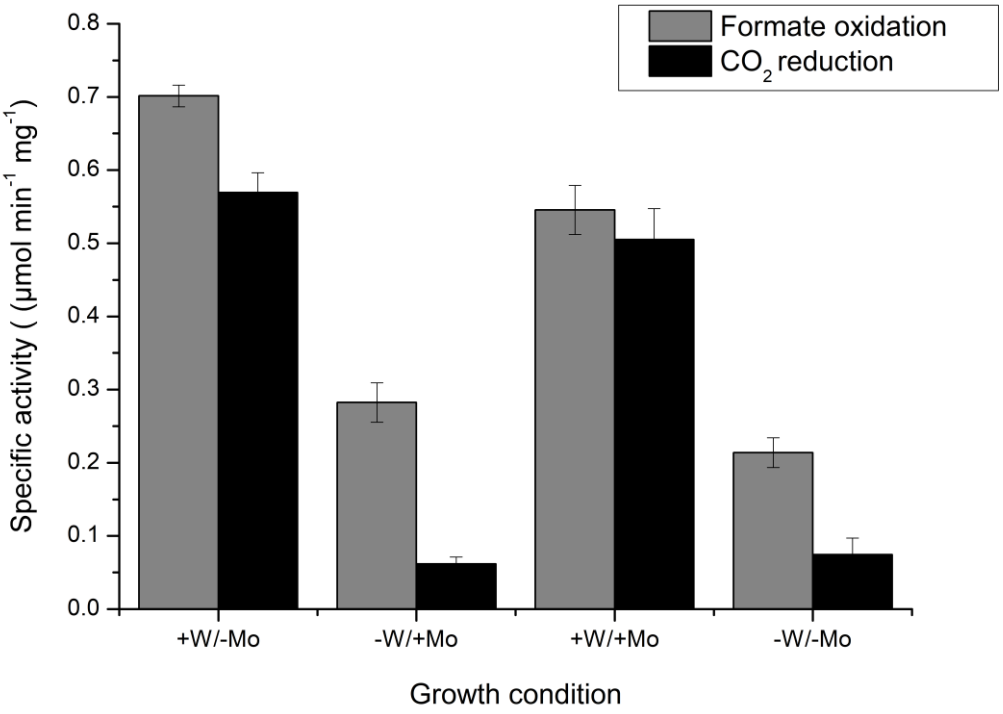

Figure 4-2 FDH and CO_2 reductase activities in response to metal supplementation.
Specific activities for S.oneidensis cells grown in minimal media supplemented with either 3 μM sodium tungstate (+W), 3 μM sodium molybdate (+Mo) supplementation of both metals (+W/+Mo) or neither metal (-W/-Mo). Activities obtained using colorimetric methyl viologen assay and normalised to protein content in samples. Data represents average of a minimum of three experimental data sets where error bars represent ± SEM.

4.3 Azide inhibition of FDH and CO_2 reductase activity.

Since both formate oxidation and CO_2 reduction were believed to be enzymatically catalysed by FDH enzymes the effect of increasing concentrations of Na azide, a known FDH inhibitor, was assessed. These experiments were performed using the assays established above with the resultant data found in Figure 4-3 with FDH inhibition shown in panel A and CO_2 reductase inhibition in panel B. Inhibition of both activities by sodium azide in a concentration dependent manner supports enzymatic catalysis. It is notable that even with 20 mM azide complete inhibition was not observed, with 78 % inhibition seen for formate oxidation and 88 % for CO_2 reduction.

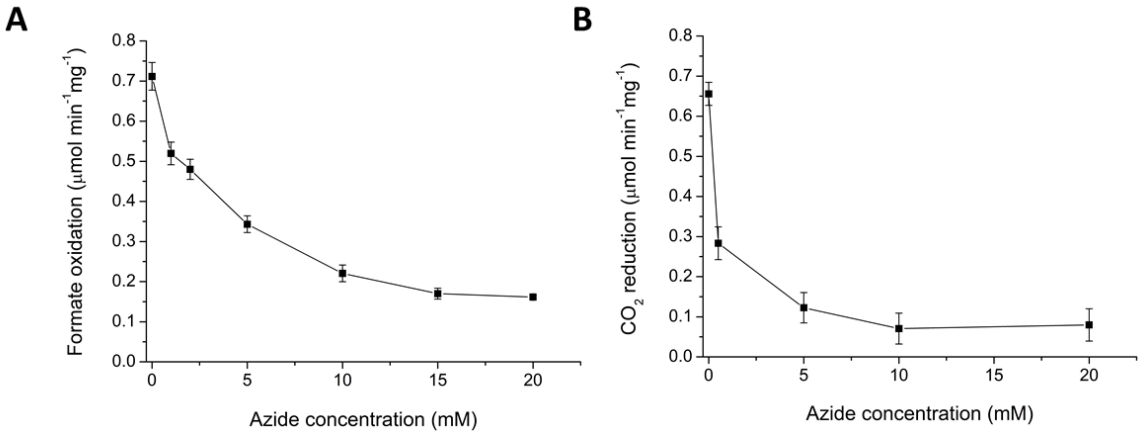

Figure 4-3 Azide inhibition of FDH and CO_2 reductase activities in S.oneidensis cells.
*For both formate oxidation **(A)** and CO_2 reduction **(B)** S.oneidensis grown in minimal growth media supplemented with 3 μM tungstate. Activities obtained using colorimetric methyl viologen assay and normalised to protein content. Data represents average of a minimum of three experimental data sets where error bars represent ± SEM.*

4.4 Confirmation of CO_2 reduction to formate by NMR

Addition of sodium carbonate to whole cells caused the oxidation of methyl viologen. To confirm that CO_2 was reduced to formate ^1H nuclear magnetic resonance spectroscopy was used to quantify formate products in methyl viologen mediated assay conditions. These experiments were conducted identically to previous CO_2 reduction assays with minor modifications to better suit NMR analysis. Previous assays contained only 125 μM dithionite to reduce methyl viologen as higher concentrations would result in inappropriately high absorbance values at 578 nm to monitor spectroscopically. The constraint of this is that even if allowed to continue to completion, only 125 μM of formate will be

formed, with the assumption that 1 M of dithionite dissociates into 2 M of SO_2^- radical in solution (Mayhew 1978) capable of reducing 2 M of methyl viologen which in turn reduces 1 M of CO_2, (the validity of these assumptions are discussed later). Since 125 µM formate proved too low to be accurately detected, 5mM dithionite was used in these experiments on the assumption that it would allow formate to be generated at quantifiable levels. This difference is highlighted here for completeness, but is unlikely to invalidate comparisons with previous assay experiments. Example NMR spectra are included in the appendix (Figure A-1) but collated formate concentration data are presented below for ease of comparison.

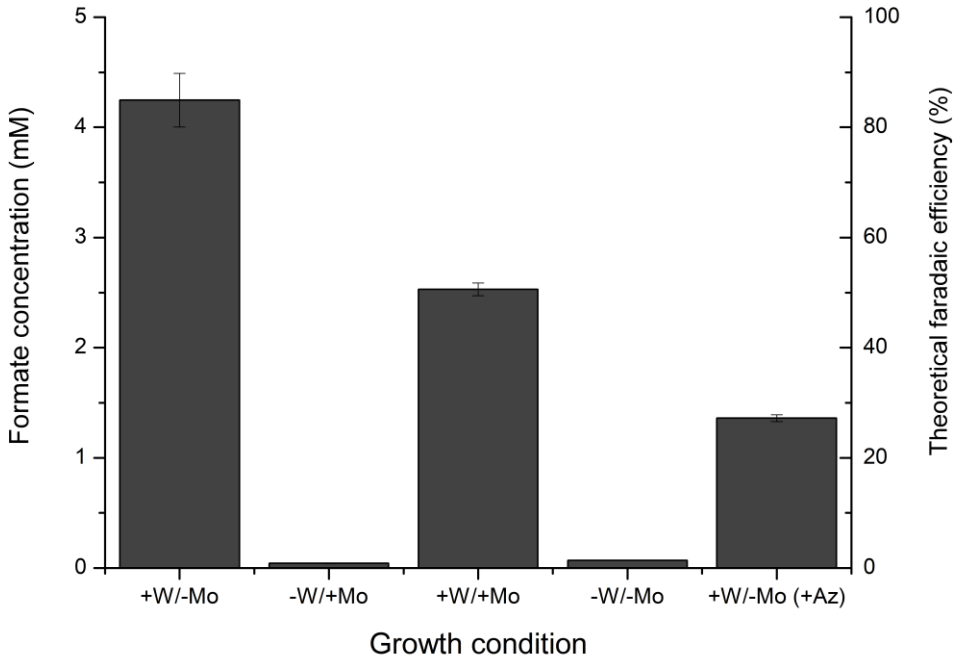

Figure 4-4 NMR analysis of CO_2 reductase assays detecting formate production.
Methyl viologen CO_2 reductase assays were conducted using cells grown in minimal growth media where +W indicates sodium tungstate supplementation at 3 µM and +Mo indicates sodium molybdate supplementation at 3 µM. Following these assays and whole cell removal, supernatant was analysed for formate content. Quantitative formate determinations are shown on left axis and theoretical faradaic efficiency on the right. This efficiency assumes 100% conversion of electrons supplied by dithionite being available for CO_2 reduction (described in text). Where present, azide (Az) at 20 mM in the CO_2 reduction assay. Data represents average of a minimum of three experimental data sets where error bars represent ± SEM.

The data from these experiments (Figure 4-4), correlated with the trends observed in the initial velocity colourimetric assays in Figure 4-2. Accounting for the assay reaction volume and dilutions in preparation for NMR analysis, 4.25 mM ± 0.24 formate was detected in assays with +W grown cells and 2.53 mM ±

0.06 when using +W/+Mo grown cells. Less than 0.1 mM formate was detected in assays containing +Mo or -W/-Mo grown cells. It is possible that despite CO_2 reductase activity being present, formate is quickly re-oxidised by the reverse reaction, to further inform on this the K_m values for both reactions are subsequently presented.

Figure 4-4 indicates not only the quantified formate concentration in these experiments, but also suggests the theoretical faradaic efficiency considering the concentration of reducing equivalents, i.e. 5 mM Na dithionite, added to the reaction. Using the above assumptions 100% efficiency would result in 5 mM formate production. Interestingly CO_2 reduction appeared to have a high faradaic efficiency, approaching 85% when cells were grown +W.

Although not graphically presented here it is important to note that a series of control experiments using NMR analysis confirmed the absolute requirement of all assay components for formate generation. If methyl viologen, dithionite, carbonate, the *S.oneidensis* cells, or any combination of the above were omitted no formate was detected. This provides strong evidence against the observed CO_2 reduction being abiotic, i.e. these results suggest that reduced methyl viologen alone is not sufficient for the reaction to proceed. This is in agreement with comparative controls in the colourimetric assay which could not measure methyl viologen oxidation at 587 nm in the presence of CO_2 without addition of *S.oneidensis* culture.

Figure 4-4 also presents data for formate generation when 20 mM azide was added to assay reactions containing cells grown +W. Only 1.36 mM ± 0.03 formate was seen compared to 4.25 mM ± 0.24 without the inclusion of azide. This is in agreement with the inhibition of CO_2 reductase activity by azide seen in Figure 4-3.

4.5 FDH and CO_2 reductase pH dependence

The effect of pH was investigated on rates of FDH and CO_2 reductase activity, again using the established methyl viologen assays. Since growth +W gave both the highest FDH and CO_2 reductase activities as well as the most formate generation according to NMR, this condition alone was used for these studies. The previous assays were conducted in 100 mM HEPES buffer pH 7.2, however HEPES is only an effective buffer over the pH range 6.8–8.2 with a pKa of 7.55 at 20°C (Good et al. 1966). As such a range of McIlvaine buffers, consisting of disodium phosphate and citric acid were used instead, due to their larger effective pH range of 2.2-8.2 (McIlvaine 1921) and frequent use in investigating pH dependence in enzymatic systems (Ruddock et al. 1996)(Michlmayr et al. 2011). As can be seen in Figure 4-5 specific activities for both reactions at pH 7.2 in this buffer were indistinguishable (within the experimental errors determined) from those at pH 7.2 in HEPES buffer. Specifically formate oxidation was 0.675 ± 0.069 μmol $min^{-1}mg^{-1}$ compared to 0.701 ± 0.014 μmol $min^{-1}mg^{-1}$ in the equivalent HEPES containing assay. CO_2 reduction was 0.692 ± 0.104 $\mu molmin^{-1}mg^{-1}$ compared to 0.569 ± 0.026 $\mu molmin^{-1}mg^{-1}$.

Regarding other pH values investigated it was observed (Figure 4-5) that specific activities for formate oxidation rise with increasing pH and the inverse is true for CO_2 reduction, i.e. specific activity decreases with increasing pH.

There is a notable discrepancy between the previous statement that McIlvaine buffers are appropriate in the pH range 2.2-8.2 and this study not investigating lower than pH6.8. This was because although the buffer was appropriate it was determined that the methyl viologen assay was not. It was found that at pH values lower than 6.8 dithionite was unable to effectively reduce the methyl viologen present, as demonstrated by being unable to reach an OD_{587} value equivalent to those obtained at higher pH experiments. Even though initial rates could be determined at these lower pH values, such experiments were not considered for analysis considering the reduced concentration of reduced methyl viologen and potential interference of bisulphite, discussed subsequently.

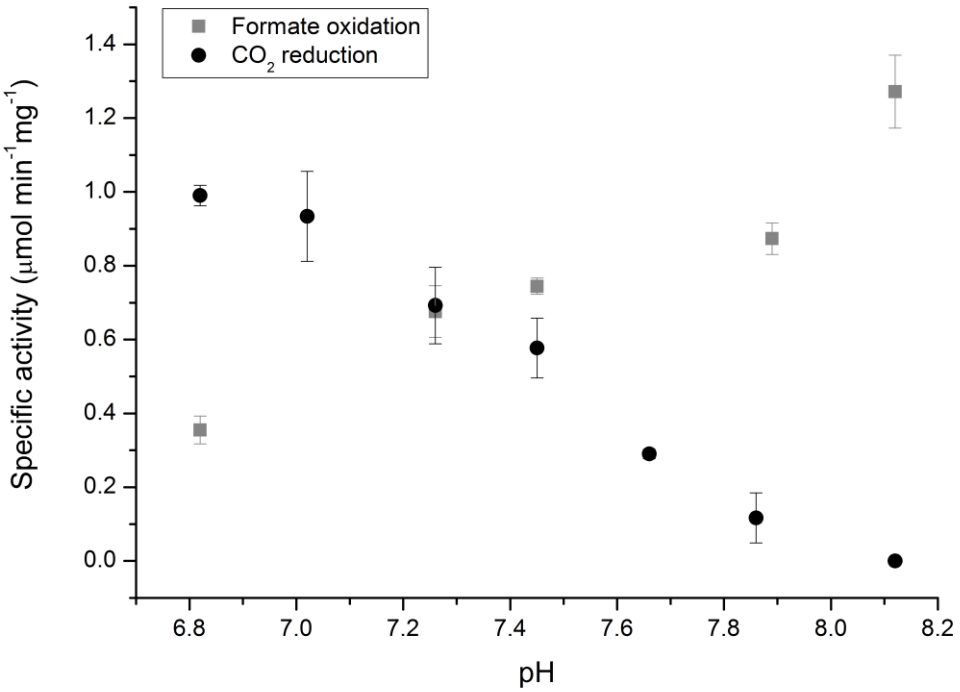

Figure 4-5 pH dependence of FDH and CO_2 reductase activities in S.oneidensis.
Cells grown in minimal growth media supplemented with 3µM tungstate. Activities obtained using colorimetric methyl viologen assay and normalised to protein content. Assays conducted in Mcilvaine buffer at varying pH values. Data represents average of a minimum of three experimental data sets where error bars represent ± SEM.

4.6 FDH and CO_2 reductase activities in cellular fractions.

To determine subcellular location of the FDH and CO_2 reductase enzymes the FDH and CO_2 reductase activities associated with membrane or soluble cell fractions were measured. Whole cells were lysed via sonication and the membrane fractions separated using ultracentrifugation. The supernatant was retained and represents the soluble cellular fractions whilst the pelleted membrane fractions were resuspended in 100 mM HEPES pH7.2.

The localisation of both FDH, CO_2 reductase and fumarate reductase activities were measured for both soluble and membrane fractions. Fumarate reductase activity was measured as *S.oneidensis* MR-1 encodes a single well characterised periplasmic fumarate reductase, FccA (Ross et al. 2011), as such fumarate reductase activity could be used as a control for successful fractionation. Fumarate reductase activity was investigated using a similar methyl viologen based colourimetric assay as described for monitoring CO_2 reduction.

For this control study the specific activities are reported normalised to the combined protein content from both soluble and membrane fractions, allowing clear visualisation of how the activity was divided between fractions.

Approximately 92% of fumarate reductase activity was observed in soluble fractions (4.6 panel A), consistent with a soluble enzyme. However a small amount of unexpected activity was also observed in the membrane fraction, but can be attributed to the relatively crude method of cell fractionation and the high abundance of FccA in the cell (Sundararajan et al. 2011) making complete separation challenging. The fumarate reductase assays show successful separation of membrane and soluble fractions. The same methodology was therefore used to localise both FDH and CO_2 reductase activity. These were studied using the previously discussed methyl viologen assays with membrane and soluble fractions in place of whole cell samples (Figure 4-6 Panel B).

The principal finding of this experiment was that all FDH and CO_2 reductase activities were membrane associated. When assayed, no activity was seen in any of the soluble fractions regardless of the growth conditions used to prepare the cells. This is in keeping with genomic predictions for all FDH enzymes in *S.oneidensis* being part of membrane associated complexes (Kane et al. 2016). Fumarate reductase activity in membrane and soluble fractions is presented in Figure 4-6 normalised to the total combined protein content in both soluble and membrane fractions to allow comparison between fractions. In contrast the lack of soluble activity made equivalent quantitative comparisons between fractions impossible for FDH and CO_2 reductase activities. Accordingly these results are presented as specific activities, normalised only to the protein content in the membrane fraction allowing comparisons with the previous whole cell specific activities instead.

Similarities can be observed in Figure 4-6 Panel B with the whole cell assays presented in Figure 4-2, with +W/-Mo and +W/+Mo growth conditions demonstrating greater FDH and CO_2 reductase activities when compared to -W/+Mo and -W/-Mo growth conditions. All specific activities are higher than their whole cell equivalents due to the partial purification achieved by removing soluble proteins. Due to this the relative differences between activities in growth conditions are exaggerated, for example formate oxidation in +W grown cells is 2.5 times higher than +Mo grown cells in whole cell assays and 4.7 times higher

in membrane fraction experiments. Despite this, the ratio between CO_2 reduction and formate oxidation should remain the same, and in +W growth conditions this is the case, with reduction:oxidation ratios of 0.81:1 for whole cells and 0.84:1 for membrane fractions. For +Mo grown cells, equivalent ratios of 0.21:1 in whole cells and 0.12:1 in membrane fractions are seen.

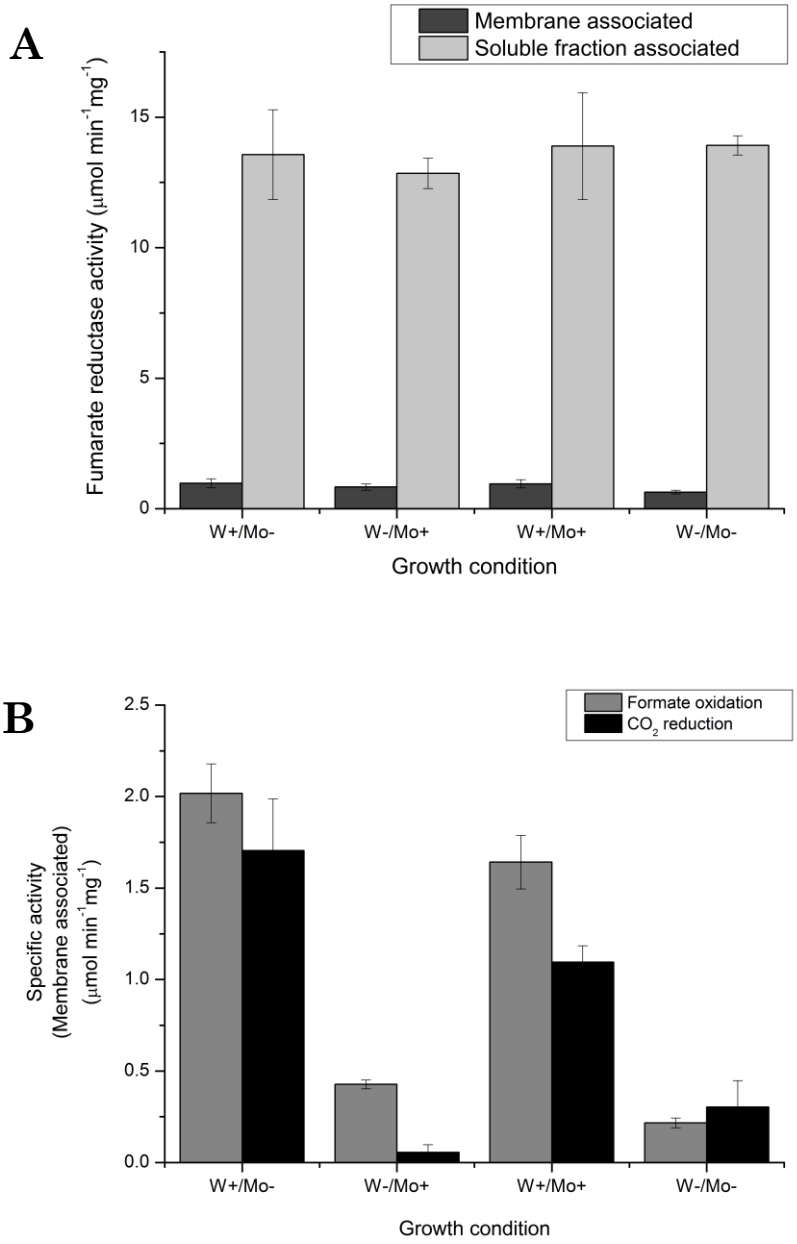

Figure 4-6 Localisation of fumarate reductase, FDH and CO_2 reductase activities.
***(A)** Fumarate reductase activity determined by methyl viologen colorimetric assay in membrane and soluble cell fractions, normalised to combined protein content in membrane and soluble fractions. **(B)** FDH and CO_2 reductase activities determined by methyl viologen colorimetric assays, normalised to protein content in membrane fraction alone. All assays conducted with fractions from S.oneidensis cells grown in minimal media supplemented with 3 µM W. FDH and CO_2 reductase activity was not detected in soluble fractions and is therefore not presented. Data represents average of a minimum of three experimental data sets where error bars represent ± SEM.*

4.7 Kinetic parameters for formate oxidation and CO_2 reduction.

Initial rate varies hyperbolically with substrate concentration for many enzymes, including previously characterised FDH enzymes (Axley et al. 1991), at low substrate concentrations not all active sites are occupied and rate is proportional to substrate concentration giving rise to first order kinetics. As the substrate concentration increases further all available active sites become saturated and zero order kinetics are observed, this can be observed graphically by plotting initial rate against substrate concentration and fitting the hyperbolic curve to the Michaelis-Menten equation (4.1):

$$v_0 = \frac{V_{max}\,[S]}{K_m + [S]} \tag{4.1}$$

Where v_0 is the initial rate, V_{max} is the limiting initial rate when all active sites are occupied, [S] is the substrate concentration and K_m is the Michaelis constant. As derived from Eq. (4.1) above, K_m is the substrate concentration at which the initial rate is half that of the V_{max} value. As such the parameter is given in units of molarity and is often given to report on the specificity of an enzyme for a substrate.

In an attempt to determine kinetic parameters for the observed formate oxidation and CO_2 reductase activities in whole cells, initial rates were determined upon addition of varying concentrations of substrate, either formate or carbonate. These experiments were otherwise identical to previous methyl viologen assays and importantly were conducted using cells grown +W as this is when the greatest activities were previously observed.

As can be seen from Figure 4-7 Panel A, oxidation increased with formate concentration before plateauing as V_{max} approached. Higher concentrations of formate were investigated from 15-50 mM, and for these concentrations of substrate specific activities actually decreased with increasing substrate concentration however these values are not included in Figure 4-7 as significant changes in pH were also observed making this data incomparable. When fitted to a hyperbolic function, the determined values for K_m and V_{max} are 39 ± 5 μM and 0.74 ± 0.02 μmol $min^{-1}mg^{-1}$ respectively with a R squared value of 0.992.

A comparable graph for CO_2 reduction can be seen in Figure 4-7 Panel B. As for formate oxidation, initial rates increased with substrate concentration before approaching V_{max}. By fitting to the same hyperbolic function parameters of 1.43 ± 0.26 mM and 0.58 ± 0.03 μmol $min^{-1}mg^{-1}$ for K_m and V_{max} were determined with an R squared value of 0.984. The data set for CO_2 reduction contains larger errors partly due to the complex behaviour of carbonate as a substrate. When using higher substrate concentrations, from 30 to 50 mM carbonate, specific activities decreased with further increases in substrate concentration as seen for formate oxidation, but as for formate oxidation, significant changes in pH were also observed so these data were excluded from analysis but addressed in the discussion.

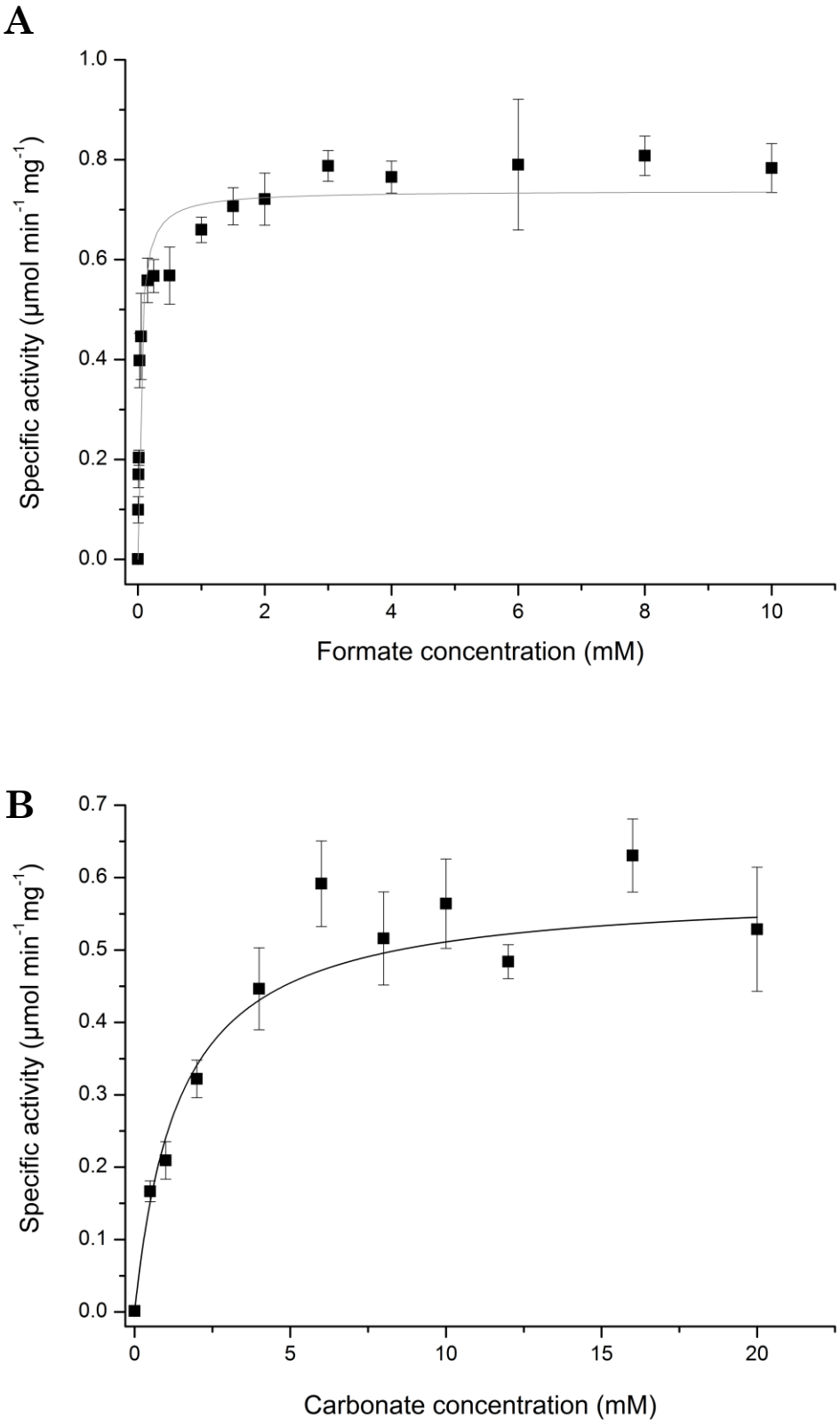

Figure 4-7 S.oneidensis formate oxidation and CO_2 reduction Michaelis-Menten plots.
*For both formate oxidation **(A)** and CO_2 reduction **(B)**, cultures were grown in +W minimal media. Initial rates determined by measuring increasing absorbance in colorimetric methyl viologen assay. Data fitted to a hyperbolic function according to the Michaelis Menten equation. Each data point represents average of a minimum of three experimental data sets where error bars represent ± SEM.*

4.8 FDH and CO_2 reductase activities of *S.oneidensis* grown in Lysogeny-broth media.

To this point all experiments had been conducted in carefully controlled minimal media for a number of reasons, for consistency, to regulate availability of cofactor metals and perceived optimisation for activities of interest. Indeed initial experiments at the start of the project failed to detect FDH activity in routine aerobically grown *S.oneidensis* cultures in LB media. This is confirmed in Figure 4-8 which also failed to detect CO_2 reductase activity in these cells.

Informed by the previous sections of work however an interesting observation was made. When Na tungstate was added to cultures at 3 μM to aerobic LB cultures, (i.e. the same concentration that increases FDH activity in minimal media), both formate oxidation and CO_2 reduction were observed (Figure 4-8). It should be noted that the addition of this tungstate had no impact on the final OD_{600} of such cultures suggesting this is not a factor limiting growth in these conditions. This was still deemed an interesting result as aerobic growth in the previously investigated minimal media is not supported and therefore this represents the only evidence for active reversible FDH enzymes under aerobic conditions in *S.oneidensis* and may bear future significance outlined in the discussion.

Also of interest were equivalent experiments in anaerobically grown LB media. For these experiments 50 mM Na fumarate was provided as a terminal electron acceptor. Even without metal supplementation both FDH and CO_2 reductase activities were observed in anaerobically grown cells, in agreement with the requirement for FDH in anaerobic respiration (Kane et al. 2016). However increases in both formate oxidation, from 0.08 ± 0.01 μmol $min^{-1}mg^{-1}$ to 1.24 ± 0.09 μmol $min^{-1}mg^{-1}$ and CO_2 reduction, from 0.03 ± 0.02 μmol $min^{-1}mg^{-1}$ to 0.41 ± 0.14 μmol $min^{-1}mg^{-1}$ were observed when 3 μM tungstate was added to growth media (Figure 4-8). Again, the addition of tungstate had no effect of the growth of these cultures, with both supplemented and non-supplemented reaching an OD_{600} of 0.23 after 24 h.

Despite these interesting observations, even when grown anaerobically with tungstate supplementation, CO_2 reductase specific activities were lower than those observed in the established minimal media supplemented with tungstate

and considering the aimed application of this project, i.e. CO_2 fixation, this was considered a significant drawback. Exacerbating this aspect was the fact that formate oxidation specific activities in these conditions were actually higher than those seen in minimal media experiments, meaning these growth condition were likely to be biased in favour of formate oxidation significantly more than the minimal media growth conditions. As such subsequent experiments continued to use the defined minimal media for growth rather than this simpler alternative.

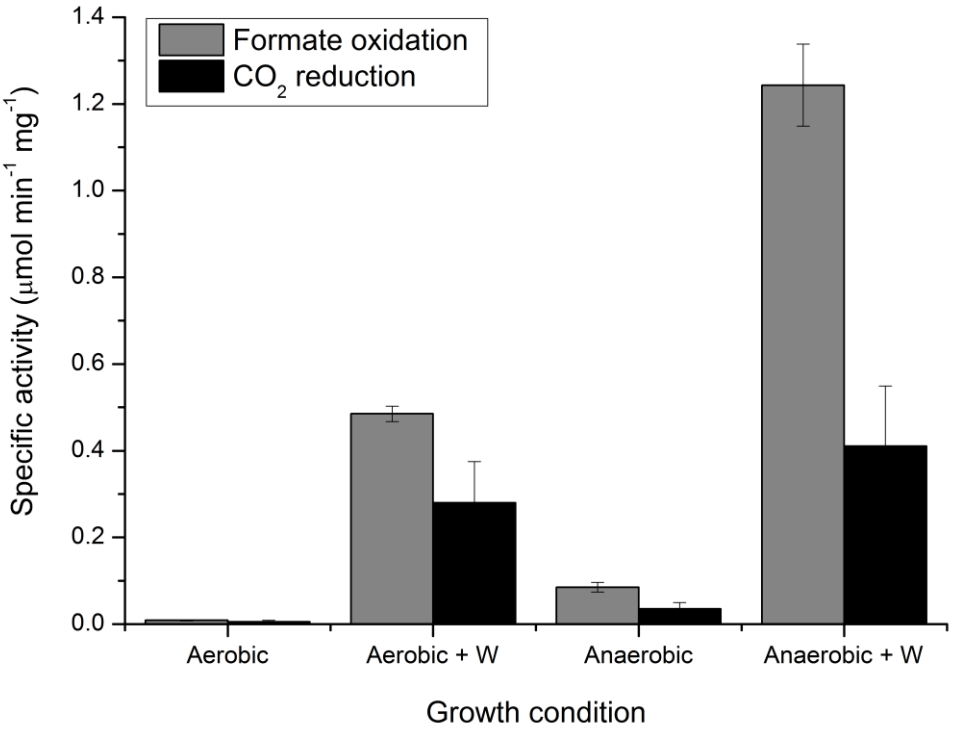

Figure 4-8 FDH and CO_2 reductase activities of S.oneidensis grown in Lysogeny-broth media. W supplemented as 3 μM sodium tungstate. Anaerobic cultures contained 50 mM fumarate as electron acceptor. Activities determined using methyl viologen assay and normalisation to protein content. Data represents average of a minimum of three experimental data sets where error bars represent ± SEM.

4.9 Purification of Fdh2α when grown in tungstate supplemented minimal media.

Due to the previous work suggesting the probable importance of *SO_4513* in both FDH and CO_2 reductase activities the encoded protein, referred to as Fdh2α from this point, was purified and analysed using ICP-MS to determine the identity of any metal cofactor present. Previous work in Chapter 3 had already highlighted that *SO_4513* expression was upregulated in response to tungstate supplementation in growth media but the identity of the cofactor metal had not been demonstrated conclusively.

Purification of Fdh2α (SO_4513) consisted of the following steps. Cell growth, lysis, cellular fractionation, (first separating membranes, then specifically the inner membrane), followed by anion exchange and size exclusion chromatography. This resulted in an isolated amount of Fdh2α which was then able to be analysed by ICP analysis.

For the purification of Fdh2α an *S.oneidensis* MR-1 mutant strain containing only the Fdh2αβγ (SO_4513-4515) Fdh isoform, i.e. a Fdnαβγ (SO_450101-0103) and Fdh1αβγ (SO_4509-4511) knock out, was used. This was primarily to avoid ambiguity, since the purification was monitored by the non-isoform specific FDH assay, it would have been hard to distinguish ineffective purification techniques from separation of different isoforms with different properties. Considering previous results showing highest enzymatic activities when growth was supplemented with tungstate, these same growth conditions in minimal media were used for protein purification.

Cell lysis was performed using a French press as opposed to sonication which was used previously for the experiments shown in Figure 4-6. Sonication was not used here due to its inability to efficiently lyse larger volumes of cells, whereas the use of a French press scales more effectively.

Ultracentrifugation separated membrane fractions of lysed cells from the soluble components, i.e. the periplasm and cytoplasm. Subsequently the use of Sarkosyl allowed the selective solubilisation of the inner membrane, since this is where Fdh2α is predicted to be localised.

Following isolation of inner membranes, Fdh2α was purified based on its ionic properties using anion exchange chromatography. This process involves maintaining the protein sample in a mobile phase with a pH higher than the pI of the protein of interest, resulting in a net anionic charge on the surface of the protein, when passed down a anion exchange chromatography column the negatively charged protein adheres to a matrix coated in cationic functional groups, common examples include diethyl-aminoethyl groups (DEAE) or quaternary amines (Q) attached to sepharose, an agarose derivative (Staby et al. 2000). Once adhered, changes in ion strength in the mobile phase, usually achieved by increasing NaCl concentration, allow the proteins to be eluted. As the concentration of negative Cl ions begins to accumulate, they compete with the bound protein to bind the positively charged groups on the column matrix, in a protein mixture those that are bound weakest to the matrix will elute first, followed by those with higher net positive charges, since each protein will vary in its electrostatic interactions, this process allows separation.

The method described in this work was found to be a good compromise between purifying Fdh2α away from large numbers of other membrane proteins, whilst retaining an acceptable yield. Other methods, including those using alternative detergents such as triton X-100 or alternative buffers (such as HEPES) were less effective in one or both of these considerations. The use of a single NaCl concentration elution step, as opposed to a linear gradient of increasing NaCl concentration followed by pooling of relevant fractions, was found to be important, with inferior recovery when using the second method.

Although anion exchange chromatography was an effective purification step several lower molecular weight proteins were still found in addition to Fdh2α. As such a further size exclusion purification step was used. This successfully isolated Fdh2α, which ran as a band on SDS-PAGE gels just under 100 kDa. NaCl was included at 150 mM in the size exclusion buffer to prevent matrix-protein and protein-protein interactions.

A coomassie blue stained gel image after the final purification and concentration step is shown in Figure 4-9 B. The successful isolation of Fdh2α was confirmed by excision of this band and analysis following tryptic digestion and peptide mass fingerprinting using mass spectrometry. This identification

was statistically significant, using a protein scoring system, score = $-10^{Log(P)}$ where P is the probability the observed match is a random event and where scores above 63 are considered significant ($p<0.05$). Fdh2α identification was significant with a score of 153.

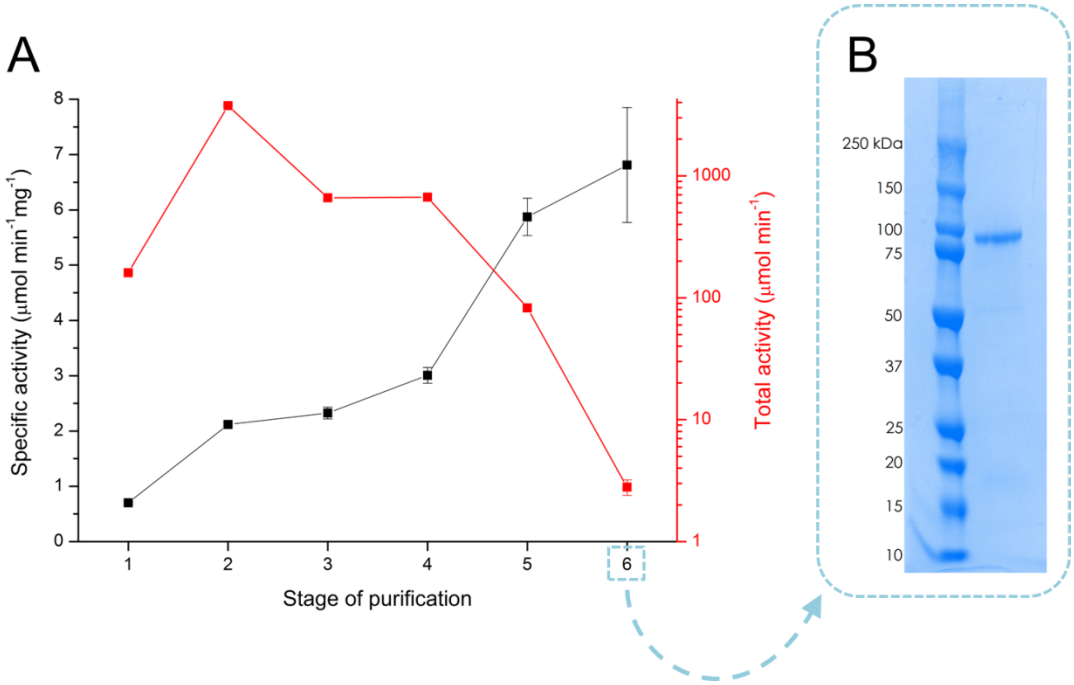

Figure 4-9 Purification of Fdh2α when grown with 3 µM tungstate.
(A) *Reporting on total and specific FDH activity throughout purification, where specific activity determined by normalising methyl viologen assay results to protein content, and total activities report on activity in entire purification step. Purification steps refer to 1) Whole cells 2) Cell lysate 3) Total membrane fractions 4) Inner membrane following sarkosyl solubilsation 5) Following anion exchange 6) Following Size exclusion. Data represents average of three measurements where error bars represent ± SEM.* ***(B)*** *Purified Fdh2α following size exclusion and concentration steps, running on a 4-20 % SDS-PAGE gel in right lane, with precision plus protein dual colour standard in the left, with associated molecular weights marked for reference.*

Throughout the purification it was possible to monitor FDH activity to report on the effectiveness of individual purification steps. By determining protein concentrations via BCA or Bradford assays, (some steps contained reagents unsuitable for the typically used BCA methodology) it was possible to record both specific and total FDH activities during the purification process. These results are shown in Figure 4-9. As would be expected for any successful purification, specific activity rose after each purification step, although only 7 fold throughout the purification. In contrast, the total activity throughout the purification decreased, this is to be expected due to the losses in each step. Explanations for the observed patterns and their relative magnitudes are explored in the discussion below.

Since rates could be determined for purified Fdh2α, turnover values, or k_{cat} values could be determined for both formate oxidation and CO_2 reduction. These values were determined according to eq. (4.2), where E_T is the concentration of enzyme active sites, assumed in this case to be equivalent to enzyme concentration. To determine the concentration of Fdh2α the given molecular weight of 105.46 kDa was used.

$$k_{cat} = \frac{V_{max}\ (\mu mol\ product\ s^{-1})}{[E_T]\ (\mu mol\ enzyme)} \tag{4.2}$$

Using eq. (4.2) turnover numbers of 12 ± 4.3 s^{-1} for formate oxidation and 10.7 ± 3.8 s^{-1} for CO_2 reduction were determined.

4.10 ICP-MS analysis of Fdh2α when grown in tungstate supplemented minimal media.

Following the purification of Fdh2α detailed above, 100 µl of 1.5 µM protein, determined by BCA assay and assuming a molecular weight of 105.46 kDa was digested using nitric acid and analysed for W and Mo content using ICP-MS. When accounting for the acid dilution step 2 µM W and 0.002 µM Mo were detected in the sample with the Mo value below the limit of detection for these experiments. From this it was concluded that Fdh2α coordinated W and not Mo, at approximately a 1.3:1 ratio of metal to protein.

4.11 Attempted purification of Fdh2α when grown in molybdate supplemented minimal media.

In addition to purifying Fdh2α when grown in minimal media containing tungstate, equivalent purifications were attempted when grown with molybdate, to determine if this metal could also be incorporated. An identical procedure to the previous protein purification was followed however the methodology was not suitable for these conditions. This can be clearly seen by comparing the maximum total activities seen in each purification, 230 µmol min^{-1} when grown with molybdate Figure 4-10 and 3700 µmol min^{-1} when grown with tungstate Figure 4-9. It was eventually concluded that the purification techniques were too inefficient to retrieve suitably pure protein for ICP-MS analysis, the initial quantities of Fdh2α in the cells were too low.

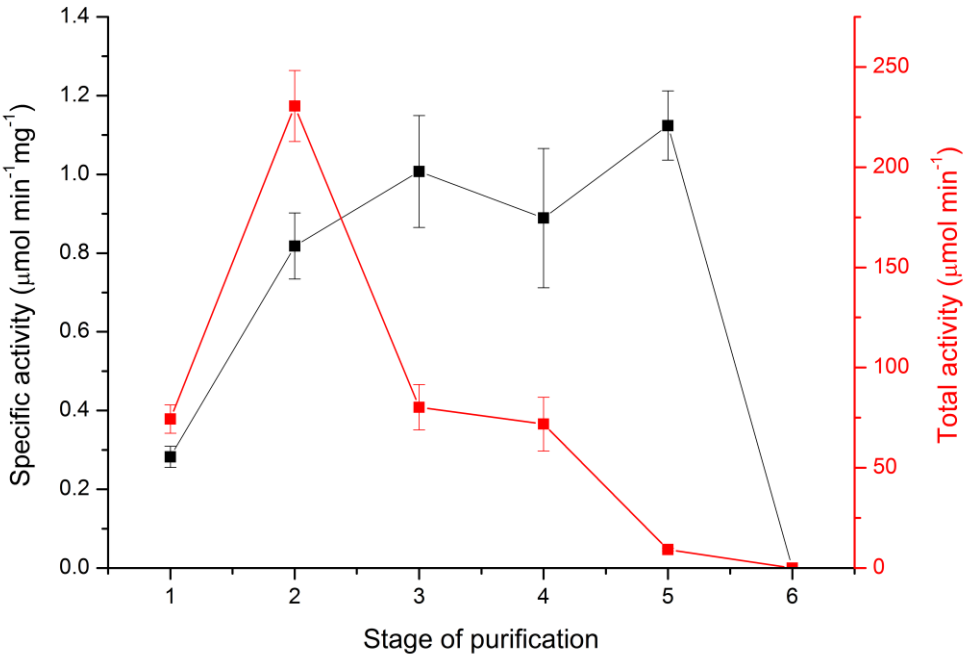

Figure 4-10 Purification of Fdh2α when grown with 3 µM molybdate.
Reporting on total and specific FDH activity throughout purification, where specific activity determined by normalising methyl viologen assay results to protein content, and total activities report on activity in entire purification step. Purification steps refer to 1) Whole cells 2) Cell lysate 3) Total membrane fractions 4) Inner membrane following sarkosyl solubilsation 5) Following anion exchange 6) Following Size exclusion. Data represents average of three measurements where error bars represent ± SEM.

4.12 Screening of alternative *Shewanella* strains for FDH and CO_2 reductase activity.

The preceding work addressed the characterisation of FDH and CO_2 reductase activity in *S.oneidensis* MR-1. This focus was principally due to *S.oneidensis* MR-1 being a well characterised model organism but the potential of other members of the *Shewanella* genus were also investigated. The principal concern of these experiments was not to characterise the metabolic or microbiological physiology aspects of FDH in these strains, merely screen them for activity.

A variety of strains capable of growth in the minimal media conditions described for *S.oneidensis* MR-1 in Chapter 3 were cultured under the same conditions, supplemented with either 3 µM tungstate or 3µM molybdate. After growth, the established FDH and CO_2 reductase assays using methyl viologen were used to investigate enzymatic activity. Those strains investigated are listed below in Table 4.1.

Table 4.1 Shewanella strains assayed for FDH and CO_2 reductase activities.
All are capable of growth in both LB media and the described minimal media and have complete genome sequences available.

Species	Strain
amazonensis	SB2B
baltica	OS185
baltica	OS195
baltica	OS223
loihica	PV-4
putrifaciens	200
putrifaciens	CN-32
putrifaciens	W3-18-1
sp.	ANA-3
oneidensis	MR-1
oneidensis	MR-7
oneidensis	MR-4

As previously, the results of the colorimetric assays were normalised to total protein concentration to present the specific activities seen in Figure 4-11. Each strain is presented with FDH and CO_2 reductase activity when grown with tungstate supplementation and molybdate supplementation.

An immediately apparent observation is that, as seen for *S.oneidensis* MR-1, formate oxidation is always significantly higher when grown with tungstate compared to molybdate with the exception of *S.baltica* OS223 which demonstrated no detectable formate oxidation in either growth condition. The same relationship is also true of CO_2 reduction, with activities being higher in all strains when supplemented with tungstate, with the notable exception of *S.amazonensis* SB2B which showed higher activity when grown with molybdate.

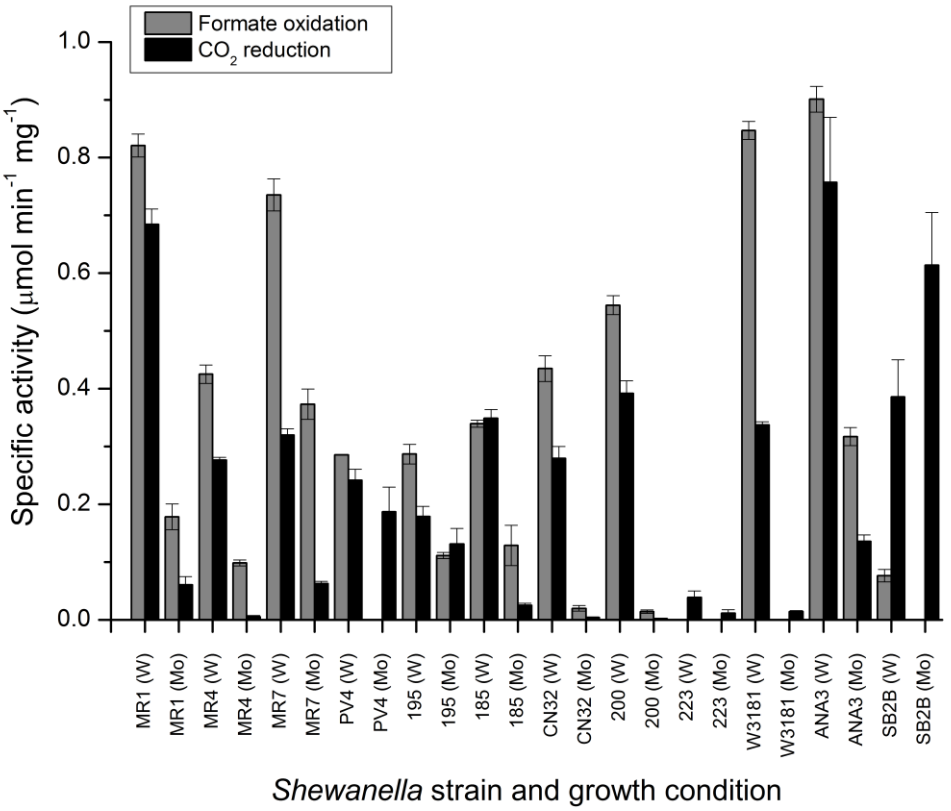

Figure 4-11 Analysis of reversible FDH activity in alternative Shewanella strains.
Cells grown anaerobically in minimal media with 50 mM sodium fumarate as terminal electron acceptor, supplemented with 3 µM tungstate or molybdate for different Shewanella strains. Determined at pH 7.2 using methyl viologen coupled redox assay. Results normalised to protein concentration as determined by BCA assay. Full strain details can be found in Table 4.1 above.

A major consideration in this experiment was the relative ratio of formate oxidation to CO_2 reduction, since those that may favour CO_2 reduction would potentially be better suited catalysts for CO_2 reduction in subsequent work. Of the strains studied most showed similar relationships to *S.oneidensis* MR-1, with slightly, or in some cases significantly, smaller CO_2 reduction rates compared to formate oxidation. Indeed in this respect *S.oneidensis* MR-1 demonstrated a suitable strain for this work as it catalysed one of the highest CO_2 reductase activities observed. Despite this the results obtained for CO_2 reduction in *S.amazonensis* SB2B were of potentially more interest. Not only were rates of CO_2 reduction for this species relatively high when compared to other strains, they were also observed regardless of which metal was supplemented, with activities of 0.39 ± 0.06 $\mu molmin^{-1}mg^{-1}$ and 0.61 ± 0.09 $\mu molmin^{-1}mg^{-1}$ when grown with tungstate and molybdate respectively. Furthermore formate oxidation in these conditions was either low, 0.07 ± 0.01 $\mu mol\ min^{-1}mg^{-1}$ when grown with tungstate, or not detected at all when grown

with molybdate, demonstrating the highest ratio of CO_2 reduction to formate oxidation observed and making *S.amazonensis* SB2B of potential interest for the future.

4.13 Discussion

4.13.1 Establishing quantitative FDH and CO_2 reductase assays.

The use of methyl viologen as a redox dye for development of FDH and CO_2 reductase assays developed in this chapter was carefully considered. As seen in Figure 4-1 the use of alternative dyes such as benzyl viologen were unable to effectively facilitate CO_2 reduction, even if they performed as well as methyl viologen for the forward reaction. The most likely explanation for this observation is the relative redox potentials of the two dyes. One of the principal reasons for using methyl viologen was its low reduction potential at -446 mV vs SHE (Illichmanová et al. 2011). In contrast benzyl viologen has a less negative redox potential (-350 mV) which may not provide a sufficient driving force for CO_2 reduction considering the published reduction potential of the CO_2/formate couple at -420 mV vs SHE (Armstrong & Hirst 2011).

Another important consideration for this redox dye was membrane permeability. Considering these assays were conducted on whole cell samples, slow or ineffective diffusion of dyes across membranes would potentially cause constraints. Indeed several classical studies demonstrated the inability of both reduced methyl and benzyl viologen species, as well as the oxidised radical form of methyl viologen, to permeate cytoplasmic membranes of gram negative bacteria (Jones et al. 1976). This is an important distinction because in contrast to methyl viologen the oxidised form of benzyl viologen is capable of diffusion into the cytoplasm (Jones et al. 1976). Since equivalent FDH activities, (i.e. the reactions requiring the oxidised form of the dyes), were observed regardless of which bipyridilium dye was used (Figure 4-1) it can be implied that all FDH activity is located in the periplasm, in keeping with genomic predictions. This logic assumes that the dyes are otherwise comparable redox partners.

Despite the minor point above, the permeability of the redox dyes was not a major consideration for these studies, it is assumed, since catalysis can be readily observed in whole cells, that all redox states of these dyes are able to

pass into the periplasm, most likely via porin structures that make the outer membranes of gram negative bacteria permeable to small molecules (Nikaido 2003).

Na carbonate was used as a substrate when investigating CO_2 reductase activity throughout this work rather than gaseous CO_2. The use of Na carbonate to provide CO_2 for CO_2 reductase assays is used in several publications (Bassegoda et al. 2014) (Maia et al. 2016). Specifically the use of Na carbonate is possible due to the dissociation of carbonate in water according to the following reactions eq. (4.3) to (4.7):

$$Na_2CO_3 \rightleftharpoons 2Na^+ + CO_3^{2-} \quad (4.3)$$

$$CO_3^{2-} + H^+ \rightleftharpoons HCO_3^- \quad (4.4)$$

$$HCO_3^- + H^+ \rightleftharpoons H_2CO_3 \quad (4.5)$$

$$H_2CO_3 \rightleftharpoons CO_2(aq) + H_2O \quad (4.6)$$

$$CO_2(aq) \rightleftharpoons CO_2(g) \quad (4.7)$$

When dissolved in water carbonate (CO_3^{2-}) undergoes a series of protonation events, first into bicarbonate (HCO_3^-) (eq.(4.4)) followed by carbonic acid (H_2CO_3) (eq.(4.5)). Carbonic acid will further equilibrate in water to produce dissolved CO_2 (CO_2 (aq)) (eq.(4.6)) (Palmer & Vaneldik 1983). Although aqueous CO_2 is the substrate used in this study it is important to note a further equilibrium (eq.(4.7)) that is established between the dissolved CO_2 and that in the surrounding atmosphere (CO_2(g)) which is dependent upon the CO_2 partial pressure in the environment. Since these complicated equilibria exist simultaneously it is difficult to determine exact substrate concentrations for CO_2 reductase assays, indeed it is possible that other carbonate species may contribute to catalysis. This said, considering equivalent CO_2 reductase activity was observed when CO_2 gas was injected into the same assay conditions, it does not seem unreasonable to assume CO_2 is indeed the substrate as found for other metal dependent FDH enzymes (Maia et al. 2016). An important note here is that changes in pH were not observed in these experiments. It could be suggested that the equilibria described above would increase the pH however

this was not observed and the buffering capacity of the 100 mM HEPES in the assay conditions proved sufficient to counter any such changes.

Whilst developing the CO_2 reductase assay the suitability of other assay components had to be considered. For example the use of HEPES as a buffer was carefully considered as it has been reported to be capable of acting as an electron donor in certain contexts (Ainsworth et al. 2016). However appropriate controls demonstrated that HEPES alone was not able to reduce methyl viologen, nor did it change assay results when replaced with Mcilvaine buffers. This is largely expected as HEPES, a well-established biochemical reagent (Good et al. 1966), is frequently used for redox studies (Ferreira et al. 2015) Phosphate buffers were avoided due to their tendency not only to inhibit a wide range of enzymatic functions, but also chelate metals, a major concern in these studies (Ferreira et al. 2015).

As mentioned above phosphate buffers were avoided due to concerns about their complexing with metal ions, such concerns were also raised about HEPES. No literature exists on the ability of HEPES to chelate or complex with Mo or W, the metals of most significance in these studies. However HEPES ability to complex other metals has received attention. Despite the majority of studies suggesting HEPES does not form metal complexes, and HEPES being specifically marketed as "non-metal-coordinating" (Sokołowska & Bal 2005), other studies have suggested low stability constants for Cu, Zn, Pb and Cd with HEPES (Sokołowska & Bal 2005)(Ferreira et al. 2015). This suggests they may complex to a small degree, although these findings are debated (Ferreira et al. 2015), and are noted as being minor compared to equivalent complexing phenomena observed when using phosphate or Tris buffers (Sokołowska & Bal 2005). Indeed HEPES and MES have been observed to be the best zwitterionic buffers to use for several metal sensitive experiments (Brom et al. 2012). Taken together HEPES and MES (for anion exchange experiments) were deemed appropriate buffer choices for these studies.

Whilst developing the CO_2 reductase assay it was apparent a reductant would be required to reduce methyl viologen prior to assessing CO_2 reduction. Na dithionite was chosen because of its frequent use in biochemistry but also because of its unusually low redox potential at pH7 and 25 ^{o}C of -0.66 V vs SHE (Mayhew 1978). Very few other compounds are capable of effectively reducing

methyl viologen. When used in this capacity, sodium dithionite ($S_2O_4^{2-}$) doesn't act directly as a reductant, instead it first transitions into the radical SO_2^- as seen below in eq. (4.8). This radical species then provides the reductive electrons, with concomitant conversion to bisulphite (HSO_3^-) (eq.(4.9).

$$S_2O_4^{2-} \rightleftharpoons 2SO_2 \cdot^- \tag{4.8}$$

$$2SO_2 \cdot^- + H_2O \rightleftharpoons HSO_3^- + H^+ + e^- \tag{4.9}$$

The conversion to bisulphite is of significance as this reaction is not unidirectional, indeed especially at lower pH values bisulphite can act to oxidise methyl viologen (Mayhew 1978) the full importance of this is discussed for pH dependent studies.

Considering the above details it was assumed that when considering CO_2 reductase activity 1 M of dithionite would dissociate into 2 M of SO_2^-. This in turn would reduce 2 M of methyl viologen according to eq. (4.10).

$$2SO_2 \cdot^- + 2MV^{2+} \rightleftharpoons 2HSO_3^- + 2MV \cdot^+ \tag{4.10}$$

Finally catalysed by CO_2 reductase, 2 M of methyl viologen would facilitate reduction of 1 M of CO_2 to formate (HCO_2^-) eq. (4.11).

$$2MV \cdot^+ + CO_2 \rightarrow HCO_2^- + 2MV^{2+} \tag{4.11}$$

Throughout CO_2 reductase studies it was assumed the above reactions were occurring. In reality however it is likely that each step was not 100% efficient.

One practical consideration for the developed CO_2 reduction assay was the extended amount of time samples were left to equilibrate with methyl viologen in an anaerobic environment before assaying for CO_2 reductase activity. First for 25 min with oxidised methyl viologen whilst sparging with nitrogen followed by 15 further minutes with reduced methyl viologen (via dithionite). These steps were found to be important as without them, estimations of CO_2 reduction varied unpredictably between replicates. One explanation for this requirement is that time was needed to allow background cellular reactions to abate, consuming any available traces of metabolites not removed during the

proceeding wash steps. However, an alternative explanation involves reduction reactivation. Many molybdopterin enzymes have been reported to need to be reduced in order to function efficiently (Field et al. 2005). Unlike the irreversible inactivation by oxygen of some proteins, examples of re-activation under prolonged reductive conditions have been reported for several nitrate reductase enzymes including NarG from *E.coli*, the cytoplasmic Nas of *Synechococcus elongatus* and periplasmic Nap from *Rhodobacter sphaeroides* (Jacques et al. 2014), enzymes from the same W/Mo bis-PGD family as FDH.

4.13.2 FDH and CO_2 reductase activities in *S.oneidensis* MR-1.

As seen in Figure 4-2 CO_2 reductase activity mirrored FDH activity in the minimal growth conditions studied. Highest activities of 0.57 ± 0.03 $\mu molmin^{-1}mg^{-1}$ were observed when growth was supplemented with tungstate, furthering the case for FDH and CO_2 reductase activities being catalysed by the same enzyme population reversibly and that tungstate is important for their maximal activity.

Assuming that W is naturally incorporated into the FDH PGD cofactor in *S.oneidensis* MR-1 cells for formate oxidation to contribute to respiration, the high levels of CO_2 reduction activity demonstrated under W growth conditions via methyl viologen assay seem counterintuitive. This is especially true considering reduction rates were almost equal to formate oxidation rates (Figure 4-2). It is assumed that the observed reduction rates are not seen under normal physiological conditions as such reversible activity would prevent PMF generation. Indeed physiologically there would be a lack of a strong reductant such as reduced methyl viologen to provide electrons at a suitable potential making such activity unlikely without external influences.

Of possible interest is the relative ratio between reduction and oxidation under these growth conditions. In Chapter 3 it was suggested that the FDH activity seen when grown with +Mo or when not supplemented with metal may be due to traces of tungstate being effectively scavenged resulting in a smaller population of functional enzyme than when grown with W supplementation. This was based partly on the assumption that only W could produce functional enzyme. Following this logic, i.e. assuming the differences in activity between growth conditions are purely based on the amount of enzyme present, and not

its physical characteristics, one would expect the ratio between oxidation and reduction to be the same regardless of growth condition.

However what is observed is that CO_2 reduction and formate oxidation are almost equivalent when grown in W containing conditions, for example 0.7 $\mu molmin^{-1}mg^{-1}$ for formate oxidation vs 0.56 $\mu molmin^{-1}mg^{-1}$ for CO_2 reduction when grown +W. In contrast formate oxidation is 3-4 fold higher than CO_2 reduction when grown without W, for example 0.28 $\mu molmin^{-1}mg^{-1}$ for formate oxidation vs 0.06 $\mu molmin^{-1}mg^{-1}$ for CO_2 reduction when grown +Mo. The CO_2 reductase activity in these conditions without supplemented W may still be due to the traces of W containing enzyme, but considering the higher FDH activity it also seems plausible that at least some proportion of formate oxidation activity is Mo associated. This will be further investigated in Chapter 5 with analysis of each FDH isoform in isolation.

From a practical perspective the results in Figure 4-2 highlight the importance of including W in growth conditions if CO_2 reductase activity is to be investigated. As such only growth in minimal media with tungstate supplementation was used for culturing cells for other biochemical investigations discussed below unless specified otherwise.

As seen in Figure 4-3, 20 mM azide inhibited over 80 % of both formate oxidation and CO_2 reduction. At first this appears a very high concentration to inhibit activity, azide is known to almost completely inhibit FDH activity at very low concentration for FDHs purified from other organisms, for example 0.01 mM azide induces 99 % inhibition in FDH from *Candida boidinii* (Schüte et al. 1976) and similar values are given for FDHs from other organisms (Axley et al. 1990) where azide is proposed to act as a transition state analog of formate oxidation (Axley et al. 1990). However these studies are normally conducted on purified enzyme and azide is a known nonspecific inhibitor of a vast range of different enzymes, many of which will be present in whole cell assays. These nonspecific interactions could decrease the concentration available for FDH inhibition by binding other enzymes as well as other cell components. Other considerations include potentially restricted access across the outer membrane or detoxification pathways employed by the cells. Despite the apparently high concentrations required, the inhibition of both oxidation and reduction by azide

supports the hypothesis that both formate oxidation and CO_2 reduction are enzymatically catalysed.

As previously mentioned pH dependent studies using the developed methyl viologen assay below pH 6.8 were unsuitable. This is attributed to the role of dithionite and its dissociation into bisulphite upon reduction of methyl viologen outlined above. At lower pH values bisulphite is capable of re-oxidising methyl viologen (Mayhew 1978) and thus an equilibrium is established between these species. In this work, methyl viologen reduction was measured spectrophotometrically at 578 nm, but below pH 6.8, even with additional concentrations of dithionite, the equilibria could not be shifted to provide an equivalent concentration of reduced methyl viologen as at higher pH experiments for the subsequent CO_2 reduction assay.

The pH dependence of reversible FDH activity seen in Figure 4-5 does largely fit with expectations, with CO_2 reduction prevailing at low pH and formate oxidation at high pH. This is in accordance with studies of FDH1 from *Syntrophobacter fumaroxidans* where increased CO_2 reduction was observed at lower pH. This is possibly due to a higher availability of protons for catalysis, (Hayashi & Ogo 2003) or more favourable protein conformation, (Choe et al. 2014) it is also possible that the changing equilibrium of carbonate species in solution at different pH may play a role, at lower pH CO_2 is the predominant form and catalysis would involve the $2e^-$, 1 proton reduction of CO_2 to formate whereas at higher pH bicarbonate and carbonate species predominate and catalysis would require the $2e^-$, $2H^+$ reduction to formate (Reda et al. 2008). Another explanation relates to proposed mechanistic model in Chapter 1 in which the protonated active site sulpho ligand (Mo^{4+}-SH), favoured at lower pH values, would be better suited for CO_2 reduction whilst the deprotonated equivalent favoured at higher pH values (Mo^{6+}=S) would enable formate oxidation (Maia et al. 2016).

Of course a combination of these different effects may contribute to the increase in observed reduction in increasingly acidic conditions. Regardless of the explanation the observed increase in reduction at acidic pH can potentially be exploited in a microbial electrosynthetic context where a lower pH bioreactor environment would increase efficiency.

4.13.3 Initial purification of FDH and CO_2 reductase activities

Fumarate reductase activity observed in Figure 4-6 panel A is in keeping with previous observations (Ross et al. 2011). More practically these results demonstrate that the methodology used here to normalise initial rates to protein concentration is appropriate as suggested by the largely similar fumarate reductase specific activities observed regardless of tungstate or molybdate supplementation which have had no reported effect on fccA activity or regulation.

The fact that CO_2 reduction and formate oxidation could be observed in membrane fractions is significant in that it suggests that no other periplasmic components are essential for catalysis. No formate oxidation or CO_2 reduction was associated with the soluble cell fractions of cultures grown in any conditions; this is in agreement with the prediction that all three primary FDH clusters in the *Shewanella oneidensis* MR-1 genome are membrane associated. It does however have an implication for the isolated single FDH subunit encoded by *SO_0988*, which does not encode membrane associated elements, it could be suggested this gene is not expressed under these conditions or is associated with another complex, possibly a FHL complex as previously described and speculated by some authors (Meshulam-Simon et al. 2007). However study of formate oxidation in deletion strains in the following chapter suggests this is not the case. Instead it seems likely that in the conditions studied here, and by others (Kane et al. 2016), *SO_0988* has no detectable role in formate oxidation or CO_2 reduction.

The ratio of formate oxidation to CO_2 reduction would be expected to remain constant between whole cells and membrane samples, since the same enzyme population is expected to catalyse both. This is true in +W growth conditions, with reduction:oxidation ratios of 0.81:1 for whole cells and 0.84:1 for membrane fractions. However in +Mo grown cells, equivalent ratios of 0.21:1 in whole cells and 0.12:1 in membrane fractions are observed. Due to the proportionally large errors on these values conclusions should be made with caution, but if correct may suggest either CO_2 reductase activity is inactivated or inhibited by the membrane separation procedure, (or that formate oxidation is augmented by the

procedure), and these effects only occur when growth is supplemented with molybdate.

4.13.4 Native protein purification of Fdh2α.

To confirm a role in active catalysis for W, and not just a role as a regulatory element, Fdh2α (*SO_4513*) was purified and analysed for metal content. Fdh2α was chosen, over Fdh1α (*SO_4509*) or Fdnα (*SO_0101*), as gene expression studies in Chapter 3 showed highest upregulation of *SO_4513* in response to W. To better monitor Fdh2α activity in isolation a genomic mutant lacking Fdh1αβγ (*SO_4509-SO_4511*) and Fdnαβγ (*SO_0101_SO_01013*) was used for the purification.

Fdh2α was successfully purified from minimal media containing W culture. The purification steps and corresponding activities are shown in Figure 4-9. Of interest is the initial rise in both specific and total activity between whole and cell lysate samples. An equivalent rise was also seen in Figure 4-10 during a Mo supplemented purification. It would be expected that total activity could not increase during a purification but this does not account for the fact that the whole cell environment may limit activity. Factors such as diffusion of methyl viologen across outer membranes, accessibility of FDH enzyme within the membrane to the redox dye, as well interactions with other cellular proteins or the redox state of the periplasm and inner membrane may influence and limit FDH activity in whole cells. Once cells are lysed such restrictions are removed allowing higher rates of catalysis to be monitored by the same enzyme population.

Whilst discussing cell lysis it is pertinent to highlight the fact that during Fdh2α purification cells were lysed using French press, but previous studies on localising enzymatic activity (Figure 4-6) used sonication for lysis. Sonication was found to not scale well at the higher volumes required for protein purification, with the extended sonication needed for complete lysis causing poor recovery of active Fdh2α. Although less damaging it was found that after lysis by French press, membrane separation by ultracentrifugation was less efficient than seen after sonication. Whereas all FDH activity was membrane associated in Figure 4-6, some activity remained in the soluble fraction when using French press for lysis, partly explaining the poor recovery of Fdh2α activity between

lysate and membrane fraction steps in Figure 4-9 and Figure 4-10. Several attempts failed to successfully isolate the Fdh2α activity found in the soluble fraction hence purification from the membrane fraction.

Although a large fraction of total activity remained in the soluble fraction, subsequent activity losses during purification were relatively low. Indeed almost all activity was retained following selective sarkosyl solubilisation, with no detectable FDH activity being associated with outer membrane fractions. This highlights that for this methodology, sarkosyl very efficiently separated FDH activity from other outer membrane proteins. This is in contrast to some studies which only found this technique to be partially effective (Yarzábal et al. 2002).

Two chromatography steps were required for isolation of Fdh2α following sarkosyl solubilisation. Optimisation of the anion exchange procedure showed that it was possible to elute active Fdh2α from anion exchange matrices without difficulty, but often with considerable concentrations of other proteins. These initial attempts used pH 7.2 HEPES buffer, since this was above the theoretical pI of Fdh2α. Following this limited success, cation exchange chromotorapghy was attempted using a CAPTO-S column instead. For this investigation pH 6 MES buffer was used as this was below the theoretical pI of Fdh2α, implying a net positive charge on the protein. In reality however Fdh2α failed to bind the cation exchange membrane at this pH. Instead it was run on the previous QSEPH anion exchange column were it was found to bind, even at pH 6. (Negatively charged sarkosyl also binds such a matrix, limiting column binding capacity.) This resolved a number of the above issues with Fdh2α eluting with far fewer other contaminants than seen at higher pH values. The fact that Fdh2α is able to effectively bind Q-sepherose matrices below its theoretical pI suggests the actual pI value may be significantly different, as is often the case between theoretical and actual pI values (Sillero & Ribeiro 1989). Whilst optimising the anion exchange procedure it was found that different elution profiles were observed if using elution gradients, i.e. gradually increasing NaCl concentrations, as opposed to step gradients, when the NaCl was changed abruptly. The latter was found to be more effective for Fdh2 purification, with elution gradients causing slow elution over a large range of salt concentrations.

After anion exchange chromatrography Fdh2α was greatly enriched, with only traces remaining of other lower molecular weight contaminants. As such the final size exclusion step was required. Size exclusion chromatography was also beneficial as it acted as an effective desalting step, with the salt eluting after the fractions containing Fdh2α as determined by a single large peak in conductivity. This step removed all other small molecular weight protein contaminants co-purified with Fdh2α after the Q-Sepherose column, with the only minor remaining contaminant running at 50 kDa. Figure 4-9 panel B. This contaminant was minor and was at first thought to be either Fdh2β (SO_4514, 20.49 kDa) or Fdh2γ (SO_4515, 36.45 kDa), proteins expected to be purified with Fdh2α (SO_4513). Considering the predicted sizes, only a complex of the two proteins would be expected to run at such a weight, unlikely considering the harsh SDS-PAGE environment. Mass spectrometry was used to try and identify the contaminant unsuccessfully, although the single larger band was identified as Fdh2α. Despite the minor contaminant, Fdh2α was considered suitably pure for metal analysis.

Despite effective purification methods such as the sarkosyl solubilsation discussed above, activity was lost throughout Fdh2α purification. When using molybdate grown cultures Fdh2α could not be isolated using the same methods used for isolation when grown +W. The purification steps were not suitable for such comparatively low starting quantities of enzyme, 230 µmol min^{-1} (Figure 4-10), compared to 3768 µmol min^{-1} when grown with tungstate (Figure 4-9). This is highlighted in Figure 4-10 where no active protein could be recovered after size exclusion chromatography.

Although specific activity rises throughout the tungsten supplemented purification, it only rises by a factor of 7 during the entire purification. This is in contrast to many protein purifications which can rise by factors of several thousand (Enoch & Lester 1975) or even more (Fox et al. 1989). This modest rise in specific activity could be explained either by FDH protein comprising a large percentage of total initial protein, or the more likely case of activity being lost throughout the preparation. It is possible that Fdh2α activity is only optimal in the presence of Fdh2β and Fdh2γ and by separating Fdh2α, activity is diminished. Alternatively many FDH proteins have been shown to be quickly and irreversibly inactivated by oxygen and although the purification steps

following lysis were conducted anaerobically these conditions only maintain oxygen concentrations below 20 ppm.

Although this work refers to Fdh2α purification it is important to specify that Fdh2α is likely purified in complex with Fdh2β and Fdh2γ for at least part of this work. Since Fdh2α is not itself predicted to be membrane associated it seems likely that this is the case as FDH activity was membrane associated after both cell fractionation and sarkosyl solubilisation. Indeed for this reason non-ionic detergents were included during both anion exchange and size exclusion purification steps. Initial experiments were conducted using triton X-100 at 1%, but due to the large micelle sizes formed, it was found to prevent effective size exclusion separation. Instead 0.01% DDM was used, which although just above the critical micelle concentration in water of 0.009% (0.17mM) (Oliver et al. 2014) did not show comparable issues. Although detergents were included to maintain membrane associated complexes, no bands corresponding to Fdh2β (20.49 kDa) and Fdh2γ (36.45 kDa) or Fdh2βγ (56.94 kDa) or the full complex, Fdh2αβγ (162.4 kDa) were seen in Figure 4-9 panel B as discussed above. This suggests that at some point during the purification Fdh2α dissociates from Fdh2βγ.

Purification of Fdh2α was achieved using classical biochemical techniques based solely on the native properties of the protein. Genetic tags were not introduced due to their tendency to induce minor conformational changes to proteins as well as the ability of some tags, (for example hexahistidine tags) to chelate and interfere with binding of metal cofactors (Lichty et al. 2005), a major drawback for such studies where minor changes may affect native metal binding.

ICP-MS analysis of the purified Fdh2α suggests an approximately a 1.3:1 ratio of W to protein. This is close to the 1:1 expected ratio arising from a single PGD cofactor per protein. The fact that W and not Mo is detected supports previous work implicating W in catalysis of FDH oxidation in *S.oneidensis*. Purified protein could not be obtained from the equivalent molybdate supplemented preparation to determine if Fdh2α is able to coordinate Mo as well as W, depending on the metal supplemented.

4.13.5 Aspects of FDH and CO_2 reductase activities for further investigation

Shewanella amazonensis SB2B demonstrated high levels of CO_2 reductase activity, not only when grown with tungsten (0.39 ± 0.06 $\mu molmin^{-1}mg^{-1}$), as was true for most other *Shewanella* strains, but also when grown with molybdate (0.61 ± 0.09 $\mu molmin^{-1}mg^{-1}$), this makes it an exciting candidate for microbial synthetic exploitation, especially as it also displayed very little formate oxidation activity avoiding complications with equilibria being established, which would reduce efficiency.

S.amazonensis SB2B grew in formate containing media supplemented +Mo despite having no detectable FDH activity. This may suggest that this species is able to grow in these media conditions without oxidising the available formate, perhaps relying entirely on the provided amino acids for both carbon and energy. Alternatively it may suggest the unsuitability of the assay to detect formate oxidation in this species, either due to the very slow kinetics or functional differences that prevent coupling to methyl viologen reduction.

Of the other strains investigated, *S.oneidensis* MR-1 displayed one of the highest CO_2 reduction rates, combined with its relatively well characterised physiology compared to the other strains it was still considered appropriate for studying electrosynthesis of formate in Chapter 6.

The investigation of FDH and CO_2 reductase activity in LB growth conditions shown in Figure 4-8 has some interesting implications. The fact that FDH activity could be observed when W was supplemented suggests that it is possible to have active FDH enzyme(s) produced under aerobic growth conditions. The exact isoform responsible for this activity may prove less oxygen sensitive than the purified Fdh2α described in this chapter. Another consideration would be whether such aerobic enzyme(s) and their formate oxidation had any role in aerobic respiration, or whether the enzyme(s) are simply expressed in response to the presence of W.

Figure 4-8 also demonstrates higher enzymatic activities in anaerobic LB supplemented with W. This is in agreement with the previous anaerobic growths in minimal media, but is somewhat surprising to see in the commonly used rich LB media, thought to contain all necessary metals. The fact that

enzymatic activity can be increased by supplementing W raises several possibilities. Either W is present in LB at insufficiently low concentrations, or is chelated/sequestered in some manner, preventing incorporation into the FDH cofactors, or W is needed for upregulation of FDH expression.

When comparing specific activities seen in LB with those in minimal media, FDH activity is higher in W supplemented LB conditions. In contrast CO_2 reductase activities are higher in minimal media, since this is the reaction of interest, minimal media were used for subsequent CO_2 reductase studies.

The kinetic parameter determinations in Figure 4-7 were estimated in whole cells, complicating analysis as these values may report on the combined action of several enzyme populations.

Whole cell K_m values of 39 ± 5 μM and 1.43 ± 0.26 mM were determined from Figure 4-7 for formate oxidation and CO_2 reduction respectively. Notably the K_m value for formate oxidation (K_m^{COO-}) is over 36 times smaller than for CO_2 reduction (K_m^{HCO3-}), implying a higher affinity for this substrate, unsurprising considering the native role of these enzymes. Similar biases have been reported for other FDH enzymes, with higher affinity for formate than carbonate. Examples include enzymes from *Pseudomonas oxalaticus* with a K_m^{COO-} of 100 μM and K_m^{HCO3-} of 40 mM (Ruschig et al. 1976), *Desulfovibrio desulfuricans* with a K_m^{COO-} of 57 μM and K_m^{HCO3-} of 15.7 mM (Maia et al. 2016) and the HDCR complex of *Acetobacterium woodii* with a K_m^{COO-} of 1 ± 0.3 mM and K_m^{HCO3-} of 37 ± 4 mM (Schuchmann & Müller 2013). Other metal dependent FDH K_m^{COO-} literature values also exist when the reverse reaction was not studied, the K_m^{COO-} value determined in this work (39 ± 5 μM) is also comparable to these values: 280 μM (*R.capsulatus*) (Hartmann & Leimkühler 2013), 8 μM (*D.vulgaris Hildenborough*) (Silva et al. 2011), 40 μM (FDH1-*S.fumaroxidans*) and 10 μM (FDH2-*S.fumaroxidans*) (de Bok et al. 2003).

In addition to K_m values, comparisons can be made with the estimated k_{cat} values for purified Fdh2α determined in this chapter, specifically 12 ± 4.3 s^{-1} for formate oxidation and 10.7 ± 3.8 s^{-1} for CO_2 reduction. It should be noted however that since Michaelis-Menten plots were not plotted for purified Fdh2α due to insufficient yield, (instead only determining activity with 10 mM substrate) these values are not true k_{cat} values. The determined turnover

number for formate oxidation ($k_{cat}^{COO^-}$, 12 ± 4.3 s^{-1}) in this work was slow in comparison to many other literature reported values: 5600 s^{-1} (FDH1 *S.fumaroxidans*), 2800 s^{-1} (FDH-H *E.coli*), 1900 s^{-1} (FDH1 *S.fumaroxidans*), 543 s^{-1} (*D.desulfuricans*), 270 s^{-1} (*R.eutropha*), 262 s^{-1} (*D.vulgaris Hildenborough*), 90 s^{-1} (*R.capsulatus*), 90 s^{-1} (*P.oxalaticus*), 39 s^{-1} (HDCR *A.woodii*) and 6.2 s^{-1} (*M.thermoacetica*) (de Bok et al. 2003; Reda et al. 2008; Maia et al. 2015; Maia et al. 2017; Maia et al. 2016).

In contrast the determined turnover number for CO_2 reduction ($k_{cat}^{HCO_3^-}$, 10.7 ± 3.8 s^{-1}) in this work was slower than several previously characterised enzymes but considerably faster than many others. Arranged from faster to slowest: 2500 s^{-1} (FDH1 *S.fumaroxidans*), 200 s^{-1} (FDH2 *S.fumaroxidans*), 46 s^{-1} (*D.desulfuricans*), 28 s^{-1} (HDCR *A.woodii*), 11 s^{-1} (*C.necator*), 3.4 s^{-1} (*D.vulgaris Hildenborough*), 3 s^{-1} (*P.oxalaticus*), 1.5 s^{-1} (*R.capsulatus*) and 0.08 s^{-1} (*C.carboxidivorans*) (Reda et al. 2008; Schuchmann & Müller 2013; Maia et al. 2015; Maia et al. 2017; Maia et al. 2016; Yu et al. 2017).

Both formate oxidation and CO_2 reduction rates decreased at higher substrate concentrations than those shown in Figure 4-7 with associated changes in pH, becoming more acidic with excess formate and more basic with excess carbonate, suggesting the buffering capacity of the assay was insufficient. Considering the above work on pH dependence this would explain the decreasing enzymatic activities in excess of substrate, with formate oxidation shown to decrease at lower pH values and CO_2 reduction to decrease at higher pH values (Figure 4-5).

The possibility of substrate inhibition should also be considered. Substrate inhibition affects 20% of all enzymes according to some estimations (Reed et al. 2010) and results in inhibited activity at high substrate concentrations, though a variety of mechanisms including allosteric effects. Substrate inhibition is sometimes considered an experimental inconvenience resulting from physiologically irrelevant levels of substrate, but there are many reported cases of substrate inhibition playing an important role in native enzymatic function (Reed et al. 2010). Examples of FDH substrate inhibition could not be found in the literature, excluding substrate inhibition by NADH in the case of a reversible NAD+ dependent FDH (Hartmann & Leimkühler 2013). Considering this, and the explanation relating to changing pH given above, the data in Figure 4-7 was considered appropriate to present without concerns of

inappropriate K_m determinations that can arise from truncating data sets suspected of being affected by substrate inhibition (Lin et al. 2001).

To conclude, this section of work established effective methods for the quantitative measurement of both FDH and CO_2 reductase activities in whole *S.oneidensis* cells and then used them to conclusively demonstrate for the first time CO_2 reduction to formate using NMR. Further study concluded that maximal activities for both reactions are dependent upon the presence of tungstate in the growth media and confirmed that both reactions were inhibited by azide and were pH dependent, with the reduction favoured at acidic pH values and oxidation during more basic conditions. Localisation studies reveal that both WT activities co-purified and were membrane associated. Work with a deletion mutant strain demonstrated the native purification of Fdh2α and the presence of W at its active site as determined by ICP-MS with an estimated turnover rate for CO_2 reduction of 10.7 ± 3.8 s^{-1}. Remaining studies suggested future avenues of research including the study of alternative *Shewanella* species including *S.amazonensis* SB2B which showed CO_2 reductase but no observable FDH activity. Other avenues include the study of less defined media, attractive from a biotechnological standpoint, which when supplemented with W were also shown to produce cultures capable of CO_2 reductase activity. Finally the kinetics of these activities were explored and although it was found results could be modelled with first order kinetics, with apparent K_m values of 39 ± 5 μM and 1.43 ± 0.26 mM for formate oxidation and CO_2 reduction respectively, following work using deletion strains is deemed necessary to fully explore the involved kinetics.

4.14 References

Ainsworth, E. V. et al., 2016. Photoreduction of *Shewanella oneidensis* Extracellular Cytochromes by Organic Chromophores and Dye-Sensitized TiO_2. *ChemBioChem*, pp.2324–2333.

Armstrong, F. a & Hirst, J., 2011. Reversibility and efficiency in electrocatalytic energy conversion and lessons from enzymes. *Proceedings of the National Academy of Sciences of the United States of America*, 108(34), pp.14049–54.

Axley, M., Grahame, D. & Stadtman, T., 1990. *Escherichia coli* formate-hydrogen lyase. Purification and properties of the selenium-dependent formate dehydrogenase component. *Journal of Biological Chemistry*, 265(30), pp.18213–18218.

Axley, M.J., Böck, A. & Stadtman, T.C., 1991. Catalytic properties of an *Escherichia coli* formate dehydrogenase mutant in which sulfur replaces selenium. *Proceedings of the National Academy of Sciences of the United States of America*, 88(19), pp.8450–4.

Bassegoda, A. et al., 2014. Reversible Interconversion of CO_2 and Formate by a Molybdenum-Containing Formate Dehydrogenase. *Journal of the American Chemical Society*, 136(44), pp.15473–6.

de Bok, F. a. M. et al., 2003. Two W-containing formate dehydrogenases (CO_2-reductases) involved in syntrophic propionate oxidation by *Syntrophobacter fumaroxidans*. *European Journal of Biochemistry*, 270(11), pp.2476–2485.

Brom, M. et al., 2012. Improved labelling of DTPA- and DOTA-conjugated peptides and antibodies with 111In in HEPES and MES buffer. *EJNMMI research*, 2, p.4.

Choe, H. et al., 2014. Efficient CO_2-Reducing Activity of NAD-Dependent Formate Dehydrogenase from *Thiobacillus* sp. KNK65MA for Formate Production from CO_2 Gas. *PloS one*, 9(7), p.e103111.

Enoch, H. & Lester, R., 1975. The purification and properties of formate dehydrogenase and nitrate reductase from *Escherichia coli*. *Journal of Biological Chemistry*.

Ferreira, C. et al., 2015. (Un)suitability of the use of pH buffers in biological, biochemical and environmental studies and their interaction with metal ions – a review. *RSC Adv.*, 5(39), pp.30989–31003.

Field, S.J. et al., 2005. Reductive activation of nitrate reductases. *Dalton Transactions*, 2005(21), pp.3580–3586.

Fox, B.G. et al., 1989. Methane Monooxygenase from *Methylosinus trichosporium* OB3B. *Journal of Bacteriology*, 264(17), pp.10023–10033.

Good, N.E. et al., 1966. Hydrogen ion buffers for biological research. *Biochemistry*, 5(2), pp.467–477.

Hartmann, T. & Leimkühler, S., 2013. The oxygen-tolerant and NAD+-dependent formate dehydrogenase from *Rhodobacter capsulatus* is able to catalyze the reduction of CO_2 to formate. *FEBS Journal*, 280(23), pp.6083–6096.

Hayashi, H. & Ogo, S., 2003. Accelerating effect of a proton on the reduction of CO_2 dissolved in water under acidic conditions. Isolation, crystal structure, and reducing ability of a water-soluble. *Journal of the American …*, pp.14266–14267.

Illichmanová, a et al., 2011. Nitrate reductase whole-cell assay: side effects associated with the use of benzyl viologen. *Folia microbiologica*, 56(1), pp.72–6.

Jacques, J.G.J. et al., 2014. Reductive activation in periplasmic nitrate reductase involves chemical modifications of the Mo-cofactor beyond the first coordination sphere of the metal

ion. *Biochimica et biophysica acta*, 1837(2), pp.277–86.

Jones, R.W., Gray, T. a & Garland, P.B., 1976. A study of the permeability of the cytoplasmic membrane of *Escherichia coli* to reduced and oxidized benzyl viologen and methyl viologen cations: complications in the use of viologens as redox mediators for membrane-bound enzymes. *Biochemical Society transactions*, 4(4), pp.671–3.

Kane, A.L. et al., 2016. Formate metabolism in *Shewanella oneidensis* generates proton motive force and prevents growth without an electron acceptor. *Journal of Bacteriology*, 198(8), pp.1337–1346.

Lichty, J.J. et al., 2005. Comparison of affinity tags for protein purification. *Protein Expression and Purification*, 41(1), pp.98–105.

Lin, Y.U.H. et al., 2001. Substrate Inhibition Kinetics for Cytochrome P450-Catalyzed Reactions Abstract : *Drug metabolism and disposition*, 29(4), pp.368–374.

Maia, L.B. et al., 2016. Reduction of Carbon Dioxide by a Molybdenum-Containing Formate Dehydrogenase: A Kinetic and Mechanistic Study. *Journal of the American Chemical Society*, 138(28), pp.8834–8846.

Maia, L.B., Moura, I. & Moura, J.J.G., 2017. Molybdenum and tungsten-containing formate dehydrogenases: aiming to inspire a catalyst for carbon dioxide utilization. *Inorganica Chimica Acta*, 455(2), pp.350–363.

Maia, L.B., Moura, J.J.G. & Moura, I., 2015. Molybdenum and tungsten - dependent formate dehydrogenases. *J Biol Inorg Chem*, 20, pp.287–309.

Mayhew, S.G., 1978. The redox potential of dithionite and SO^{-}_{2} from equilibrium reactions with flavodoxins, methyl viologen and hydrogen plus hydrogenase. *European journal of biochemistry / FEBS*, 85(2), pp.535–547.

McIlvaine, T., 1921. A buffer solution for colorimetric comparison. *Journal of Biological Chemistry*, pp.183–186.

Meshulam-Simon, G. et al., 2007. Hydrogen metabolism in *Shewanella oneidensis* MR-1. *Applied and environmental microbiology*, 73(4), pp.1153–65.

Michlmayr, H. et al., 2011. Characterization of two distinct glycosyl hydrolase family 78 α-L-rhamnosidases from *Pediococcus acidilactici*. *Applied and Environmental Microbiology*, 77(18), pp.6524–6530.

Mordkovich, N.N. et al., 2013. Effect of NAD+-dependent formate dehydrogenase on anaerobic respiration of *Shewanella oneidensis* MR-1. *Microbiology*, 82(4), pp.404–409.

Nikaido, H., 2003. Molecular basis of bacterial outer membrane permeability revisited. *Microbiology and molecular biology reviews : MMBR*, 67(4), pp.593–656.

Oliver, R.C. et al., 2014. Tuning Micelle Dimensions and Properties with Binary Surfactant Mixtures. *Langmuir*, 30(October), pp.13353–13361.

Palmer, D.A. & Vaneldik, R., 1983. the Chemistry of Metal Carbonato and Carbon-Dioxide Complexes. *Chemical Reviews*, 83(6), pp.651–731.

Reda, T. et al., 2008. Reversible interconversion of carbon dioxide and formate by an electroactive enzyme. *Proceedings of the National Academy of Sciences of the United States of America*, 105(31), pp.10654–8.

Reed, M.C., Lieb, A. & Nijhout, H.F., 2010. The biological significance of substrate inhibition: A mechanism with diverse functions. *BioEssays*, 32(5), pp.422–429.

Ross, D.E. et al., 2011. Towards electrosynthesis in shewanella: energetics of reversing the mtr pathway for reductive metabolism. *PloS one*, 6(2), p.e16649.

Ruddock, L.W., Hirst, T.R. & Freedman, R.B., 1996. pH-dependence of the dithiol-oxidizing activity of DsbA (a periplasmic protein thiol:disulphide oxidoreductase) and protein disulphide-isomerase: studies with a novel simple peptide substrate. *The Biochemical journal*, 1005(Pt 3), pp.1001–5.

Ruschig, U. et al., 1976. CO_2 reduction to formate by NADH catalysed by formate dehydrogenase from *Pseudomonas oxalaticus*. *European journal of biochemistry / FEBS*, 70(2), pp.325–330.

Schuchmann, K. & Müller, V., 2013. Direct and Reversible Hydrogenation of CO_2 to Formate by a Bacterial Carbon Dioxide Reductase. *Science*, 342(December), pp.1382–1386.

Schüte, H. et al., 1976. Purification and properties of formaldehyde dehydrogenase and formate dehydrogenase from *Candida boidinii*. *European journal of biochemistry / FEBS*, 62(1), pp.151–60.

Sillero, A. & Ribeiro, J.M., 1989. Isoelectric points of proteins: Theoretical determination. *Analytical Biochemistry*, 179(2), pp.319–325.

Silva, S.M. da et al., 2011. Tungsten and molybdenum regulation of formate dehydrogenase expression in *Desulfovibrio vulgaris Hildenborough*. *Journal of bacteriology*, 193(12), pp.2909–16.

Sokołowska, M. & Bal, W., 2005. Cu(II) complexation by "non-coordinating" N-2-hydroxyethylpiperazine-N-2-ethanesulfonic acid (HEPES buffer). *Journal of Inorganic Biochemistry*, 99(8), pp.1653–1660.

Staby, A., Jensen, I.H. & Mollerup, I., 2000. Comparison of chromatographic ion-exchange resins. *Journal of Chromatography A*, 897(1–2), pp.99–111.

Sundararajan, a et al., 2011. *Shewanella oneidensis* MR-1 sensory box protein involved in aerobic and anoxic growth. *Applied and environmental microbiology*, 77(13), pp.4647–56.

Yarzábal, A. et al., 2002. The High-Molecular-Weight Cytochrome c Cyc2 of *Acidithiobacillus ferrooxidans* Is an Outer Membrane Protein The High-Molecular-Weight Cytochrome c Cyc2 of Acidithiobacillus ferrooxidans Is an Outer Membrane Protein. *J. Bacteriol.*, 184(1), pp.313–317.

Yu, X. et al., 2017. Efficient reduction of CO_2 by the molybdenum-containing formate dehydrogenase from *Cupriavidus necator* (*Ralstonia eutropha*). *Journal of Biological Chemistry*, pp.1–20.

5 FDH characterisation in *Shewanella oneidensis* MR-1 deletion mutants in response to metal supplementation

WT *S.oneidensis* MR-1 contains three FDH gene clusters that respond differently to the addition of W or Mo in growth media. Chapter 3 began to investigate this area by studying gene expression of the three catalytic subunit isoforms Fdh1α, Fdh2α and Fdnα, encoded by SO_4509, SO_4513 and SO_0101 respectively but was unable to determine the contributions of each to the observed growth phenotypes in minimal media when supplemented with tungstate or molybdate. Similarly, Chapter 4 was also unable to determine the contributions of the three isoforms to the WT FDH and CO_2 reductase activities, or their contributions to the observed whole cell K_m values for formate and carbonate. The purification of SO_4513α went some way to confirming that this enzyme demonstrates CO_2 reductase activity when grown with tungstate, but the contribution of the other heterotrimeric isoforms remains unknown.

To resolve these issues seven in-frame deletion mutants were studied in detail in this section, their growth phenotypes in minimal media conditions, corresponding enzymatic activities and K_m values for formate and carbonate were all studied to compliment the previous work in these areas. The experimental approach for each element of study is briefly described below along with the nomenclature used throughout this section to avoid ambiguity.

Seven deletion mutants were studied. The first three of these mutants are referred to as single cluster mutants, and lack only a single FDH isoform, for example ΔFdh1, a Δ*SO_4509-4511* deletion mutant. The next three strains investigated are referred to as double cluster mutants, for example Fdh1+, which lacks both Δ*SO_0101-0103* and Δ*SO_4513-4515* and is named after the cluster that remains, in this example Fdh1. The final triple cluster mutant investigated is referred to as ΔFDH and lacks all three *fdh* gene clusters. The importance of each mutant lacking not only the α catalytic subunit, but the entirety of the heterotrimeric isoform, including the α, ß and γ subunits is

discussed later. A summary table of the mutants studied are provided for ease of reference in Table 5-1.

Table 5-1 Details of mutant strains used in Chapter 5 and corresponding genotypes. Full details in Chapter 2.

Deletion in *Shewanella oneidensis* MR-1 background	Genotype	Notation
ΔFdh1	ΔSO_4509-4511	ΔFdh1
ΔFdh2	ΔSO_4513-4515	ΔFdh2
ΔFdn	ΔSO_0101-0103	ΔFdn
ΔFdn ΔFdh2	ΔSO_0101-0103 ΔSO_4513-4515	Fdh1+
ΔFdn ΔFdh1	ΔSO_0101-0103 ΔSO_4509-4511	Fdh2+
ΔFdh1 ΔFdh2	ΔSO_4509-4511 ΔSO_4513-4515	Fdn+
ΔFdn ΔFdh1 ΔFdh2	ΔSO_0101-0103 ΔSO_4509-4511 ΔSO_4513-4515	ΔFDH

To enable comparison with the wildtype data from Chapter 3, the same growth conditions were investigated for growth of the seven deletion mutants, specifically growth in the minimal media developed containing 50mM sodium formate and 50mM sodium fumarate as terminal electron acceptor grown anaerobically supplemented either with 3μM sodium tungstate (+W), 3μM sodium molybdate (+Mo), both metals at 3μM (+W/+Mo) or supplemented with neither (-W/-Mo).

In addition to the study of growth, the whole cell FDH and CO_2 reductase specific activities of these strains was also determined using the colourimetric assays established in Chapter 4. All assays were conducted on whole cell samples after 24 h growth in minimal media; as such the activity data presented here represents cells from the final time points in the growth curves in Figure 5-2, Figure 5-6 and Figure 5-9. Experiments were conducted on whole

cell samples as for wildtype. Since each assay is normalised to protein content both the mutant and wildtype data are comparable.

K_m and V_{max} determinations were made for both formate oxidation and CO_2 reduction for certain mutant strains. These determinations were performed according to the procedure described in Chapter 4, varying the substrate concentration and plotting the corresponding specific activities to generate Michaelis-Menten plots from which the presented kinetic parameters were derived.

Since this work generated large amounts of data it has been organised into two sections, the first relating to study of formate oxidation in these mutant strains and their relevant growth phenotypes and the second addressing the non-physiologically relevant CO_2 reductase activity and all associated experiments. To ensure clarity these two sections are further split into sub-sections relating to the study of each FDH isoform, Fdh1, Fdh2, and Fdn in turn.

5.1 Microbial physiology and formate oxidation.

5.1.1 Growth and formate oxidation of triple deletion strain (ΔFDH)

Before studying Fdh1, Fdh2 and Fdn in isolation it is first appropriate to present the results obtained for the triple cluster deletion strain, ΔFdnΔFdh1ΔFdh2 i.e. that without any of the above FDH isoforms.

This triple deletion strain was unable to grow in the studied minimal media growth conditions regardless of whether tungstate or molybdate were supplemented (Figure 5-1). This confirms that no other *fdh* gene(s) in the genome are capable of supporting growth on formate under these conditions, in agreement with genomic predictions.

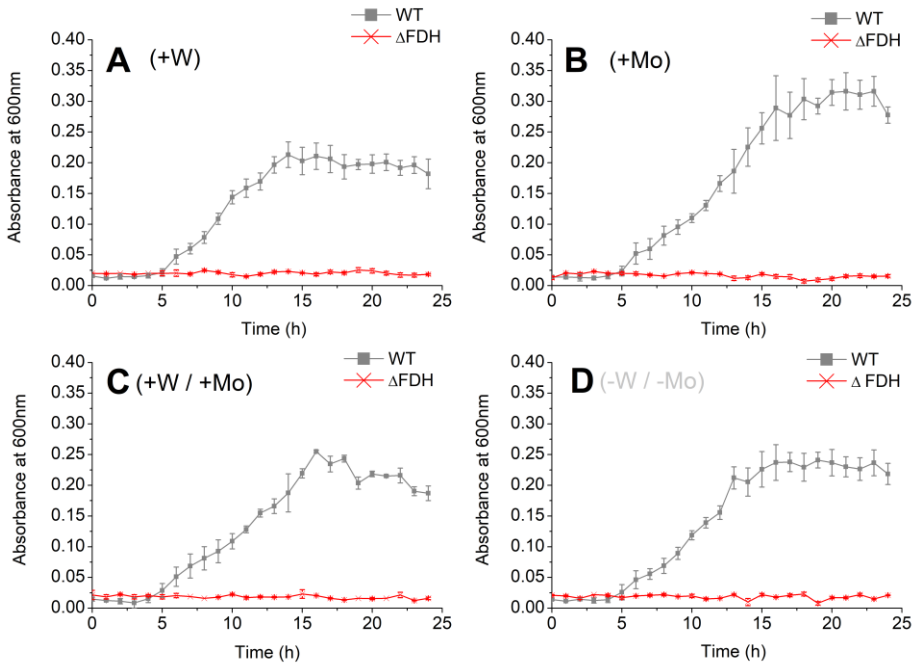

Figure 5-1 Growth of triple deletion strain ΔFDH in minimal media.
*Media supplemented with **(A)** 3μM sodium tungstate (+W), **(B)** 3μM sodium molybdate (+Mo) **(C)** 3μM sodium tungstate and molybdate (+W/+Mo) or **(D)** With neither metal (-W/-Mo). All panels represent anaerobic growth in minimal media with 50mM fumarate as terminal electron acceptor. Wildtype growth shown in grey for comparative purposes. Data represents average of a minimum of three experimental data sets where error bars represent ± SEM.*

5.1.2 Importance of Fdh1 for growth and formate oxidation

Fdh1 is the first of three isoforms to be studied in detail. To do this data from two strains are presented, ΔFdh1, which allows assessment of the effect of removing Fdh1, and Fdh1+, which allows the study of Fdh1 in isolation, i.e. with the other two isoforms deleted.

The growth of these strains in minimal media supplemented with tungstate and or molybdate is presented in Figure 5-2 with WT growth under the same conditions shown for comparison. As seen in all four panels the ΔFdh1 strain reached lower OD_{600} readings after 24 h growth than WT or Fdh1+ suggesting that deletion of Fdh1 limits final cell density. Fdh1+ reaches final OD_{600} readings comparable to WT suggesting that Fdh1 in isolation is capable of supporting growth. When combined, analysis of ΔFdh1 and Fdh1+ strains both corroborate an importance for Fdh1 for WT growth under all four growth conditions.

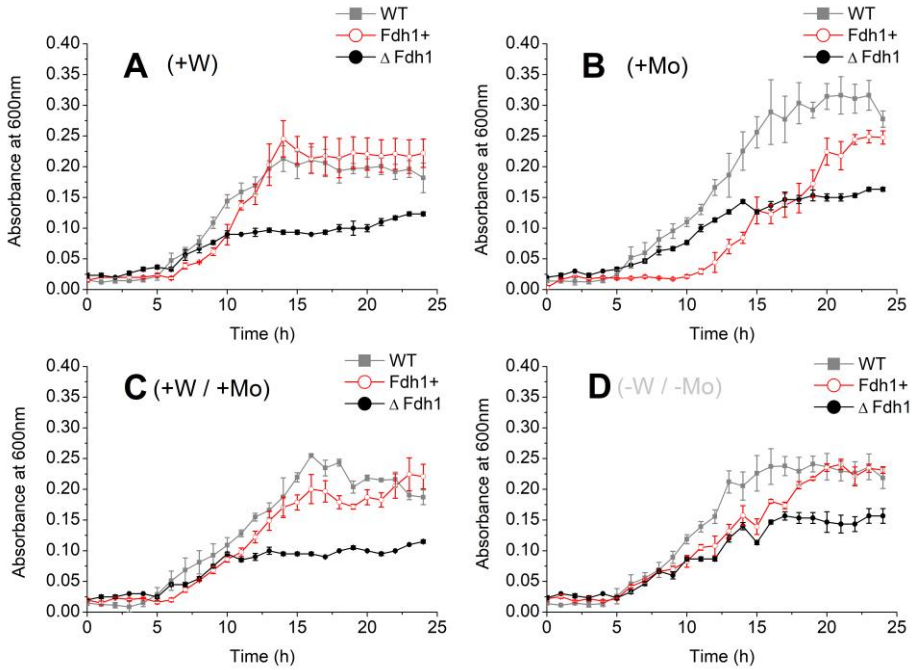

Figure 5-2 Growth of deletion strains ΔFdh1 and Fdh1+ in minimal media.
*Media supplemented with **(A)** 3μM sodium tungstate (+W), **(B)** 3μM sodium molybdate (+Mo) **(C)** 3μM sodium tungstate and molybdate (+W/+Mo) or **(D)** With neither metal (-W/-Mo). All panels represent anaerobic growth in minimal media with 50mM fumarate as terminal electron acceptor. Wildtype growth shown in grey for comparative purposes. Data represents average of a minimum of three experimental data sets where error bars represent ± SEM.*

The specific FDH activities of these strains was next determined and presented in Figure 5-3 as a relative proportion of that seen in WT. The ΔFdh1 strain shows significantly decreased activity compared to WT in all growth conditions except when grown +Mo alone, where the activity is within error of that seen for WT. This suggests that Fdh1 is responsible for a proportion of WT activity when grown +W, +W/+Mo and -W/-Mo yet may not contribute during +Mo growth.

Specific activities seen for Fdh1+ largely support these conclusions. Around 50% of WT activity is retained when grown +W or +W/+Mo, suggesting Fdh1 is responsible for around half of WT FDH activity when grown with W. In contrast Fdh1 in isolation is responsible for less than 20% of WT activity when grown +Mo or -W/-Mo.

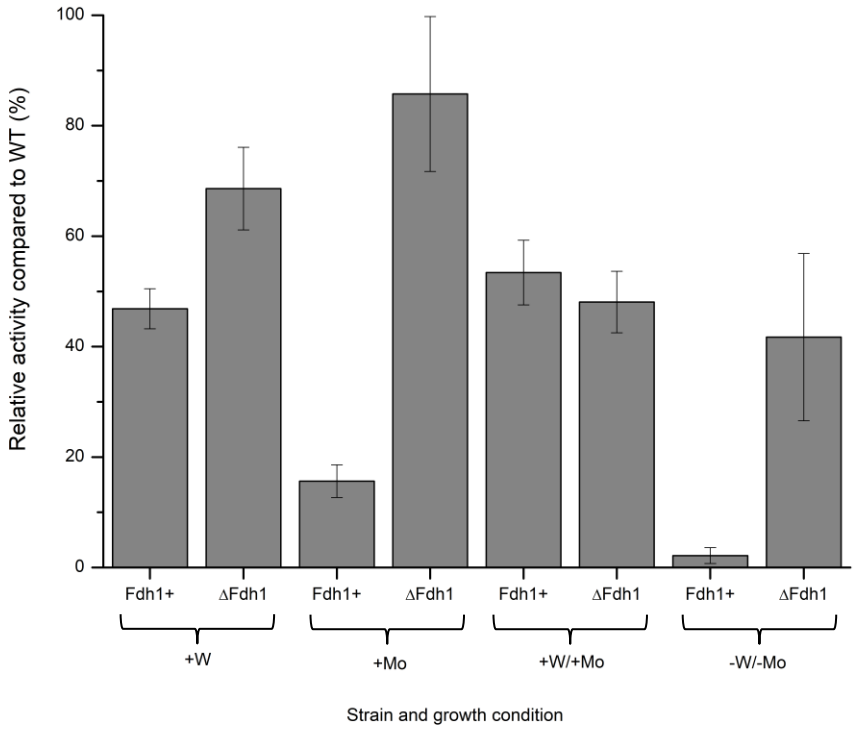

Figure 5-3 Relative FDH activities of ΔFdh1 and Fdh1+ compared to WT.
Activity measured after growth in minimal media for 24 h when growth supplemented with 3μM sodium tungstate (+W), 3μM sodium molybdate (+Mo), 3μM sodium tungstate and molybdate (+W/+Mo) or neither metal (-W/-Mo). Activities obtained using colorimetric methyl viologen assay and normalised to protein content in sample. Presented as % of WT specific activity seen for the same growth condition. Data represents average of a minimum of three experimental data sets where error bars represent ± SEM.

Following this demonstration that Fdh1 is likely to contribute to WT formate oxidation activity, in particular those seen when grown +W or +W/+Mo, K_m and V_{max} values for formate when grown +W were established for the Fdh1+ strain, to allow comparison with those seen in whole cells under equivalent conditions. K_m and V_{max} for formation oxidation +W were determined from Figure 5-4 as 0.07 ± 0.03 mM and 0.32 ± 0.02 μmol $min^{-1}mg^{-1}$ respectively.

Since the role of Fdh1 was unclear during +Mo growth conditions K_m and V_{max} values were also established under this condition for Fdh1+. This was to determine whether Fdh1 had a particularly high affinity for formate, potentially explaining why despite its relative unimportance for native formate oxidation rates it was seen to be essential for maximal growth under this condition. This study was also of interest as a different K_m value to that determined when grown +W may suggest a different enzyme population, indirect evidence for distinct W and Mo containing forms of Fdh1. K_m and V_{max} for formation oxidation +Mo were determined from Figure 5-5 as 0.22 ± 0.03 mM and 0.04 ± 0.002 μmol $min^{-1}mg^{-1}$ respectively.

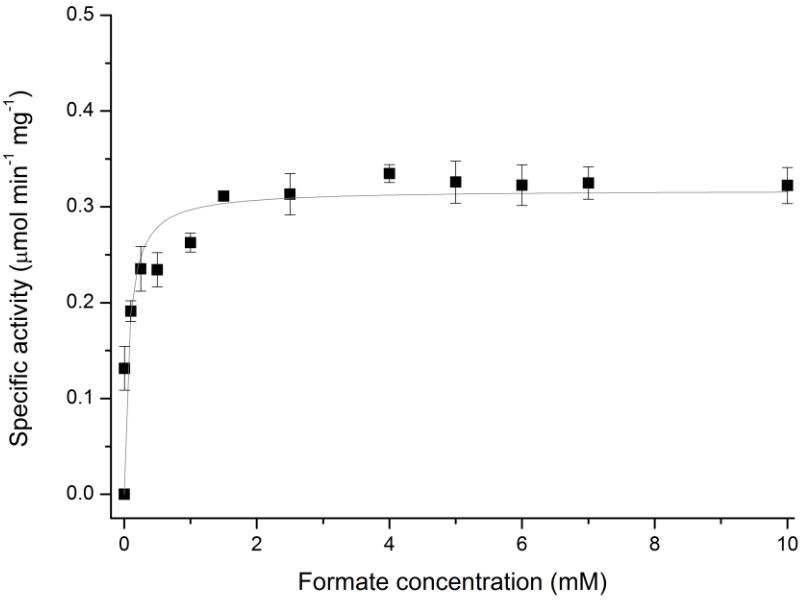

Figure 5-4 Michaelis-Menten plot for formate oxidation in Fdh1+ cells grown +W.
Initial rates determined by measuring increasing absorbance in colorimetric methyl viologen assay. Each data point represents average of a minimum of three experimental data sets where error bars represent ± SEM. Data fitted to a hyperbolic function according to the Michaelis Menten equation. K_m and V_{max} for formate oxidation determined as 0.07 ± 0.03 mM and 0.32 ± 0.02 µmol $min^{-1}mg^{-1}$ respectively.

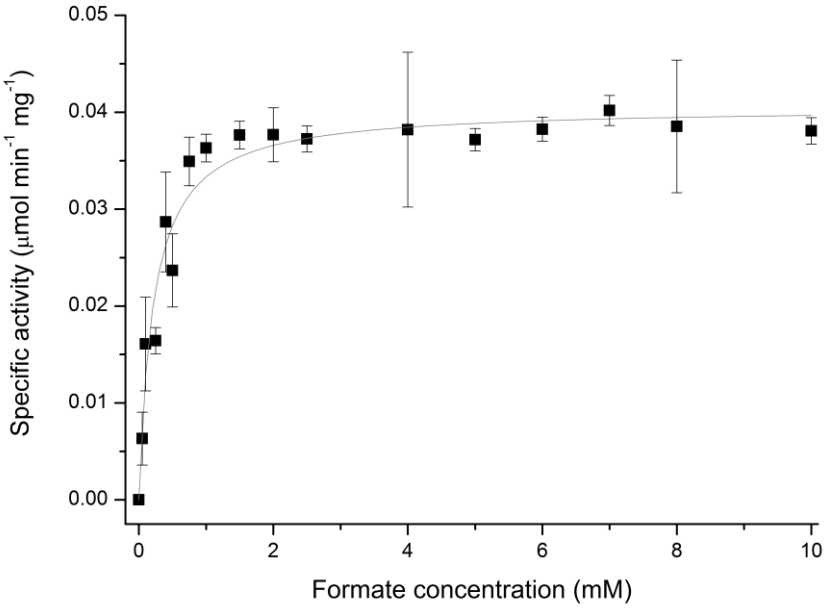

Figure 5-5 Michaelis-Menten plot for formate oxidation in Fdh1+ cells grown +Mo.
Initial rates determined by measuring increasing absorbance in colorimetric methyl viologen assay. Each data point represents average of a minimum of three experimental data sets where error bars represent ± SEM. Data fitted to a hyperbolic function according to the Michaelis Menten equation. K_m and V_{max} for formate oxidation determined as 0.22 ± 0.03 mM and 0.04 ± 0.002 µmol $min^{-1}mg^{-1}$ respectively.

5.1.3 Importance of Fdh2 for growth and formate oxidation

Fdh2 was the second of the three isoforms to be studied. For this isoform data for ΔFdh2, (which allows assessment of the effect of removing Fdh2), and Fdh2+, (which allows the study of Fdh2 in isolation), are presented.

The growth of ΔFdh2 can be seen in Figure 5-6 with the strain reaching stationary OD_{600} values within error seen for WT for all four growth conditions except +Mo (0.22 ± 0.01 vs 0.30 ±0.05 for WT). This suggests that deletion of Fdh2 alone does not limit final cell density except under this condition.

Also shown in Figure 5-6 is the growth of Fdh2+. Of those mutants that grew, Fdh2+ reached the lowest final OD_{600} in all four studied conditions, only reaching stationary phase when supplemented +W/+Mo. Fdh2+ remained in exponential growth after 24 h for all three of the other conditions suggesting that although Fdh2 is capable of supporting growth in isolation it cannot maintain the population supported by WT or Fdh1 alone.

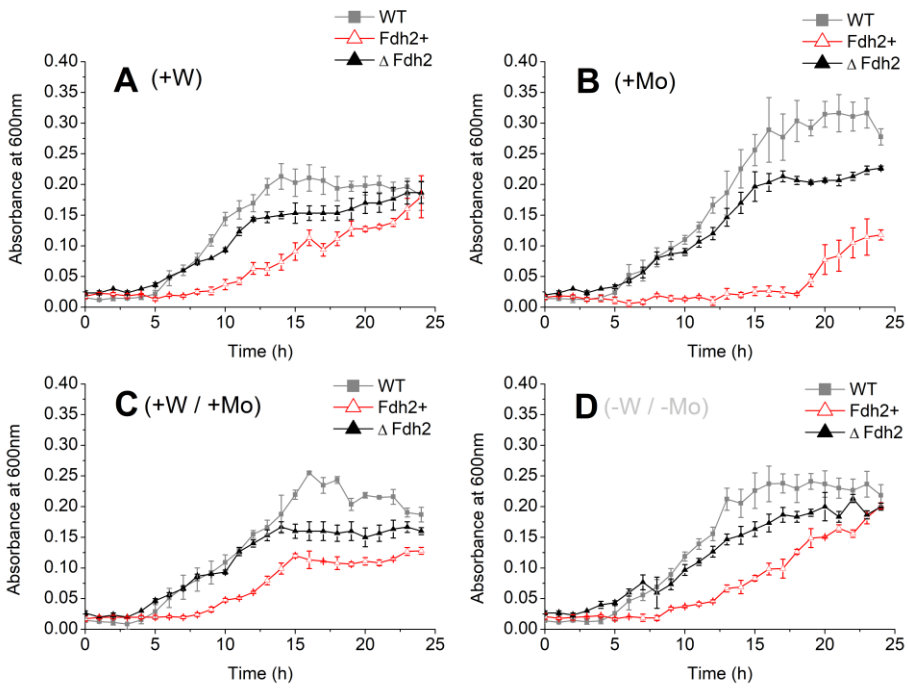

Figure 5-6 Growth of deletion strains ΔFdh2 and Fdh2+ in minimal media.
*Media supplemented with **(A)** 3μM sodium tungstate (+W), **(B)** 3μM sodium molybdate (+Mo) **(C)** 3μM sodium tungstate and molybdate (+W/+Mo) or **(D)** With neither metal (-W/-Mo). All panels represent anaerobic growth in minimal media with 50 mM fumarate as terminal electron acceptor. Wildtype growth shown in grey for comparative purposes. Data represents average of a minimum of three experimental data sets where error bars represent ± SEM.*

Although Fdh2 was observed to contribute less to growth than Fdh1 under these formate containing growth conditions the FDH activity of both ΔFdh2 and Fdh2+ were determined and are presented in Figure 5-7 below as percentages of WT activity under the same conditions.

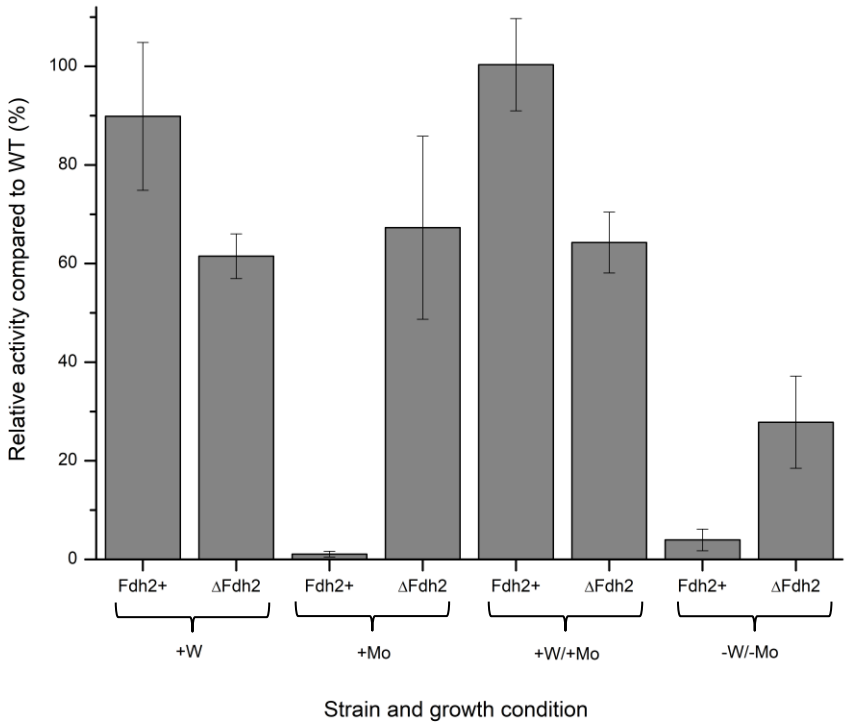

Figure 5-7 Relative FDH activities of ΔFdh2 and Fdh2+ compared to WT.
Activity measured after growth in minimal media for 24 h when growth supplemented with 3μM sodium tungstate (+W), 3μM sodium molybdate (+Mo), 3 μM sodium tungstate and molybdate (+W/+Mo) or neither metal (-W/-Mo). Activities obtained using colorimetric methyl viologen assay and normalised to protein content in sample. Presented as % of WT specific activity seen for the same growth condition. Data represents average of a minimum of three experimental data sets where error bars represent ± SEM.

Deletion of Fdh2 caused large decreases in formate oxidation activity compared to WT in all four growth conditions, with activities around 60% of WT when grown +W, +Mo or +W/+Mo and around 25% when grown -W/-Mo. These results do not correlate with the previous described growth data which suggested a growth defect in ΔFdh2 only when grown +Mo.

Analysis of Fdh2+ in Figure 5-7 suggest that Fdh2 alone is capable of comparable formate oxidation specific activities to WT when grown +W or +W/+Mo. In contrast activities seen for Fdh2+ grown +Mo or -W/-Mo are effectively non-existent, at 1 or 3% of WT activities respectively. These results for Fdh2+ are of considerable interest as they not only suggest that in isolation

Fdh2 requires tungstate containing conditions to show activity, but also that these activities are comparable to those seen in WT.

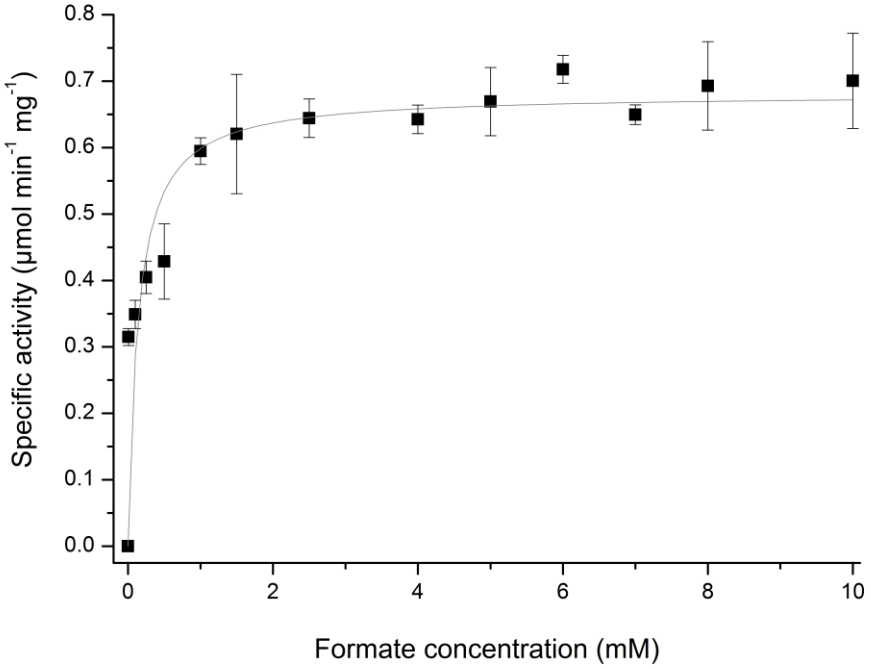

Figure 5-8 Michaelis-Menten plot for formate oxidation in whole Fdh2+ cells grown +W.
Initial rates determined by measuring increasing absorbance in colorimetric methyl viologen assay. Each data point represents average of a minimum of three experimental data sets where error bars represent ± SEM. Data fitted to a hyperbolic function according to the Michaelis Menten equation. K_m and V_{max} for formation oxidation determined as 0.14 ± 0.05 mM and 0.68 ± 0.03 µmol $min^{-1}mg^{-1}$ respectively.

Considering the perceived importance of the Fdh2 isoform for maximal FDH activities in tungsten supplemented growth conditions, K_m and V_{max} values were determined using Fdh2+ whole cells grown +W. Figure 5-8 demonstrated K_m and V_{max} values for formation oxidation determined as 0.14 ± 0.05mM and 0.68 ± 0.03 µmol $min^{-1}mg^{-1}$ respectively.

5.1.4 Importance of Fdn for growth and formate oxidation

Fdn was the final FDH isoform to be studied. Relevant data for ΔFdn and Fdn+ (i.e. Fdn in isolation), are presented.

Growth of ΔFdn is seen in Figure 5-9 with the strain reaching the same stationary OD_{600} values as WT, indeed growth traces in all four growth conditions matched those seen in WT suggesting that deletion of Fdn had no significant effect on any aspect of the ability of *S.oneidensis* to grow under these conditions.

In support of this statement is the growth of Fdn+ also seen in Figure 5-9. Fdn+, seen in red, was unable to grow in any of the four growth conditions suggesting Fdn alone is not capable of supporting growth.

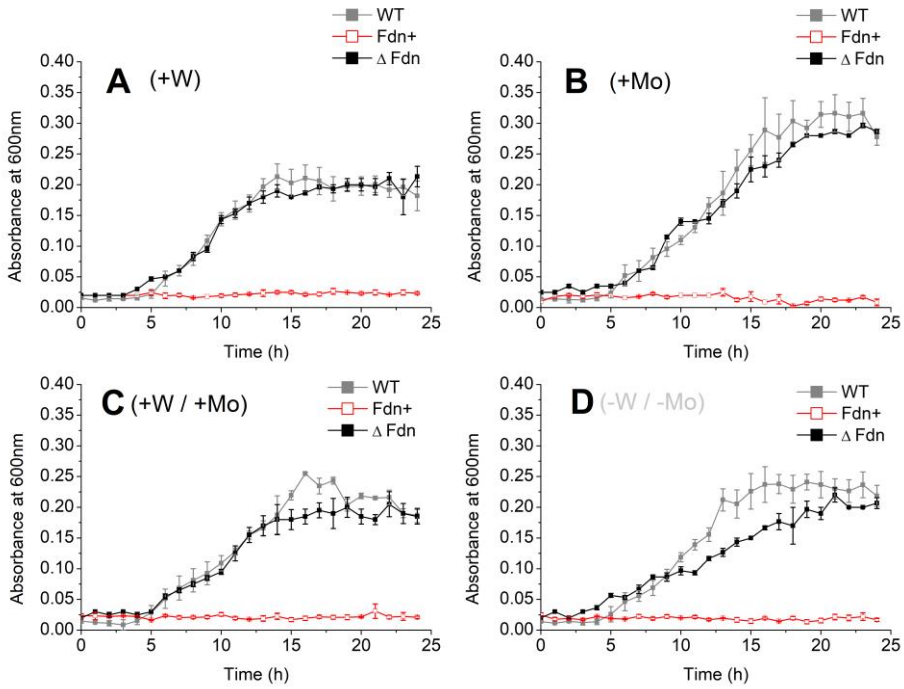

Figure 5-9 Growth of deletion strains ΔFdn and Fdn+ in minimal media.
*Media supplemented with **(A)** 3μM sodium tungstate (+W), **(B)** 3μM sodium molybdate (+Mo) **(C)** 3μM sodium tungstate and molybdate (+W/+Mo) or **(D)** With neither metal (-W/-Mo). All panels represent anaerobic growth in minimal media with 50mM fumarate as terminal electron acceptor. WT growth shown in grey for comparative purposes. Data represents average of a minimum of three experimental data sets where error bars represent ± SEM.*

Since Fdn+ was unable to grow in the studied media conditions only formate oxidation data for ΔFdn can be reported. Relative formate oxidation by ΔFdn is presented below in Figure 5-10 and shows that formate oxidation when grown

+W or +W/+Mo is unchanged in the absence of Fdn, but significantly lower when grown +Mo or -W/-Mo.

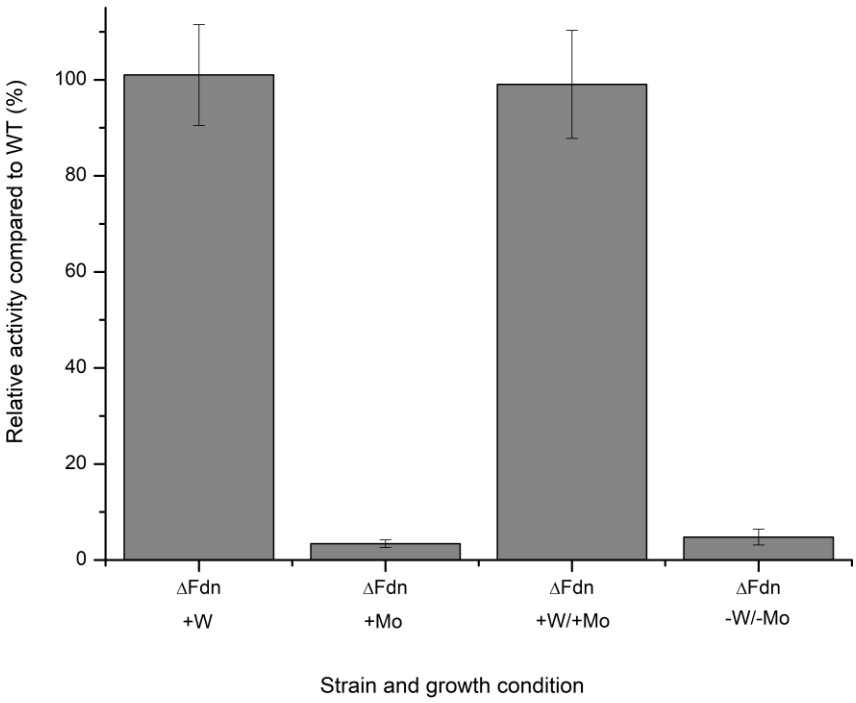

Figure 5-10 Relative FDH activities of ΔFdn compared to WT.
Activity measured after growth in minimal media for 24 h when growth supplemented with 3μM sodium tungstate (+W), 3μM sodium molybdate (+Mo), 3μM sodium tungstate and molybdate (+W/+Mo) or neither metal (-W/-Mo). Activities obtained using colorimetric methyl viologen assay and normalised to protein content in sample. Presented as % of WT specific activity seen for the same growth condition. Data represents average of a minimum of three experimental data sets where error bars represent ± SEM.

5.1.5 Relative isoform contributions to WT growth and FDH activity

A full compilation of the data presented above, including lag phase durations, specific growth rates, final OD values after 24 h growth and non-comparative formate oxidation specific activities for all seven deletion strains in all four media conditions are presented in the appendix.

When comparing isoforms, deletion of both Fdh1 and Fdh2 result in impaired growth phenotypes in at least one growth condition whilst deletion of Fdn causes no changes compared to WT. It is tempting therefore to dismiss Fdn as not playing any physiological role in the studied conditions. However the FDH activity of ΔFdh1, ΔFdh2 and ΔFdn disputes this, showing that individual deletion of each of the three isoforms affects the ability of *S.oneidensis* to oxidise formate in at least one growth condition. Indeed analysis of the growth of the double cluster mutants Fdh1+ and Δ Fdh2+ support that Fdn has a role, albeit minor, in normal growth. This support comes in the form of two points, presented in turn below for clarity.

The first point relates to the duration of lag phase seen in different deletion strains. All three of the single cluster mutants grew with lag phase durations indistinguishable from the error determined for WT values, with slightly longer values determined for ΔFdh1 -W/-Mo (5.6 h) and for ΔFdn +Mo (5.3 h). In contrast the double mutants Fdh1+ and Fdh2+ showed extended lag phases in almost every growth condition with the exception of Fdh1+ -W/-Mo. Of these extended lag phases, the most extended were seen when supplemented with molybdate (10 ± 1 h for Fdh1+ and 16.3 ± 1.2 h for Fdh2+). Together this information suggests that any two of the three isoforms together, including Fdn, are able to recreate lag phase durations seen in WT, but in isolation neither Fdh1, (evidenced by Fdh1+) or Fdh2, (evidenced by Fdh2+) or Fdn, evidenced by the absence of growth of Fdn+, are able.

The second point relates to the observed specific growth rates. All of the single cluster mutant strains showed specific growth rates between 40-61% of the WT rates (except ΔFdnΔFdh2 +W), suggesting a requirement for all three isoforms for WT growth rates. This effect would be expected to be cumulative, with double cluster mutants showing even lower rates than mutants with only one isoform removed, interestingly however the double cluster mutants that grew

either demonstrated comparable growth rates to single mutants, when grown +Mo or -W/-Mo, or higher growth rates than the single cluster mutants when grown with +W or +W/+Mo. It would be expected that if all three isoforms contributed to maximal growth rates these double cluster mutants would show lower growth rates than their single counterparts. This discrepancy is exemplified by Fdh1+ +W showing comparable growth rates to WT. Since Fdh1+ showed growth rates comparable to WT, but the ΔFdh2 mutant, which retains Fdh1 and Fdn, showed reduced growth rates, it could be suggested that Fdn inhibits Fdh1 linked growth rates when grown with tungstate. The same trend, although less pronounced, is seen when grown +W/+Mo, not only for Fdh1, but also Fdh2.

To summarise the above results it is seen that a combination of any two of the three isoforms are required to maintain WT lag phase duration, and deletion of any one of the three isoforms causes decreases in the specific growth rate. Regarding final OD_{600}, deletion of the Fdn isoform causes no significant changes; deletion of Fdh1 causes minor growth attenuation and deletion of Fdh2 the most pronounced phenotype. These last results do not correlate with the observed FDH activities where Fdh2 and Fdh1 are thought to contribute to FDH activities when grown +W or +W/+Mo, whilst all three isoforms are thought to be involved when grown +Mo or -W/-Mo, although under these conditions Fdh2 and Fdn could not be shown to catalyse formate oxidation alone.

Although to study the nuances of formate oxidation in this section activities are presented in relation to those seen for WT, it should be highlighted that for all mutant strains, consistently lower specific activities were observed when grown +Mo or -W/-Mo compared to +W or +W/+Mo, as was previously seen for WT in Chapter 3. None of the mutants demonstrated higher activities when grown +Mo or -W/-Mo.

To allow easy comparison of the determined kinetic parameters in the following text the K_m and V_{max} values obtained from Figure 5-4 Figure 5-5 and Figure 5-8 are presented in Table 5-2.

Table 5-2 Collection of kinetic parameters determined for formate oxidation.

Strain (Growth)	Km for oxidation (μM)	Vmax for oxidation (μmol min^{-1} mg^{-1})
Wildtype (+W)	39 ± 5 μM	0.74 ± 0.02
Fdh2+ (+W)	140 ± 50 μM	0.68 ± 0.03
Fdh1+ (+W)	70 ± 30 μM	0.32 ± 0.02
Fdh1+ (+Mo)	220 ± 30 μM	0.04 ± 0.002

As can be seen from Table 5-2 when growth was supplemented with tungstate WT cells had the lowest K_m value for formate (39μM), followed by Fdh1+ (70μM) followed by Fdh2+ (140μM), suggesting that of the two isoforms Fdh1 has a higher affinity for formate. The highest V_{max} rate is seen for WT cells (0.74 μmol min^{-1} mg^{-1}) followed by Fdh2+ (0.68 μmol min^{-1} mg^{-1}) and then Fdh1+ (0.32 μmol min-1 mg^{-1}) suggesting that the Fdh2 isoform can reach the highest rates of catalysis, in keeping with previous analysis of specific activities in Figure 5-7.

Interestingly when grown +Mo, the Fdh1+ strain showed a higher K_m value for formate (220 ± 30μM) than when grown with +W (140 ± 30μM). The implications of this are subsequently discussed. The V_{max} value for those cells grown +Mo was lower (0.04 ±0.002 μmol min^{-1} mg^{-1}) than seen when grown +W (0.32 ± 0.02 μmol min^{-1} mg^{-1}), in agreement with previous specific activity analysis.

5.2 Contribution of FDH isoforms to WT CO_2 reductase activity

Although sharing a number of the techniques used to study formate oxidation above, the ability of *S.oneidensis* deletion strains to reduce CO_2 is presented here separately to avoid ambiguity and highlight the different approach to data analysis. In this context the principal focus is in identification of the isoforms responsible for native CO_2 reductase activity to inform on targets for future optimisation. This work does not concern the native physiology of *S.oneidensis* as CO_2 reduction is not thought to be a physiologically relevant conversion, seen only under artificial conditions such as those presented here.

5.2.1 Importance of Fdh1 for CO_2 reduction

The first isoform to be studied in the context of CO_2 reduction is Fdh1. To do this the relevant data for ΔFdh1 and Fdh1+ are presented. The growth data for these strains has already been presented in the previous section, but it is worth noting that the cells for these CO_2 reduction assays, like those for formate oxidation, were harvested after 24 h growth in minimal media supplemented either with 3μM sodium tungstate (+W), 3μM sodium molybdate (+Mo), both metals at 3μM (+W/+Mo) or supplemented with neither (-W/-Mo).

Using the colourimetric methyl viologen assay established in Chapter 4, CO_2 reductase rates were determined for ΔFdh1 and Fdh1+ and are presented in Figure 5-11. It should be noted that the values presented are not presented as proportions of WT activity as for formate oxidation, instead the absolute specific activities are presented, with the corresponding WT activities in red. This is because in this context the fastest rates, rather than the fastest relative rates are of most interest.

ΔFdh1 shows comparable CO_2 reductase activity to WT when grown +W or +W/+Mo suggesting Fdh1 does not contribute to the WT rates in these conditions. Analysis of growth +Mo or -W/-Mo is more complicated, under these conditions ΔFdh1 actually shows higher CO_2 reductase rates than WT suggesting Fdh1 may actually limit CO_2 reduction under these conditions although the observed rates are still significantly slower than those seen +W or +W/+Mo.

CO_2 reduction of Fdh1+, in contrast to study of ΔFdh1, suggests that when grown +W and +W/+Mo, Fdh1 in isolation does contribute to CO_2 reductase activity. To further complicate matters study of Fdh1+ after growth +Mo demonstrate higher rates of CO_2 reduction than WT, although these values are close to the determined errors and conclusions based on these data are made with caution.

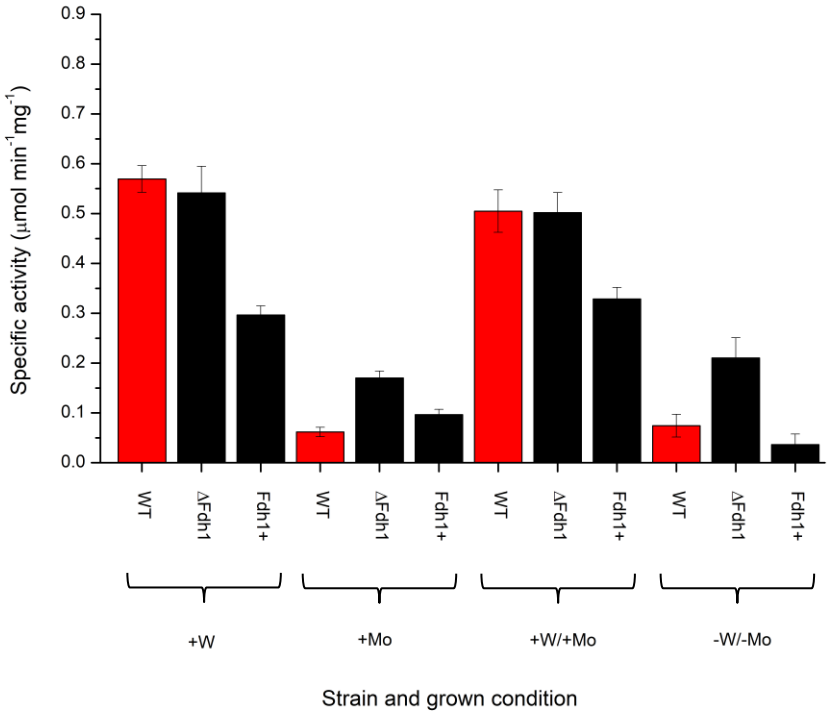

Figure 5-11 CO_2 reductase activities of ΔFdh1 and Fdh1+.
Activity measured after growth in minimal media for 24 h when growth supplemented with 3µM sodium tungstate (+W), 3µM sodium molybdate (+Mo), 3µM sodium tungstate and molybdate (+W/+Mo) or neither metal (-W/-Mo). Activities obtained using colorimetric methyl viologen assay and normalised to protein content in sample. Presented as specific activities and including WT values (shown in red) for comparative purposes. Data represents average of a minimum of three experimental data sets where error bars represent ± SEM.

Since study of Fdh1+ in tungstate containing growth conditions suggested that Fdh1 may contribute to CO_2 reduction, K_m (2.18 ± 0.31 mM) and V_{max} (0.32 ± 0.01 µmol $min^{-1}mg^{-1}$) values for CO_2 reduction were determined as described in Chapter 4, presented from data in Figure 5-12.

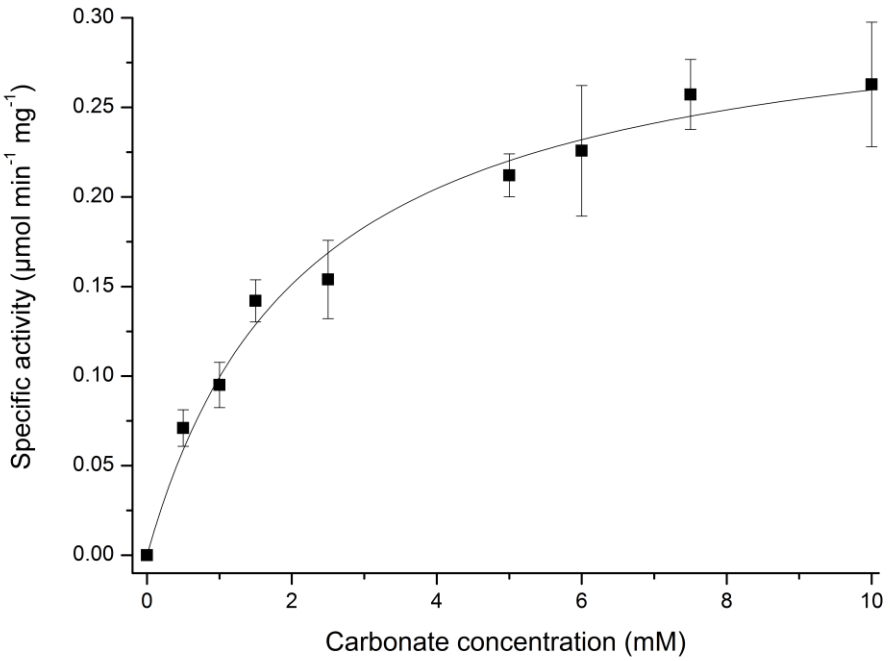

Figure 5-12 Michaelis-Menten plots for CO_2 reduction in whole Fdh1+ cells grown +W.
Initial rates determined by measuring increasing absorbance in colorimetric methyl viologen assay. Each data point represents average of a minimum of three experimental data sets where error bars represent ± SEM. Data fitted to a hyperbolic function according to the Michaelis Menten equation. K_m and V_{max} for CO_2 reduction determined as 2.18 ± 0.31 mM and 0.32 ± 0.01 µmol $min^{-1}mg^{-1}$ respectively.

5.2.2 Importance of Fdh2 for CO_2 reduction

CO_2 reductase activity was next studied in the deletion strains relating to Fdh2, ΔFdh2 and Fdh2+. CO_2 reductase activities for these strains are found below (Figure 5-13) in the same format seen for Figure 5-11.

Analysis of the CO_2 reductase activity for ΔFdh2 is surprisingly complicated. When grown +W or +W/+Mo, deletion of Fdh2 results in a significant drop in CO_2 reductase activity, suggesting Fdh2 contributes to these activities. In contrast when grown +Mo or -W/-Mo, activities are significantly higher than those seen for WT suggesting that, as seen for Fdh1, deletion of these isoforms in isolation causes increase in CO_2 reductase activities. Also similarly to Fdh1 however, the rates of these activities when grown +Mo or -W/-Mo are not as high as those seen in tungstate supplemented conditions.

Fdh2+ represents potentially the most interesting of the mutant strains when considering CO_2 reductase activity. When grown +W or +W/+Mo, Fdh2+ shows

CO_2 reduction rates comparable or even higher (although not statistically significant) than WT, suggesting that Fdh2 in isolation is capable of producing comparable rates of CO_2 reduction. In contrast when grown +Mo or -W/-Mo negligible amounts of CO_2 reductase activity are observed suggesting that Fdh2 associated CO_2 reductase activity is strictly dependent on the availability of tungstate.

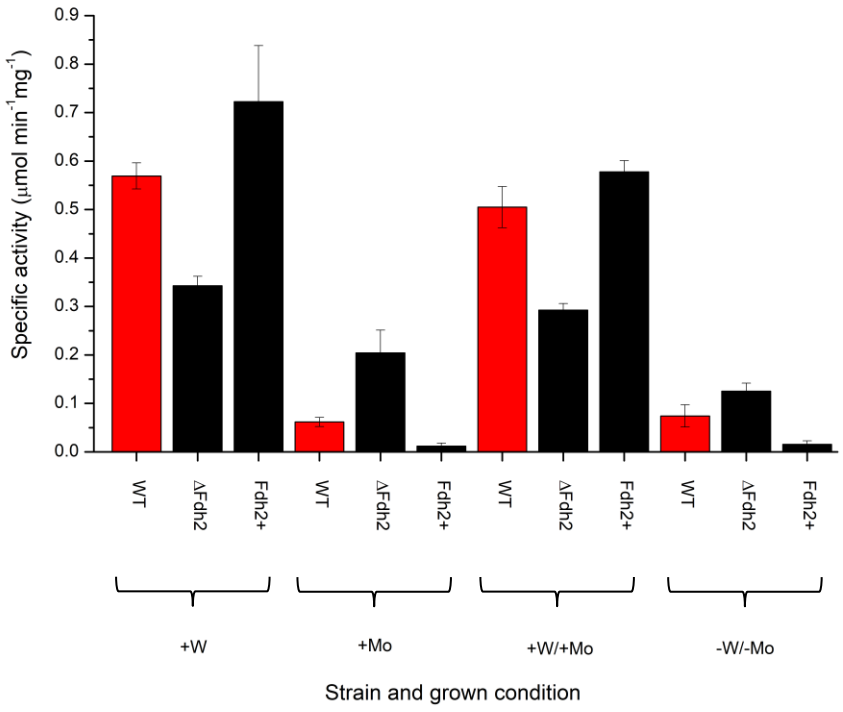

Figure 5-13 CO_2 reductase activities of ΔFdh2 and Fdh2+.
Activity measured after growth in minimal media for 24 h when growth supplemented with 3µM sodium tungstate (+W), 3µM sodium molybdate (+Mo), 3µM sodium tungstate and molybdate (+W/+Mo) or neither metal (-W/-Mo). Activities obtained using colorimetric methyl viologen assay and normalised to protein content in sample. Presented as specific activities and including WT values (shown in red) for comparative purposes. Data represents average of a minimum of three experimental data sets where error bars represent ± SEM.

Due to the high levels of CO_2 reductase activity seen for Fdh2+ when grown +W, K_m (1.05 ± 0.13 mM) and V_{max} (0.86 ± 0.03 µmol $min^{-1}mg^{-1}$) values were determined from Figure 5-14.

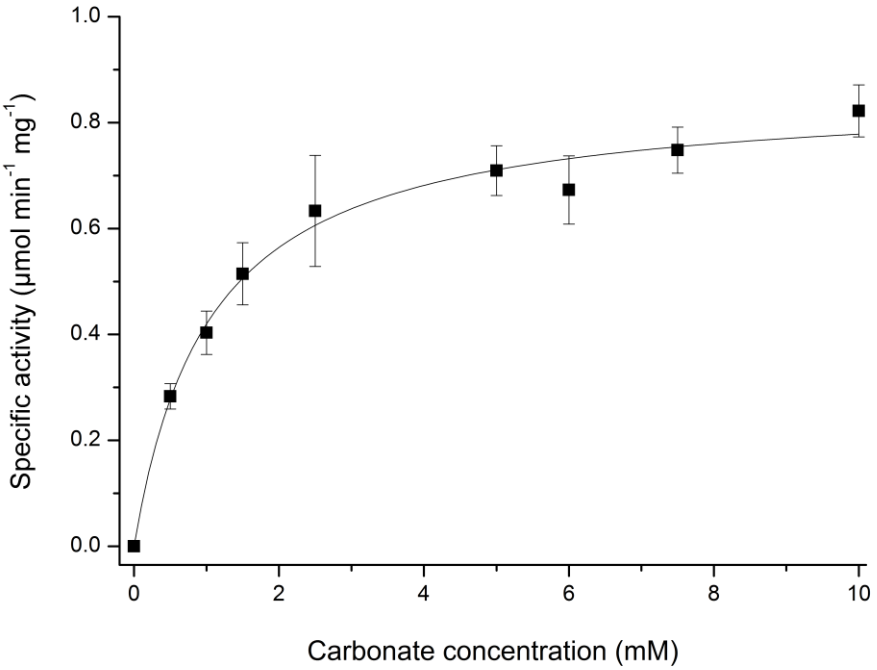

Figure 5-14 Michaelis-Menten plot for CO_2 reduction in whole Fdh2+ cells grown +W.
Initial rates determined by measuring increasing absorbance in colorimetric methyl viologen assay. Each data point represents average of a minimum of three experimental data sets where error bars represent ± SEM. Data fitted to a hyperbolic function according to the Michaelis Menten equation. K_m and V_{max} determined as 1.05 ± 0.13 mM and 0.86 ± 0.03 µmol $min^{-1}mg^{-1}$ respectively.

5.2.3 Importance of Fdn for CO_2 reduction

Fdn was the final isoform to be studied for CO_2 reduction, using the mutant strain ΔFdn alone. As already noted for formate oxidation, the inability of ΔFdh1ΔFdh2 to grow in the described minimal media made its subsequent study by colourimetric assay impossible.

CO_2 reductase activities of ΔFdn after growth in the four described growth conditions are seen in Figure 5-15. The values for CO_2 reductase activity after growth +W or +W/+Mo are comparable to WT, suggesting Fdn does not contribute to CO_2 reductase activity in these conditions. In contrast, and as seen for ΔFdh1 and ΔFdh2 previously, when grown with +Mo or -W/-Mo, activities were higher than WT, but significantly lower than comparative activities from tungstate supplemented conditions.

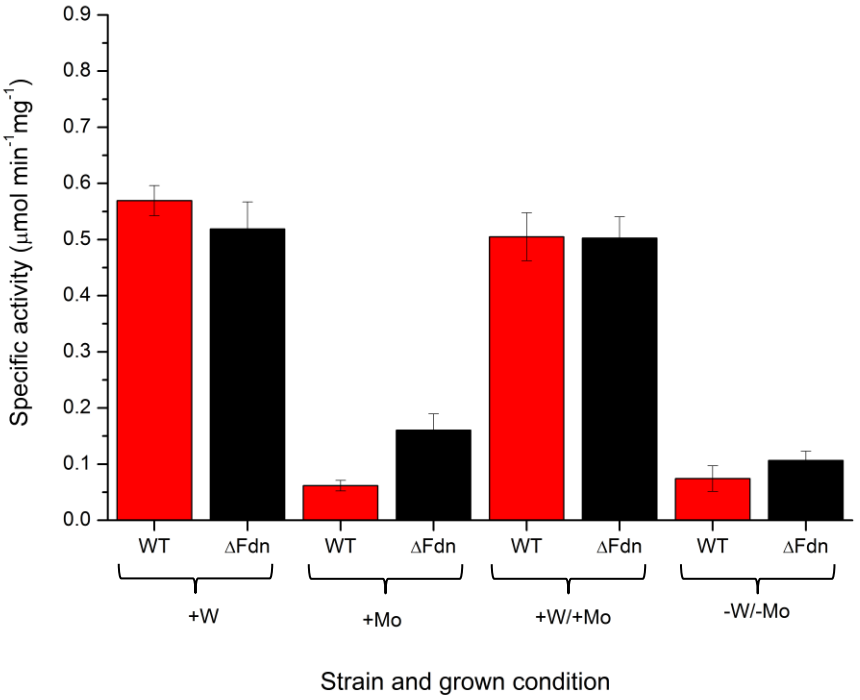

Figure 5-15 CO_2 reductase activities of ΔFdn.
Activity measured after growth in minimal media for 24 h when growth supplemented with 3µM sodium tungstate (+W), 3µM sodium molybdate (+Mo), 3µM sodium tungstate and molybdate (+W/+Mo) or neither metal (-W/-Mo). Activities obtained using colorimetric methyl viologen assay and normalised to protein content in sample. Presented as specific activities and including WT values (shown in red) for comparative purposes. Data represents average of a minimum of three experimental data sets where error bars represent ± SEM.

5.2.4 Relative isoform contributions to WT CO_2 reductase activity

To better compare between the CO_2 reduction kinetic parameters determined for +W grown Fdh2+ and Fdh1+ cells, the relevant values are combined in Table 5-3 below.

Table 5-3 Collection of kinetic parameters determined for CO_2 reduction.

Strain (growth)	K_m for reduction (mM)	V_{max} for reduction (µmol min^{-1} mg^{-1})
Wildtype (+W)	1.43 ± 0.26 mM	0.58 ± 0.03
Fdh2+ (+W)	1.05 ± 0.13 mM	0.86 ± 0.03
Fdh1+ (+W)	2.18 ± 0.31 mM	0.32 ± 0.01

The lowest K_m for CO_2 reduction in Table 5-3 is not seen for WT, but Fdh2+ (1.05 ± 0.13 mM). WT shows the second lowest K_m (1.43 ± 0.26mM) followed by Fdh1+ (2.18 ± 0.31 mM). In contrast to formate oxidation this suggests that the Fdh2 isoform not only has a higher affinity for CO_2 than Fdh1, but also WT when grown +W, an interesting observation discussed further below. It is notable that these K_m values are all several orders of magnitude larger than those determined for formate suggesting a much higher affinity for formate over CO_2.

The highest V_{max} determined for CO_2 reduction was for Fdh2+ (0.86 ± 0.03 μmol min^{-1} mg^{-1}) followed by WT (0.58 ± 0.03 μmol min^{-1} mg^{-1}) and Fdh1+ (0.32 ± 0.01 μmol min^{-1} mg^{-1}). It should be highlighted that such high specific activities were not reported in Figure 5-13 for Fdh2+ +W but the large error on this previous value (0.72 ± 0.12 μmol min^{-1} mg^{-1}) does not necessarily make the data contradictory.

5.3 Kinetics of FDH deletion mutants in lysogeny broth

Since the previous studies investigated growth and subsequent enzymatic activity on minimal media it was impossible to determine the enzymatic activity of both the double cluster mutant Fdn+ and triple mutant ΔFDH as neither of these strains were able to grow in the defined minimal media.

As such equivalent rich lysogeny broth experiments were performed, capable of supporting the growth of these strains allowing for their subsequent analysis for formate oxidation and CO_2 reduction assays, the other double cluster mutants, Fdh1+ and Fdh2+, were also studied under these conditions. After anaerobic growth for 24 h with 50mM sodium fumarate as terminal electron acceptor and supplemented with 3μM sodium tungstate, cells were washed and assayed for activity as described previously. The resultant data is seen in Figure 5-16.

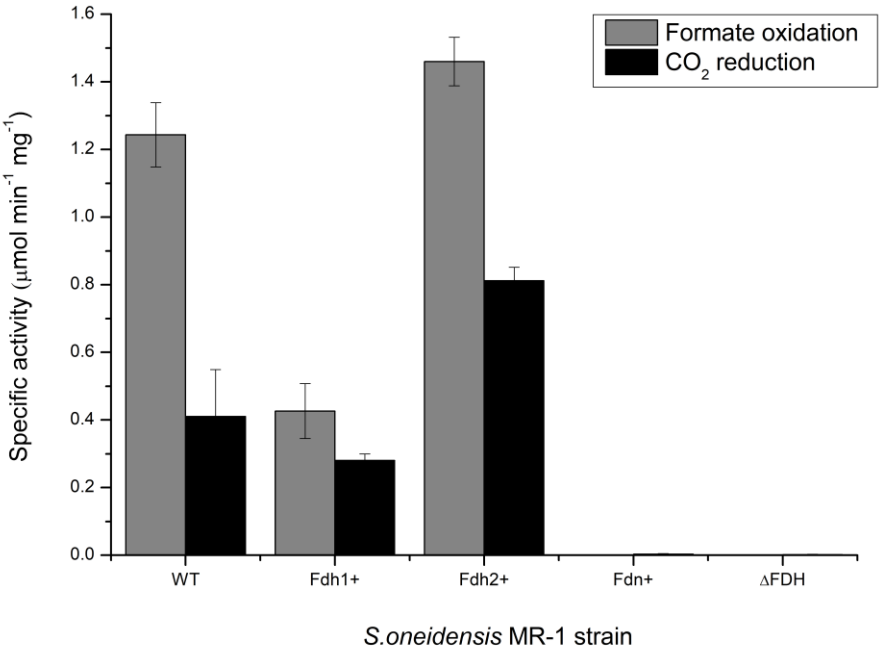

Figure 5-16 FDH and CO_2 reductase activities in FDH mutant strains after growth in LB.
Cultured for 24 h in LB supplemented with 3µM sodium tungstate (+W). Activities obtained using colorimetric methyl viologen assay and normalised to protein content in sample. Data represents average of a minimum of three experimental data sets where error bars represent ± SEM.

No formate oxidation or CO_2 reduction was seen in Fdn+ or the triple mutant ΔFDH grown in LB media +W in Figure 5-16. The double mutants that did show activity, Fdh1+ and Fdh2+, showed similar trends to tungstate supplemented minimal media conditions, with Fdh1+ showing attenuated activity for both formate oxidation and CO_2 reduction, suggesting Fdh1 has a minor contribution to WT activity. In contrast the Fdh2+ mutant not only showed higher CO_2 reduction rates than WT, (0.81 ± 0.04 compared to 0.41 ± 0.14 µmol min^{-1} mg^{-1})as seen after growth in tungstate supplemented minimal media, but higher formate oxidation activities as well (1.46 ± 0.07 compared to 1.24 ± 0.09 µmol min^{-1} mg^{-1}).

5.4 Discussion

This chapter of work aimed to elucidate which of the three identified FDH isoforms in *S.oneidensis* MR-1 contributed to wildtype growth and formate oxidation/CO_2 reduction. It is evident after studying the preceding data that the relationship between these three isoforms and their growth and activity phenotypes are complex, subtle and interlinked.

5.4.1 Comparing FDH specific activity and cell growth

A strain with a high FDH specific activity might be expected to correlate with an ability to grow in minimal media containing formate as sole electron donor. However this is not the case. The best example of this is the study of the ΔFdn strain in minimal media supplemented with molybdate. Under these conditions exceptionally low rates of formate oxidation were observed, 0.009 ± 0.01 μmol min^{-1} mg^{-1} compared to 0.282 ± 0.027 μmol min^{-1} mg^{-1} for WT (+Mo). It might then be assumed that such a defect would inhibit the ability of this strain to grow on formate, but as seen in Figure 5-9 ΔFdn grew to comparable OD_{600} values as wildtype during stationary phase, 0.29 ± 0.01 vs 0.30 ± 0.05, albeit with a slower growth rate. Since this OD_{600} during stationary phase is the highest observed of any strain, in any condition, it is considered that the rate of formate oxidation does not limit population size in any of the four of the growth conditions studied.

Although no correlation could be made between stationary population size and formate oxidation specific activity it seems more plausible to look for a correlation between formate oxidation specific activity and specific growth rate. When examined however no convincing correlations can be made. Again the best illustration of this point is using the strain Fdh1+ (+W) as a counter example. This strain showed the second highest specific growth rate of 0.35 ± 0.05 h^{-1}, behind only WT (+W) at 0.37 ± 0.06 h^{-1}. However this strain showed the lowest formate oxidation specific activity of all strains under this growth condition with a rate of 0.329 ± 0.095 μmol min^{-1} mg^{-1}.

Considering the physiology underlying a bacterial lag phase, i.e. insufficient supply of a particular metabolite or inactivity of a required enzyme (Monod 1949), most frequently resolved by changes in gene expression (Rolfe et al.

2012), it is perhaps unsurprising that no correlation is observed between formate oxidation activity during stationary phase and duration of lag phase.

As concluded above no correlations can be made between the formate oxidation specific activity data shown in Figure 5-3, Figure 5-7 and Figure 5-10 and any aspect of growth in minimal media, not the specific growth rate, the lag phase duration nor stationary phase OD_{600}. It should be realised however that comparisons between bacterial growth, even in a defined growth media, will not be directly comparable with the artificial conditions established for measuring enzymatic activity using non-endogenous redox partners, in this case methyl viologen. The caveats associated with these comparisons are detailed below.

Under normal physiological conditions, i.e. those seen during growth, oxidation of formate to CO_2 (standard reduction potential -420mV vs SHE (Ruschig et al. 1976) is coupled to the reduction of menaquinone to menaquinol, with a reduction potential of -50 to -100 mV vs SHE (Richardson et al. 2012). In contrast the reduction potential of methyl viologen at -446mV vs SHE (Illichmanová et al. 2011) is considerably more negative, more negative even than the formate/CO_2 couple, highlighting the distinctly different thermodynamics between growth and activity assay experiments. In addition, during the normal physiological reaction, the oxidation of formate generates electrons that are proposed to pass via the β and γ subunits of the FDH complexes (Jormakka et al. 2002), although this may also be the case when coupled to methyl viologen as an electron acceptor, it is also possible the redox dye interacts directly with the catalytic α subunit and electrons bypass the remainder of the FDH complex, again highlighting the incomparability of the two experiments. Finally it should also be highlighted that during growth, catalysis would likely be influenced by the redox state of the menaquinone pool, and the number of other metabolic processes that contribute to this state. During the colourimetric assays however these constraints would not limit the reaction, the only limitation being the availability of the redox dye. Finally all assay experiments were conducted on cells after 24 h growth, i.e. during stationary phase, both protein expression and redox state of the cells are likely to be subtly different between lag phase and exponential growth, complicating comparisons.

5.4.2 Comparing kinetic parameters for deletion strains

Although comparisons are made cautiously in light of the above discussion, the determination of kinetic parameters for the Fdh1 and Fdh2 isoforms summarised in Table 5-2 and Table 5-3 might be suggested to explain the observed growth phenotypes of the deletion strains.

When analysing the K_m and V_{max} values for formate oxidation it is first worth considering that the WT determinations represent contributions from all isoforms capable of oxidising formate. Under tungstate supplemented conditions, the activity of mutant strains in Figure 5-3 and Figure 5-7 suggest that Fdh1 and Fdh2 are the two isoforms responsible for catalysis of formate and therefore responsible for contributing to the WT K_m and V_{max} values.

In such examples where the kinetics of enzyme mixtures have been studied it has been hard to identify individual enzyme populations from kinetics data alone, with estimations not possible with similar K_m values (Brown et al. 2014). Even in those examples where the contributions of different isoforms were able to be separated, the importance of very accurate data sets is stressed, (Brown et al. 2014), accuracy that proved unfeasible with the WT whole cell methodology in Chapter 4. As such the isoforms were examined in isolation, i.e using the double cluster mutants Fdh1+ and Fdh2+.

Of the two double cluster mutants studied a K_m value of 70 μM was determined for Fdh1+ and 140 μM for Fdh2+ suggesting that of the two isoforms Fdh1 has a higher affinity for formate. It is possible that this higher affinity for formate is linked to the importance of Fdh1 for growth in minimal media over Fdh2 seen in Figure 5-2 and Figure 5-6. However the concentration of formate in these experiments, supplemented at 50 mM, is considerably higher than both of these K_m values suggesting that formate concentration shouldn't limit the kinetics of either isoform or their ability to support bacterial growth. The importance of Fdh1 relative to Fdh2 under these growth conditions may also be linked to their intracellular redox partners. Although both Fdh1 and Fdh2 are predicted to couple to the menaquinone pool, they may do so with altered thermodynamics, the structural variation between them causing changes in reduction potential. Although there is no current evidence, it is not impossible that they may even

interact with other intracellular redox partners, resulting in one or other being of considerable more importance for effective metabolism.

It should be noted that although the Fdh1 isoform is predicted to be of most significance for *S.oneidensis* growth, and has the lowest determined K_m value of the mutants, it is in fact Fdh2, evidenced by analysis of Fdh2+, which shows the higher V_{max} value at 0.68 μmol min^{-1} mg^{-1} suggesting that this higher rate of formate oxidation attained by Fdh2 does not provide a growth advantage, in keeping with previous discussion either suggesting functionally distinct roles for the two isoforms or other metabolic processes, other than formate oxidation, limiting bacterial growth.

Again, such discussion must be cautious making such comparisons between those experiments conducted using methyl viologen and their physiological counterparts involved in respiration where K_m and V_{max} values may be significantly different (Bassegoda et al. 2014).

5.4.3 FDH isoform contributions to WT CO_2 reductase activity

CO_2 reduction will now be discussed with a focus on biotechnological significance as this reaction has not been convincingly demonstrated to be of importance for the normal metabolism of *S.oneidensis MR-1*.

Although Fdh1 is considered the most important isoform for growth and has the lowest K_m for formate oxidation, Fdh2 is the isoform of most interest for CO_2 reduction. The strain containing only the Fdh2 isoform (Fdh2+) has the lowest K_m value for CO_2 seen in Table 5-3 and the highest V_{max} value for CO_2 reduction (0.86 μmol min^{-1} mg^{-1}), making this strain an attractive target for future biotechnological exploitation for CO_2 reduction. The importance of this particular strain is emphasised as when grown with tungstate it shows higher rates of CO_2 reduction than WT, (V_{max}: 0.86 μmol min^{-1} mg^{-1} vs 0.58 μmol min^{-1} mg^{-1}), whilst growing to comparable OD_{600} values (0.18 ± 0.03 vs 0.20 ± 0.03). The reasons behind the lower K_m and higher V_{max} for this strain compared to WT are currently unclear but are possibly linked to the absence of Fdn as the strain containing Fdh2 and Fdn (ΔFdh1) did not show specific activities higher than wildtype, this was only observed when Fdn was also not present in the double deletion mutant Fdh2+.

5.4.4 Regulatory role of Fdn under tungstate containing growth

For Fdn in isolation (Fdn+), no formate oxidation was observed when grown in lysogeny broth +W, and no growth was seen in the formate containing minimal media conditions (+W) suggesting the lack of any formate oxidation capable of supporting growth. In addition in the ΔFdn mutant strain formate oxidation rates are comparable to WT in tungstate supplemented conditions, further suggesting Fdn does not contribute to formate oxidation when grown with tungstate.

Despite these facts, although Fdn does not appear to contribute to formate oxidation directly, its deletion does seem to affect the ability of the other isoforms to oxidise formate effectively when grown with tungstate. Deletion of Fdn appears to have contrasting effects on formate oxidation by Fdh1 and Fdh2. Fdh1 appears less able to oxidise formate when Fdn is absent, as seen by comparing the activities for Fdh1+ (0.291 μmol min^{-1} mg^{-1}), and ΔFdh2 (0.35 μmol min^{-1} mg^{-1}) which retains Fdh1 in addition to Fdn. In contrast, Fdh2 appears better able to oxidise formate when Fdn is absent as seen by comparing the activities for Fdh2+ (0.55 μmol min^{-1} mg^{-1}), and ΔFdh1 (0.291 μmol min^{-1} mg^{-1}) which retains Fdn in addition to Fdh2.

Further complicating this relationship is the observation that when both of the other isoforms Fdh1 and Fdh2 are present, deletion of Fdn does not appear to affect formate oxidation (0.54 ± 0.01 μmol min^{-1} mg^{-1}), showing values equivalent to WT (0.545 ± 0.03 μmol min^{-1} mg^{-1}).

Together these results suggest that under tungstate supplemented conditions Fdn appears redundant when both of the other isoforms are present, but when in isolation Fdn apparently acts to either increase the FDH activity in strains containing Fdh2 or decrease the activity in strains containing only Fdh1. These changes however are not thought to be due to a role oxidising formate directly and may be caused by Fdn acting in a regulatory role. Future gene expression and protein interaction studies would help to clarify the complicated relationship between these isoforms.

5.4.5 Role of Fdn in the absence of tungstate

The Fdn isoform has a more important role for formate oxidation during molybdate containing growth conditions, with ΔFdn (+Mo) impaired in ability to oxidise formate, (0.009 ± 0.01 μmol min^{-1} mg^{-1}). Although this would suggest that Fdn is capable of oxidising formate the strain Fdn+ containing only Fdn was not able to grow under these molybdate supplemented conditions suggesting a distinction between ability to oxidise formate and the ability to oxidise formate capable of supporting growth, drawing parallels with earlier discussion regarding the exact interactions of these isoforms with other metabolic elements.

5.4.6 Fdh1 significance under both tungstate and molybdate supplementation

The Fdh1 isoform appears to play a role under both tungstate and molybdate supplemented growth conditions, not only regarding the assay determined activities, but also growth phenotype. The K_m determinations in Table 5-2 suggest that the Fdh1+ strain shows different K_m values for formate when grown with tungstate (70 ± 30μM) and molybdate (220 ± 30 μM). This may suggest a structurally distinct form of Fdh1 containing either W or Mo at the active site depending on growth condition. This could be confirmed by purification of SO_4509, the catalytic subunit of Fdh1 although the difficulty of such native purifications when using molybdate grown cells and their low associated activity is already highlighted in the inability to purify SO_4513 when grown +Mo in Chapter 4.

Considering that the K_m values for Fdh1+ were determined to be different when grown +W and +Mo an equivalent methodology may also be helpful for investigating whether SO_4513, the catalytic subunit of Fdh2, is capable of co-ordinating either W or Mo depending on growth conditions by determining K_m values for Fdh2+, grown +Mo.

5.4.7 Extended lag phase duration

Of all studied strains the longest lag phases are observed for Fdh1+ and Fdh2+ when grown +Mo (10 ± 1h and 16.3 ± 1.2 h respectively). Since both Fdh1 and Fdh2 have been concluded to require tungstate for maximal activity and both these strains lack Fdn, considered important for molybdate associated formate

oxidation, this is perhaps not surprising. These particularly extended lag phases reflect the time needed by these strains to begin effectively oxidising formate. As already suggested in Chapter 3, if an excess of molybdenum competitively inhibits the activity of tungstate dependent enzymes, such as Fdh1 and Fdh2, this lag time may represent the time needed to upregulate elements needed to produce active versions of Fdh1 or Fdh2, either by removal of inhibitory molybdate or upregulation of tungstate uptake, for example by the specific transporter *TupA* (SO_4719) (Kolker et al. 2005). In agreement with this theory is the slightly extended lag phase observed by ΔFdn +Mo (5.3 ± 0.3 h) suggesting that in the absence of Fdn an extended lag phase is always seen when supplemented with molybdate, but this lag is less severe when both Fdh1 and Fdh2 are present suggesting that together they are better able to adapt to such conditions and produce the conditions required for effective catalysis.

5.4.8 Areas for future research

This chapter of work aimed to bring greater clarity and detail to the study of FDH activity in *S.oneidensis*. The previous two chapters studied wildtype *S.oneidensis* activity and growth and as such were unable to identify relevant proteins. This more systematic study of each isoform in turn has revealed only part of a complicated relationship, yet nonetheless has provided a significant advance in understanding the biochemistry behind formate oxidation in *S.oneidensis* MR-1.

To act as a basis for future research the following questions still remain to be answered.

Does the suggested importance of Fdn for activity when grown with molybdate correspond to a Mo containing enzyme? What is the mechanism behind the apparent regulation of Fdh1 and Fdh2 by Fdn?

Is the ability of Fdh1 to influence catalysis under tungstate or molybdate supplemented conditions with distinct K_m values a reflection of an enzyme capable of coordinating either a Mo-MGD or a W-MGD cofactor? Importantly previous QPCR work (Chapter 3) suggested SO_4509, the catalytic subunit of Fdh1, is expressed when growth is supplemented with either tungstate or molybdate. This is in agreement with the proposed flexibility to utilise W or Mo

suggested here and the requirement of Fdh1 for maximal growth in all conditions regardless of supplementation.

Finally future work should identify why the Fdh1 isoform is more important for WT growth than Fdh2, whether the distinction is structural or related to how they couple to subsequent metabolism.

The study of the deletion strains has provided answers to questions posed in Chapter 3. When considering the previous observation that *SO_0101* expression was upregulated in growth conditions without tungstate or molybdate supplementation it was questioned whether SO_0101 (Fdn), could catalyse formate oxidation without W or Mo as a cofactor, or is better able to scavenge these metals to make an active FDH population to support growth even when these metals are scarce. Neither of these hypotheses are supported by the current work, evidenced by the inability of the Fdn+ strain to grow under these conditions.

Other possibilities raised in Chapter 3, like the newer questions posed above, require a detailed genome wide expression study to determine whether these deletion strains correctly represent the wildtype regulatory elements involved in the expression of these three isoforms.

Since the investigation of CO_2 reductase activity is not trying to inform on native metabolic importance, the conclusions made can be far more definitive. For the purposes of CO_2 reduction by *S.oneidensis* MR-1, Fdh2 is the isoform of most interest for future study. When coupled to methyl viologen, strains containing this isoform are capable of the highest rates of CO_2 reduction with the lowest K_m values, in particular the strain Fdh2+ will be of considerable interest as it not only supports higher rates of CO_2 reduction than WT, but does not compromise by showing the attenuated growth seen by some other strains.

5.5 References

Bassegoda, A. et al., 2014. Reversible Interconversion of CO_2 and Formate by a Molybdenum-Containing Formate Dehydrogenase. *Journal of the American Chemical Society*, 136(44), pp.15473–6.

Brown, S. et al., 2014. The Kinetics of Enzyme Mixtures. *Molecular Biology Research Communications*, 3(1), pp.21–32.

Illichmanová, a et al., 2011. Nitrate reductase whole-cell assay: side effects associated with the use of benzyl viologen. *Folia microbiologica*, 56(1), pp.72–6.

Jormakka, M. et al., 2002. Molecular basis of proton motive force generation: structure of formate dehydrogenase-N. *Science*, 295(March), pp.1863–1868.

Kolker, E. et al., 2005. Global profiling of *Shewanella oneidensis* MR-1: expression of hypothetical genes and improved functional annotations. *Proceedings of the National Academy of Sciences of the United States of America*, 102(6), pp.2099–104.

Monod, J., 1949. The growth of bacterial cultures. *Annual Reviews in M*, 3(Xl), pp.371–394.

Richardson, D.J. et al., 2012. Exploring the biochemistry at the extracellular redox frontier of bacterial mineral Fe(III) respiration. *Biochemical Society transactions*, 40(3), pp.493–500.

Rolfe, M.D. et al., 2012. Lag phase is a distinct growth phase that prepares bacteria for exponential growth and involves transient metal accumulation. *Journal of Bacteriology*, 194(3), pp.686–701.

Ruschig, U. et al., 1976. CO_2 reduction to formate by NADH catalysed by formate dehydrogenase from *Pseudomonas oxalaticus*. *European journal of biochemistry / FEBS*, 70(2), pp.325–330.

6 Electrode driven reversible *S.oneidensis* FDH activity

Previous chapters have focussed on characterising the CO_2 reductase and FDH activity of *S.oneidensis* MR-1, concluding that the highest rates of catalysis are observed when sodium tungstate is supplemented to growth and under such conditions catalysis is due to the combined action of the Fdh1αβγ and Fdh2αβγ isoforms. This chapter builds on the established findings to investigate the feasibility of driving these intracellular reactions with an electrode. Study of CO_2 reductase activity was the principal focus due to its potential as an energy storage mechanism with simultaneous CO_2 fixation.

To introduce the experiments discussed in this chapter a brief overview of the relevant electrochemical techniques and the underlying principles are described. Electrochemistry is the study of electron exchange at the surface of an electrode, such exchange can be bidirectional with electron transfer to an electrode (positive, oxidative current) or from an electrode (negative, reductive current), illustrated below in Figure 6-1.

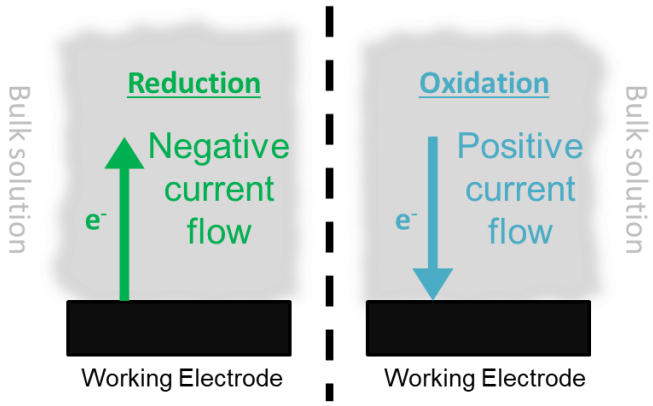

Figure 6-1 Fundamental concept underlying following electrochemical techniques.

When discussing a protein or bacterial culture interacting with an electrode, electron transfer can occur either spontaneously or as a result of exogenously added mediators, which shuttle between the electrode and sample, ensuring effective electron exchange. Methyl Viologen (MV) is commonly used as an electrochemical mediator when an electrode in isolation is unable to exchange electrons with a material or molecule of interest. In such contexts MV

transitions between a dicationic form and a monocationic radical. At low potentials a second reduction to a neutral species can also take place (-0.88 V vs SHE) but since such low potentials are not studied in this work all future references refer exclusively to cycling between the radical and oxidised form, a reaction found to be fully reversible without side reactions between pH 5-13 (Bird & Kuhn 1981). When acting as a mediator the MV radical can either be observed in a freely diffusing form or absorbed to an electrode in a film. The proportion of the two regimes is influenced by the properties of the working electrode and in turn can influence the redox potential, with a reduction potential of -0.432 vs SHE observed in a previous study using graphite (Barroso-Fernandez et al. 1998). Several examples of electrodes deliberately coated with or modified by MV to increase electrochemical interactions exist in the literature with many stable over the course of many days (Bird & Kuhn 1981).

In all experiments described in this work current flow is measured to inform on catalysis by *S.oneidensis* MR-1 cultures in a simple electrochemical cell using a three electrode configuration. The working electrode (WE) is the site of electron exchange with the sample, the counter electrode (CE) enables electron transfer at the WE by maintaining charge balance and the reference electrode (RE) regulates the potential (E) of the working electrode, allowing a chosen voltage to be applied during an experiment.

Chronoamperometry (CA) represents the simplest type of electrochemical experiment, in which the WE is poised at a desired potential and current measured over time. In the following results the potential is maintained (typically at -0.56 vs SHE) and changes in current are observed with the introduction of reactants to the electrochemical cell.

Cyclic voltammetry is a more complex but powerful electrochemical technique capable of providing large amounts of information about an analyte of interest including formal reduction potentials, diffusion coefficients, the presence of reaction intermediates and reaction stoichiometry. It is a versatile technique used in a wide range of fields but in a biochemical context is most commonly used for protein film voltammetry experiments (PFV) which inform on the redox properties of a purified enzyme immobilised on an electrode (Legér et al. 2003). Despite being far more complicated systems than immobilised proteins the

electrochemical interactions of whole microbial cells have also been explored extensively using cyclic voltammetry (Harnisch & Freguia 2012).

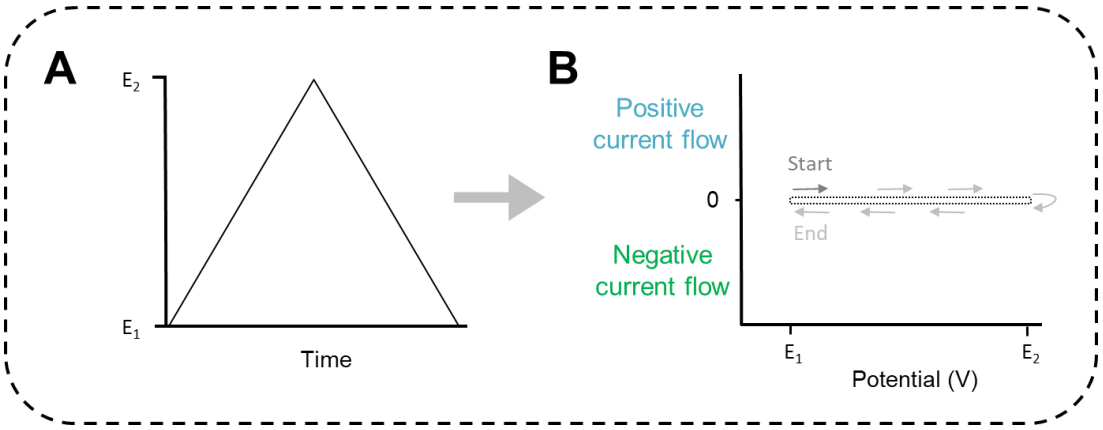

Figure 6-2 Cyclic voltammetry (CV) conceptualisation.
*(**A**) During a CV experiment potential is swept from an initial potential (E_1) to a final potential (E_2) and back. (**B**) Throughout current is measured and is plotted against the applied potential in a cyclic voltammogram. Featureless baseline trace demonstrating small capacitive current 'envelope' in the absence of redox signals.*

The principles underlying a cyclic voltammetry experiment are outlined in Figure 6-2. During a cyclic voltammetry experiment a changing potential is imposed on the working electrode, measured against the reference electrode. This changing potential will sweep linearly from an initial potential (E_1) to a final potential (E_2) before returning to the initial potential Figure 6-2 (**A**). Throughout the experiment the corresponding current flowing between working and counter electrodes is plotted as a function of the applied potential (Kissinger & Heineman 1996) (Figure 6-2 (**B**)). During these experiments scan rate (v) is the change of potential as a function of time, i.e. $v = dE/dt$.

It is necessary to carefully consider the potential window studied for cyclic voltammetry experiments (E_2-E_1) as only a limited range of potentials hold biological relevance. Since all biology occurs in water the anodic and cathodic water decomposition points, i.e. at -0.414 V vs SHE at pH 7 for the reduction of H^+ to H_2 and +0.815 vs SHE at pH 7 for the oxidation of H_2O to O_2, constrain physiologically relevant electrochemistry experiments (Becking et al. 1960). Indeed studies significantly above or below these limits have been shown to interfere with biological study, the production of hydrogen at low potentials causing poor sample interaction at the electrode or at higher potentials the unfolding or oxidative damage of protein samples (Marsili, Rollefson, et al. 2008).

When making such cyclic voltammetric measurements it is important to appreciate the two types of current that can result from changing a potential at an electrode. Faradaic currents result from oxidation or reduction reactions of the analyte; these are normally the signals of interest. In addition however changes in applied potential at the electrode cause changes in charge density at the electrode/electrolyte interface resulting in a balancing current unrelated to redox reactions in the analyte referred to as capacitive currents (Harnisch & Freguia 2012) (represented by the CV trace in Figure 6-2 (**B**)). Since these capacitive currents increase with scan rate Faradaic signals can be completely masked at higher scan rates. Partially for this reason slow scan rates were used for all cyclic voltammetry experiments in this study. The other consideration was that at higher scan rates slower enzymatic reactions may not have time to establish and the kinetics of interfacial electron transfer to the working electrode will dominate Faradaic signals (Marsili, Rollefson, et al. 2008). As such, slow scan rates of 1 mV/s were used where the current limitations are likely to be due to enzyme kinetics, referred to as an enzyme controlled regimes (Srikanth et al. 2008), or mass transfer (Harnisch & Freguia 2012).

Cyclic voltammetry experiments using whole cells, or indeed using enzymes, can be studied under two distinct conditions. Under non-turnover conditions, substrates for catalysis are not added and all redox transformations rely on the working electrode alone to regenerate and transition between oxidised and reduced forms of compounds as illustrated in Figure 6-3 (**A**). During such conditions the current returns to zero after the complete oxidation (or reduction) of all present redox active species resulting in peaks in cyclic voltammetry traces as seen in Figure 6-3 (**B**). The position of these peaks indicates the potential at which a species is oxidised or reduced. In the case of a single reversible redox reaction (as illustrated in Figure 6-3) the peak positions can be used to determine a formal potential for the reaction of interest.

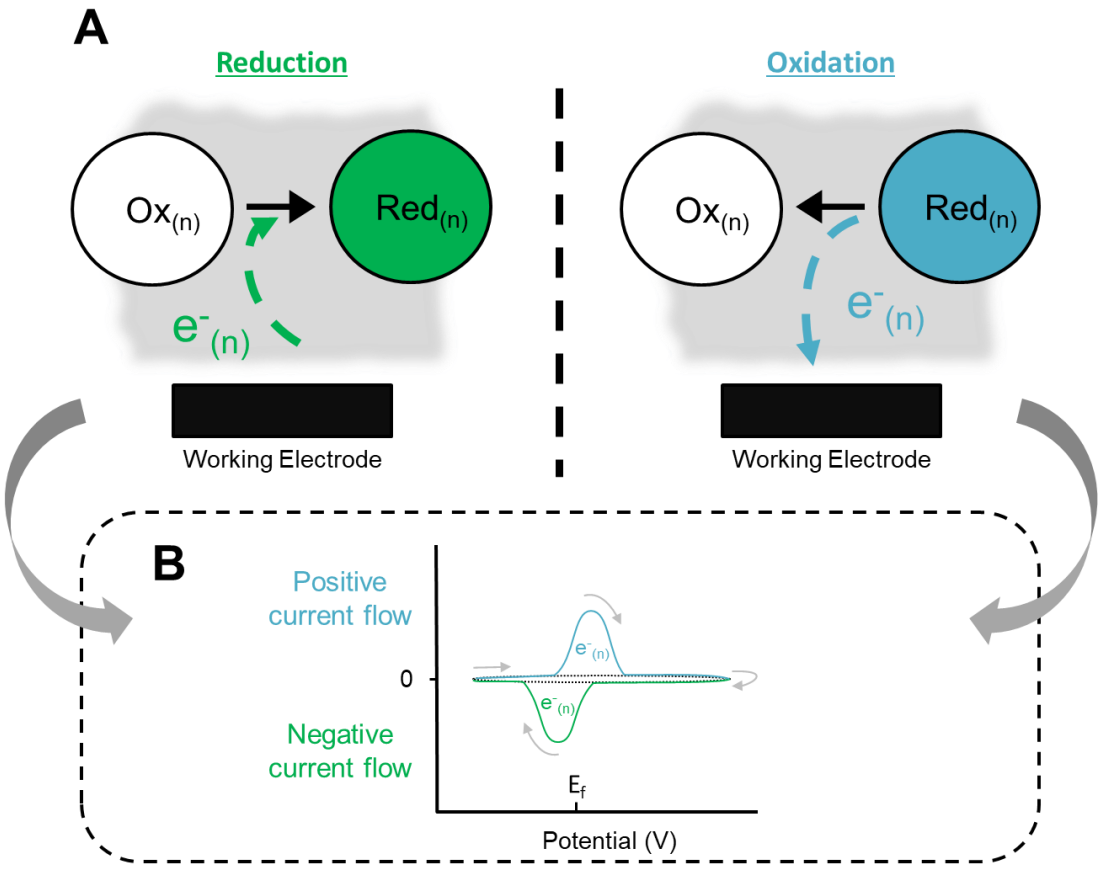

Figure 6-3 Non-catalytic electrochemistry and CV traces.
(A) *Reduction or oxidation of a species capable of exchanging electrons with an electrode (Ox or Red).* ***(B)*** *Corresponding CV trace for a simple reversible redox couple showing oxidation as potential becomes more positive (left to right) and reduction on the reverse sweep as potentials become more negative (right to left) Formal potential (E_f) for a simple redox process defined as average of positive (oxidative) and negative (reductive) peak potentials.*

In contrast cyclic voltammetry can also be performed on cells under turnover conditions, i.e. in the presence of a substrate for a redox enzyme, illustrated in Figure 6-4 (**A**). For such catalytic cyclic voltammograms only capacitive currents are observed until a suitably negative potential (in the case of a reduction reaction) or a suitably positive potential (in the case of an oxidation reaction) is approached whereby the reaction begins to proceed, resulting in catalytic Faradaic currents that continue at all sufficiently positive/negative potentials as long as substrate remains at the electrode Figure 6-4 (**B**). At these potentials the observed current represents the continuous electron transfer to or from the substrate in solution via continuous redox cycling of the enzyme active site.

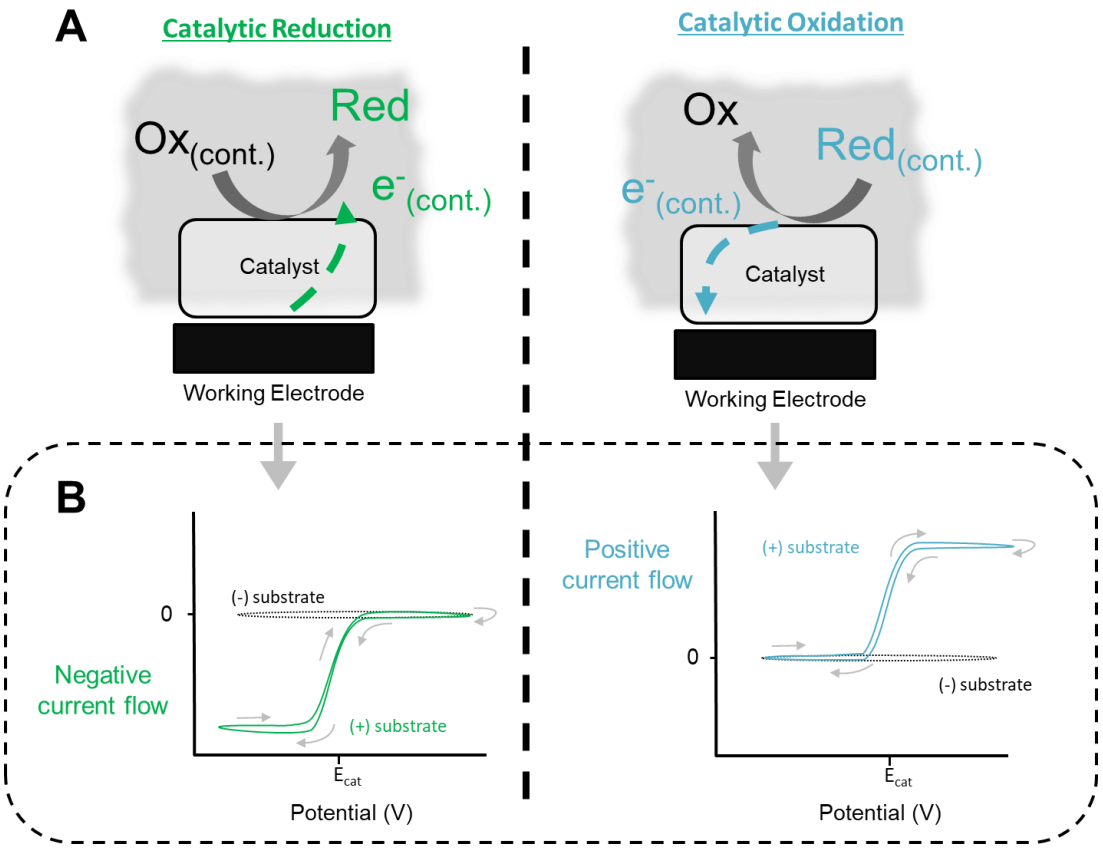

Figure 6-4 Catalytic (turnover) electrochemistry and CV traces.
(A) *Reduction or oxidation of a substrate by a catalyst capable of exchanging electrons with an electrode for catalysis.* ***(B)*** *Example CV trace for reductive catalysis where negative currents are recorded at suitably low (reducing) potentials (green) and example CV trace for oxidative catalysis where positive currents are recorded at suitably high (oxidising) potentials (blue). In both cases clear sigmoid (S) shaped catalytic CV traces are observed on both forward and reverse scans. The inflection point of such traces (E_{cat}) can be best visualised by plotting di/E.*

Due to the sustained electron transfer to (or from) the electrode during turnover conditions a characteristic sigmoidal shaped voltammetric trace is observed. The inflection point(s) of such traces where the gradient changes most is often used to characterise such traces and such features are often visualised by plotting the first derivative of the catalytic current with respect to applied potential (Harnisch & Freguia 2012). The peak potentials in such derivative graphs are defined in this work simply as simply inflection points (Zhang et al. 2013) (Marsili, Rollefson, et al. 2008) or catalytic potentials (E_{cat}) being terminology adopted from the related field of protein film voltammetry (Srikanth et al. 2008)(Field et al. 2005). Confusingly a number of alternative/interchangeable terms are used within the literature for these values including formal potentials (Millo 2012), (Harnisch & Freguia 2012), onset potentials (Marsili, Baron, et al. 2008) redox centre potentials (Jain et al. 2011), half wave potentials (Carmona-Martinez et al. 2011), and midpoint potentials (Baron et al. 2009). Regardless of

terminology, when applied to whole cell electrochemistry these potentials can either reflect the potential of the catalytic process or the potential of another intermediate electron transfer site that limits the rate of electron transfer to the electrode (Marsili, Rollefson, et al. 2008).

6.1 Results

6.1.1 Electrode driven reversible FDH activity with *S.oneidensis* and MV.

To establish whether an electrode can serve as a redox partner for FDH catalysis a custom made three electrode bioreactor was used. This consisted of a single chamber containing a platinum counter electrode and Ag/AgCl reference electrode, both isolated from the experiment by conductive glass frits. Experiments were conducted using 30ml of electrolyte (100 mM HEPES, 8.7 mM NH_4Cl, 1.3 mM K_2HPO_4, 1.7 mM KH_2PO_4 and 1 mM $MgSO_4$) in the presence of a graphite working electrode to which cultures of *S.oneidensis* MR-1, the mediator MV (10 μM) or substrates (50 mM sodium formate or carbonate) could be added. Before experimentation abiotic baseline measurements were run confirming comparative capacitive currents for all bioreactors with only those displaying smooth featureless cyclic voltammetry traces used for subsequent experimentation.

Experiments were performed for both *S.oneidensis* MR-1 cultures grown in the presence of 3 μM sodium tungstate (+W) or 3 μM sodium molybdate (+Mo) to better corroborate previous findings that this distinction results in significantly different FDH activities. Growth duration and wash preparation steps were identical to those used for colourimetric assays. To ensure normalisation cultures were diluted so cell suspensions of the same OD were introduced into the electrochemical cells, subsequent analysis showed comparable protein content (20 mg/ml) as determined by BCA assay. When adding such cultures to bioreactors 2 ml of previous electrolyte was removed and replaced by 2 ml of *S.oneidensis* culture, maintaining a reaction volume of 30 ml. Regardless of growth condition cyclic voltammograms of cultures without addition of MV or substrate were featureless (Figure 6-5, dashed traces) acting as effective baseline comparisons for turnover conditions.

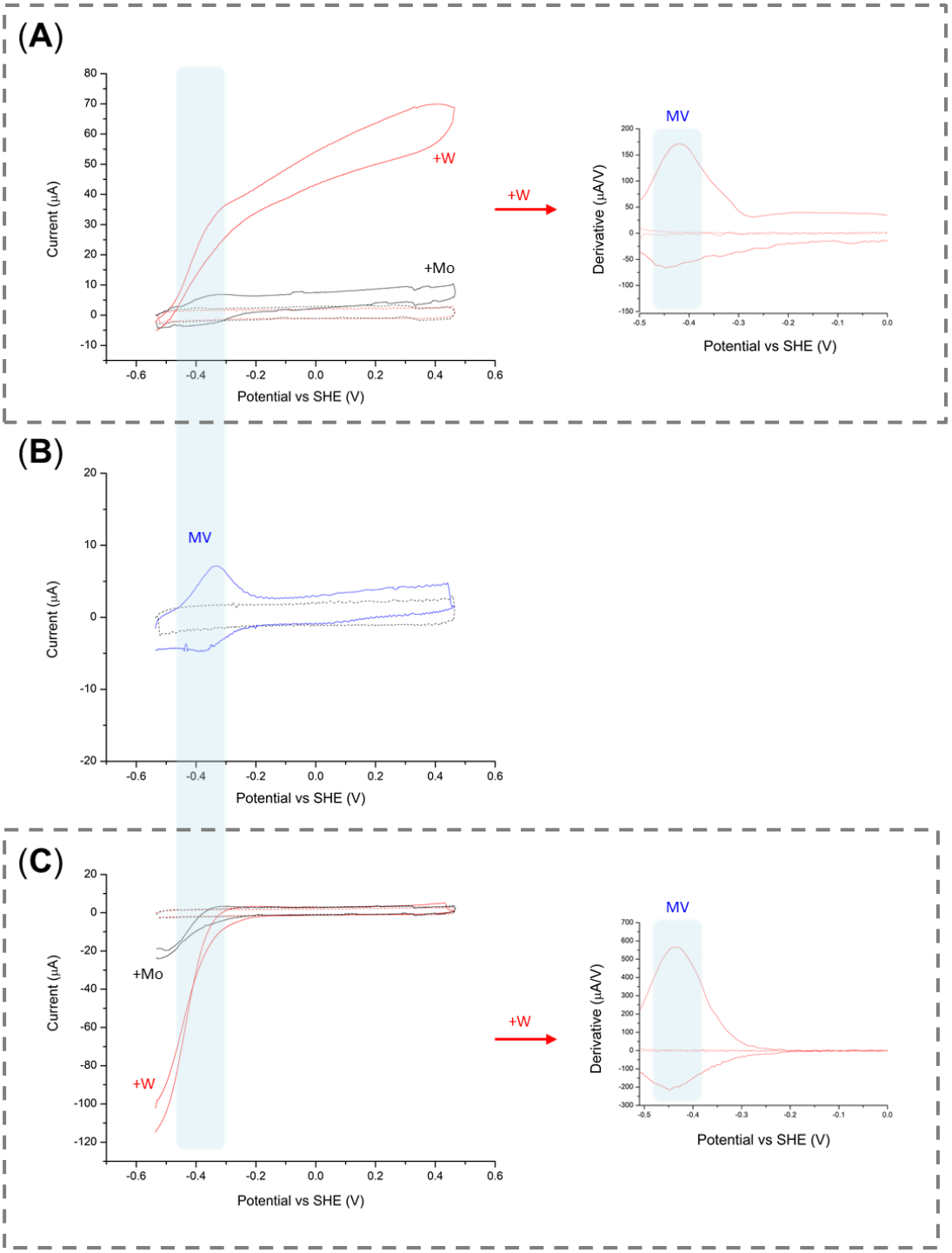

Figure 6-5 Reversible electrochemical FDH activity of S.oneidensis MR-1 with MV.
*For all panels, dashed traces indicate absence of substrate or MV and solid traces indicate the presence of substrate (50 mM) and 10 μM MV (i.e. turnover conditions). Red traces indicate experiments using S.oneidensis cells grown with 3 μM sodium tungstate (+W) and black traces with 3 μM sodium molybdate (+Mo). (**A**) Formate oxidation by S.oneidensis cells and corresponding di/E plot for +W conditions, showing a single feature at -0.438 V vs SHE under turnover conditions. (**C**) CO_2 reduction by S.oneidensis cells and corresponding di/E plot for +W conditions, showing a single feature at -0.436 V vs SHE under turnover conditions. (**B**) S.oneidensis cells (+W) in presence of 10 μM MV without sodium formate or carbonate, shown in blue, highlighting comparable E_{cat} values during turnover conditions to E_f of MV. All traces show second of two cyclic voltammetry scans, measured and controlled by μStat 8000P potentiostat, scan rate 1 mV/s, pH7.2.*

Although *S.oneidensis* MR-1 has been previously reported to exchange electrons directly with an electrode the mediator MV was included due to its proven ability to drive reversible FDH activity in assay based experiments in addition to its known ability to interact well with graphite electrodes for electron exchange. Addition of 10μM MV to cultures resulted in the appearance of a small reversible cyclic voltammogram feature as seen for +W grown cells in Figure 6-5 panel B (identical traces were recorded for cells +Mo). This feature is indicative of a single reversible redox reaction as expected for redox cycling of MV at the surface of the electrode.

To confirm reversible FDH activity, both sodium formate (Figure 6-5, (A)) and sodium carbonate (Figure 6-5, (C)) were added to *S.oneidensis* MR-1 cultures in addition to 10 μM of the mediator MV, with each experiment described in turn.

Addition of sodium formate resulted in increased positive currents at all potential values above approximately -0.5 V vs SHE for both +W and +Mo grown cells as seen in Figure 6-5 (A) red and black solid traces respectively. This increase in current corresponds to the electron flow to the graphite electrode from the catalytic oxidation of formate. When grown +W these currents were considerably higher, > 7 times higher at +0.4 V vs SHE (72 μA) than corresponding currents for cells grown +Mo (9 μA). In addition +W grown cells show a clear sigmoidal shaped CV, indicative of catalysis (Armstrong & Hirst 2011).

Addition of sodium carbonate resulted in increased negative currents at all potential values below approximately -0.3 V vs SHE for both +W and +Mo grown cells as seen in Figure 6-5 (C) red and black solid traces respectively. This negative current corresponds to the electron flow from the graphite electrode for the catalytic reduction of CO_2. Comparatively these cathodic currents were larger for +W cells, with currents 4.5 times higher at -0.53 V vs SHE compared to those for +Mo cells. Both +W and +Mo experiments demonstrated a clear sigmoidal shaped CV. As in previous work the phrase CO_2 reduction is used here to describe the reduction observed when sodium carbonate, and its solvation products are used as substrate.

To quantify the position of the catalytic waves during both formate oxidation and CO_2 reduction, the E_{cat} of turnover +W traces was determined by plotting

the first derivative di/E as seen in Figure 6-5 (A) and (C). The signal/noise ratio proved too low to perform equivalent analysis of +Mo derivative traces. The derived E_{cat} values, -0.438 V vs SHE for formate oxidation and -0.436 V vs SHE for CO_2 reduction are in good agreement with the observed position of non catalytic MV signals in Figure 6-5 (B) (emphasised by extrapolated blue window) and literature reported reduction potentials for MV on graphite at -0.432 V vs SHE (Barroso-Fernandez et al. 1998) collectively suggesting MV mediated electron exchange.

To complement the above cyclic voltammetry data demonstrating CO_2 reduction, chronoamperometry measurements were also taken on cells grown in +W containing media. This was done following the experimental description above but rather than taking cyclic voltammograms, the current was continuously measured whilst the working electrode remained poised at -0.56 V vs SHE, i.e. a suitably reducing potential for CO_2 reduction determined by the previous CV analysis. During these experiments 10 μM MV was added first followed by 50mM sodium carbonate and finally increasing concentrations of the known CO_2 reductase inhibitor, sodium azide, see Chapter 4. As can be seen from Figure 6-6 when bacterial culture was present 10 μM MV addition caused a small increase in reductive current, augmented significantly by addition of carbonate and partially attenuated by increasing concentrations of azide. To confirm that the observed reduction of CO_2 was due to the bacterial cells and not a spontaneous effect of reductively poising the electrode, the experiment was repeated abiotically as seen in the grey trace in Figure 6-6, MV, sodium carbonate and sodium azide did not cause any significant changes to current production.

It is important to highlight that compared to the previous cyclic voltammetry experiments only a quarter of the cell culture was used for the experiment presented in Figure 6-6, i.e. 250 ml of culture was prepared rather than 1 L. The cells were otherwise prepared identically, resulting in an inoculum containing 5mg/ml protein being added to the bioreactor. As a result of this the maximum currents reached upon addition of carbonate are smaller, 22 μA rather than the 115 μA seen in Figure 6-5 (**C**) when using 1 L of culture.

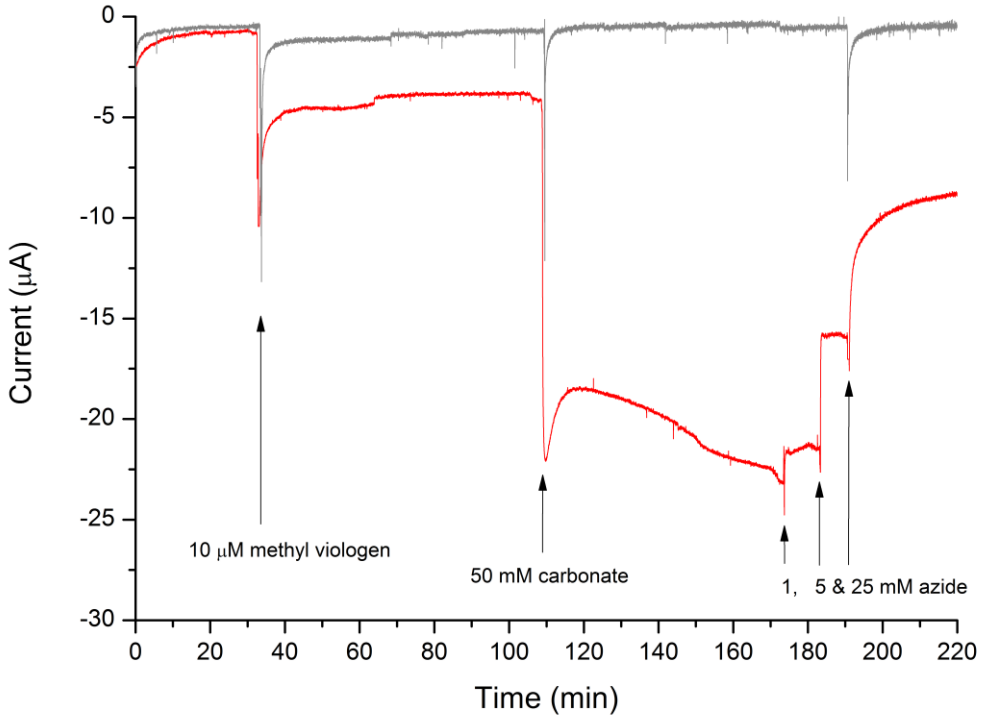

Figure 6-6 Chronoamperometry of S.oneidensis in response to sodium carbonate, MV and azide. S.oneidensis culture (+W) (red) and abiotic control (grey) exposed to poised graphite electrode at -0.56 V vs SHE monitoring effect on current after addition of 10 μM MV, 50mM sodium carbonate and increasing additions of sodium azide. Each addition followed by mixing for 5 s.

6.1.2 Electrochemically driven non-mediated CO_2 reduction by *S.oneidensis*

The inclusion of the costly and toxic MV to mediate catalysis was undesirable and so subsequent experimentation investigated catalytic responses without exogenously added mediator. Only the biotechnologically relevant CO_2 reductase activity (and not formate oxidation) was studied in this context. Experiments were otherwise performed under the same experimental conditions as seen in Figure 6-5 (C) using 50 mM sodium carbonate as substrate for a range of *S.oneidensis* cultures collectively shown in Figure 6-7.

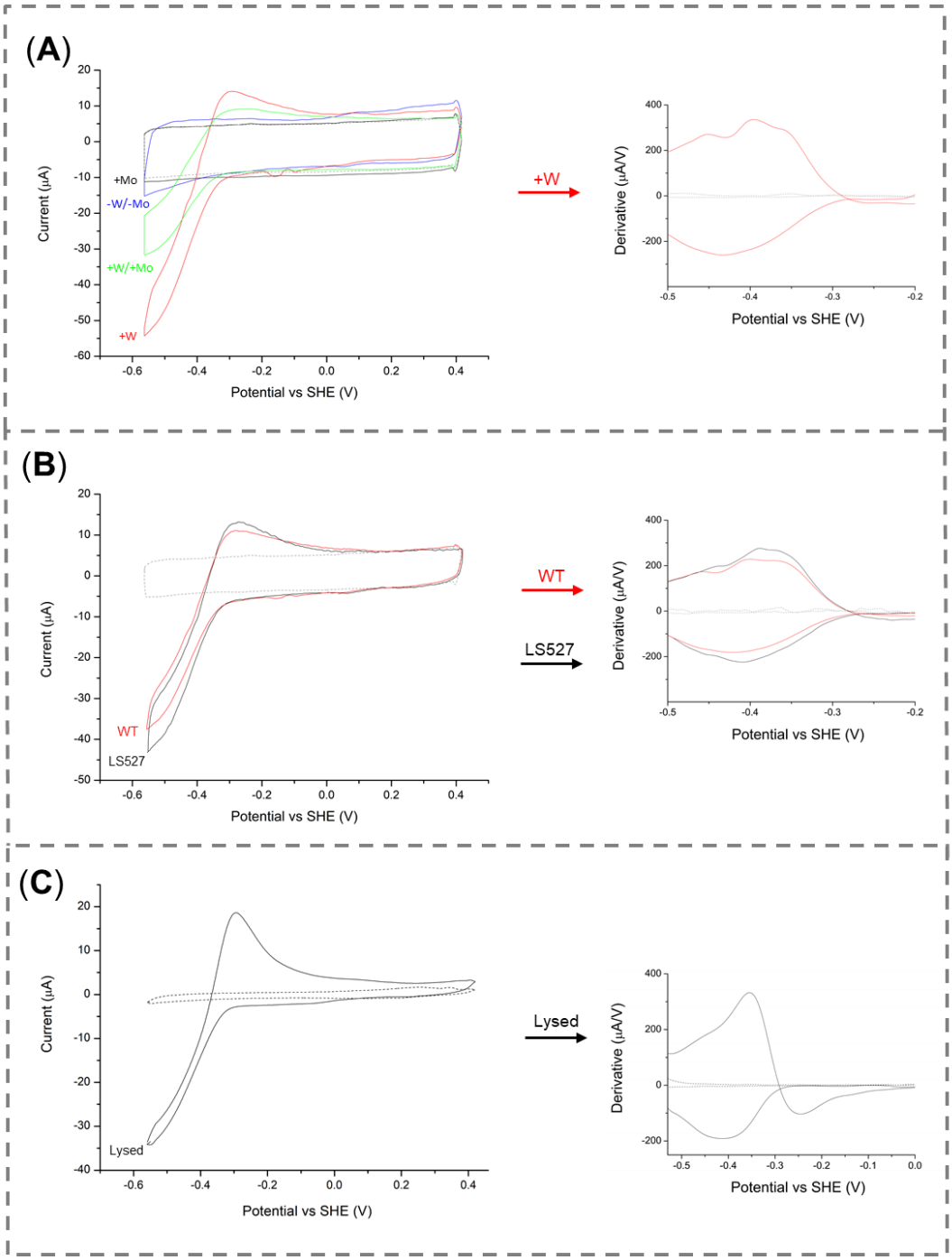

Figure 6-7 CO_2 reductase activity of WT S.oneidensis MR-1, LS527 and lysed WT MR-1 cultures without exogenously added mediator.

*For all panels dashed grey traces indicate absence of substrate and solid traces indicate the presence of 50 mM sodium carbonate (i.e. turnover conditions). (**A**) Cyclic voltammetry traces (using μStat 8000P potentiostat) for WT S.oneidensis MR-1 cultures grown +W (red) +W/+Mo (green) +Mo (black) and -W/-Mo (blue), Derivative plot of +W turnover trace (also in red) showing features at -0.454, -0.393 and -0.356 V and a single broader peak on the cathodic sweep centred at -0.434 V vs SHE. (**B**) Wildtype MR-1 (+W) (red) and LS527 (+W) (black), each trace representing mean of three biological replicates, for each using the second of two CV scan recordings. Derivative plot of turnover traces for both strains (left). Both MR-1 in red and (LS527 in black) derivative show three features at -0.458 (-0.439), -0.401 (-0.388) and -0.363 (-0.362) V vs SHE and a single broader peak on the cathodic sweep centred at -0.426 (-0.411) V vs SHE. (**C**) Lysed WT MR-1 (+W) with corresponding derivative, anodic sweep of the turnover trace contains small (at -0.445 V) and large (at -0.35 V) reductive peaks followed by an oxidative feature at -0.243 V. On the reverse cathodic sweep a single reductive peak is seen centred at -0.414 V vs SHE. All traces show second of two CV scan recordings measured and controlled by AUT73338 potentiostat unless specified, scan rate 1mV/s, pH7.2.*

Figure 6-7 Panel A displays cyclic voltammetry responses of WT *S.oneidensis* MR-1 cultures in response to 50 mM sodium carbonate addition when cultured in the presence 3 μM sodium tungstate (+W, red), 3 μM sodium molybdate (+Mo, black), 3 μM sodium tungstate and sodium molybdate (+W/+Mo, green) or in the presence of neither metal (-W/-Mo, blue). Panel B shows equivalent experiments performed for both WT MR-1 (+W, red) and a genomic knockout strain, LS527 (black), lacking components of the Mtr pathway (*mtrCAB* (SO_1776-SO_1778) *mtrDEF* (SO_1780-SO_1782) and *omcA* (SO_1779)) which have been previously implicated in electron exchange with an electrode (Ross et al. 2011). Finally Panel C shows the response of intentionally lysed (via sonication) WT *S.oneidensis* MR-1 (+W) cells. This was done according to section 2.16 (Cell lysis- sonication) except the protease inhibitor cocktail was omitted due to its possible interference with CV measurements. This cell lysate was then used in lieu of whole cells, containing comparable protein content (20 mg/ml) to previous experiments (determined by BCA assay).

In all three panels clear catalytic features are seen in response to the addition of 50 mM sodium carbonate, showing negative currents below approximately -0.35V vs SHE corresponding to the electron flow from the graphite electrode for the catalytic reduction of CO_2. The magnitude of these currents varies, especially in panel A, where the tungstate containing conditions show more negative currents than those without, for example at -0.56 V SHE -55 μA (+W), -33 μA (+W/+Mo), vs -16 μA (-W/-Mo) and -12 μA (+Mo). As a result +W growth conditions were used for subsequent study in panel B and C. These panels show comparative currents to those seen for WT cells (+W) with currents of -44 μA for LS527 and -25 μA for lysed WT (+W) cells at -0.56 V vs SHE respectively.

In addition to the negative (reductive) catalytic feature of these CV traces a small positive (oxidative) peak can also be seen centered at -0.25 V vs SHE, most distinctly seen for lysed MR-1 in panel C, likely due to the reverse direction of catalysis and the re-oxidation of formate generated by CO_2 reduction, supported by the fact that the feature forms a peak rather than a catalytic wave suggesting depletion of substrate.

First derivative plots (di/E) are also seen for all panels in Figure 6-7 (right) to quantify the position of the catalytic waves and reveal the finer details of

catalytic responses seen for WT cells. Unlike previous mediated derivative plots these contain multiple features. For WT +W cultures the forward sweep (from negative to more positive potentials) contains three features, centred at -0.454, -0.393 and -0.356 V vs SHE respectively. In contrast only a single broad feature is seen on the reverse cathodic sweep, centred at -0.434 V vs SHE.

Since multiple peaks can be seen in the derivative of WT cells a comparative approach with a strain lacking the Mtr pathway (a principal candidate for the signals seen in WT cells) was used. It was hypothesised that the native Mtr pathway of *S.oneidens*is MR-1 that under normal physiological conditions couples intracellular respiration with reduction of external minerals (Coursolle et al. 2010) may be working in reverse to provide electrons to the intracellular CO_2 reductases. The derivative plot of LS527 however is similar to that seen for WT cells (Figure 6-7: derivative of **A** vs **B**), suggesting (in combination with the comparable catalytic currents) that the Mtr pathway is not likely to mediate electron exchange during catalysis.

It was also proposed that all of the signals seen for WT cells may result from cell lysis and direct interaction of FDH with the electrode, if this was the case the derivative of the intentionally lysed MR-1 cells would be expected to look identical, with overlapping peaks in the first derivative plot. However this is not the case (Figure 6-7: derivative of **A** vs **C**), suggesting at least a proportion of the activity in whole cells proceeds via a mechanism other than cell lysis. The distinctions between the two plots are subtle, with a more pronounced formate re-oxidation peak for lysed cells and only a single clear reductive peak (at -0.35 V vs SHE) whilst the peak for formate oxidation in unlysed cells is not seen on the derivative and features multiple broader reductive features centred at -0.458, -0.401 and -0.363 V vs SHE.

To confirm that formate is formed during such non-mediated experiments using +W cultured *S.oneidensis* MR-1, chronoamperometry experiments were performed, with the working electrode potential set to -0.56 V vs SHE whilst recording current. Catalysis was initiated by addition of 50 mM sodium carbonate, added after 180 s when current was equivalent to that seen in the abiotic control as seen in Figure 6-8. Quantification of formate production at the end of the experiment was performed using ^{1}H NMR.

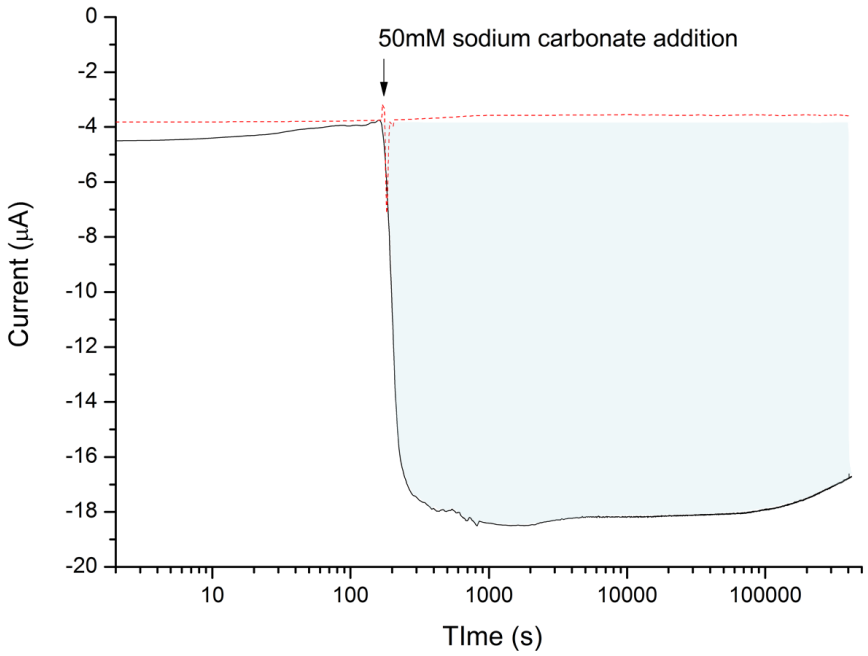

Figure 6-8 Extended CO_2 reductase activity of S.oneidensis MR-1 (+W) after addition of 50 mM sodium carbonate.
Working electrode poised at -0.56 V vs SHE controlled by AUT73338 potentiostat throughout the 4.8 day experiment. Chronoamperometry of abiotic (red dashed trace) and MR-1 culture grown +W (black trace) in response to addition of 50 mM carbonate, bioreactors were mixed thoroughly after addition of carbonate but were not agitated subsequently. Integration of Faradaic current after addition of carbonate to MR-1 cells show by shaded blue region with a calculated area of 4.499 coulombs., y= 4 μA used as baseline for integration.

The lack of current after addition of carbonate to the abiotic control in Figure 6-8 indicates a requirement for the cells to catalyse the non-mediated CO_2 reduction and disproves that a reductively poised electrode alone is capable of comparable catalysis. In contrast the experiment containing WT culture shows a significant reductive current (-16 μA within 400 s) in response to carbonate addition, with current being maintained over the course of several days (4.8 (388,800 s) without agitation.

During the course of this experiment it was assumed that the charge transferred from the working electrode was being used to generate formate. Making this assumption that observed charge drives exclusively the $2e^-$ reduction of CO_2 to formate, and considering the reaction volume of 30 ml, the theoretical formate concentration at the end of the experiment can be given by eq (6.1) where F is Faraday's constant (96485.33).

$$[Formate]\ (M) = \frac{Charge\ (C)}{Reactor\ volume\ (L)\ \times\ F\ \times\ 2} \qquad (6.1)$$

As such the 4.5 coulombs of charge integrated from Figure 6-8 would result in a theoretical concentration of 0.771 mM formate assuming 100% Faradaic efficiency.

^{1}H NMR spectra quantified 0.728 ± 0.019 mM formate in samples taken from the bioreactor containing the bacterial culture at the end of the experiment In contrast no formate was detected in samples taken before addition of sodium carbonate. The abiotic control showed no detectable formate before addition of carbonate or after its addition.

Interestingly very small concentrations of succinate (10.5 ± 0.6 μM) were also detected in the experiment containing the bacterial culture after 4.8 days. No succinate was detected at the start of this experiment or at the end of the equivalent abiotic experiment suggesting that a small proportion of the supplied electrons may be diverted to alternative metabolic pathways, but considering the calculated efficiencies (below) this diversion is considered to be negligibly small (0.061 coulombs).

By comparing the value of 0.777 mM formate assuming 100% faradaic efficiency and the experimentally determined value of 0.728 mM formate generated in the reaction containing *S.oneidensis* an actual Faradaic efficiency of 107 % is calculated. This good agreement suggests a highly promising system for effectively catalysing the reduction of CO_2 to formate with low over-potentials and further developments are explored in the following discussion.

6.2 Discussion

Considering the wide range of electrochemical techniques and analyses available to probe systems on an electrode (Léger 2013) those used here are relatively simple. Fundamentally this is due to the extremely complicated nature of whole bacterial cell interactions with electrodes and the propensity for inappropriate over-analysis (Marsili, Rollefson, et al. 2008). Both cyclic voltammetry and chronoamperometry hold numerous precedents in the literature for the study of electrode-bacterial interactions (Babauta et al. 2012) and were considered the most informative and appropriate techniques for the current study. Commonly cyclic voltammetry is used to determine the potentials of those redox couples involved in electron transfer but even with this simple technique care must be taken with analysis as factors such as mass-transfer limitations, resolved in the field of PFV by use of rotating electrodes (Angove et al. 2002), have not been similarly resolved for whole cell experiments (Babauta et al. 2012). The assignment of potentials for such CV analyses have been most convincingly shown in combination with other studies including comparisons with gene deletion strains (Coursolle et al. 2010) or the replacement of analytes thought to contain soluble mediators contributing to voltammetry signals (Marsili, Baron, et al. 2008). Even in such elegant demonstrations however the relevance of such redox signals to those currents seen in after extended interactions can be debated and so such techniques are typically complimented by chronoamperometric studies (Babauta et al. 2012).

As demonstrated in Figure 6-5, both anodic currents resulting from formate oxidation and cathodic currents resulting from CO_2 reduction mediated by MV could be observed when using grown cultures of *S.oneidensis* as biocatalysts. These currents were greatest when cultures grown with 3 μM sodium tungstate were used rather than those grown with equivalent concentrations of sodium molybdate. This is in agreement with the previously studied colourimetric assays (Chapter 4) and suggests that reducing equivalents derived from both chemical compounds such as dithionite or a cathode can drive formate production Figure 6-9(A).

Surprisingly this is not always the case as observed for the molybdate containing formate dehydrogenase FDH-H isolated from *E.coli* for which CO_2

reductase activity could readily be observed when reducing equivalents were provided by an electrode, but not in equivalent MV mediated assays (Bassegoda et al. 2014). It has been suggested that this lack of CO_2-MV oxidase activity was due to the single Fe-S cluster in this protein limiting catalysis, other examples including FDH1 from *Syntrophobacter fumaroxidans* have ten (Reda et al. 2008), and the relevant FDH of *Shewanella* here contain at least four, the larger number of clusters being thought to better suit buffering of electron supply and demand (Bassegoda et al. 2014). An alternative explanation involves the requirement of a reductive reactivation event not seen during the time course of the solution assay, as previously reported for the related nitrate reductase enzymes (Field et al. 2005). This discussion is interesting as many studied FDH enzymes have been claimed to be incapable of CO_2 reduction on the basis of colourimetric redox assays alone, re-evaluation by electrochemical methods may demonstrate otherwise.

It is notable that no redox features were seen for *S.oneidensis* cultures under any non-turnover conditions regardless of growth method. This is thought to be partially due to the previous wash steps which aimed to remove metabolites that would interfere with analysis. Despite this the reversible redox transitions of outer membrane cytochromes and signals from molecules such as flavins normally observed in similar studies of *S.oneidensis* (Marsili, Baron, et al. 2008) (Coursolle et al. 2010) (Harnisch & Freguia 2012) would still be expected. The likely difference is that these studies deliberately encouraged the generation of *S.oneidensis* biofilms and direct cell adhesion to an anode before electrochemical study (Babauta et al. 2012), whilst this study used planktonic cells with no prior electrode acclimatisation/biofilm promotion. As such the CV signals resulting from such associations were likely indistinguishably small within the background capacitive current.

The formation of biofilms were deliberately not encouraged here primarily because the generation of biofilms is typically performed using anodes poised at suitably high potentials, (for example +0.4 V vs SHE (Carmona-Martínez et al. 2012)) over several hours if not days, making the process time intensive and potentially costly when considering future biotechnological uses, in addition since the principal application of this work was the reduction of CO_2 using a

cathode poised at -0.56 V vs SHE (Figure 6-8), the acclimatisation to a positively poised electrode may prove counterproductive.

6.2.1 Mechanistic discussion of non-mediated CO_2 reductase activity.

Analysis of the features seen in the first derivative plots of non-mediated CO_2 turnover traces of *S.oneidensis* cultures in Figure 6-7 is incredibly difficult and requires further study to resolve satisfactorily. The peaks in such first derivative plots inform on redox active elements that limit the rate of electron transfer to the electrode during the catalytic process (Marsili, Rollefson, et al. 2008). Typically such derivative traces are symmetrical with respect to the X axis for common reversible processes (Rapson et al. 2008). The features in the described figures are not symmetrical suggesting from a classical electrochemical perspective the existence of quasi – reversible or irreversible redox processes (Kim et al. 1993), unfortunately with the available information no definitive conclusions about the identity of these sites can be made. Possible mechanisms are illustrated in Figure 6-9 Panels B through F and the merits of each are discussed in turn.

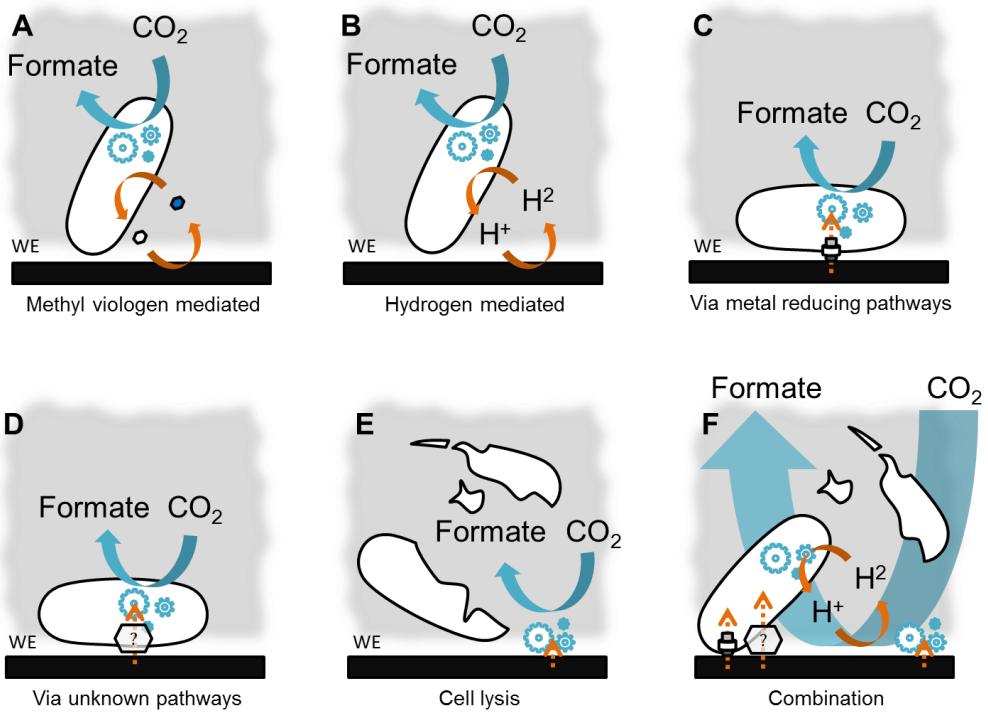

Figure 6-9 Possible mechanisms for CO_2 reductase activity at the working electrode (WE).
(A) *Mediation by exogenous MV capable of shuttling between electrode and active site.* ***(B)*** *Mediation by abiotically produced hydrogen evolved at cathode.* ***(C)*** *Direct electron transfer via the Mtr pathway* ***(D)*** *Direct electron transfer via currently unidentified native metabolic elements* ***(E)*** *Cell lysis resulting in catalytic machinery (FDH) accepting electrons directly from cathode.* ***(F)*** *A combination of the above mechanisms.*

It can be speculated that since similar features are observed in the derivative of the turnover trace of the LS527 mutant compared to WT (Figure 6-8) the absent elements of the Mtr pathway in LS527 are unlikely to solely contribute to any of the observed first derivative features in the WT trace. This is in agreement with the observation that comparable levels of reductive catalysis are observed in this strain compared to WT. This result is in contrast to the only other electrosynthetic study of *Shewanella* which demonstrated an absolute requirement for the components of the Mtr pathway for acceptance of electrons from a cathode to drive intracellular reduction of fumarate to succinate (Ross et al. 2011). However this study supplied the driving force for the reduction of fumarate with a cathode poised at -0.36 V vs SHE (Ross et al. 2011) whilst the reduction of CO_2 in this study requires significantly lower potentials down to -0.56 V vs SHE, considerably below many of the reported heme potentials in the pathway which range from -500 mV to +100 mV (Hartshorne et al. 2007).

Since electron transfer does not appear to proceed via the Mtr pathway alternative mechanisms must be proposed, these include the possibility that in response to the experimental environment cell lysis occurs allowing direct electron transfer to those elements required for catalysis (Figure 6-9 Panel E). Although not conclusive, indirect evidence from the analysis of the features of the CV obtained using lysed cells in Figure 6-7 (**C**), and the comparative differences to whole cells suggest the contributions of other mechanisms.

Other mechanisms other than cell lysis include the possibility of hydrogen generation at the cathode acting as a freely diffusible mediator able to drive CO_2 reduction (Figure 6-9 Panel B), as seen for nitrite or acetate production in previous systems (Sakakibara & Kuroda 2004). Although reductive features in baseline CV readings that might indicate abiotic hydrogen production were not seen, despite suitably low potentials, it is difficult to disprove the generation of small quantities of hydrogen due to the inability to perform appropriate controls in aqueous analytes. Regardless this particular mechanism is considered unlikely from a thermodynamic perspective considering the similarity of the reduction potentials of the CO_2/formate couple at -0.42 V vs SHE (Ruschig et al. 1976) and the H^+/H_2 couple at -0.41 V vs SHE (Becking et al. 1960) , although similar it has been shown that due to the low solubility of hydrogen such low

potentials can only be maintained under high H_2 partial pressures (Rabaey & Rozendal 2010).

Alternatively the observed catalysis may proceed via other metabolic elements including other conductive outer membrane proteins other than the well-studied Mtr pathway (Figure 6-9 Panel C and D). Candidates for such proteins include other cytochromes of as yet undetermined function or even the known outer membrane DMSO reductase (Gralnick et al. 2006). Extraceullular polymeric substances (EPS) may even play a role (Babauta et al. 2012), with excreted protein found in the EPS of *Shewanella* sp. HRCR-1. Of this excreted protein homologs of mtrC and omcA represented only a tenth of that found, the remainder consisting of many more redox active proteins of currently unknown function (Cao et al. 2011).

6.2.2 Biotechnological development

Importantly this is the first work to report the ability of *S.oneidensis* to reduce CO_2 to formate not only using colourimetric redox assays as shown in Chapter 4, but also electrochemically with the work presented here. The fact that such reduction could be seen with or without MV mediation presents a number of options for future biotechnological exploitation. The Faradaic reductive currents (determined by the subtraction of capacitive current from total) produced by mediated +W grown *S.oneidensis* cultures was observed to be 112 μA at -0.56 V vs SHE Figure 6-5 (C) whilst in equivalent non-mediated experiments only 42 μA (Figure 6-7 (A)) of reductive current was transferred. The lower rate of electron transfer for formate generation in the non-mediated system is not unexpected, with the addition of MV allowing a larger number of the planktonic cells to interact with the electrode. Regardless the non-mediated system still represents the regime of most interest for future study, despite the catalytic current consumption being only 37% of the mediated rate, due to the exclusion of the costly and toxic mediators (Suntres 2002).

Regardless of the mechanisms behind the observed non-mediated catalysis the described system represents a simple method for the generation of an effective CO_2 reductase biocatalyst. Previously isolated FDH enzymes with the capacity for CO_2 reduction to formate at an electrode have been proposed for biotechnological exploitation (Rabaey & Rozendal 2010), their main constraint

being the considerable cost required to isolate and immobilise the purified enzyme on an electrode (Bassegoda et al. 2014) or the slow culture time of those organisms they are purified from (Reda et al. 2008). This system circumvents this requirement, requiring only the materials needed to culture the fast growing *S.oneidensi*s (Yang et al. 2008) with no purification steps required and using only cheap graphite electrodes.

In order to become an attractive technology the described system would have to demonstrate benefits over other developing technologies for the reduction of CO_2. These include a range of chemical catalysts that function at ambient temperature and pressure including those derived from iridium (Hull et al. 2012) or cobalt (Jeletic et al. 2013), but both currently demonstrate either slow rates of catalysis and/or the use of expensive chemicals or solvents.

It has already been addressed that this system remains attractive in comparison to those systems where enzymes require expensive purification steps, but a number of other recent studies have also proposed whole cell systems to drive the reduction of CO_2 to formate (Schuchmann & Müller 2013) and (Pinske & Sargent 2016).

The first demonstrates the use of whole cultures of *Acetobacterium woodii* to produce formate from gas mixtures containing hydrogen and CO_2. This system exploits the native hydrogen dependent carbon dioxide reductase (HDCR) enzyme complex which contains an iron-iron hydrogenase, two electron transfer subunits and a Mo containing FDH component (Schuchmann & Müller 2013). This system is doubly attractive due to the native carbon monoxide dehydrogenase (CODH) of *A.woodii*, which allows such cultures to convert not just CO_2 and hydrogen gas mixes into formate, but also those containing carbon monoxide as well, allowing it to generate formate from syngas (Schuchmann & Müller 2013). The main drawback of this system is that it requires the addition of expensive sodium ionophores to prevent generation of biomass, acetate and other side products (Schuchmann & Müller 2013).

The second proposed whole cell strategy uses *E.coli* cultures grown in the presence of formate to stimulate production of the FHL complex, consisting of electron transfer subunits, a Ni-Fe hydrogenase and the previously described Mo containing FDH, FDH-H (Bassegoda et al. 2014). By exposing such cells to

an environment with high pressure of both CO_2 and H_2 at pH7.4, the intracellular FHL is able to couple hydrogen oxidation to CO_2 reduction. i.e. the reverse of the reaction catalysed by the complex under physiological conditions (Pinske & Sargent 2016). This system was capable of operating for 10.5 h before formate production plateaued, with a quoted initial rate of 4 nmole of formate produced per min per mg of protein (Pinske & Sargent 2016) although even higher rates have been since demonstrated with higher pressures of hydrogen and CO_2 (Sargent, F, personal communication). To provide a comparison with the current work 23 μmol of formate was produced in Figure 6-8 from culture containing 40 mg of protein over 7013 min, giving an equivalent value of 0.083 $nmolmin^{-1}mg^{-1}$. Although this value is considerably lower it does not take into consideration the relative longevity of the two systems or the fact that the *in vivo* FHL system requires a pressurised CO_2/H_2 environment to function optimally, a potential setback for economic viability.

Of course comparisons with either of these systems are somewhat misleading because both the HDCR *A.woodii* and FHL *E.coli* systems require hydrogen as the electron donor for the reduction of CO_2 to formate. Neither has been studied with the use of a cathode acting as electron donor, (although HDCR can also use ferredoxin as an electron donor (Schuchmann & Müller 2013). These whole cell systems instead rely on the permeability of hydrogen into cells, making them similar but not necessarily competing technologies with the cathode driven system described here.

The continual catalysis and high Faradaic efficiency of this system seen over several days (Figure 6-8) supports its future investigation. It is envisaged that significant improvements to various aspects of the design could be tested, including the use of agitation, as the present system does not address the possibility of diffusion limitations, both those of the substrate to the active sites but also of protons/hydroxyl ions that balance charge. This would need to be assessed carefully however as the power required for agitation and its scaling is a common issue for the viability of several BES systems (Recio-garrido et al. 2016).

The present electrochemical set up was designed to be simple and cost effective, lacking any costly components. It also does not feature a coupled anode because

to effectively study such bacterial systems it is essential to determine which electrode limits current (Babauta et al. 2012) and this system removes this extra complication. Future developments would need to consider how the described system could be integrated into a BES device. From an engineering perspective the described cathodic system could be coupled to a biotic anode as described previously in other MEC or MES devices (Pant et al. 2012) to limit the costs of driving CO_2 reduction or alternatively more traditional chemical anodes could also be used. Other options include driving the cathode with energy from renewable solar sources to chemically store the produced energy (Lovley 2011).

From a biological perspective it could be envisioned that syntrophic relationships could be established with other organisms, converting the produced formate into molecules of higher economic worth, using the produced formate as a feedstock molecule, as described previously (Rabaey & Rozendal 2010). Alternatively, and considering the known genome, extensive metabolic study and genetic tractability of *Shewanella*, the required metabolic functions for subsequent reductive transformations could be introduced using synthetic biology approaches.

6.3 References

Angove, H.C. et al., 2002. Protein Film Voltammetry Reveals Distinctive Fingerprints of Nitrite and Hydroxylamine Reduction by a Cytochrome c Nitrite Reductase. *The Journal of Bological Chemistry*, 277(26), pp.23374–23381.

Armstrong, F. a & Hirst, J., 2011. Reversibility and efficiency in electrocatalytic energy conversion and lessons from enzymes. *Proceedings of the National Academy of Sciences of the United States of America*, 108(34), pp.14049–54.

Babauta, J. et al., 2012. Electrochemically active biofilms: facts and fiction. A review. *Biofouling*, 28(8), pp.789–812.

Baron, D. et al., 2009. Electrochemical measurement of electron transfer kinetics by *Shewanella oneidensis* MR-1. *The Journal of biological chemistry*, 284(42), pp.28865–73.

Barroso-Fernandez, Ä. et al., 1998. Electrochemical behavior of methyl viologen at graphite electrodes modified with Nafion sol-gel composite. *Analytica Chimica Acta*, 370, pp.221–230.

Bassegoda, A. et al., 2014. Reversible Interconversion of CO_2 and Formate by a Molybdenum-Containing Formate Dehydrogenase. *Journal of the American Chemical Society*, 136(44), pp.15473–6.

Becking, L., Kaplan, I. & Moore, D., 1960. Limits of the Natural Environment in Terms of pH and Oxidation-Reduction Potentials. *The Journal of Geology*, 68(3), pp.243–284.

Bird, C.L. & Kuhn, a. T., 1981. Electrochemistry of the viologens. *Chemical Society Reviews*, 10(1), p.49.

Cao, B. et al., 2011. Extracellular polymeric substances from *Shewanella sp* . HRCR-1 biofilms : characterization by infrared spectroscopy and proteomics. *Environmental microbiology*, 13, pp.1018–1031.

Carmona-Martinez, A. a et al., 2011. Cyclic voltammetric analysis of the electron transfer of *Shewanella oneidensis* MR-1 and nanofilament and cytochrome knock-out mutants. *Bioelectrochemistry (Amsterdam, Netherlands)*, 81(2), pp.74–80.

Carmona-Martínez, A. a et al., 2012. Electron transfer and biofilm formation of *Shewanella putrefaciens* as function of anode potential. *Bioelectrochemistry*, 93, pp.23–9.

Coursolle, D. et al., 2010. The Mtr respiratory pathway is essential for reducing flavins and electrodes in *Shewanella oneidensis*. *Journal of bacteriology*, 192(2), pp.467–74.

Field, S.J. et al., 2005. Reductive activation of nitrate reductases. *Dalton Transactions*, 2005(21), pp.3580–3586.

Gralnick, J. a et al., 2006. Extracellular respiration of dimethyl sulfoxide by *Shewanella oneidensis* strain MR-1. *Proceedings of the National Academy of Sciences of the United States of America*, 103(12), pp.4669–74.

Harnisch, F. & Freguia, S., 2012. A basic tutorial on cyclic voltammetry for the investigation of electroactive microbial biofilms. *Chemistry, an Asian journal*, 7(3), pp.466–75.

Hartshorne, R. et al., 2007. Characterization of *Shewanella oneidensis* MtrC : A cell-surface decaheme cytochrome involved in respiratory ... decaheme cytochrome involved in respiratory electron transport to extracellular electron acceptors. *J Biol Inorg Chem*, 12(October), pp.1083–1094.

Hull, J.F. et al., 2012. Reversible hydrogen storage using CO_2 and a proton-switchable iridium catalyst in aqueous media under mild temperatures and pressures. *Nature Chemistry*, 4(5), pp.383–388.

Jain, A. et al., 2011. Visible spectroelectrochemical characterization of *Geobacter sulfurreducens* biofilms on optically transparent indium tin oxide electrode. *Electrochimica Acta*, 56(28), pp.10776–10785.

Jeletic, M.S. et al., 2013. A Cobalt-Based Catalyst for the Hydrogenation of CO_2 under Ambient Conditions. *J. Am. Chem. Soc*, 135, p.11533−11536.

Kim, M., Smith, V.P. & Hong, T., 1993. First- and Second-Order Derivative Polarography / Voltammetry for Reversible , Quasi-Reversible , and Irreversible Electrode Processes. *J.*

Electrochem. Sac., 140(3).

Kissinger, P. & Heineman, W.R., 1996. *Laboratory Techniques in Electroanalytical Chemistry, Second Edition, Revised and Expanded* 2nd ed. P. Kissinger & W. R. Heineman, eds., CRC Press.

Legér, C. et al., 2003. Enzyme Electrokinetics : Using Protein Film Voltammetry To Investigate Redox Enzymes and Their Mechanisms. *Biochemistry*, 42(29), pp.8654–8662.

Léger, C., 2013. An Introduction to Electrochemical Methods for the Functional Analysis of Metalloproteins. *Practical Approaches to Biological Inorganic Chemistry*, pp.179–216.

Lovley, D.R., 2011. Powering microbes with electricity: direct electron transfer from electrodes to microbes. *Environmental microbiology reports*, 3(1), pp.27–35.

Marsili, E., Rollefson, J.B., et al., 2008. Microbial biofilm voltammetry: direct electrochemical characterization of catalytic electrode-attached biofilms. *Applied and environmental microbiology*, 74(23), pp.7329–37.

Marsili, E., Baron, D.B., et al., 2008. *Shewanella* secretes flavins that mediate extracellular electron transfer. *Proceedings of the National Academy of Sciences of the United States of America*, 105(10), pp.3968–73.

Millo, D., 2012. Spectroelectrochemical analyses of electroactive microbial biofilms. *Biochemical Society transactions*, 40(6), pp.1284–90.

Pant, D. et al., 2012. Bioelectrochemical systems (BES) for sustainable energy production and product recovery from organic wastes and industrial wastewaters. *RSC Advances*, 2, pp.1248–1263.

Pinske, C. & Sargent, F., 2016. Exploring the directionality of *Escherichia coli* formate hydrogenlyase : a membrane- - bound enzyme capable of fixing carbon dioxide to organic acid. *MicrobiologyOpen*, 5(5), pp.721–737.

Rabaey, K. & Rozendal, R. a, 2010. Microbial electrosynthesis - revisiting the electrical route for microbial production. *Nature reviews. Microbiology*, 8(10), pp.706–16.

Rapson, T.D., Kappler, U. & Bernhardt, P. V, 2008. Direct catalytic electrochemistry of sulfite dehydrogenase : Mechanistic insights and contrasts with related Mo enzymes. *Biochimica et Biophysica Acta*, 1777, pp.1319–1325.

Recio-garrido, D., Perrier, M. & Tartakovsky, B., 2016. Modeling , optimization and control of bioelectrochemical systems. *Chemical Engineering Journal*, 289, pp.180–190.

Reda, T. et al., 2008. Reversible interconversion of carbon dioxide and formate by an electroactive enzyme. *Proceedings of the National Academy of Sciences of the United States of America*, 105(31), pp.10654–8.

Ross, D.E. et al., 2011. Towards electrosynthesis in *Shewanella*: energetics of reversing the mtr pathway for reductive metabolism. *PloS one*, 6(2), p.e16649.

Ruschig, U. et al., 1976. CO_2 reduction to formate by NADH catalysed by formate dehydrogenase from *Pseudomonas oxalaticus*. *European journal of biochemistry / FEBS*, 70(2), pp.325–330.

Sakakibara, Y. & Kuroda, M., 2004. Electric Prompting and Control of Denitrification. *Biotechnology and Bioengineering*, 42(4), pp.535–537.

Schuchmann, K. & Müller, V., 2013. Direct and Reversible Hydrogenation of CO_2 to Formate by a Bacterial Carbon Dioxide Reductase. *Science*, 342(December), pp.1382–1386.

Srikanth, S. et al., 2008. Electrochemical characterization of *Geobacter sulfurreducens* cells immobilized on graphite paper electrodes. *Biotechnology and bioengineering*, 99(5), pp.1065–73.

Suntres, Z.E., 2002. Role of antioxidants in paraquat toxicity. *Toxicology*, 180, pp.65–77.

Yang, Y. et al., 2008. Characterization of the *Shewanella oneidensis* Fur gene : roles in iron and acid tolerance response. *BMC Genomics*, 12, pp.1–12.

Zhang, X., Epifanio, M. & Marsili, E., 2013. Electrochemical characteristics of *Shewanella loihica* on carbon nanotubes-modified graphite surfaces. *Electrochimica Acta*, 102, pp.252–258.

7 Discussion

Metalloenzymes are a varied and complex aspect of biochemistry, the requirement for metal uptake and incorporation into apoproteins representing a considerable challenge for organisms, one that can be metabolically expensive due to the requirement for a host of accessory/assembly/metal uptake proteins and/or the energy required for active uptake of the metals from the environment. The metal containing FDH enzymes of *S.oneidensis* MR-1 represent a fascinating example, with multiple isoforms encoded by the genome highlighting the importance of the reaction they collectively catalyse. Formate oxidation in *S.oneidensis* MR-1 has been shown to be a key part of anaerobic respiration, contributing to PMF generation and removal of cytoplasmic formate from precursor molecules like pyruvate and lactate (Kane et al. 2016). Despite metal dependent FDH enzymes from other organisms containing either W or Mo, it was initially expected that due to the higher abundance of Mo in environments where *S.oneidensis* is usually found (Chapter 3 discussion) and the annotation of these enzymes as molybdoenzymes in online databases such as KEGG (Kanehisa et al. 2017), Mo would be required for FDH activity in *S.oneidensis*. However W (in the form of sodium tungstate) was found to be essential for maximal catalysis and not Mo (Chapter 3). Such a result was unexpected but since the hallmark of Shewanella species is their ability to couple to a wide range of electron acceptors, many of which also require Mo containing enzymes (TMAO reductase, DMSO reductase, nitrate reductase etc. (Gralnick et al. 2006)) the use of W in place of Mo in FDH enzymes would help alleviate the competition for these metals, presenting a selective advantage to those organisms capable of making use of a full complement of terminal reductases even when environmental Mo concentrations are low.

Although the overall requirement for W for maximal FDH activity in *S.oneidensis* MR-1 is interesting it does not adequately resolve the individual contributions of the three isoforms. It is interesting to note that gene expression of these three isoforms seems differentially regulated by the presence of 3μM tungstate or molybdate in the growth medium, with the Fdh1αβγ and Fdh2αβγ isoforms expressed under both conditions, whilst Fdnαβγ expression is not seen when supplemented with tungstate (Chapter 3). The study of a range of FDH

deletion strains suggests that the Fdh1αβγ and Fdh2αβγ isoforms are responsible for the formate oxidation activity observed in colourimetric assays in WT cells when grown with tungstate, but that when grown with molybdate the Fdnαβγ isoform plays a more important role (Chapter 5). This is supported by the observation that Fdh2αβγ (when grown with tungstate) can be natively purified and has been shown to be active with W at the active site (Chapter 4).

These collective observations could be taken to suggest a simple system with two of the isoforms (Fdh1αβγ and Fdh2αβγ) oxidising formate during tungstate supplemented growth and the third (Fdnαβγ) during molybdate supplemented growth. However this appears not to be the case, with the Fdh1αβγ and Fdh2αβγ isoforms partially contributing to colourimetrically assessed FDH activity and growth when supplemented with molybdate and the presence of Fdnαβγ regulating the assayed FDH activity seen by Fdh1αβγ and Fdh2αβγ when grown with tungstate. Further study will be required to tease apart the complicated relationship between these three isoforms, but it appears that as a generalisation the Fdh1αβγ and Fdh2αβγ isoforms are collectively responsible for growth and FDH activity in formate and tungstate containing growth conditions, i.e. those conditions of most interest for the majority of this work.

The requirement for W supplementation for maximal FDH activity in *S.oneidensis* MR-1 has not been previously reported. It is worth noting that since the oxidation of formate is considered an important part of the catabolism of *S.oneidensis* when grown on an anode in MFC devices (Luo et al. 2016), this result may hold applicational significance. The addition of W to growth media when culturing *S.oneidensis*, or indeed other *Shewanella* species studied in Chapter 4, may enhance current production in MFC experiments by intensifying formate oxidation in the periplasm and therefore increasing the flow of electrons from the terminal reductases in the Mtr pathway to an electrode. This may even be the case for 'rich' growth media such as LB which are normally considered to contain an excess of all required metals, despite this, experiments in LB (Chapter 4) suggest that the addition of 3 μM tungstate significantly increases FDH activity even in this growth medium.

The development of a CO_2 reductase activity for *S.oneidensis* demonstrated for the first time that the FDH enzymes of *S.oneidensis* MR-1 are reversible. This was not necessarily expected as many metal containing FDHs have been shown

to be irreversible (Oh & Bowien 1998), and in light of the native role of many of these enzymes catalysing formate oxidation the ability to drive CO_2 reduction would offer no immediately evident advantage. It should be stressed that the reported CO_2 reductase activity described throughout this work is not suggested to be physiologically relevant in *S.oneidensis* MR-1 and is only observed in the presence of a strong exogenous reductant, either dithionite (Chapter 4-5) or a cathode (Chapter 6). Despite not being relevant for native metabolism the observed CO_2 reductase activity is an exciting observation for biotechnological exploitation.

CO_2 reductase activity in *S.oneidensis* MR-1 is highest when cultures are grown in the presence of W, and the isoform Fdh2αβγ (with a lesser role for Fdh1αβγ) catalyse this CO_2 reduction (Chapter 3 and 5). Accordingly CO_2 reductase activity is entirely found in membrane fractions of cells and is associated with natively purified Fdh2αβγ containing W with an estimated turnover value of $10.7 \pm 3.8\ s^{-1}$ (Chapter 4).

This activity can be seen to be maximal at acidic pH values, in line with the proposed mechanism where a protonated active site (Mo^{4+}-SH) is thought to be required to drive CO_2 reduction. Catalysis is also inhibited in a concentration-dependent manner by the known FDH inhibitor azide and the measured reduction of CO_2 to formate can be confirmed using ^1H NMR (Chapter 4), which when driven by an electrode is seen with a high (107 %) coulombic efficiency (Chapter 6).

Together these observations allow an informed development of CO_2 reductase activity in a microbial electrosynthetic system. The work in Chapter 6 confirms this possibility with CO_2 reductase activity being seen in both mediated (by MV) and non-mediated electrochemical experiments, requiring W supplementation during growth to reach maximal catalysis. The mechanism behind electron transfer from the cathode for reductive catalysis in the non-mediated system remains unclear, with the Mtr pathway usually implicated in electron exchange with an electrode in *S.oneidensis* not thought to play a role. Other possibilities, including a role of hydrogen mediation or alternative outer membrane pathways would provide an interesting avenue for further characterisation.

Despite the mechanisms behind the observed CO_2 reductase activity on an electrode not being completely understood the system presented here still represents an important paradigm. Regardless of whether a proportion of the cells are lysing and enzymes are interacting directly with an electrode the system here presents an efficient cost effective way of producing a selective biocatalyst for the reduction of CO_2 to formate. As mentioned in Chapter 1, the major constraint of using biologically derived enzymes for such transformations is the time and costs associated with their purification and immobilisation on an electrode, this system requires no previous purification steps, functioning with a planktonic culture interacting with an unmodified graphite electrode without the need for exogenous mediators and capable of sustained catalysis for an extended (5 day) timeframe.

Excitingly the field of whole cell biocatalysts (Reshamwala et al. 2014) or "microbial factories" (Pandit & Mahadevan 2011) has been gaining momentum in the last few years, with multiple groups focusing more and more on microbial electrosynthesis (Khosravanipour et al. 2017)(Sadhukhan et al. 2016). Indeed the idea of using Mo and W containing FDH enzymes for biotechnological CO_2 reduction too has been gathering momentum (Bassegoda et al. 2014)(Maia et al. 2017). The work here combines these two areas with the currently proposed system using *S.oneidensis* considered an ideal point for further study.

The current electrochemical design could be further developed with the introduction of stirring during experiments to assess whether diffusion limits the observed rates of catalysis. Equally the information derived from previous biochemical studies (Chapters 4-5) could be used to further refine the design, running the experiments at lower pH to increase CO_2 reductase rates or by using the ΔFdnΔFdh1 strain instead of WT, which showed higher CO_2 reduction rates. Although the work in Chapter 6 suggested that *S.oneidensis* is capable of catalysis over 5 days a true lifespan for such a system could also be investigated, running the device until either substrate was depleted or reductive currents were no longer observed.

Careful evaluation of use of sodium carbonate as a substrate for CO_2 reduction assays would be another aspect for future study. Although comparable rates were seen in MV coupled assays using sodium carbonate or gaseous CO_2 (Chapter 4) the effect of adding exogenous carbonic anhydrase to increase the

available substrate concentration could be studied as another possible method for intensifying catalysis. It is interesting to note that the genome of *S.oneidensis* MR-1 contains a gene annotated as a carbonic anhydrase (SO_2474) but whether it is functionally expressed under the described conditions has not been studied. The aceogenic *A.woodii* that naturally catalyses CO_2 reduction to formate has been shown to possess an equivalent carbonic anhydrase (Schuchmann & Müller 2013).

Considering electrochemical CO_2 reductase activity in *S.oneidensis* MR-1 does not seem to require the Mtr pathway the possibility of driving comparable catalysis in other organisms could also be explored. Since the FDH-H of *E.coli* has already been demonstrated to be reversible on an electrode when purified this gram negative bacterium would make an interesting comparison. Equivalent experiments to those performed here using planktonic *E.coli* cultures may indicate whether the mechanisms for non-mediated catalysis seen in Chapter 5 are present in other comparable gram negatives.

In addition to *E.coli* other bacterial species or strains could be studied in comparative experiments. The use of *Shewanella* cultures other than *S.oneidensis* MR-1 would prove an interesting route, especially study of those strains that demonstrated high rates of CO_2 reduction compared to formate oxidation in Chapter 4. A good example is *S.amazonensis* SB2B, which showed high rates of MV coupled CO_2 reduction when grown with Mo or W, but almost no formate oxidation, making it an interesting target for electrochemical study.

The use of bacterial strains that physiologically use iron or a cathode as an electron donor (e.g. *Mariprofundus ferrooxydans* PV-1 (Summers et al. 2013)) would be another area of particular interest as these would theoretically be predisposed to accept electrons from a cathode. Although the limitations of these species is their typically slow growth rate, if the relevant iron oxidising machinery proved suitable it could be transferred to a faster growing organism such as *S.oneidensis*.

Although other bacterial species are discussed here one of the key advantages of using *S.oneidensis* MR-1 for such experiments is its plasticity. The genome of *S.oneidensis* MR-1 is well characterised and is genetically tractable allowing easy introduction of other metabolic elements. These could include the

machinery required for subsequent transformation of formate to molecules of higher worth or complexity whilst using the same single organism system. It also would allow incorporation of non-native FDH enzymes to assess if CO_2 reduction can be intensified should more suitable non-native FDH isoforms be identified. Importantly however *S.oneidensis* is one of a limited number of organisms with the required metabolic machinery for correct assembly of complex multi cytochrome proteins, which the majority of extracellular electron transfer proteins tend to be (Liang et al. 2009). As such this work establishes an important premise, showing the native ability of *S.oneidensis* MR-1 to catalyse CO_2 reduction allowing informed future studies in this biotechnologically attractive organism.

7.1 References

Bassegoda, A. et al., 2014. Reversible Interconversion of CO_2 and Formate by a Molybdenum-Containing Formate Dehydrogenase. *Journal of the American Chemical Society*, 136(44), pp.15473–6.

Gralnick, J. a et al., 2006. Extracellular respiration of dimethyl sulfoxide by *Shewanella oneidensis* strain MR-1. *Proceedings of the National Academy of Sciences of the United States of America*, 103(12), pp.4669–74.

Kane, A.L. et al., 2016. Formate metabolism in *Shewanella oneidensis* generates proton motive force and prevents growth without an electron acceptor. *Journal of Bacteriology*, 198(8), pp.1337–1346.

Kanehisa, M. et al., 2017. KEGG as a reference resource for gene and protein annotation. *Nucleic acids research*, 44(September), pp.457–462.

Khosravanipour, A. et al., 2017. Microbial electrosynthesis of solvents and alcoholic biofuels from nutrient waste: A review. *Journal of Environmental Chemical Engineering*, 5(1), pp.940–954.

Liang, S. et al., 2009. The roles of outer membrane cytochromes of *Shewanella* and *Geobacter* in extracellular electron transfer. *Environmental microbiology reports*, 1(4), pp.220–7.

Luo, S. et al., 2016. (13)C Pathway Analysis for the Role of Formate in Electricity Generation by *Shewanella Oneidensis* MR-1 Using Lactate in Microbial Fuel Cells. *Scientific reports*, 6(February), p.20941.

Maia, L.B., Moura, I. & Moura, J.J.G., 2017. Molybdenum and tungsten-containing formate dehydrogenases: aiming to inspire a catalyst for carbon dioxide utilization. *Inorganica Chimica Acta*, 455(2), pp.350–363.

Oh, J.-I. & Bowien, B., 1998. Structural Analysis of the fds Operon Encoding the NAD^+-linked Formate Dehydrogenase of *Ralstonia eutropha*. *The Journal of biological chemistry*, 273(41), pp.26349–26360.

Pandit, A. V & Mahadevan, R., 2011. In silico characterization of microbial electrosynthesis for metabolic engineering of biochemicals. *Microbial cell factories*, 10(1), p.76.

Reshamwala, S.M.S. et al., 2014. Construction of an efficient *Escherichia coli* whole-cell biocatalyst for D -mannitol production. *Journal of Bioscience and Bioengineering*, 118(6), pp.628–631.

Sadhukhan, J. et al., 2016. A critical review of integration analysis of microbial electrosynthesis (MES) systems with waste biorefineries for the production of biofuel and chemical from reuse of CO_2. *Renewable and Sustainable Energy Reviews*, 56, pp.116–132.

Schuchmann, K. & Müller, V., 2013. Direct and Reversible Hydrogenation of CO_2 to Formate by a Bacterial Carbon Dioxide Reductase. *Science*, 342(December), pp.1382–1386.

Summers, Z.M., Gralnick, J. a & Bond, D.R., 2013. Cultivation of an obligate Fe(II)-oxidizing lithoautotrophic bacterium using electrodes. *mBio*, 4(1), pp.e00420-12.

Appendix

Table A1 Collection of growth and kinetic data for deletion mutants in different conditions.
Growth condition refers anaerobic growth for 24 h when supplemented either with 3 µM Na tungstate (+W), 3 µM Na molybdate (+Mo), 3 µM Na tungstate and molybdate (+W/+Mo) or not supplemented with either (-W/ -Mo). Lag phase: Duration of lag phase in hours, green indicating a lag phase between 4 to 5 h, light green between 5 and 6 h, yellow between 6 and 8 h, light orange between 8 and 10 h and dark orange denoting 16+ h. Exponential phase: Specific growth rate (µ) during exponential growth, green indicating a specific growth rate between 0.3 and 0.35 h^{-1}, light green between 0.25 and 0.3 h^{-1}, yellow between 0.2 and 0.25 h^{-1}, light orange between 0.15 and 0.2 h-1 and dark orange between 0.1 and 0.15 h^{-1} .Stationary phase: Average OD600 during stationary phase where green indicates an OD600 reading between 0.25 and 0.3, light green between 0.2 and 0.25, yellow between 0.15 and 0.2, and orange between 0.1 and 0.15, where those marked with (*) did not reach stationary phase within 24 hours and instead describe OD600 values after 24 hours growth. Formate oxidation: Specific activity, determined by methyl viologen assay and normalised to total cell protein content where green indicates an formate dehydrogenase specific activity between 0.7 and 0.56 $\mu molmin^{-1}mg^{-1}$, light green between 0.56 and 0.42, yellow between 0.42 and 0.28, light orange between 0.28 and 0.14 and dark orange between 0.14 and 0 $\mu molmin^{-1}mg^{-1}$. (-) indicates strains where growth was not detected.

Growth condition	Strain	Lag phase	Exponential phase	Stationary phase	Formate oxidation
+W	Wild Type	4.9 ± 0.7	0.37 ± 0.06	0.20 ± 0.03	0.701 ± 0.015
	ΔFdh1	4 ± 0.7	0.18 ± 0.02	0.11 ± 0.01	0.481 ± 0.002
	ΔFdh2	4 ± 0.4	0.17 ± 0.01	0.18 ± 0.04	0.431 ± 0.224
	ΔFdn	4.6 ± 0.3	0.18 ± 0.02	0.2 ± 0.04	0.708 ± 0.028
	Fdh1+	6 ± 0	0.35 ± 0.05	0.22 ± 0.06	0.328 ± 0.095
	Fdh2+	8.8 ± 1.2	0.17 ± 0.01	0.18* ± 0.03	0.630 ± 0.138
	Fdn+	-	-	-	-
	ΔFDH	-	-	-	-
+Mo	Wild Type	5 ± 0.4	0.29 ± 0.08	0.30 ± 0.05	0.282 ± 0.027
	ΔFdh1	4 ± 0.57	0.13 ± 0.03	0.16 ± 0.01	0.242 ± 0.029
	ΔFdh2	4.7 ± 0.3	0.15 ± 0.01	0.22 ± 0.01	0.189 ± 0.013
	ΔFdn	5.3 ± 0.3	0.12 ± 0.04	0.29 ± 0.01	0.009 ± 0.009
	Fdh1+	10 ± 1	0.16 ± 0.03	0.25* ± 0.01	0.044 ± 0.002
	Fdh2+	16.3 ± 1.2	0.18 ± 0.04	0.12* ± 0.01	0.003 ± 0.001
	Fdn+	-	-	-	-
	ΔFDH	-	-	-	-

Table A1 (cont.)

Growth condition	Strain	Lag phase	Exponential phase	Stationary phase	Formate oxidation
+W/+Mo	Wild Type	4.6 ± 0.4	0.34 ± 0.04	0.21 ± 0.02	0.545 ± 0.033
	ΔFdh1	5 ± 0	0.21 ± 0.02	0.1 ± 0.01	0.262 ± 0.072
	ΔFdh2	4 ± 0.57	0.16 ± 0.02	0.16 ± 0.03	0.35 ± 0.009
	ΔFdn	4.7 ± 0.3	0.15 ± 0.02	0.19 ± 0.03	0.54 ± 0.013
	Fdh1+	5.6 ± 0.3	0.25 ± 0.04	0.2 ± 0.04	0.291 ± 0.027
	Fdh2+	7.7 ± 0.3	0.23 ± 0.01	0.12 ± 0.01	0.547 ± 0.055
	Fdn+	-	-	-	-
	ΔFDH	-	-	-	-
-W/-Mo	Wild Type	5 ± 0.4	0.25 ± 0.03	0.23 ± 0.04	0.214 ± 0.0.02
	ΔFdh1	5.6 ± 0.3	0.13 ± 0.02	0.15 ± 0.03	0.089 ± 0.01
	ΔFdh2	4.6 ± 0.3	0.14 ± 0.02	0.2 ± 0.03	0.059 ± 0.001
	ΔFdn	4 ± 0.57	0.13 ± 0.02	0.2 ± 0.02	0.01 ± 0.005
	Fdh1+	4.7 ± 0.3	0.14 ± 0.02	0.23 ± 0.02	0.004 ± 0.001
	Fdh2+	8.3 ± 0.3	0.15 ± 0.01	0.2* ± 0.01	0.008 ± 0.001
	Fdn+	-	-	-	-
	ΔFDH	-	-	-	-

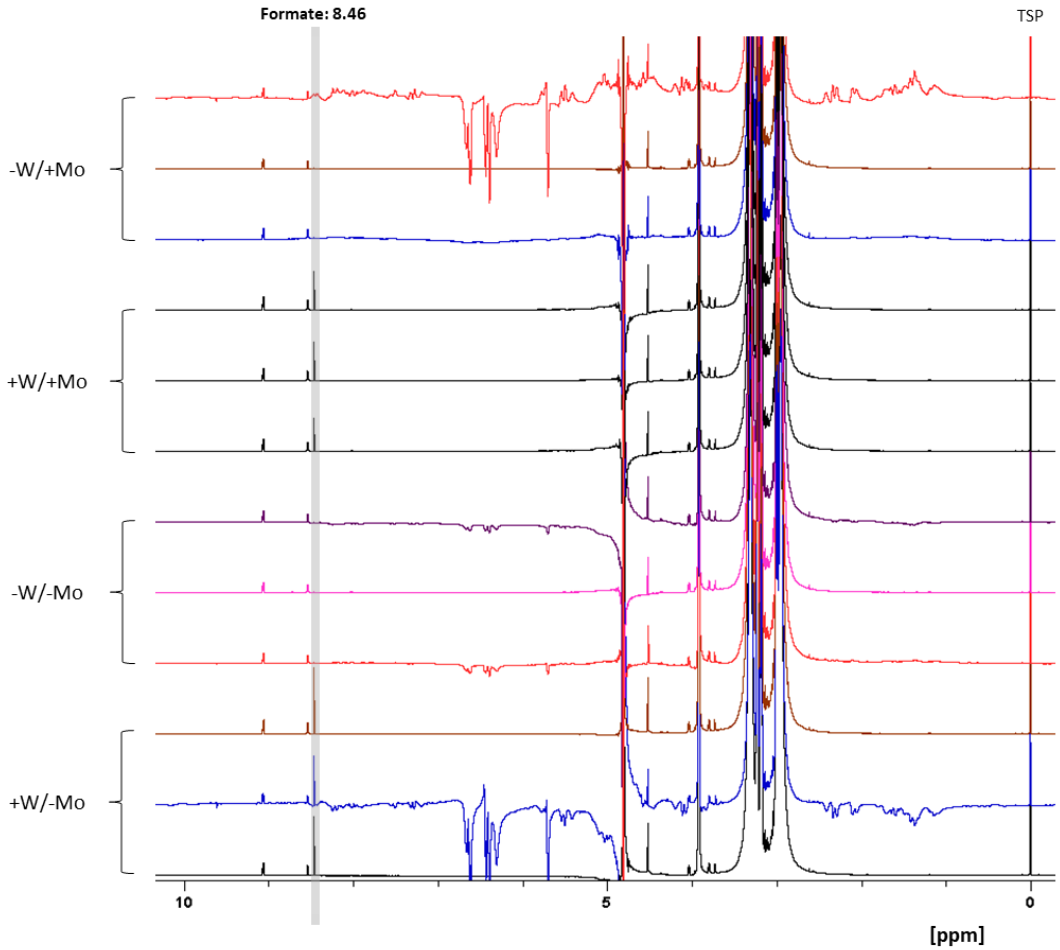

Figure A-1 Example NMR traces for analysis of CO_2 reductase assays
Methyl viologen CO_2 reductase assays were conducted using cells grown in minimal growth media where +W indicates sodium tungstate supplementation at 3 μM and +Mo indicates sodium molybdate supplementation at 3 μM. Following these assays and whole cell removal, supernatant was analysed for formate content by ^1H NMR. Shown are example NMR traces highlighting the formate feature at 8.46, this peak was integrated and compared with standards to quantify formate concentration presented in Figure 4-4. Other signals represent contributions from assay reagents including HEPES, dithionite and methyl viologen, all spectra normalised to TSP methyl peak (0).